Drought Assessment in South Indian River Basins using Reconstructed GRACE Data to Examine Terrestrial Water Storage and Teleconnections

Submitted in partial fulfilment of the requirements
for the award of the degree of

DOCTOR OF PHILOSOPHY

in

CIVIL ENGINEERING

by

K Satish Kumar
(Roll No. 717005)

Supervisor
Prof. P Anand Raj

DEPARTMENT OF CIVIL ENGINEERING
NATIONAL INSTITUTE OF TECHNOLOGY
WARANGAL – 506004 (T.S.), INDIA
JUNE 2022

Drought Assessment in South Indian River Basins using Reconstructed GRACE Data to Examine Terrestrial Water Storage and Teleconnections

Submitted in partial fulfilment of the requirements
for the award of the degree of

DOCTOR OF PHILOSOPHY

in

CIVIL ENGINEERING

by

K Satish Kumar
(Roll No. 717005)

Supervisor
Prof. P Anand Raj

DEPARTMENT OF CIVIL ENGINEERING
NATIONAL INSTITUTE OF TECHNOLOGY
WARANGAL – 506004 (T.S.), INDIA
JUNE 2022

Dedicated to Late Prof. E. Venkata Rathnam, to my beloved parents and to my wife.

APPROVAL SHEET

This Dissertation Work entitled **"DROUGHT ASSESSMENT IN SOUTH INDIAN RIVER BASINS USING RECONSTRUCTED GRACE DATA TO EXAMINE TERRESTRIAL WATER STORAGE AND TELECONNECTIONS"** by **Mr. K Satish Kumar** is approved for the degree of Doctor of Philosophy.

Examiners

_____

_____

_____

Supervisor

_____

Chairman

_____

Date:_____ Place:_____

DECLARATION

This is to certify that the work presented in the thesis entitled **"DROUGHT ASSESSMENT IN SOUTH INDIAN RIVER BASINS USING RECONSTRUCTED GRACE DATA TO EXAMINE TERRESTRIAL WATER STORAGE AND TELECONNECTIONS"** is a bonafide work done by me under the supervision of Prof. P Anand Raj and was not submitted elsewhere for the award of any degree.

I declare that this written submission represents my ideas in my own words and where others' ideas or words have been included, I have adequately cited and referenced the original sources. I also declare that I have adhered to all principles of academic honesty and integrity and have not misrepresented or fabricated or falsified any idea / data / fact /source in my submission. I understand that any violation of the above will be a cause for disciplinary action by the Institute and can also evoke penal action from the sources which have thus not been properly cited or from whom proper permission has not been taken when needed.

_____

(K SATISH KUMAR)

(Roll No: 717005)

Date:_____

NATIONAL INSTITUTE OF TECHNOLOGY
WARANGAL

CERTIFICATE

This is to certify that the thesis entitled **"DROUGHT ASSESSMENT IN SOUTH INDIAN RIVER BASINS USING RECONSTRUCTED GRACE DATA TO EXAMINE TERRESTRIAL WATER STORAGE AND TELECONNECTIONS"** that is being submitted by **K SATISH KUMAR** for the award of the degree of **DOCTOR OF PHILOSOPHY** in the Department of Civil Engineering, National Institute of Technology, Warangal, is a record of bonafide research work carried out by him under my supervision and it has not been submitted elsewhere for award of any degree.

Prof. P. Anand Raj
Supervisor
Department of Civil Engineering
National Institute of Technology
Warangal-506004 (T.S.), India.

ABSTRACT

Drought is a complex natural hazard that affects ecosystems and society in several ways and it is important to quantify drought at the river basin scale. Drought is difficult to model and predict due to the complicated relationships between the components of the water cycle and the land surface atmospheric interactions. One of the most significant challenges is the lack of spatial and temporal consistency in the in-situ measurements available for drought monitoring. Droughts can also be caused due to the deficiency of water from a variety of sources/components, including surface water, groundwater, and soil moisture. Consistent and accurate measurement of each of these components independently and then integrating them into a total water storage measurement is difficult. As a result, the Gravity Recovery And Climate Experiment (GRACE) mission's measurements are exceptionally valuable. In recent years, researchers have been evaluating the potential of Terrestrial Water Storage (TWS) anomalies in drought monitoring methodologies. The GRACE provides consistent spatial and temporal global TWS observations, and studies have demonstrated that TWS anomalies are suited for drought related studies worldwide. Therefore, it is proposed to use remote sensing products to help understand drought conditions in four basins of South India.

In the first section, monthly and seasonal correlation among six drought indices namely GRACE Drought Severity Index (GRACE DSI), Standardized Precipitation Index (SPI), Self-Calibrated Palmer Drought Severity Index (SC_PDSI), Standardized Precipitation Evapotranspiration Index (SPEI), Combined Climatologic Deviation Index (CCDI) and GRACE Groundwater Drought Index (GGDI) with Terrestrial Water Storage Anomalies (TWSA) are analysed using the Pearson's correlation coefficient (r) from 2003 to 2016 for four river basins of South India. The considered river basins are Godavari River Basin (GRB), Krishna River Basin (KRB), Cauvery River Basin (CRB) and Pennar and East flowing rivers between Pennar and Cauvery River Basin (PCRB). Basin scale drought events are evaluated using CCDI, GRACE DSI, SC_PDSI, SPI12 and SPEI12 at seasonal and monthly time scale. The four seasons considered are (i) post-monsoon rabi (Jan-Mar), (ii) pre-monsoon (Apr-Jun), (iii) monsoon (Jul-Sep) and (iv) post-monsoon kharif (Oct-Dec) respectively. Characteristics of drought event analysis are calculated for monthly CCDI. The results showed that TWSA is highly correlated with GGDI and CCDI. Seasonally, high spatial correlations between CCDI and GGDI with TWSA are evident for all the river basins. KRB experienced severe drought that lasted for 29 months, longer than in the rest of basins between 2003 and 2005. Overall, GGDI and CCDI indices are found to be effective for examining and evaluating the drought conditions at the basin scale.

In the second section, the drought characteristics are analysed and assessed using GGDI during 2003 to 2016. The spatial distribution, temporal evolution of drought, and trend characteristics are also analysed. Then, the relationship between GGDI and climate factors are evaluated by the method of Wavelet Coherence. The results indicate the following points: (i) GRACE's quantitative results are consistent and robust for drought assessment, (ii) Out of the four basins, severe drought is noticed in CRB between 2012 and 2015, with severity 27 and duration of 42 months, (iii) Other than GRB, the remaining three basins displayed significant negative trends at monthly and seasonal scales and (iv) The Wavelet Coherence method revealed that climate factors have a substantial effect on GGDI, and the impact of Southern Oscillation Index (SOI) on drought is significantly high, followed by Sea Surface Temperature (SST) Index (namely, NINO3.4) and Multivariate El Niño–Southern Oscillation Index (MEI) in all the basins. This study provides reliable and robust quantitative result of GRACE water storage variations that shares new insights for further drought investigation.

In the third section, the reconstruction of TWSA is performed using Multi Layer Perceptron's (MLP) to obtain a continuous TWSA time series from 1960 to 2020. The MLP model is developed by considering Global Land Data Assimilation System (GLDAS) evaluated TWSA, precipitation and temperature as predictors and GRACE TWSA as predictand. The predictor and predictand datasets from January 2003 to December 2013 (75% of the samples) are used for training the MLP model, and those from January 2014 to June 2017 (25% of the samples) are used for testing the performance of trained model at both grid and basin scales. During the testing period (2014 to 2017), the MLP modeled TWSA is highly correlated with the observed TWSA in four basins with correlation coefficient varying between 0.89 to 0.95. Then, the model developed TWSA is converted to seasonal GroundWater Storage Anomalies (GWSA) ($GWSA_{GRACE}$) and validated using observation well based GWSAs ($GWSA_{OBS}$) which are evaluated from a dense network of groundwater well measurements from 1996 to 2020. At grid and basin scale, a good correlation is observed between seasonal $GWSA_{GRACE}$ and $GWSA_{OBS}$. PCRB and CRB exhibited high correlations between $GWSA_{GRACE}$ and $GWSA_{OBS}$ in all the seasons at all grids when compared with GRB and KRB. At basin scale the highest correlation between $GWSA_{GRACE}$ and $GWSA_{OBS}$ is observed in PCRB (r= 0.81) followed by CRB (r= 0.79) and GRB (r= 0.72).

In the fourth section, drought frequency analysis is performed only for GRB by developing Severity-Duration-Frequency (SDF) and Severity-Area-Frequency (SAF) curves using CCDI and 12-month SPI (SPI12) from 1960 to 2020. CCDI is calculated from the reconstructed TWSA and SPI12 is evaluated using precipitation data from India Meteorological Department (IMD). In this section, SPI12 based SAF and SDF

curves are compared with the CCDI based SAF and SDF curves. Using Fuzzy C-Means (FCM) clustering approach, homogeneous drought regions are identified and therefore, optimum number of clusters are assigned as four. The best fit copula for observed and simulated severity and duration are: region 1-Clayton, Region 2 and 3 -Gumbel, Region 4- Frank copula. SDF and SAF curves are developed and analysed using the best fit copulas. The research findings conclude that the SDF curves are concave upward indicating an increase in severity with an increase in duration. The rate of increase of severity is small for shorter durations compared to that of longer durations of drought. The SAF curves with steeper slopes and high variability in topographical and hydrological characteristics have been observed over GRB. From these curves, for a specified percentage of area and return period, the drought severity can be calculated and the information can be used for crop management and agricultural water demands. Good agreement is observed between SPI12 and CCDI based SAF and SDF curves. Therefore, drought frequency analysis can be performed using the reconstructed TWSA for any river basin in India.

The results obtained based on the application of different statistical techniques used in this study, make it possible to recommend GRACE mascon solutions for drought and groundwater related studies over the region with similar climatic, hydrogeological and groundwater withdrawal conditions. Also, the reconstructed TWSA from 1960 to 2020, resulting in a 60-year TWSA time series can be utilised to research any long-term climate related applications. Overall, the findings of this research offer a view of potential conditions of drought in the four basins of South India.

Keywords: Drought, GRACE, Terrestrial Water Storage, Drought Indices, CCDI, GGDI, SPI, Severity, Duration, Teleconnections, Reconstruction, Groundwater Storage, Drought Frequency Analysis.

ACKNOWLEDGEMENT

This thesis is the fruit of effort and guidance of many persons that I would like to thank. Above all, I sincerely thank ***National Institute of Technology, Warangal*** *for providing me with the opportunity to work with such wonderful people and their support to complete this dissertation in spite of all its conditions.*

First and foremost, I would like to express my sincere gratitude to my research supervisor ***Late Prof. E. Venkata Rathnam****, for the guidance, direction, and pearls of wisdom, but more importantly for his encouragement precisely when needed and without which it would have been nearly impossible to produce this piece of work. From bottom of my heart, I am in your debt for your help and support.*

I would like to express my sincere gratitude to my research supervisor ***Prof. P. Anand Raj****, for his encouragement, guidance, and support throughout my doctoral study and research. He provided me with valuable insights of advice not only about research and the process of accomplishing it, but also about life. I am indebted to him and the present work would not have been possible without his continuous support.*

Besides my supervisors, I would like to thank ***Dr. Venkataramana Sridhar****, Associate Professor, Virginia Tech, USA for his continuous guidance and support throughout my research work. I approached him uncountable times, when I have faced a research problem that seemed to be insuperable. He always been willing to guide me to find a solution and also intervened when the problem became too big for me to handle. I am indebted to him for all the creative inputs provided and putting up the pieces together to obtain a fruitful output.*

Besides my supervisor, I would like to thank the rest of my Doctoral committee members: ***Prof. P Rathish Kumar****, Chairman of the Doctoral Committee & Head of the Civil Engineering Department,* ***Prof. N V Umamahesh****, Internal Member,* ***Dr. K***

***Venkata Reddy**, Internal Member and **Prof. Debashis Dutta**, External Member, Department of Mathematics, for their encouragement, insightful comments and constructive suggestions.*

*My sincere thanks also goes to **Prof. N V Ramana Rao**, Director, National Institute of Technology Warangal for rendering all help and support needed for completion of my Ph.D. work. I gratefully acknowledge **National Institute of Technology Warangal**, for providing me financial support to carry out my research.*

*Special thanks and acknowledgment goes to **Dr. K. V. Jayakumar**, Emeritus Professor, **Sri. Kameswara Rao V N**, Associate Professor and **Dr. Umesh B**, Assistant Professor, Civil Engineering Department, NIT Warangal for their valuable suggestions and immense help rendered in bringing out this work.*

*I thank my fellow research scholar **Mrs. K Sreelatha** for her encouragement, and help whenever I needed and for creating an environment congenial to my work and study. Special thanks goes to **Mr. Sagar Banavath**, **Mr. Venkat Rao Gundapuneni**, **Mrs. Soumyashree Dixit**, **Mr. Rudraswamy G K**, **Mr. Komali Bharath Narayana Reddy**, **Mr. Subbarao Yarramsetty** and **Dr. Goutham Veerapu**, for their direct or indirect help throughout the period of my research work and creating an enjoyable and fun work environment.*

*Last but not the least, I always gonna be truly grateful and thankful to my parents **Mr. K Narasimhulu** and **Mrs. K Gowramma**, family members: **Mr. K Kishore Kumar** (brother), **Mrs. K Saroja** (sister-in-law), **Dr. Tulasi K** (sister), **Ms. K Aarohi** (niece), **Mr. K Mokshith** (nephew) for standing by me in testing times and offering good moral support all these years. They always encouraged and helped me even with this long geographical distance between us. Without them, I would not be the person I am today.*

*Thanks are due to my wife **Mrs. M Chaitanya** for her love, affection,encouragement and constant support, for all the late nights and early mornings. Thank you for being my best friend in difficult times throughout the research period. I owe you everything.*

K Satish Kumar

TABLE OF CONTENTS

LIST OF SYMBOLS

a_k	Hidden neurons
$C(\bullet)$	Copula distribution function
$C(u, v)$	Cumulative distribution function
$\overline{CWS_{2004-2009}}$	Average canopy water storage w.r.t the base line period from January 2004 to December 2009
$CWSA_t$	Canopy water storage anomaly w.r.t time t
C_ψ	Admissibility constant
d	Distance between the particles
E	Evapotranspiration
F	Force
f	Mapping function
Fpi	Fuzziness Partition Index
$F_D(d)$	Cumulative distribution function of drought duration
$F_{S,D}(s, d)$	Joint cumulative distribution function
$F_{S\|D}(s \mid d)$	Conditional cumulative distribution function
$F_X(x)$	Marginal cumulative distribution function for random variable X
$F_Y(y)$	Marginal cumulative distribution function for random variable Y
$F_{XY}(x, y)$	Joint cumulative distribution function
G	Universal gravitational constant
$GWSA_t$	Groundwater storage anomaly w.r.t time t
GWS_{OBS}	Observed groundwater storage
$GWSA_{OBS}$	Observed groundwater storage anomaly
$\overline{GWS_{2004-2009}}$	Average groundwater storage w.r.t the base line period from January 2004 to December 2009
H_0	Null hypothesis
H_1	Alternative hypothesis

I_i	Incoming masses
m_1, m_2	Two point masses
M	Predictors
n	Sample size
O_i	Outgoing masses
P	Precipitation
Pe	Partition Entropy
R	Runoff
r	Pearson's correlation coefficient
s	Scale factor
S	Smoothing operator
Si	Separation Index
S_y	Specific yield
$SMSA_t$	Soil moisture storage anomaly w.r.t time t
$\overline{SMS_{2004-2009}}$	Average soil moisture storage w.r.t the base line period from January 2004 to December 2009
$TWSA_t$	Terrestrial water storage anomaly w.r.t time t
$T_{S\|D}(s \mid d)$	Conditional recurrence interval
u, v	Two uniformly distributed random variables
$V(S)$	Variance
W	Weight
$W_s(\tau, s)$	Wavelet transform
$W_{xy}(s, \tau)$	Cross wavelet transforms between two series x and y
x_i, y_i	x and y variable samples indexed with i
$\bar{x}, \bar{y}$	Mean of values in x and y variables
Z	Trend test statistics

$\frac{\delta S}{\delta t}$	Derivative of total mass with respect to time t
ΔTWS	Change in terrestrial water storage
ΔGWS	Change in groundwater storage
ΔSMS	Change in soil moisture storage
ΔSWE	Change in snow water equivalent
ΔSWS	Change in surface water storage
ΔCWS	Change in canopy water storage
Δh	Groundwater level anomalies
$\Gamma(\alpha)$	Gamma function
α	Shape parameter
β	Scale parameter
σ	Standard deviation
μ	Mean
$\psi(t)$	Mother wavelet transformation basis function
$\Psi(\omega)$	Fourier transform
$\|.\|$	Magnitude
τ	Time shift
φ_0	Mother wavelet
ω_0	Frequency
ε	Noise
γ	Arrival rate

Glossary of Terms

AD	Anderson–Darling
AIC	Akaike Information Criteria
ANN	Artificial Neural Network
AO	Arctic Oscillation
ARX	AutoRegressive eXogenous
BIC	Bayesian Information Criteria
BNN	Bayesian Neural Network
CCA	Canonical Correlation Analysis
CCDI	Combined Climatologic Deviation Index
CDF	Cumulative Distribution Function
CGWB	Central Ground Water Board
CLM	Community Land Model
CMIP5	Coupled Model Inter-comparison Project phase 5
CNN	Convolutional Neural Network
CRB	Cauvery River Basin
CRI	Coastline Resolution Improvement
CSR	Center for Space Research
CWS	Canopy Water Storage
CWT	Continuous Wavelet Transform
DAS	Data Assimilation System
DLR	Deutsches Zentrum für Luft- und Raumfahrt
DMI	Dipole Mode Index
DNN	Deep Neural Network
DWT	Discrete Wavelet Transform
EML	Exact Maximum Likelihood
ENSO	El Niño Southern Oscillation
EWH	Equivalent Water Height
FCM	Fuzzy C-Means clustering

GA	Genetic Algorithm
GCM	Global Climate Model
GGDI	GRACE Groundwater Drought Index
GHDI	GRACE Hydrological Drought Index
GIA	Glacial Isostatic Adjustment
GLDAS	Global Land Data Assimilation System
GPCC	Global Precipitation Climatology Centre
GPS	Global Positioning System
GRACE	Gravity Recovery And Climate Experiment
GRACE DSI	GRACE Drought Severity Index
GRACE FO	GRACE Follow-On
GRB	Godavari River Basin
GSFC	Goddard Space Flight Center
GWL	GroundWater Level
GWS	GroundWater Storage
GWSC	GroundWater Storage Change
GWSD	GroundWater Storage Deviation
GWSA	GroundWater Storage Anomaly
HWBM	Hydrological Water Balance Model
IAF	Intensity-Area-Frequency
ICA	Independent Component Analysis (ICA)
IDW	Inverse Distance Weightage
IFM	Inference From Margins
IMD	India Meteorological Department
IOD	Indian Ocean Dipole
JPL	Jet Propulsion Laboratory
KBR	K-Band microwave Ranging
KRB	Krishna River Basin
KS	Kolmogorov–Smirnov

L-L	Log Likelihood
LSM	Land Surface Model
LULC	Land Use-Land Cover
mascon	Mass Concentration
MDHI	Modified Drought Hazard Index
MEI	Multivariate ENSO Index
MERRA	Modern-Era Retrospective Analysis for Research and Applications
MJO	Madden-Julian Oscillation
MLP	Multi Layer Perceptron
MLR	Multiple Linear Regression
MMK	Modified Mann-Kendall
MOM	Method Of Moments
MPL	Maximum Pseudo-Likelihood
NAO	North Atlantic Oscillation
NASA	National Aeronautics and Space Administration
NSE	Nash-Sutcliff Efficiency
NOAA	National Oceanic and Atmospheric Administration
PCA	Principal Component Analysis
PCRB	Pennar and East flowing rivers between Pennar and Cauvery River Basin
PDF	Probability Density Function
PDSI	Palmer Drought Severity Index
PET	Potential Evapotranspiration
PRISM	Parameter-elevation Regressions on Independent Slopes Model
PSO	Particle Swarm Optimization
QBO	Quasi-Biennial Oscillation
RCP	Representative Concentration Pathway
RF	Random Forest
RMSE	Root Mean Square Error

SAF	Severity-Area-Frequency
SARIMAX	Seasonal Auto Regressive Integrated Moving Average with EXogenous variables
SC_PDSI	Self-Calibrated PDSI
SDF	Severity-Duration-Frequency
SH	Spherical Harmonics
SMS	Soil Moisture Storage
SOI	Southern Oscillation Index
SPI	Standardized Precipitation Index
SPEI	Standardized Precipitation Evapotranspiration Index
SSFI	Standardized StreamFlow Index
SST	Sea Surface Temperature
SVM	Support Vector Machine
TRMM	Tropical Rainfall Measuring Mission
TSDI	Total Storage Deficit Index
TWS	Terrestrial Water Storage
TWSA	Terrestrial Water Storage Anomaly
TWSC	Terrestrial Water Storage Change
VIC	Variable Infiltration Capacity
WGHM	WaterGAP Global Hydrology Model
WSDI	Water Storage Deficit Index
XGB	eXtreme Gradient Boost

LIST OF TABLES

LIST OF FIGURES

CHAPTER 1

INTRODUCTION

1.1 GRAVITY RECOVERY AND CLIMATE EXPERIMENT (GRACE)

1.1.1 GRACE Mission Overview

Many of today's most critical climate science problems are dependent on understanding how water moves across the planet. However, this isn't always straightforward to quantify. Water can be found in plain sight, such as in a lake or it might be hidden underground. It can evaporate in a matter of seconds as sunlight heats the Earth's surface or it can be held as ice in a glacier for years. Irrespective of whether water is visible or invisible, liquid, solid or vapour, mass of water remains constant and has a gravitational pull. The changing pull of gravity around Earth is tracked precisely by **G**ravity **R**ecovery **A**nd **C**limate **E**xperiment (GRACE) by observing the movement of Earth's water masses from deepest ocean depths to the top of the Himalayas.

The GRACE and GRACE **F**ollow-**O**n (GRACE FO) satellite gravity missions are jointly launched by United States and German space agencies i.e., **N**ational **A**eronautics and **S**pace **A**dministration (NASA) and **D**eutsches Zentrum für **L**uft- und **R**aumfahrt (DLR). GRACE mission is launched on 17 March 2002 and ended on 27 October 2017, providing more than 15 years of continuous Earth's gravity field variations. GRACE FO mission launched on 22 May 2018 will continue in observing and monitoring the movement of Earth's water changes in rivers, lakes, soil moisture, underground water storage, ice sheets and glaciers.

The GRACE mission consists of two co-orbital satellites with the inter-satellite separation of approximately 220 km, flying in tandem in a polar, near-circular orbit at an altitude of 450 km with 89.5° inclination (see Fig. 1.1). The GRACE mission is unique among the Earth observation satellite missions, as it detects the gravity changes by measuring the inter-satellite distance, rather than imaging the Earth. The change in distance between the satellites is undoubtedly invisible to the naked eye, but extremely precise minuscule changes in the distance are measured by the **K**-**B**and microwave **R**anging (KBR) system with an accuracy of 1 $\mu m.s^{-1}$ located on each satellite (Tapley et al., 2004). Non-gravitational accelerations are measured and filtered out, leaving

only gravity-induced accelerations to be evaluated. The satellite's precise location over the Earth is then determined by satellite **G**lobal **P**ositioning **S**ystem (GPS) receivers to within a centimetre or less. GRACE satellites will use all of this precise data to create monthly maps of the Earth's average gravity field with unprecedented accuracy.

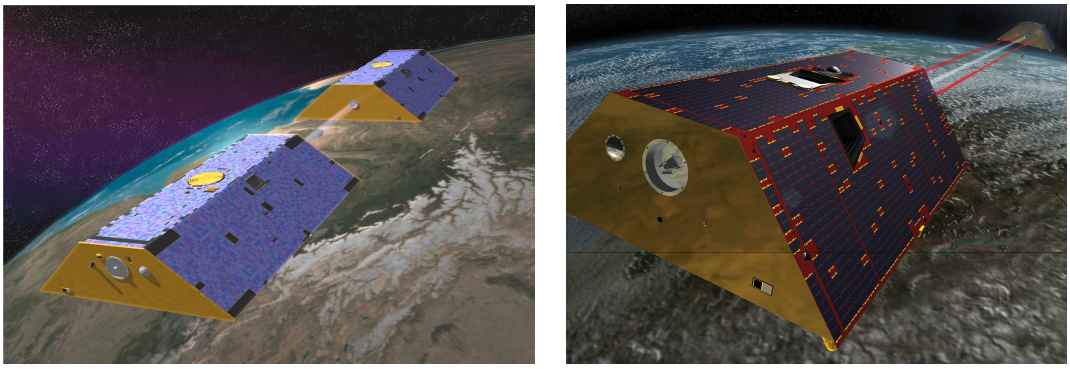

(a) (b)

Figure 1.1: (a) GRACE mission and (b) GRACE FO mission. Source: https://www.jpl.nasa.gov/

1.1.2 Satellite Gravimetry

One of the fundamental forces that emerges from the presence of mass is gravity. According to Newton's law of gravitation, every particle attracts every other particle by a force F pointing along the line intersecting both points. The magnitude of the force is proportional to the product of the two point masses (m_1 and m_2) and inversely proportional to the square of the distance between the particles (d).

$$F = G\frac{m_1 \cdot m_2}{d^2} \tag{1.1}$$

where, G= universal gravitational constant. Redistribution of masses on or near the Earth's surface (m_1) creates a change in the gravitational field that affects the satellite (m_2) when Eq. 1.1 is applied to an Earth-satellite system. Over short periods of time, changes in water storage create the most substantial redistribution of mass on the Earth's surface (Wahr et al., 2004). No other substance moves as quickly as water storage changes, with the exception of sudden land mass shift during earthquakes (Han et al., 2005). Analysing temporal fluctuations in the gravity field is a useful technique for estimating mass movements, whether one is investigating hydrology, climatology, or oceanography.

GRACE gravity observations have been processed using various approaches. The global **S**pherical **H**armonics (SH) basis function is the traditional processing approach that has been applied over the decade in parameterizing the Earth's gravity field (Bettadpur, 2012; Wahr et al., 1998). Regional **mas**s **con**centration (mascon) function

is an alternative processing strategy that has been operational in parameterizing the gravitational field over the recent years (Luthcke et al., 2015; Save et al., 2016; Watkins et al., 2015). The gravity field variations based on GRACE measurements are represented in Fig. 1.2.

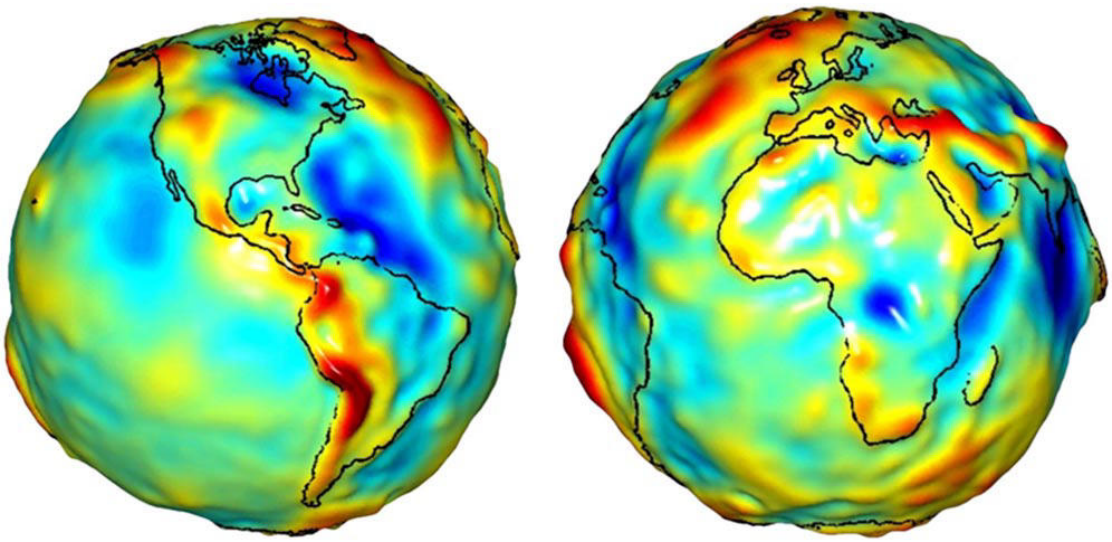

Figure 1.2: Gravity field variations based on GRACE measurements.
(red bulges: stronger gravity; blue depressions: weaker gravity)

The observed monthly changes in gravity are caused by fluctuations in mass. These mass variations (estimated by either spherical harmonic or mascon functions) are considered/assumed as a thin layer of water thickness over the surface of Earth. In reality, majority of the changes in gravity are caused by water storage fluctuations in land ice masses, hydrologic reservoirs and in atmosphere by moving ocean. The vertical extent of these changes are estimated in centimeters of **E**quivalent **W**ater **H**eight (EWH). EWH is an imaginary uniform water layer (density = 1000 kg/m^3) of thickness h which denotes the **T**errestrial **W**ater **S**torage (TWS) anomaly.

1.1.3 GRACE Data Products

Multiple processing stages are used to process data from GRACE satellite sensors (KBR, GPS, accelerometer, and star camera). The output of each processing step is labelled as a different data product (Bettadpur, 2012). Level-0, Level-1A, Level-1B, Level-2 and Level-3 are the official five classifications for GRACE data. In this thesis, Level-3 data products known as GRACE mascon's are used for the analysis.

1.1.3.1 Level-3 mascon's

The monthly gravity anomalies from Level-2 are converted into surface mass anomalies (EWH) and maps it to a geographical grid in Level-3. Different post-processing filters and geophysical data adjustments are implemented depending

on the Level-2 input data type. Mascon's are equivalent to Level-3 products, that predict mass changes (in terms of EWH) in concentrated blocks over Earth's surface. There is no need for further filtering and the method promises to be more effective than existing methods at preventing signal leakage. Presently three agencies are providing mascon solutions from GRACE mission namely: (i) **G**oddard **S**pace **F**light **C**enter (GSFC) (Luthcke et al., 2015), (ii) **J**et **P**ropulsion **L**aboratory (JPL) (Watkins et al., 2015) and **C**enter for **S**pace **R**esearch (CSR) (Save et al., 2016). These mascon products do not need post-processing and hence can be used directly in studies related to hydrology, climatology, or oceanography. In this thesis, GRACE datasets from JPL centre are used for the drought analysis over South Indian River Basins.

1.1.4 Total Water Storage (TWS)

Water can be stored in the atmosphere, biosphere, lithosphere, cryosphere and other parts of the Earth's system. Water is constantly moving through the atmosphere, on the surface and beneath the Earth's surface. The total amount of water remains relatively constant, but the location in which it is held varies greatly. Hydrological analyses are performed to estimate where and how much water is present at any given time. All the hydrological analyses are performed using the application of a mass balance. The mass balance for every system can be calculated using the Reynold's transport theorem. The mass balance within a control volume can be defined as

$$\frac{\delta S}{\delta t} = \sum_i I_i - \sum_i O_i \tag{1.2}$$

where, $\frac{\delta S}{\delta t}$ = derivative of total mass with respect to time t; $\sum_i I_i$ = sum of all incoming masses; $\sum_i O_i$ = sum of all outgoing masses. The above equation states that the difference in the storage is due to the difference between inflow and outflow masses within a system.

Because the total water storage on Earth is constant, a mass balance is only applicable when a specific control volume is defined. In most of the hydrological studies, the basins, sub basins and other watersheds are considered as control volumes. The fact that a watershed has only one lateral flow, run-off at the outlet, makes it an ideal control volume. Precipitation and evapotranspiration are the other vertical fluxes that influence total water storage. Considering these fluxes, mass balance is written as

$$\frac{\delta S}{\delta t} = P - E - R \tag{1.3}$$

where, S= change of water stored in the system in time t; P= precipitation entering into the system; E and R are evapotranspiration and runoff leaving the system respectively.

When examining a river basin, water can be stored in a variety of ways. Water is mostly stored on the surface (rivers, lakes and snow accumulation), in the soil (soil moisture), or in the deeper earth (aquifers in the form of groundwater). TWS is the combination of all waters present above and below the earth's surface. Changes in the Earth's gravity field, as measured by the GRACE and GRACE FO missions, can be used to identify variations in TWS. According to GRACE, it's unclear which part of the hydrological cycle caused the change in the mass. Only data regarding the overall mass change within a given area is retrieved. By removing the mean of a specific period, mass anomalies are calculated and they are frequently denoted as EWH.

When employing GRACE for hydrological purposes, there are two distinct goals. Eq.1.3 is used to compare the storage fluctuations to the sum of precipitation, evaporation and run-off within the basin. The alternative method focuses on the various components that make up the word "terrestrial water storage". These components include surface water, groundwater, soil moisture, snow water equivalent and canopy water storage, as given in Eq.1.4.

$$\Delta TWS = \Delta GWS + \Delta SMS + \Delta SWE + \Delta SWS + \Delta CWS \tag{1.4}$$

where, $\Delta TWS =$ change in terrestrial water storage; $\Delta GWS =$ change in groundwater storage; $\Delta SMS =$ change in soil moisture storage; $\Delta SWE =$ change in snow water equivalent; $\Delta SWS =$ change in surface water storage; $\Delta CWS =$ change in canopy water storage. From the above equation, often it is assumed that temporal variations in the surface water (ΔSWS) are insignificantly small. The snow component (ΔSWE) is minimal or absent in some warmer locations. Then Eq.1.4 can be rewritten as

$$\Delta TWS = \Delta GWS + \Delta SMS + \Delta CWS \tag{1.5}$$

The variations in TWS are directly related to the changes in the components that make up TWS. By rearranging Eq.1.5, the changes in groundwater storage can be derived as shown in Eq.1.6 .

$$\Delta GWS = \Delta TWS - (\Delta SMS + \Delta CWS) \tag{1.6}$$

1.1.5 Applications of GRACE

The GRACE dataset over land denotes the time variation in TWS that represents the vertically integrated water column comprising groundwater, surface water, snow water, soil moisture and canopy water storages. TWS interacts with the water balance and climate energy on a variety of scales and fronts, making it an important part of the

Earth system (Famiglietti, 2004). Understanding and defining the Earth's climate system requires accurate information of TWS. However, little is known about global water storage prior to the GRACE project because in-situ measurements are expensive and difficult to maintain and earlier remote sensing missions are limited to surface water and groundwater storage (Ramillien et al., 2008).

Each component of TWS contributes to the water cycle in different ways with respect to space and time. On seasonal to annual time scales, soil moisture and snow are important components of climate modelling (Dirmeyer et al., 2005). Groundwater storage, on the other hand, is a sign of long-term mechanisms and, as a result, has a longer memory in land surface activities. Groundwater is a major source for drinking and irrigation which makes it vulnerable to anthropogenic influences throughout the world (Famiglietti et al., 2011a). These effects, however, are difficult to predict and characterise in models, and groundwater monitoring is lacking throughout the globe. As a result, GRACE measurements provide a plethora of data for monitoring and tracking the global hydrological cycle at all levels.

GRACE data can be used for a variety of purposes in hydrology, including drought monitoring, groundwater monitoring, assessment of flood potential, ice mass change, **G**lacial **I**sostatic **A**djustment (GIA), sea-level budget, earthquakes and weather forecasts. The extent and applicability of this knowledge will expand when improvements to the existing GRACE product and increased accuracy from future missions are made. In this thesis, GRACE datasets are used for drought evaluation over South India River Basins.

1.2 DROUGHT MONITORING

Drought has been defined in a variety of ways throughout the course of several decades of research. Despite the fact that all the definitions are linked, distinct types of droughts vary in length and impact local resources in different ways. Meteorological drought is described as periods of unusually low or no precipitation. The impacts of precipitation working through reservoirs, streamflow and groundwater are referred to as hydrological drought. Agriculture drought refers to how crops react to increasing heat stress and lack of water in the soil. Finally, socioeconomic drought is linked to economic supply and demand of water and agricultural products, which are impacted significantly by hydrological, meteorological and agricultural droughts. Therefore, monitoring drought is an essential feature to study in all these sectors (Tallaksen and Van Lanen, 2004).

In recent decades, with changing climate, drought-related calamities have escalated worldwide (Allen et al., 2011; Kang and Sridhar, 2017, 2018; Thilakarathne and Sridhar, 2017). Like many other countries, the frequency of occurrence of droughts

increased several fold in India since 1965 (Bisht et al., 2018a; Setti et al., 2020; Shewale and Kumar, 2005). The average drought length and severity in India will continue to increase in the future (2010 to 2099) compared to the historic period (1979 to 2005), which leads to serious regional drought problems (Bisht et al., 2019). Drought depends mainly on seasonal variations in precipitation resulting in the occurrence of extreme events (Bisht et al., 2018b; Van Loon and Van Lanen, 2013). Drought conditions are exacerbated by rising water demand as a result of population growth, irrigated agriculture and industrialization. The geographical area of India is approximately 3.28 million km^2, of which around 1.07 million km^2 are exposed to various types of drought conditions (Mishra et al., 2009). Increased demand for water leads to overexploitation of surface and subsurface water resources, resulting in conflicts among water users during drought periods. Drought monitoring at the river basin level is therefore necessary for proper evaluation of water resources, management and mitigation strategies.

Drought is a recurrent feature of climate occurring in all climatic regimes. Precipitation, timing, intensity, duration, temperature, humidity and wind speed play significant roles in the occurrence of droughts and its effect accumulate gradually over a significant period of several months to years. Subsequently, drought management plans have uncertainties as it is difficult to accurately assess the start and end time, known as a creeping phenomenon. Drought indices are suitable tools for monitoring, quantifying, evaluating droughts and become predominant in drought characterisation as they reduce the complexity of the drought phenomenon to a single numerical value. Drought indicators have become key and decisive features over time for drought monitoring and early warning systems (Vicente-Serrano et al., 2011). Despite the fact that there are various drought indexes accessible, there is substantial controversy about their efficiency and applicability (Sehgal et al., 2017).

Over the last few decades, **S**tandardized **P**recipitation **I**ndex (SPI), **P**almer **D**rought **S**everity **I**ndex (PDSI) and **S**tandardized **P**recipitation **E**vapotranspiration **I**ndex (SPEI) have been the most extensively used drought indices worldwide (Hayes et al., 2011). Despite their suitability for a variety of water-related sectors, these indices have their limitations. For instance, SPI is extensively related to precipitation, which does not take into account other important variables that bias the characterisation of drought. Similarly, PDSI is calculated using duration and weighting factors derived from the dataset observed over United State regions and therefore limits its implementation to other climate zones (Palmer, 1965; Zhang et al., 2018). PDSI also lacks multi time scale features compared to SPI, making it difficult to compare with runoff and reservoir storage. Wells et al. (2004) proposed a new drought index called **S**elf-**C**alibrated PDSI (SC_PDSI), which can be applied to any region considering the local variations. Some

studies by Dai (2011a); Kang and Sridhar (2019); Mishra and Singh (2010); Zhang et al. (2015a) examined the competency and shortcomings of PDSI, SPI and SPEI in depth. It can be inferred from the above discussion that more than one drought index is to be used to analyse and evaluate drought at regional or basin scales.

1.3 DROUGHT MONITORING USING GRACE

For global socio-economic security, monitoring and understanding the droughts, as well as how they are evolving in space and time, is critical. At present, remote sensing capabilities have increased several fold, capturing the spatial and temporal variations in land surface fluxes at larger scales than before. Hydrological, meteorological and agricultural droughts are therefore monitored using remote sensing products. Despite the fact that satellite remote sensing has greatly benefited us in this challenge, most satellite missions only observe Earth's near surface features. Therefore, GRACE mission assessed changes in water storage both above and below the earths surface, making it unique for drought related studies. TWS has been recently applied in monitoring and characterizing regional droughts and water availability conditions (Girotto et al., 2017; Zhao et al., 2017a,b). Cao et al. (2015) introduced the **T**otal **S**torage **D**eficit **I**ndex (TSDI) from TWS changes over Northwest China. Yi and Wen (2016) developed the **G**RACE **H**ydrological **D**rought **I**ndex (GHDI). For the quantification of drought, Sinha et al. (2017) developed the **W**ater **S**torage **D**eficit **I**ndex (WSDI). Zhao et al. (2017b) developed a new global gridded **D**rought **S**everity **I**ndex (DSI) from TWS changes called GRACE DSI. Sinha et al. (2019) proposed the **C**ombined **C**limatologic **D**eviation **I**ndex (CCDI) utilizing TWS and precipitation over Indian River Basins. From the previous studies, spatial and temporal evaluations of drought were identified using TWSA and these studies reported that longer duration and higher severity of drought causes long recovery time (Chang et al., 2019; Zhang et al., 2019). Therefore, monitoring and understanding the properties of drought using GRACE datasets, and how are they evolving at continental to global scales in space and time is the biggest challenges in drought research.

1.4 GRACE TWS CHANGES AND LINKS WITH TELECONNECTIONS

Drought is a dynamic natural phenomenon with high frequency and long duration characteristics that impact ecosystems and society in many ways (Kang and Sridhar, 2017, 2018; Mishra and Singh, 2011). Drought is a common natural calamity that, due to its long-term persistence and frequency, has a significant impact on agriculture, water resources and socio-economic development (Cammalleri et al., 2017; Kang and Sridhar, 2018; Sahoo et al., 2015). Thus, effective evaluation and monitoring of droughts are extremely necessary. Drought monitoring mainly depends on the

observed station data (hydrological and meteorological). Due to the lack of observed data and the spatial heterogeneity of the regional environment, obtaining exact drought characteristics is difficult (Long et al., 2014). Due to large-scale climate variations in India, the spatio-temporal availability of surface and groundwater is very diverse and affects the agricultural and industrial productivity of the country (Bhuvaneswari et al., 2013). The drought occurred in India during 2016 affected 330 million people with more than $100 billion loss in the economy (ASSOCHAM Report, 2016). From this perspective, it is crucial to understand the variations of surface and groundwaters and its association with teleconnections for the conservation of water resources.

GRACE assess the changes in water storage both above and below the Earth's surface, making it unique and useful for drought related studies when compared to the traditional univariate drought indicators. Utilizing the GRACE data, many studies have investigated drought characteristics throughout the world. These studies only verified the drought characteristics using GRACE data but not the association between GRACE based droughts and teleconnection factors. It is clear from earlier studies that teleconnection factors have a major effect on drought (Dai, 2011b; Wang et al., 2015a). Many attempts have been made in the past to establish the relationship between climate variability and TWS from GRACE, with most studies focused on **E**l **N**iño **S**outhern **O**scillation (ENSO). To evaluate the association between **M**ultivariate **E**NSO **I**ndex (MEI) and GRACE mass anomalies, Phillips et al. (2012) utilized monthly TWS. Huang et al. (2016) concluded that hydrological drought over the Columbia River Basin is greatly influenced by ENSO and **A**rctic **O**scillation (AO). Over the entire world, Ni et al. (2018) examined the links between ENSO and TWS. Vissa et al. (2019) evaluated the relationship between ENSO induced groundwater changes derived from GRACE and **G**lobal **L**and **D**ata **A**ssimilation **S**ystem (GLDAS) over India. Liu et al. (2020) explored the role of teleconnections over TWS variations within the Asian and Eastern European regions. Other studies related to linkage between GRACE and teleconnections include Anyah et al. (2018); Han et al. (2019); Ndehedehe et al. (2017); and Wang et al. (2020). Thus, climate variables influence the drought directly or indirectly that results in detailed investigation between them.

1.5 GROUNDWATER STORAGE CHANGES

From water balance perspective, **G**round**W**ater **S**torage (GWS) change is considered as the difference between recharge (lateral inflow, seepage from surface water etc.) and discharge (groundwater withdraws and lateral outflow) within the aquifer system. However, in-situ hydrological observations make it challenging to directly calculate groundwater recharge and discharge rates (Alley et al., 1999). On the other hand, observation well measurements are the principal source of groundwater system.

Groundwater levels can be further converted to GWS changes by multiplying them with storage coefficients. Hydrological models, such as **L**and **S**urface **M**odels (LSMs) and **H**ydrological **W**ater **B**alance **M**odels, can monitor GWS variations in addition to in-situ well measurements (HWBMs). The majority of established LSMs are capable of simulating water and energy fluxes between the land surface and the atmosphere, but they fall short of simulating GWS variations (Rodell et al., 2004). On the other hand, HWBMs are designed to assess global water resources. Thus, human water uses, such as irrigation, household and industrial water consumption are taken into account (Bierkens, 2015). As a result, groundwater is often simulated in these models in arid and semi-arid regions. However, due to the inadequate parameterization of HWBMs, limited knowledge regarding recharge/abstractions of groundwater and estimation of accurate GWS changes remains a challenge (Döll et al., 2014). At regional or basin scales, groundwater flow models can be employed to evaluate regional/basin specific GWS variations. However, extensive hydrogeological data (water level readings, hydraulic parameters, aquifer characteristics, geology) and climatic forcing data are required to build a reliable regional groundwater model, which are often difficult to obtain.

At present, remote sensing capabilities have increased many folds, capturing the spatial and temporal water storage changes above and below the Earth's surface when compared to observation well measurements and global models. Therefore, remote sensing based estimates of water storage changes can be used to track global GWS variations from space. For almost two decades, the GRACE and GRACE FO missions have provided unprecedented monthly TWS fluctuations globally (Tapley et al., 2004). GWS changes can be estimated by subtracting soil moisture, snow water and surface water from TWS (Yeh et al., 2006). As a result, GRACE is a useful tool for estimating GWS changes, particularly in areas where monitoring groundwater levels is poor or unmonitored. Many studies have used GRACE data to assess GWS changes, particularly its depletion, in many regions, including USA (Famiglietti et al., 2011b; Scanlon et al., 2012), India (Long et al., 2016; Rodell et al., 2009; Tiwari et al., 2009) and California's Central Valley (Longuevergne et al., 2010; Strassberg et al., 2007).

1.6 RECONSTRUCTION OF GRACE TWS

The GRACE twin satellites have provided the gravitational field changes with unprecedented spatio-temporal resolution over the earth, that can interpret TWS changes, giving a novel method to evaluate hydrological features (Tapley et al., 2004). GRACE missions have been so effective that the result is now widely used in a variety of sectors, considerably advancing our understanding of TWS, ice melting, sea-level change, earthquakes etc. (Tapley et al., 2004, 2019). But GRACE applications are still

limited to study the long-term water cycle behaviour as the data is limited to short period i.e., 2002 to 2017 (GRACE) and 2018 to date (GRACE FO).

The GRACE product of the earth's gravity field began in April 2002. The GRACE mission was originally planned for a period of 5 years producing perfect monthly gravity variations till 2010. In spite of this, GRACE mission has been operational for another seven years till 2017, with regular rest intermissions to extend the life of the deteriorated power supply (Flechtner et al., 2014). GRACE data was last available in June 2017, however the GRACE FO satellite mission started delivering the output from June 2018, creating an 11-month missing data between the two operations. The extended GRACE FO data improves GRACE applications and increases the potential to detect previously unknown processes. However, the one year lag between two missions have hampered the continuous investigation of GRACE and GRACE FO's 18 years of observations to date. In the GRACE and GRACE FO dataset, a total of 34 data gaps are found in which majority are solitary or paired as shown in Fig. 1.3 and hence do not pose a significant difficulty. However, filling the one year gap between GRACE and GRACE FO missions (between July 2017 to May 2018) is challenging.

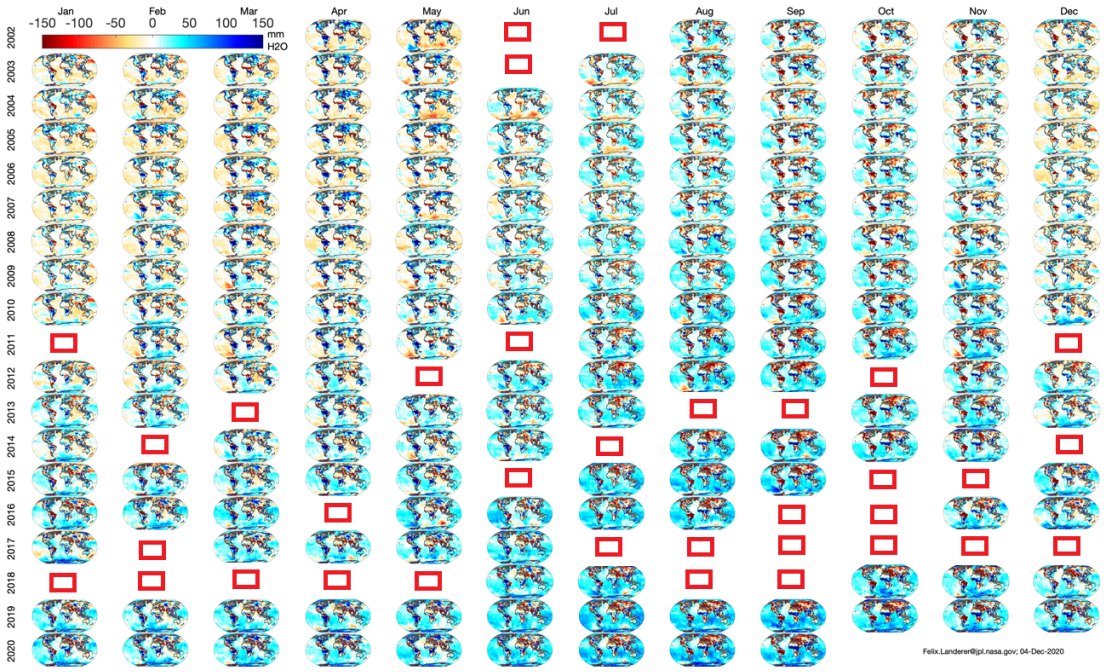

Figure 1.3: GRACE and GRACE FO data records with gaps (The red boxes indicates the missing months GRACE gravity fields).

Global LSM and HWBM can simulate historical hydrology and energy fluxes using long-term climate datasets (Rodell et al., 2004). The model simulations can then be used to estimate long-term TWS. However, present model uncertainties, combined with the poor quality of forcing data, severely limit the model's capacity to reproduce real-world

conditions (Qian et al., 2006). As a result, inconsistencies between TWS **A**nomalies (TWSA) derived from GRACE and surface/hydrological models should be expected. In recent years, there has been a growing interest in combining GRACE data with outputs from global LSMs to improve TWSA estimation (Long et al., 2014; Nie et al., 2016). GRACE data provide a more reliable estimate of TWS changes than global models and the model simulations of historical hydro-meteorological variables can predict long term TWS time series. Although the TWS simulations from the models include uncertainties, their close fitting correlations with GRACE measurements allow for the development of reliable long-term TWSA datasets.

Because of GRACE's high sensitivity in detecting TWSA, researchers have previously attempted to reconstruct TWSA by developing empirical relationships between TWSA and meteorological and hydrological variables. TWS variations predicted in many basins on the basis of water balance are linearly correlated with TWSA from GRACE. In the Amazon Basin, Nie et al. (2016) used a linear model to relate the TWS estimated from GLDAS with GRACE and rebuilt TWSA from 1948 to 2012. Humphrey et al. (2017) took it a step further by building a polynomial regression model between GRACE TWSA and precipitation and temperature in the Amazon Basin, based on a similar principle used by Nie et al. (2016). Increase of machine learning technologies has greatly improved our ability to mimic and anticipate the environment throughout the world. Machine learning approaches contributed in developing new possibilities in earth system modelling and successfully used in land cover mapping, weather prediction and soil type mapping etc. (Bauer et al., 2015; Rogan et al., 2008). For the reconstruction of TWSA, machine learning approaches are beneficial where physical models are indeterminate and standard statistical approaches are inadequate. Machine learning techniques like **A**rtificial **N**eural **N**etwork (ANN) (Long et al., 2014) and deep **C**onvolutional **N**eural **N**etwork (CNN) (Sun et al., 2019) have been used to reconstruct TWSA over recent years. Also, many researchers have used multiple learning-based techniques to reconstruct TWSA. Liu et al. (2020) used ANN, **M**ultiple **L**inear **R**egression (MLR) and **A**uto**R**egressive e**X**ogenous (ARX) models to predict (2017 to 2018) and reconstruct (1992 to 2002) TWSA with climate inputs. Sun et al. (2020) predicted and reconstructed the GRACE TWSA using MLR, **S**easonal **A**uto **R**egressive **I**ntegrated **M**oving **A**verage with e**X**ogenous (SARIMAX) variables and **D**eep **N**eural **N**etwork (DNN) covering 60 river basins throughout the world. Though the machine learning based reconstructed TWSA may have the effect of climate variability and human intervention, the reconstructed TWSA results over high human intervention basins may not correlate well with GRACE measurements.

1.7 DROUGHT FREQUENCY ANALYSIS

Drought is a natural threat considered when precipitation deficits are encountered for extended periods. Drought is the temporary deviation from normal weather conditions that may occur in a variety of climates. Whereas, aridity is a permanent climate feature based on long-term climatic conditions in an area (Araghi et al., 2018; Karamouz et al., 2012). As a result of climate change, aridity and drought are expected to increase, that may have significant implications on agriculture and ecosystem (Dai, 2013; Lobell et al., 2008). The characteristics of dryness are recognized as an important factor in water resource planning and management (Shiau, 2006). Drought can be characterized by various factors such as severity, intensity and duration, and is therefore described as a complex natural disaster (Kang et al., 2019; Mishra and Singh, 2010). In contrast to other natural disasters, droughts also impact over a large region (Kang and Sridhar, 2017; Sehgal and Sridhar, 2019; Sehgal et al., 2017; Wilhite et al., 2014). Thus, during the analysis of drought condition, multivariate complexity and spatial variations should be considered.

Almost every three years, India faces drought in different parts of the country. Over the last few decades, India has experienced long and severe droughts, and similarly, in recent times, frequency has also increased in many parts of the country (Bisht et al., 2019). During June to September, a significant amount (about 70-90 %) of annual rainfall occurs due to the Southwest monsoon in India (Bisht et al., 2018a,b). Since most of the country depends on monsoon rainfall, drought may be caused when monsoon fails (Kumar et al., 2013). In India,the distribution of drought conditions have been studied by several researchers (Das et al., 2016; Gupta et al., 2020; Janga Reddy and Ganguli, 2012). Vulnerability of drought is amplified by climate change that adversely affects India's water supplies. Therefore, the regional study of near-future spatial and temporal characteristics of drought will provide immense knowledge for decision-makers and planners to frame policies to mitigate the impacts of drought hazards.

Numerous research on the spatial and temporal distribution of monsoon rainfall have been carried out. Few researchers find a rise in average precipitation over the monsoon season along with inter-annual variability (Chaturvedi et al., 2012; Fan et al., 2012). Globally, various regional studies have been carried out to understand the characteristics of spatial and temporal drought. Multivariate modeling, such as Severity-Duration-Frequency (SDF) and Severity-Area-Frequency (SAF) curves can help to assess the regional drought risk (Mishra and Singh, 2010; Reddy and Ganguli, 2013). These drought curves are evaluated for different return periods based on mathematical relationships between severity, intensity, interarrival time, duration and area coverage. To denote all characteristics of droughts, these curves quantitatively

relate the severity, duration/area and return period (Kang and Sridhar, 2020; Rajsekhar et al., 2015a).

1.8 OBJECTIVES OF THE STUDY

The focus of the present work is to monitor TWSA and evaluate its effect on drought over South Indian River Basins namely, **G**odavari **R**iver **B**asin (GRB), **K**rishna **R**iver **B**asin (KRB), **C**auvery **R**iver **B**asin (CRB) and **P**ennar and East flowing Rivers between Pennar and **C**auvery **R**iver **B**asins (PCRB)
This main objective, for the sake of more clarity, is subdivided into four sub objectives as given below.

- Assessment of monthly and seasonal droughts using GRACE terrestrial water storage.
- Utilizing GGDI for drought characterization and its linkage to Teleconnection factors.
- Reconstruction of TWSA and its validation with in-situ groundwater well measurements.
- Analysis of Severity-Duration-Frequency and Severity-Area-Frequency curves for GRB.

1.9 OUTLINE OF THE THESIS

The work carried out in this investigation is presented in the following chapters. The thesis comprises of eight chapters: introduction, literature review, study area and data collection, four chapters for each sub objective, and conclusions.

The introduction chapter (chapter 1) provides an overview of the GRACE satellite mission, its various data products and contributions to understanding the earth system mass change. Then monitoring of drought using drought indices, understanding drought properties (duration and severity) and their evolution in space and time are discussed.

Chapter 2 deals with the literature review covering each of the problems studied by earlier research. The summary of each of the research paper is critically reviewed and briefly explained.

Chapter 3 deals with the study area and data collection. This chapter is followed by four chapters for each sub objective under consideration.

Chapter 4 deals with spatial and temporal variations of GRACE terrestrial water storage with respect to various drought indices to offer insights into assessing future droughts using remote sensing data.

Chapter 5 deals with GRACE groundwater drought index for drought characterization and its linkage to teleconnection factors.

Chapter 6 deals with the reconstruction of GRACE terrestrial water storage beyond GRACE period (1990 to 2020) and its validation with the in-situ groundwater well measurements.

Chapter 7 deals with the drought frequency analysis and development of Severity-Duration-Frequency and Severity-Area-Frequency curves for Godavari River Basin. (Note: Similar studies can be done for all other basins in Southern India.)

Chapter 8 deals with summary of the study followed by conclusions and an outlook for possible future extensions of this work.

CHAPTER 2

LITERATURE REVIEW

A detailed review of the research work carried out by the previous investigators on drought assessment using GRACE, reconstruction of TWSA and its linkage with teleconnection factors are discussed in this chapter.

2.1 DROUGHT MONITORING USING GRACE

Rodell and Famiglietti (2002) computed TWS as the sum of soil moisture, surface water (reservoir storage), groundwater (observation wells) and snow depth from 1982-1996 over Illinois, United States. Monthly, seasonal and yearly TWS changes are estimated with expected uncertainty in TWS changes in Illinois over 145,800 km^2. Uncertainty was typically too large to allow detection of monthly TWS changes, while seasonal and annual changes are detectable about half the time. However, given a 200,000 km^2 or larger area, and assuming that the estimated water storage changes are representative of progressively bigger regions, the same monthly, seasonal and annual fluctuations are often detectable. Results conclude that the rate of detectability increases and the uncertainty decreases with the increase of spatial extent of the study region i.e., 300,000 km^2 or larger for monthly changes and 200,000 km^2 and larger for seasonal and annual changes. According to the authors, the most influenceable component of TWS is the soil moisture followed by groundwater, snow depth and reservoir storage.

Syed et al. (2008) compared the TWS Changes (TWSC) derived from GRACE and GLDAS worldwide. The results of TWSC matched well with the GLDAS simulations. The GLDAS simulated TWSC revealed a number of critical features of spatial and temporal land water storage fluctuations. Although global TWSC averages are evenly split between soil moisture and snow water equivalent, zonal TWSC averages show the importance of soil moisture storage at low latitudes against snow storage at high latitudes. According to the findings, GRACE can aid with a better knowledge of how TWS responds to climate change and variability with longer time series.

Chen et al. (2010) demonstrated the capability of TWS from GRACE to observe and quantify the 2005 Amazon drought event (worst drought of the century) and to compare GRACE results with climate and LSMs over the same 2005 drought event. In the summer of 2005, GRACE detected a large drop in TWS in the Central Amazon

Basin, compared to the average of five previous summers in the GRACE era. On the other hand, climate and LSMs underestimated the intensity of drought in 2005. TWS observations from GRACE are supported by in-situ water level data from river gauge stations, as well as collected precipitation data from satellite remote sensing. The results displayed how GRACE gravity measurements can be used to monitor large scale drought and flood occurrences, as well as to test advanced climate and LSMs.

Houborg et al. (2012) used GRACE Data Assimilation System (DAS) for drought assessment over United States. This study developed drought indicators to investigate the possibility of more comprehensive drought conditions over the United States. Previous drought monitor studies lacked the continuous observed measurements of groundwater and soil moisture, which are both important for drought research. Extensive observed groundwater and soil moisture datasets are used in this study to measure advances in hydrological modelling competence as a result of TWS data assimilation. This study illustrates that data assimilation may be the key to attaining TWS's full potential in hydrological applications.

Thomas et al. (2014) used GRACE's TWSA to develop a quantitative approach for evaluating hydrological and meteorological drought occurrence and severity. Further GRACE is used to estimate the associated regional water storage deficit. The storage deficit method accurately predicted the onset, termination and duration of hydrological droughts and correlated well with the meteorological drought databases. The findings of this study could eventually be used to develop a complete framework for hydrological drought monitoring.

Yi and Wen (2016) estimated TWS changes in the continental United States (US) using GRACE from 2003 to 2012 and developed GRACE Hydrological Drought Index (GHDI) for drought monitoring. From 2003 to 2012, TWS showed opposing patterns in the North and South of the continental US. In 2006, the equivalent water thickness is decreased by -5.1 cm in the Central South. A good correlation was observed between GHDI and Palmer Hydrological Drought Index, indicating that the index can be used for drought monitoring. GHDI can be expanded for global drought monitoring because of its minimal dependence on hydrological parameters. This is especially advantageous for countries that lack adequate hydrological monitoring equipment.

Zhao et al. (2017b) developed a new monthly global gridded GRACE DSI dataset using TWS changes from 2002-2014. The GRACE DSI captured key worldwide drought occurrences over the last decade and has good spatio-temporal agreement with PDSI and SPEI. The findings of study conclude that GRACE DSI can be used for drought monitoring in the regions where ground observation are limited. The study

concludes that the developed global gridded GRACE DSI dataset can used to evaluate droughts at regional or global scale.

Sinha et al. (2017) derived and analysed Water Storage Deficit Index (WSDI) for India river basins. The method relies on fluctuations in TWS from GRACE to calculate drought intensity and severity. Results showed that drought severity and duration coincide well with the major meteorological droughts reported in India. Drought events between April 2002 to April 2015 have been well recognised and quantified using this method across four homogeneous rainfall zones of India. WSDI values displayed an increasing trend in West-Central India and a decreasing trend in in North-Western and Central India. The findings suggest a high level of confidence in WSDI's ability to accurately characterise drought at wide spatial scales.

Sun et al. (2018) used GRACE CSR mascon data from 2003 to 2015 to assess drought conditions in the Yangtze River Basin. **W**ater **S**torage **D**eficits (WSD) are used to evaluate drought events, while the drought severity is assessed using the WSDI and compared with SPI, PDSI, SPEI and **S**tandardized **R**unoff **I**ndex (SRI). The findings showed that there exists a good correlation between WSDI and SPI, PDSI, SRI and SPEI. The droughts identified by the WSDI are in good agreement with the previous studies. GRACE CSR mascon data may be used to analyse drought features in the YRB, and the WSDI provides for strong and reliable drought characterization across large areas, according to the findings. This study accurately captured major drought occurrences over a huge geographic area, making it a good substitute for large-scale regions and regions with few hydro-meteorological sites, where typical approaches based on rich site observations are impractical to adopt.

Sinha et al. (2019) proposed a novel drought index named CCDI that incorporates all the aspects of agricultural, meteorological, hydrological and human-induced drought occurrences. CCDI is evaluated as a combined effect of variations in TWS from GRACE and precipitation over Ganga, Godavari, Krishna and Mahanadi River Basins in India. In addition, CCDI is compared to SPI, SPEI, PDSI, SRI and GRACE DSI in order to assess the index ability to predict the occurrence of droughts. The CCDI proved to be effective in identifying drought events over the study regions. In comparison to other drought indices, the results have shown a better understanding of overall drought conditions. The findings reveal an appreciable level of confidence in CCDI's ability to quantify droughts, which will further improve with better quantification and expanded availability of TWS information from GRACE and GRACE FO missions.

Vishwakarma (2020) reviewed the potential of GRACE TWS for drought monitoring. As a result of continuous climate change, droughts may become more

severe and last for longer durations in the future. So, for global socio-economic security, monitoring and understanding the duration and intensity of droughts, as well as how they evolve in place and time, is critical. Although satellite remote sensing aided us much in this attempt, most satellite missions only observe Earth's near-surface features. GRACE, a recent geodetic satellite mission, assessed changes in water storage both above and below the earth's surface, making it unique and useful for drought studies. Before using this innovative dataset, one need be aware of its specific challenges and characteristics. The author discussed key properties of several GRACE products. The author also went through some of the limitations of the GRACE mission that one should be aware of, as well as some of the most recent improvements in GRACE data processing that could open up a lot of doors in the near future.

2.2 TWSA AND ITS LINKAGE TO TELECONNECTIONS

Zhang et al. (2015b) examined TWS changes from GRACE in combination with **T**ropical **R**ainfall **M**easuring **M**ission (TRMM) and in-situ river gauges; along with hydrological models: GLDAS and **W**aterGAP **G**lobal **H**ydrology **M**odel (WGHM) in the Yangtze River Basin for 2006 and 2008 droughts. Then links between TWS and ENSO are evaluated. The droughts are clearly quantified by TWS deficit estimations and a normalized TWS anomaly provided an alternative and relevant hydro-climatological index in the basin. Findings showed that the association between TWS anomalies and drought occurrences are closely related to ENSO variability.

Ndehedehe et al. (2017) examined the association of three global climate teleconnections named **A**tlantic **M**ulti-decadal **O**scillation (AMO), **I**ndian **O**cean **D**ipole (IOD) and ENSO with changes in TWS from GRACE and **M**odern-**E**ra **R**etrospective Analysis for **R**esearch and **A**pplications (MERRA) over West Africa. The positive phase of AMO coincided with above-normal rainfall (wet conditions) in the Sahel region, while the negative phase coincided with drought conditions, confirming the statistically significant relationship (r = 0.62) between AMO and SPI. In the Volta basin, ENSO appeared to be more linked with TWS from GRACE. Also, a strong association between TWS from MERRA and AMO, ENSO events are observed throughout the coastal West African countries. The findings suggest that ENSO and AMO are the two key climatic indices that affect TWS in West Africa.

Anyah et al. (2018) employed **I**ndependent **C**omponent **A**nalysis (ICA) method to evaluate the relationship between TWS changes and teleconnections namely ENSO, IOD, **N**orth **A**tlantic **O**scillation (NAO), **M**adden-**J**ulian **O**scillation (MJO) and **Q**uasi-**B**iennial **O**scillation (QBO) over Africa for the period 2003–2014. The linkages between **C**limatic **I**ndices (CIs) and TWS are extracted using Pearson correlation

analysis and certain strong CI-rainfall associations are discovered. The findings revealed that there exists a substantial link between CIs and TWS over the study region. Furthermore, the findings showed that the CIs' first prominent **I**ndependent **C**omponent (IC) is linked to NAO and characterised by large TWS reductions over Southern Africa.

Forootan et al. (2019) used probabilistic methodologies to evaluate drought indices based on TWS for 156 river basins during 2003-2016. The drought features such as trends, occurrences, area-extent and frequency are extracted for 3, 6, 12 and 24 month timescales. Using **C**anonical **C**orrelation **A**nalysis (CCA), link between global hydro-meteorological droughts and **S**ea **S**urface **T**emperature (SST) fluctuations are determined. This association is then utilised to identify areas where droughts and teleconnections are closely linked. The findings showed that hydrological droughts (3 to 6 months) occur more frequently than other periods. The ENSO displayed a significant impact on hydrological droughts in Northern Asia and much of the Australian continent from 2006 to 2011. At regional scale, hydrological droughts are also influenced by IOD and NAO.

Vissa et al. (2019) aimed to quantify the inter-annual variations of **G**round**W**ater **S**torage **C**hanges (GWSCs) over India. GWSCs are calculated using GRACE and GLDAS-Noah LSM model during 2003 to 2015. Over the six lake sites, the estimated GWSCs are validated using satellite altimetry. Cross correlation and plotting analysis are used to examine the variability of GWSC and altimetry water level heights. The non-parametric Mann–Kendall trend test and Sen's slope method are used to evaluate annual changes in TWSA from GRACE and GWSC. The findings showed a decrease in GWSC and TWSA over Northern India, Southern and Western Central India. The decline of GWSC is enhanced during El Niño, whereas increment of GWSC is evident during the La Niña phase. The results concluded that variations in inter-annual GWSCs over India are mainly due to precipitation changes.

Han et al. (2019) investigated the TWSA dynamics and assessed their relationships with teleconnections in the Yunnan Province, China. Results concluded that TWSA showed a decreasing trend during different time scales. In humid areas, the main driving factor for variations in TWSA is precipitation magnitude. Good correlation is observed between TWSA and AO, ENSO. This study adds to our understanding of how teleconnections may affect TWSA dynamics in a changing environment.

Wang et al. (2020) used the GRACE Groundwater Drought Index (GGDI) as a metric for assessing drought in North China plain from 2003 to 2015. The spatial temporal evolution of drought characteristics and trends are comprehensively identified

during 2003 to 2015. Following that, utilising cross wavelet transform technology, the linkages between GGDI and teleconnection factors are explained. The GRACE's quantitative results for drought evaluation are reliable and robust. The cross-wavelet transform revealed a significant influence of teleconnection factors on drought evolution. The GRACE gravity satellite can provide new insight into drought monitoring and can be used to other locations, according to the findings.

Liu et al. (2020) characterized the spatiotemporal variations in TWS based on GRACE, LSM and precipitation observations over Asian and Eastern European regions. The linkages between TWS and the global major teleconnections are then investigated. From 2002 to 2017, there was a general decrease in TWS, with five hotspots of negative TWS trends. TWS partitioning demonstrated that these negative trends are mostly caused by excessive groundwater exploitation and warming-induced surface water loss. The findings also revealed that ENSO, AO, and NAO are the three most powerful factors influencing TWS fluctuations. The findings offer light on differences in TWS and its components in Asian and Eastern European areas with limited food and water availability.

2.3 RECONSTRUCTION OF TWSA

Sun (2013) predicted the groundwater level changes by downscaling GRACE satellite data. In many places around the world, in-situ groundwater monitoring networks have declined in recent years. Because of the uncertainty in GRACE data and the difficulty in disaggregating specific TWS components, the use of GRACE data for local-scale groundwater resource management has been limited. The nonparametric ANN models used in this study are developed using Parameter-elevation Regressions on Independent Slopes Model (PRISM) monthly precipitation, maximum and minimum temperatures and GRACE ΔTWS as inputs; and groundwater level change as the target variable. Monthly and seasonal water level fluctuations for numerous wells across the United States are estimated using ensemble ANN models. Results conclude that, GRACE displayed a considerable impact on the performance of ANN ensembles, especially when the cyclic pattern of groundwater hydrograph is interrupted by extreme climate events. When continuous in-situ measurements are unavailable, the results support the basic hypothesis that downscaled ΔTWS can be used to infer or predict groundwater level changes.

Zhang et al. (2016) used GRACE TWS to characterize the hydrological drought in the Yangtze River Basin. ANN method is used to extend the TWSA data to a longer period (1979–2012). The reconstructed TWSA using ANN model matched well with the observed TWSA from GRACE (Nash–Sutcliff efficiency = 0.83). Then using a

multi-decadal TWS time series, WSD and drought recovery time are defined. A simple statistical approach is used to evaluate the drought recovery time. The results conclude that YRB experienced hydrological drought 29 times between 1979 and 2012. The average drought recovery time for the entire basin is 3.3 months. Drought conditions prevailed from 2003 to 2008, owing to below-average precipitation, high temperatures, and intense human activity. The findings show that GRACE data may be used to rebuild the TWS time series for a wide river basin, which can be used to define hydrological drought and investigate spatio-temporal trends.

Humphrey et al. (2017) proposed a new approach which statistically relates anomalies in atmospheric drivers (e.g., precipitation and temperature) to monthly GRACE anomalies. The study statistically correlated GRACE TWSA with the anomalies observed by the major atmospheric factors. The gridded subdecadal TWS changes are reconstructed for the period 1985–2015. The findings show that the proposed product, and more broadly, the offered approach, can be used as a simple benchmark for evaluating TWS. Finally, this method is employed to bridge the gap between the GRACE and GRACE FO missions in terms of data. The data set presented here is best suited for regional and global investigations of climate-driven TWS variability from monthly to subdecadal time scales.

Jing et al. (2020) aimed to develop a data-driven model for simulating TWS dynamics by correlating climate forcings with GRACE TWSAs over the Pearl River Basin in China. **R**andom **F**orest (RF) and e**X**treme **G**radient **B**oost (XGB) are two ensemble learning techniques that are used to learn the relationships. TWSA of the basin is reconstructed from prior decades and compared to the TWSA generated by global LSMs. Results conclude that the RF and XGB algorithms performed well and reproduced the spatial pattern. The temporal characteristics of the reconstructed TWSA are closely matched with the GRACE and LSMs. This study proposed a multi scale GRACE drought index and the index matched well with SPEI at different time scales. The outcomes of this study show that machine learning may be used to forecast TWS dynamics from climatic forcing data and produce results that are comparable to complicated physical models.

Li et al. (2020) aimed to compare multiple data-driven algorithms and find the most reliable ones for predicting gridded TWSC from GRACE in 2017-2018 and reconstructing them using climate inputs up to 1992. To compare alternative methodologies, such as the MLR, ANN, and ARX approaches, a methodological framework is first constructed. Second, metrics are created to assess the predictability of the results. Finally, utilising the identified approaches, gridded TWSC within 26 regions is predicted and reconstructed. The results conclude that the projected TWSC

correlated well with the observed TWSC, which is better than the TWSC simulated using hydrological models. In summary, MLR is more robust and feasible approach for both filling the gap between GRACE missions and reconstructing long period TWSC fields globally.

Sun et al. (2020) reconstructed missing monthly data at grid size in 60 river basins around the world using six GRACE solutions and three learning-based models, including DNN, MLR, and SARIMAX. The three learning-based models were proven to be reliable for reconstructing GRACE data in humid environments with little or no human participation. In most of the basins, DNN models slightly outperformed SARIMAX model and significantly outperformed MLR model. At the basin scale, the three GRACE mascon datasets outperformed the spherical harmonics. Models with spherical harmonic solutions performed similarly in all the basins, whereas the model with mascon solution differed significantly in some basins. The findings can be used to fill in data gaps between the GRACE missions, as well as selecting appropriate GRACE solutions for regional hydrological studies.

Li et al. (2021) presented a new long-term global reconstructed TWSA fields by merging machine learning with time series and statistical decomposition approaches. According to the findings, the reconstructed TWSA matched well with the GRACE FO observation at global scale. The reconstruction approach is more reliable when compared to satellite laser ranging solutions and observed global mean sea level change. The findings offered a realistic method for recreating historical TWSA as well as filling the GRACE data gap.

2.4 GROUNDWATER STORAGE CHANGES AND ITS VALIDATION WITH WELL MEASUREMENTS

Rodell et al. (2007) estimated GWS variations using GRACE (which includes groundwater, soil moisture and snow) and GLDAS (soil moisture and snow) datasets over Mississippi River Basin, USA. Water level records from 58 observation wells in the basin's unconfined aquifers are used to validate the findings. The GRACE-GLDAS based GWS variations for the Mississippi River Basin and the two sub-basins $>$900,000 km^2 matched well with the observation well-based GWS. The performance of the technique is poor for sub-basins with an extent of around 500,000 km^2. Continuing to improve GRACE processing methods will certainly improve the technique's skill in the future while also boosting the temporal resolution.

Strassberg et al. (2007) considered TWS from GRACE as the combination of GWS and SMS. Then SMS from GLDAS is subtracted from TWS to obtain GWS (i.e., GWS=TWS-SMS). These GRACE-GLDAS based GWS are compared with GWS

variations obtained from 2,719 observation well datasets. Results conclude that a favourable correlation is observed between seasonal GWS obtained from GRACE and observation well network with R = 0.58. These findings suggest usage of GRACE to track GWS fluctuations in semiarid areas where irrigation pumping causes considerable seasonal GWS variations.

Rodell et al. (2009) evaluated the GWS variations for Indian states using TWSC observations from GRACE and simulated soil-water variations from hydrological modelling system. According to the findings, groundwater depletion amounted to a net loss of 109 km^3 of water, which is twice the capacity of India's largest reservoir. Other TWS components did not appear to play a substantial role in the reported drop in overall water levels. According to the study, unsustainable groundwater extraction for irrigation and other anthropogenic activities are most likely to blame. If efforts to ensure sustainable groundwater usage are not done promptly, the repercussions for residents of the region include a decline in agricultural output and potable water shortages, resulting in severe socioeconomic stress.

Shamsudduha et al. (2012) tested the ability of GRACE satellite measurements to trace intra-annual (seasonal) and interannual ΔGWS in the Bengal Basin using in-situ groundwater levels and distributed specific yield estimates during January 2003 to December 2007. The results conclude that the GRACE (CSR, GRGS) based ΔGWS correlated well with in-situ well measurements. Spherical harmonic product of CSR correlated well when compared with the GRGS products. Groundwater depletion estimated from borehole hydrographs is within the range of ΔGWS estimated from GRACE. The significant increase in groundwater abstraction for dry-season irrigation and extensive public water supply during the last two decades is principally responsible for groundwater depletion from 2003 to 2007.

Chen et al. (2014) re-assessed long-term GWS variation in the Northwest India using TWS and global forward modeling method. Using the global forward modelling method, this study successfully reduced the leakage errors in GRACE estimates and increased the accuracy of GWSC from GRACE. According to the results, the groundwater loss remained pronounced from January 2003 to December 2012, particularly in the first five years (01/2003–12/2007). The depletion rates are 20.4$\pm$7.1 **G**iga**t**onnes (Gt) per year on average over a ten-year time frame and 29.4$\pm$8.4 gigatonnes per year in the first five years. The study region's yearly GWS fluctuations are highly associated with yearly precipitation anomalies. Groundwater depletion reached over 80 Gt in 2009, the driest season of the decade, while net additions of roughly 24 and 35 Gt are seen in the two comparatively rainy seasons of 2008 and 2011, respectively.

Bhanja et al. (2016) validated the GWSAs obtained from a combination of GRACE and LSM with GWSA obtained from in-situ groundwater level measurements over 12 Indian River Basins from 2005-2013. For comparison with in-situ data, two GRACE products, RL05 SH and mascon products, are used. This study also produced a high-resolution specific yield map for India which is used for calculating GWS. The GRACE-estimated GWSA corresponded well with observed GWSA in most of the River Basins, according to the findings. GRACE-SH estimates matched well in terms of RMSE when compared to the observed GWS anomaly, but GRACE-mascon estimates showed superior correlation. This study used the Hodrick-Prescott filter, a non-parametric trend estimation approach, to compare the performance of two GRACE estimations. GRACE-mascon estimates clearly outperformed the GRACE-SH estimates in reproducing observed GWSA trends, with GRACE-mascon estimates showing significant strong association in 10 of the 12 basins. This study recommends GRACE-mascon solutions for groundwater related studies with similar meteorological, hydrogeological, or groundwater depletion conditions.

Asoka et al. (2017) used GRACE groundwater anomaly, groundwater well observations, daily precipitation dataset and irrigated area map to explore the driving mechanisms of groundwater variability. The analysis showed that long-term precipitation changes are influencing GWS variability in most parts of India. Between 2002 and 2013, this study discovered that GWS in Northern India decreased by 2 cm/yr while increasing by 1 to 2 cm/yr in Southern India. According to the findings, changes in precipitation account for a considerable portion of the total variability in GWS over North-Central and Southern India. Variations in GWS in North Western India are mostly explained by variations in irrigation abstraction, which is driven by changes in precipitation.

Bhanja and Mukherjee (2019) estimated the usable GWS using both satellite and in-situ measurements in India. In-situ observation well data are utilised to estimate the total useable GWS. Despite increased precipitation, the usable GWS estimations suggest substantial rates of GWS depletion (>5 km^3/yr) in North-East India (Assam). According to GRACE estimations, the growth of recent GWS-depletion zones in the Indus, Ganges, and Brahmaputra Basins is centred in unconsolidated sediments or lithotype. In contrast, Southern and Central Indian states displayed replenishing GWS trends. The study discovered that the states with highest rates of groundwater depletion are subjected to water-intensive agricultural methods. The authors suggest that the developed approach is useful to develop management alternatives for sustainable groundwater usage in various parts of the world.

Chen et al. (2019) compared different TWS solutions from GRACE and their effects on the spatial and temporal variations of GWS estimated from 2003 to 2013 in the Songhua River Basin. Monthly TWSA data from 1982 to 2002 are reconstructed using ANN technique, which performed well according to correlation coefficient **N**ash-**S**utcliff **E**fficiency (NSE). The GWS fluctuations are validated using in-situ groundwater level measurements. The main drivers of GWS spatio-temporal changes, as well as their inter- and intra-annually changing properties are investigated. According to the study, changes of GWS showed a "downward fluctuation" (1982–1994), a "stable upward" (1998–2008) and a "decreasing dramatically" (2009–2013) period, respectively. The results conclude that, declining GWS trend is observed at a rate of 1.04$\pm$0.59 mm/yr from 1982 to 1994. With increased climatic and anthropogenic influences, several severe fluctuations characterised the GWS variations.

Meghwal et al. (2019) examined the linkage between climate and groundwater variability in Western India using GRACE and well measurement data from 1996 to 2016. TWS and GWS, as measured by GRACE, have decreased (at a rate of -3.67 km^3/yr) in WI between 2002 and 2016. Analysis of GWS change associated with the monitoring wells and GRACE revealed distinct patterns in two states (Gujarat and Rajasthan). During 1996-2016, the variability of GWS associated with observation wells is strongly coupled with the precipitation. However, GWS is strongly linked with groundwater pumping and policies related to lowering groundwater abstraction for irrigation. Groundwater pumping for irrigation is the primary cause of groundwater depletion in Rajasthan. The findings highlighted the importance of controlling groundwater supplies in India.

Rateb et al. (2020) compared GWS changes from GRACE with groundwater level monitoring data and with regional, global hydrological and LSMs over 14 major U.S. aquifers from 2002–2017. The GRACE data revealed declining GWS trends in the six aquifers, which are linked to long-term droughts. In most aquifers, GWS changes agreed well with observed data. Regional groundwater models (eight) showed similar or greater GWS trends when compared to GRACE. Global hydrological models that include groundwater pumping, overestimated GWS depletion in South-Central and South Western U.S. According to the findings, global LSMs tend to track GWS dynamics better than global hydrological models. By combining remote sensing, monitoring, and modelling data, this study emphasises the importance of considering all data sources to constrain GWS uncertainties.

Bhanja et al. (2020) assessed GWS changes from GRACE using in-situ observation well measurements over India's major river basins for the period 2003–2014. The long-term trends in GWS are computed and analysed with respect to

changing precipitation trends. The authors also looked at long-term changes in precipitation patterns using SPI1 and SPI12 from 1961 to 2014. Both 1961-2014 and 2003-2014 (the study period), experienced long-term decreasing precipitation patterns in the Ganges and Brahmaputra Basins. Whereas, indeterminate or increasing precipitation trends are observed in other basins. However, in-situ measurements found decreased GWS (at rates of >0.4 km^3/yr) in the Ganges-Brahmaputra River Basin due to its agricultural productivity. The findings are utilized to better understand and predict long-term GWS conditions, as well as their relationship with precipitation patterns and thus used to develop sustainable groundwater management techniques in India's water-stressed regions.

Sarkar et al. (2020) examined the GWS changes from GRACE during 2003-2016 for Indian regions that are stressed with groundwater crisis. The study revealed that maximum GWS change is occurred in Delhi, Northern Uttar Pradesh and some parts of Haryana by -7.52 cm/yr. The groundwater depletion rates are also increased in the study regions between 2003 to 2016. The results conclude that, in spite of quantified rainfall, metro cities (Delhi, Chennai, Bengaluru, Kolkata and Mumbai) suffered a major depletion in GWS. The GWSC derived from GRACE agreed reasonably with in-situ well observations thereby justifying remote sensing approach.

2.5 DROUGHT FREQUENCY ANALYSIS

Kim et al. (2002) investigated the spatio-temporal characteristics of drought for sustainable water resource management in the Conchos River Basin, Mexico. PDSI is used as indicator to evaluate the drought characteristics. Frequency analysis method is adopted to investigate the spatio-temporal variations of drought based on drought intensity. Then kriging estimator is used to examine the spatial distribution of drought. The spatial and temporal characteristics of PDSI are utilized in developing the drought intensity-areal-frequency curves. The developed curves contain drought severity and area with respect to the return period to describe the spatial and recurrence patterns of droughts. The analysis showed occurrence of severe drought in the year 1990 with a large areal extent and with a return period of 80 to 100 years.

Shiau (2003) introduced a theoretical derivation for univariate and bivariate distribution return periods based on stochastic approach. As the extreme hydrological events are complex in nature, the bivariate distribution is considered as a better approach to represent these events (droughts and floods) than the univariate distribution. The return periods are defined using either two joint random variables or separate single variable for bivariate distribution. Assuming the bivariate distribution with the Gumbel marginal distributions, flood peak and flood volume are modelled for

Pachang River, Southern Taiwan using the daily streamflow data. Also, the properties associated with the univariate and bivariate distributions are discussed. The results exhibited a good agreement between the models and observed streamflow data.

Mishra and Desai (2005) analysed the spatial and temporal variations of drought using SPI at multiple timescales (1, 3, 6, 9, 12 and 24 month) in the Kansabati River Basin, India. The basin is divided into 25 grid cells and at each grid inverse distance method is adopted for spatial interpolation of precipitation dataset. The monthly SPI is evaluated using the rain gauge station data for the period 1965–2001. Using the gridded SPI series drought severity, duration and frequency are evaluated at multiple timescales. Then, SAF curves are developed using the spatio-temporal characteristics of SPI. The SAF curves are constructed to depict drought severity and area at different return periods so as to describe the spatial and recurrence patterns of drought. Results conclude that SPI1 and SPI3 based droughts (short-term) are high in 1979 with return periods of 80 to 100 years over the entire basin. Medium and long-term droughts are frequent in 1980's with a return period of 50 to 100 years. The 1980 droughts affected agriculture, reservoir storage and groundwater in the basin.

Shiau (2006) constructed a two-dimensional copula for drought severity and duration. The copula parameters are estimated using **I**nference **F**unction for **M**argins (IFM) method. The drought severity and duration are assumed to be distributed as gamma and exponential distributions. Then several copulas are tested for drought severity and duration to determine the best fitted copula and Galambos copula is concluded as the best fit to the observed drought. SPI is used to determine the drought severity and duration for Wushantou (Taiwan). The results conclude that the copula is fitted well for the drought severity and duration, considered as useful tool in exploring the relations of drought variables.

Shiau et al. (2007) examined the hydrological droughts using copulas in the Yellow river, China. The drought characteristics (severity and duration) are evaluated using the monthly streamflow data. Since droughts are complex in nature, single index is insufficient for comprehensive drought evaluation. Therefore, bivariate distribution is applied to model drought severity and duration jointly for drought assessment and copulas is used to achieve this purpose. Clayton copula is used to jointly describe the drought severity and duration. Then the bivariate return periods are also evaluated to explore the noticeable historic droughts. The results conclude that severe drought has occurred during 1930-1933 with a return period of 105 years. Also, low return period of 4.4 years is encountered during 1997–1998 drought because of drastically reduced streamflow in the Yellow River during 1997 due to human activities.

Bondarabadi et al. (2008) evaluated the spatial characteristics of drought over Razavi and Southern Khorasan provinces in Iran using SPI12. Drought maps are generated using thin plate smoothing splines method. The SPI12 maps are classified into several clusters and then the area enclosed by each SPI category is evaluated and **P**robability **D**ensity **F**unctions (PDFs) are fitted with different return periods. Then, SAF curves corresponding to different return periods are developed for the study region. Results conclude that droughts with 2 to 5 year return period are anticipated to cover $\sim$30% of the region. And droughts with 20 to 50 year return periods may cover $\sim$70% of the region. Thus, severe droughts are expected to occur with high return periods and less areal coverage.

Mishra and Singh (2009) used SPI to investigate the impact of climate change on SAF curves in the Kansabati River Basin, India. The generated SAF curves based on expected rainfall using a specified **G**lobal **C**limate **M**odel (GCM) and scenario uncertainty are compared to past droughts. To project precipitation from six GCMs, the **B**ayesian **N**eural **N**etwork (BNN) downscaling method is used. Then SPI is evaluated at 3 and 12-month timescale and SAF curves are constructed for 2001-2050 and 2051-2100 periods. The results have shown that the basin experienced severe droughts during 2001-2050 compared to the drought occurred in 1980. The SAF curves described the spatial and return patterns of droughts in the study region and are useful in anticipating the drought severity with percentage of areal extent over the future periods. The authors suggested to derive SAF curves using several GCMs to overcome the biases in GCM simulations and uncertainties in scenarios.

Shiau and Modarres (2009) investigated the multi-attributes of drought based on copula in terms of SDF curves for two rain gauge stations in Iran. The drought properties: severity, duration and frequency are defined using SPI3 calculated from rainfall series during 1954-2003. A joint distribution function is employed for drought severity and duration using copulas. The drought frequency is then related to the copula-based distribution function to develop SDF curves. From the developed SDF curves, for a given return period and duration, Anzali station experienced greater drought severity compared to Abadan station. These SDF curves are concave downwards indicating that drought severity increases with duration.

Janga Reddy and Ganguli (2012) developed SDF curves using copula-based bivariate probabilistic approach over Western Rajasthan, India. SPI at 6-month time scale is used to analyse the drought characteristics. The joint distribution of severity and duration are modelled using Plackett, Archimedean, Elliptical and Extreme Value copula families. The Gumbel-Hougaard and Extreme Value copulas are performed better in modelling the drought characteristics compared to other copulas based on

upper tail dependence coefficient and statistical techniques. Then SDF curves are derived with the conditional return periods evaluated using the best performing copula. The results conclude that SDF curves are helpful in planning and management of water resources at drought prone areas.

Reddy and Ganguli (2013) analysed the spatio-temporal variations of drought and developed **I**ntensity-**A**rea-**F**requency (IAF) curves for Western Rajasthan, India. The meteorological droughts are analysed using SPI6 at spatial resolution of 0.5°×0.5°. Seasonal trends are evaluated using Mann Kendall trend test and results showed increased number of grids under drought for the study region. Then three copula families namely Frank, Gumbel-Hougaard and Plackett are used to model the joint dependence between intensity and areal extent of drought. The drought properties are best represented by Gumbel-Hougaard copula based on upper tail dependence and goodness of fit tests. Then IAF curves are derived with the conditional return periods evaluated using the best performing copula. The developed IAF curves could estimate drought intensities for a specified areal extent and return periods. The results conclude that for a drought event with 8.8 **P**ercentage **A**rea **U**nder **D**rought (PAUD) and 50-year return period produced an intensity of 1.55. Whereas, drought event with 90 PAUD and 50-year return period produced an intensity of 2.13. Therefore, the developed IAF curves are useful in spatial assessment of drought events and the associated risks.

Reddy and Singh (2014) examined the usefulness of two metaheuristic methods namely **P**article **S**warm **O**ptimization (PSO) and **G**enetic **A**lgorithm (GA) in estimating the copula parameters and developing SDF curves over Texas, USA. In this study, drought characteristics are evaluated using SPI and drought risk analysis is performed by copula methods. For accurate estimation of copula model, GA and PSO techniques are applied. First, the drought characteristics are modelled separately with different probability distribution functions and the best model is concluded for copula modelling. Then three copula families namely Extreme Value, Plackett and Student's-t are used to model the joint dependence between drought severity and duration and the performance is evaluated using **K**olmogorov–**S**mirnov (KS), **A**kaike **I**nformation **C**riteria (AIC) and tail dependence tests. The performance measures conclude that Gumbel-Hougaard copula is the best fitted model and used for the development of SDF curves. The results conclude that the meta-heuristic techniques are useful in accurate estimation of copula parameters and derivation of SDF curves.

Rajsekhar et al. (2015b) developed the hydrologic drought atlas that describes the spatial variation of severity for 3, 6, 12 and 24-months durations and corresponding to 10, 25, 50 and 100-year return periods for Texas state. The drought characteristics are derived using the **V**ariable **I**nfiltration **C**apacity (VIC) model from stream flow data at

monthly timescale. The drought severity and duration are evaluated using **S**tandardized **S**tream**F**low **I**ndex (SSFI) and suitable marginal distributions are selected from Gamma, Exponential, Weibull and Log-normal distributions. Then the joint dependence between drought severity and duration is modelled using various copula families and SDF curves are developed using the best performed copula. The developed SDF curves are used to prepare the drought atlas for Texas which depicts the drought severity for a given duration and return period. The results conclude that SDF curves displayed convex (concave) pattern in arid and semiarid regions. Also, decreasing pattern are observed for drought severities from West to East of Texas.

Rajsekhar et al. (2015a) evaluated the socioeconomic impacts of drought due to climate change for the state of Texas. The author reviewed the effects of changing climate variability on the features of various drought kinds. Through a relative entropy technique, downscaled and bias-corrected data from five GCMs are utilised to produce an ensemble of precipitation, temperature and wind speed for drought study. After that, a unique multivariate drought index is used to quantify all physical types of droughts in one place. The geographical patterns of drought features are studied using multivariate frequency analysis for each planning zone in Texas to identify the distribution of prospective drought hazard areas as a result of climate change, resulting in the drought hazard index. A drought vulnerability assessment is also conducted, with numerous socioeconomic aspects taken into account, resulting in the formulation of socioeconomic drought vulnerability index. A set of composite drought risk maps are created, which combined hazard and vulnerability analyses. Overall, the findings are expected to aid Texas in developing an efficient drought mitigation strategy.

Amirataee et al. (2018) developed SAF curves using one-month SPI during 1971-2013 in Lake Urmia Basin, Iran. The joint probability distribution of drought severity and drought area is then modelled using seven distinct copula functions. Using AIC, **B**ayesian **I**nformation **C**riteria (BIC), and **R**oot **M**ean **S**quare **E**rror (RMSE), the Frank copula is identified as the best acceptable copula for constructing the joint probability distribution of severity and percentage of area under drought.The drought SAF curves are developed using the Frank copula. According to the findings, majority of the study areas are affected by severe/extreme drought and non-drought (wet) behaviours.

Ahmed et al. (2019a) used **G**lobal **P**recipitation **C**limatology **C**entre (GPCC) gauge-based gridded precipitation data to reconstruct historical droughts and downscale future precipitation projected by seven GCMs from the **C**oupled **M**odel **I**nter-comparison **P**roject phase 5 (CMIP5) under four **R**epresentative **C**oncentration **P**athway (RCP) scenarios. Downscaling and bias correction are accomplished using the **S**upport **V**ector **M**achine (SVM) and quantile mapping respectively. Statistical

measures are used to evaluate the model's performance. The SPI is utilised to describe the seasonal droughts for distinct crop growth periods using historical and future precipitation data. Drought SAF curves are produced for the historical period (1961–2010) and three future periods (2010-2039, 2040-2069 and 2070-2099). At 95 percent confidence level, the uncertainty band of future drought SAF curves is computed using Bayesian bootstrap. Results conclude that droughts with longer return periods affect bigger areas than droughts with shorter return periods, according to historical SAF curves. Drought estimates for the future revealed an increase in impacted area for droughts of lower severity, return period and reduction for droughts of higher severity and return period.

Alamgir et al. (2020) examined variations in SAF curves of seasonal droughts in Bangladesh using SPI from nineteen CMIP5 GCMs. Drought properties are estimated for the four climatic seasons namely: winter, pre-monsoon, monsoon and post-monsoon. For three time periods (2010–2039, 2040-2069 and 2070-2099), changes in the SAF curves are calculated. The Bayesian bootstrap approach is used to calculate the SAF curves. The results conclude that moderate and severe droughts occurred for longest return periods and are more likely to damage the region than other drought types. During all return periods and severity categories, the kharif season drought is found to be the most acute and affected major areas of the country. Droughts in the monsoon and kharif seasons are expected to become more severe and last longer in Bangladesh, according to projections.

2.6 CONCLUDING REMARKS

A detailed review is carried out in the above sections and the following observations are made:

- The pertinence and robustness of GRACE satellite remote sensing data can be used to estimate total water storage necessary for drought studies at regional and basin scales.
- GRACE can help to a better understanding of how terrestrial water storage responds to climate change and variability with longer time series.
- Spatial correlation analysis is useful in identifying the drought areas that are strongly affected with TWSA by considering the relationship between drought indices and TWSA. Therefore, utilizing the existing indices to identify the right index in the river basins where hydro-meteorological datasets are scarce is expected to offer insights in assessing droughts using remote sensing data.

- Teleconnection factors have a major effect on drought and very few studies have investigated the associations between droughts evaluated using GRACE and teleconnections. A comprehensive and systematic analysis between GRACE and teleconnections is vague and in particular for India. Therefore, this study addresses the drought situation in South Indian River Basins with GGDI and identifying the linkages between drought and teleconnections.

- Machine learning techniques have recently advanced and proved to be effective in data prediction and reconstruction. In this study, a learning-based model, namely **M**ulti **L**ayer **P**erceptron (MLP) is used to reconstruct TWSA to obtain a continuous time series from 1960 to 2020.

- In evaluating groundwater variations and trends, GRACE-based estimates have proven valuable at regional and basin scales. Very few studies, particularly in India, have compared GRACE groundwater storage estimates with observation well measurements. In this study, the reconstructed TWSA using MLP is converted to groundwater storage anomalies and validated with observation well measurements.

- The SAF and SDF curves can describe the spatial and return patterns of droughts and can be useful in anticipating the drought severity with percentage of areal extent over the future periods.

- The SAF and SDF curves can be helpful in planning and management of water resources at drought-prone areas.

CHAPTER 3

STUDY AREA AND DATA COLLECTION

3.1 STUDY AREA

India is the seventh largest country in the world comprising 22 major river basins (India-WRIS, 2012) of which four are selected for the present study. The **G**odavari **R**iver **B**asin (GRB) is located in the Deccan Plateau and has a tropical climate with annual precipitation from 760 mm to 1550 mm and annual maximum temperature from 31° C to 34° C. Major part of the basin is covered by agricultural land (60%) followed by forest area (30%) and water bodies (2%) as per the 2005–06 **L**and **U**se-**L**and **C**over (LULC) (www.india-wris.nrsc.gov.in) data. The **K**rishna **R**iver **B**asin (KRB) falls in the Deccan Plateau and Western Ghats and its annual precipitation and mean temperature are 860 mm and 26 °C, respectively. Approximately 76% of the basin is covered by agricultural areas and 10% by forests. The **C**auvery **R**iver **B**asin (CRB) falls in three agro-climatic zones with tropical and sub-tropical climates. The mean annual precipitation is 1075 mm and mean monthly temperature varies from 23 °C to 28 °C. The basin is dominated by agricultural lands with 66% followed by forest areas with 21%. The **P**ennar **R**iver **B**asin (PRB) falls in two agro-climate zones with mean annual precipitation of 770 mm, and mean minimum and maximum temperature of 21 °C and 32 °C. From the LULC assessment of 2005–06, 59%, 20%, and 5% of the basin are covered with agricultural lands, forests, and water bodies, respectively. Additional details of these river basins are shown in Table. 3.1 and Fig. 3.1.

Table 3.1: River basin details considered in the study

S. No	Basin Name	Area (Sq.km)	Mean Annual Rainfall (mm)	Maximum Temperature (°C)	Minimum Temperature (°C)	Elevation (m)
1	Godavari River Basin (GRB)	3,12,810	1095	33	20	1665
2	Krishna River Basin (KRB)	2,54,750	860	32	20	1900
3	Pennar and East flowing rivers between Pennar and Cauvery River Basin (PCRB)	1,17,890	770	32	21	1440
4	Cauvery River Basin (CRB)	85,630	1075	34	17	2630

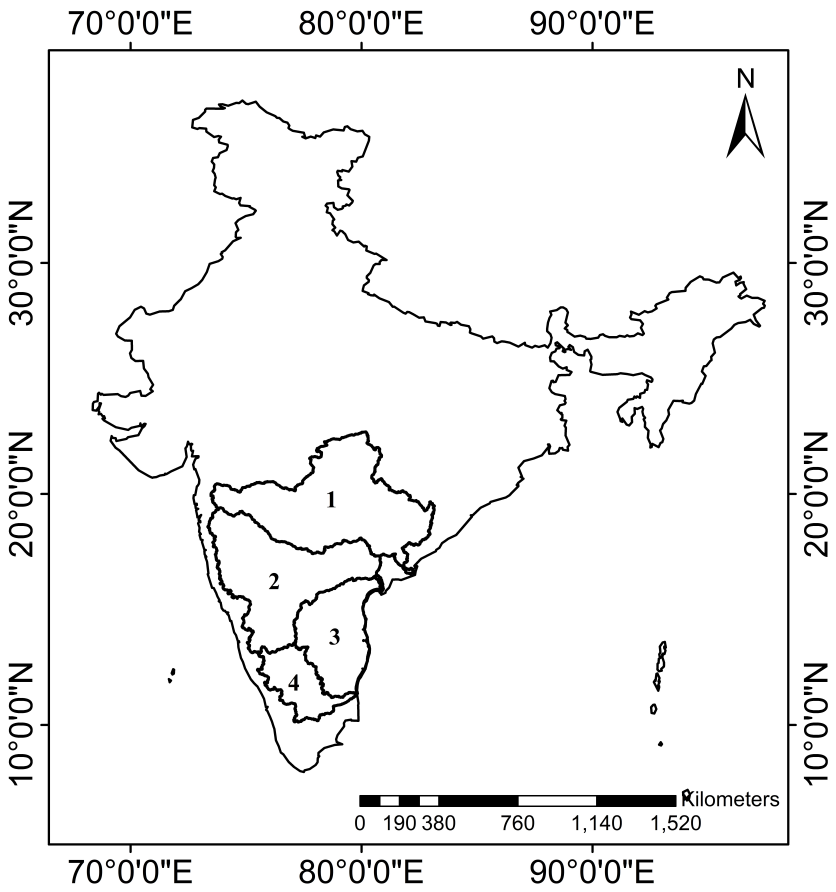

Figure 3.1: Study region showing river basins considered in the study. (1. GRB, 2. KRB, 3. PCRB and 4. CRB)

3.2 DATA

3.2.1 Meteorological Data

In the present study, gridded precipitation and temperature data from the **I**ndia **M**eteorological **D**epartment (IMD) are considered for 1960–2020 with a spatial resolution of 1° × 1° and monthly temporal resolution for the study area (Rajeevan et al., 2008; Srivastava et al., 2009).

3.2.2 Self-Calibrated Palmer Drought Severity Index (SC_PDSI)

The SC_PDSI dataset is collected from the **C**limate **R**esearch **U**nit (CRU) website at a spatial resolution of 0.5°×0.5°. New updated versions are available each year, and CRU TS4.03 is the current update (http://www.cru.uea.ac.uk/data).

3.2.3 GRACE Terrestrial Water Storage Anomaly

In this study, the latest release of GRACE monthly mass grids (RL 06) processed at JPL (https://grace.jpl.nasa.gov) are used for analysis. The GRACE data is considered

from 2002–2017 and GRACE FO is considered from 2018-2020. The JPL RL06 surface mass data form a unique framework, which estimates monthly gravity fields at 3 × 3 degree equal-area spherical cap mass concentration using a priori constraints that minimise the impact of measurement errors (Wiese et al., 2016). Correction of the **G**lacial **I**sostatic **A**djustment (GIA) has been applied. GRACE JPL mascon data does not need a smoothing filter, as the spherical cap mascon performs as a smoothing function by decreasing the signal strength at spatial scales below 3°. Lost signals are restored by applying gridded scaling factors. Despite its effectiveness, there are long-term limitations for scaling factors in the application of groundwater variations (Landerer and Swenson, 2012). Dataset leakage errors are effectively reduced by the use of scaling factors and **C**oastline **R**esolution **I**mprovement (CRI) filters. Residual errors interpret GRACE measurement errors in addition to lost inter-annual signals.

3.2.4 Global Land Data Assimilation System (GLDAS)

The latest release of the GLDAS Noah model, namely NOAH10_M 2.0 and NOAH10_M 2.1 products that are consistent with the GRACE product, is used in this study (https://disc.gsfc.nasa.gov/). Because GLDAS products are not available continuously from 1960 to 2020, both GLDAS Noah versions 2.0 and 2.1 are selected to obtain data from 1960 to 2020. GLDAS NOAH10_M 2.0 version products are considered form 1960-2000, and GLDAS NOAH10_M 2.1 version products are considered for the period 2000-2020, with the spatial resolution of 1° × 1°. From GLDAS, TWSA is calculated by incorporating soil moisture storage (ΔSMS) and canopy water storage (ΔCWS). Because the GLDAS Noah model cannot evaluate changes in groundwater storages (ΔGWS), TWSA is calculated using only two components ($GLDAS_{TWSA} = \Delta SMS + \Delta CWS$). As, GLDAS products are as reliable as GRACE products, GLDAS-based TWSA is used as a predictor for GRACE TWSA reconstruction and prediction.

3.2.5 In-situ Groundwater Well Measurements

In this study, seasonal (during January, May, August and November, respectively) in-situ observation well data from 1973 locations covering GRB (822), KRB (550), CRB (275), and PCRB (326) basins, accessed from Central Ground Water Board (CGWB, India) between January 1996 and December 2020 are used (see Fig. 3.2). The groundwater observation well data is available for four seasons namely: (i) Post-monsoon rabi (January), (ii) Pre-monsoon (May), (iii) Monsoon (August) and (iv) Post-monsoon kharif (November) respectively. Most (>87%) of the studied wells are considered to be within shallow, unconfined aquifers (CGWB, 2014b), though certain areas of Southern Indian states are found to have higher percentage of confined wells.

The data is processed to have temporal continuity i.e., at least three seasonal data should be available out of four from 1996-2020 over the study region.

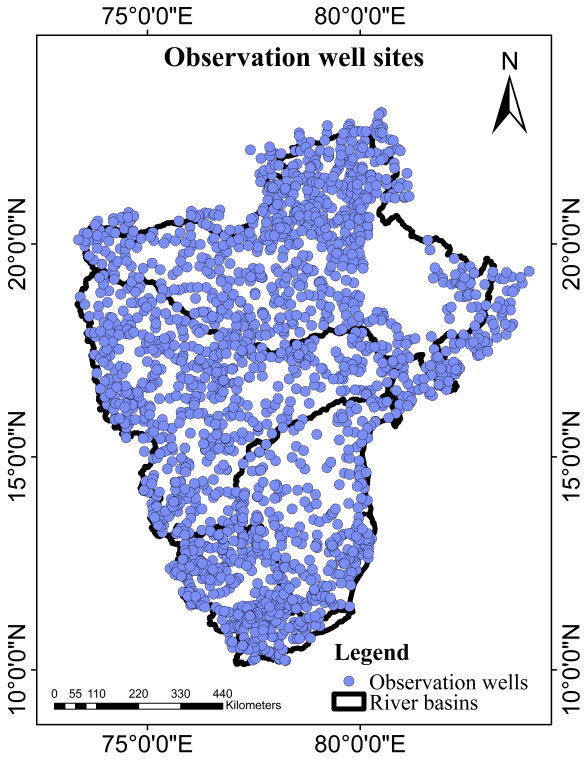

Figure 3.2: Study region showing major river basins of South India and groundwater observation well locations.

3.2.6 Climate Data

Monthly climate oscillations namely NINO 3.4, **M**ultivariate **E**NSO **I**ndex (MEI), **S**outhern **O**scillation **I**ndex (SOI), and **D**ipole **M**ode **I**ndex (DMI) during 2003–2016 are utilized in the study. Monthly **S**ea **S**urface **T**emperature (SST) anomaly data (NINO3.4) is obtained from http://www.esrl.noaa.gov/. For ENSO, the MEI is selected and obtained from https://www.esrl.noaa.gov/. The SOI data is obtained from the NOAA Earth System Research Laboratory (https://psl.noaa.gov/). The **I**ndian **O**cean **D**ipole (IOD) is measured as DMI due to the dipole mode in the tropical Indian Ocean, and the DMI data is obtained from http://www.jamstec.go.jp.

CHAPTER 4

ASSESSMENT OF MONTHLY AND SEASONAL DROUGHTS USING GRACE TERRESTRIAL WATER STORAGE

The purpose of the present work is to monitor TWSA and assess its impact on drought in the South Indian River Basins. This main objective is subdivided into four sub objectives, each of which is examined in depth and presented in different chapters. The first sub objective is covered in the chapter. The first sub objective deals with spatial and temporal variations of TWS with respect to various drought indices to offer insights into assessing future droughts using remote sensing data.

4.1 INTRODUCTION

Drought is one of the extremes of water availability and one of most serious threat to sustainable socio-economic development of a region (Nagarajan, 2010). According to the **W**ater **R**esource **I**nstitute (WRI), a quarter of the world's population is experiencing severe water stress in 2019 and this percentage is expected to double by 2050. These forecasts are based on models and they are only as accurate as our current understanding of drought's spatio-temporal properties. As a result, number of research groups are investigating into current and past drought events to get novel insights.

Drought indices are suitable tools for monitoring, quantifying and evaluating drought. These drought indices become predominant in drought characterisation as they reduce the complexity of drought phenomenon to a single numerical value. GRACE-related drought indices have been recently applied in monitoring and characterizing regional droughts and water availability conditions. Despite their suitability for a variety of water-related sectors, these indices have their limitations. Identifying the right index to quantify storage or drought becomes a problem when it is not known and what suitable index is to be considered over the study regions. Therefore, there is a need in understanding the correlation between GRACE TWS and other drought indices, to validate and illustrate the relevance of these indices to forecast drought in certain areas (Yang et al., 2020; Zhao et al., 2017b).

The distinguishing features of this study includes the assessment of spatial correlation on a seasonal scale between TWSA from GRACE and other indices (SPI, SPEI, SC_PDSI, GRACE DSI, GGDI and CCDI). This is considered important in

identifying the spatial extent of drought-hit areas as the relationship between drought indices and TWSA has some physical significance. These insights are important as seasonal correlations analysis between drought indices and TWSA can be useful to examine the applicability of certain drought indices for individual river basins. It should be noted that accurate quantification of beginning and end of drought period is difficult. However, a drought event captured by a drought index offers the signal of both past and future drought. As each drought index is different by construct and variables involved, differences in characterizing drought events are expected among the indices. Therefore, analysis of several indices is performed in this study. Seasonal and monthly drought events offer additional insights into identifying suitable ones from among the indices including SPI, SPEI, SC_PDSI, CCDI, GRACE DSI and GGDI. The four basins considered in this study are driven by monsoon rainfall where 75% of the annual rainfall generally occurs during this period.

Spatial correlation analysis is useful in identifying the drought areas that are strongly affected with TWSA by considering the relationship between drought indices and TWSA. As the influence of TWSA with drought indices is spatially unrevealed. With the above perspective, significant seasonal correlation analysis between drought indices and TWSA could be considered as a standard to examine the applicability of certain drought indices for individual river basins. Therefore, utilizing the existing indices to identify the right index in the basins where hydro-meteorological datasets are scarce is expected to offer insights in assessing droughts using remote sensing data. The flowchart of the first sub-objective is presented in Fig. 4.1.

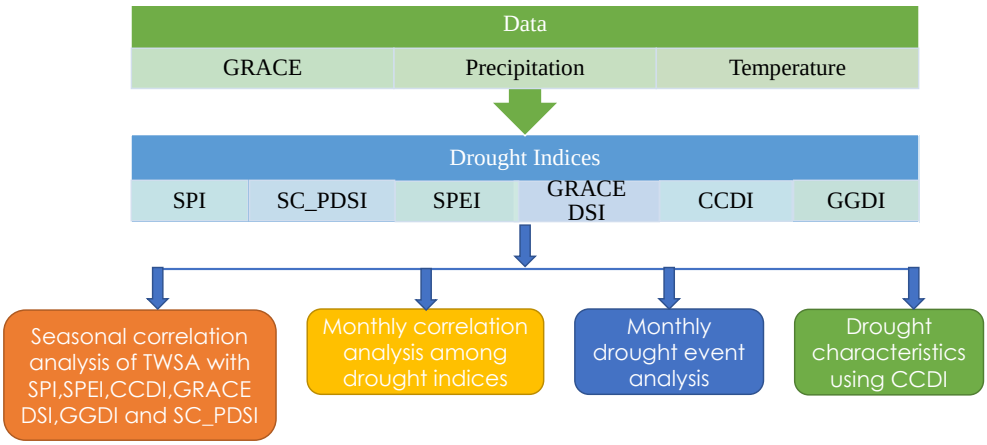

Figure 4.1: Flow chart of first sub objective

For analysis purpose, the first sub objectives is further divided as given below.

- To quantify six drought indices: SPI, SPEI, SC_PDSI, GRACE DSI, GGDI and CCDI using precipitation, temperature and TWSA datasets.

- To analyse the correlation between above mentioned six drought indices and TWSA using statistical techniques.
- To determine suitable drought indices based on correlation analysis, and
- Apply drought indices to detect seasonal drought patterns impacted by the changes in TWSA over a decade between 2002 and 2016.

4.2 METHODOLOGY

4.2.1 Processing and Analysis of Data

Drought indices namely SPI and SPEI are evaluated using gridded precipitation and temperature datasets. GRACE is also increasingly used in water availability assessments (Sridhar et al., 2019) and a similar approach is employed for drought assessment in this study. The missing monthly GRACE datasets are filled by the linear interpolation method (Sun et al., 2018). The indices SPI and SPEI are evaluated using R-Studio (package: SPEI; version 3.5.1; https://www.r-project.org/) for the 3, 6 and 12-month time scales. For the calculation of CCDI, GGDI and GRACE DSI, GRACE monthly mass grids (RL 06) are used. The potential impact of short reference period (2002-2016) and long reference period (1975-2016) are evaluated over TWSA (Cammalleri et al., 2019). From the analysis, major variations are not observed in between short and long reference period. For this study the base line period is considered from January 2004 to December 2009, i.e., a short reference period. Furthermore, evaluation of different 5-year periods to consider the reference period has shown no significant differences. Positive TWSA indicates more water and negative value indicates less water than in the past. SC_PDSI dataset is collected from the CRU TS website at a spatial resolution of 0.5°×0.5° is directly used for the analysis. The considered variables are resampled and clipped to the same spatial extent of 1°×1° using the MATLAB toolkit.

The study analysed correlation of drought indices, such as SPI, SPEI, SC_PDSI, GRACE DSI, GGDI and CCDI with the TWSA dataset. Correlation analysis is performed for four seasons: post-monsoon rabi (January to March), pre-monsoon (April to June), monsoon (July to September) and post-monsoon kharif (October to December). The indices SPI and SPEI are evaluated for 3, 6 and 12-month time scales. GRACE DSI, GGDI and CCDI are calculated by following the procedures of Sinha et al. (2019); Thomas et al. (2017); Zhao et al. (2017a) respectively. The Pearson's correlation analysis (see Eq. 4.1) is performed for all grids covering the river basins between each drought index and the TWSA to obtain the correlation coefficients.

$$r = \frac{\sum_{i=1}^{n}(x_i - \bar{x})(y_i - \bar{y})}{\sqrt{\sum_{i=1}^{n}(x_i - \bar{x})^2 \sum_{i=1}^{n}(y_i - \bar{y})^2}} \tag{4.1}$$

where r = Pearson's correlation coefficient; x represents the TWSA dataset; and y represents the drought index. i is $1, 2 \ldots .n$; $\bar{x}$,$\bar{y}$ are the means of x and y scores respectively; n = the total number of observations; r ranges between -1 and +1, the highest r (positive or negative) represents the higher correlation between x and y.

Then t-test is performed to determine the significant difference between the means of two datasets (e.g., TWSA and SPI) and is calculated for their corresponding p values at the 95% confidence level. Significance is indicated when $p < 0.05$. Spatial maps are prepared using ArcGIS 10.3 for the correlation coefficients along with p values.

The drought categories for SPI are considered from McKee et al. (1993). For GRACE DSI and CCDI, the drought categories are considered from the **U**nited **S**tates **D**rought **M**onitor (USDM) that are classified into D0, D1, D2, D3 and D4 categories (Svoboda et al., 2002; Zhao et al., 2017a). Note that the categories of drought presented in this study depend on the range of drought indices obtained for four river basins.

4.2.2 Standardized Precipitation Index (SPI)

The SPI is a dimensionless meteorological drought index which requires single hydrological variable i.e., precipitation, to characterize drought events. It is simple to analyse, spatially invariant and can be applied to evaluate meteorological, hydrological and agricultural drought phenomenon with this index. Using SPI, the temporal analysis of drought events can be evaluated at 3, 6, 9, 12, 24, 36 and 48-month time scales. To evaluate SPI for a given year i, month j and for time scale of k, the following steps are used:

- For a specific period of interest j, cumulative precipitation series is evaluated $X_{ij}^{k}(i = 1, 2, \ldots, n)$, where each term denotes the sum of precipitation of $k - 1$ previous successive months.
- The aggregated monthly precipitation series (say $k = 12$ months) is fitted with cumulative probability distributions (for e.g., gamma distribution). The gamma distribution function is defined as

$$g(x) = \frac{1}{\beta^{\alpha}\Gamma(\alpha)} x^{\alpha-1} e^{\frac{-x}{\beta}} \tag{4.2}$$

  where, $\Gamma(\alpha)$= gamma function, α= shape parameter and β= scale parameter. The shape and scale parameters are estimated using method of maximum likelihood.

- For a specific month and time, the estimated parameters are utilized in finding the cumulative probability distribution of the precipitation event. The cumulative

probability, $G(x)$ is obtained by integrating $g(x)$ i.e.,

$$G(x) = \int_0^x g(x)dx = \int_0^x \frac{1}{\hat{\beta}^{\alpha}\Gamma(\hat{\alpha})} x^{\hat{\alpha}-1} e^{-\frac{x}{\hat{\beta}}} dx \tag{4.3}$$

- A mixed (containing zero values and continuous precipitation amount) two parameter gamma distribution function is employed and the corresponding **C**umulative **D**istribution **F**unction (CDF) is given as

$$F(x) = q + (1-q)G(x) \tag{4.4}$$

where, q= probability of zero precipitation and $G(x)$= distribution function calculated for non-zero precipitation.

- An equiprobability transformation (Panofsky et al., 1958) is carried out from the CDF of mixed distribution to the CDF of standard normal distribution (zero mean and unit variance), which is given as

$$SPI = \psi^{-1}(F(x)) \tag{4.5}$$

- This transformed probability in Eq. 4.5 is the SPI. The negative SPI value specifies that the precipitation is below average (dry condition) and positive SPI value indicates above average precipitation (wet condition).

A drought period is defined as the successive number of SPI values below a threshold (approximately 0.8). According to McKee et al. (1993), droughts are classified into four categories namely mild (D0), moderate (D1), severe (D2) and extreme (D3) droughts as given in Table 4.1. In this study, SPI is computed over 3, 6 and 12-month time scales with monthly gridded precipitation data at a spatial resolution of 1°×1° from 2002 to 2016.

Table 4.1: Drought categories related to **D**ry (D) conditions for SPI

Drought Category	SPI
D0: Mild (abnormal) Drought	0 to -0.99
D1: Moderate Drought	-1.00 to -1.49
D2: Severe Drought	-1.50 to -1.99
D3: Extreme Drought	≤ -2

4.2.3 Standardized Precipitation Evapotranspiration Index (SPEI)

Several drought indices have been developed to characterise droughts by considering one or more climatic variables like precipitation, temperature, runoff,

evapotranspiration and soil moisture. To quantify meteorological drought, SPI is considered as the most widely used drought index because it is less data intensive and simple to calculate. As SPI can be calculated at different time scales, it helps in understanding the effect of rainfall deficit on various hydrological components (McKee et al., 1993). The limitation of SPI is that it does not consider other climate variables like evapotranspiration in quantifying the droughts. Therefore, SPI may not reproduce the true water deficit that is intensified by climate change. By considering all the advantages of SPI, Vicente-Serrano et al. (2010) developed SPEI which can be calculated at 1 to 48-month time scale representing hydrological, agricultural and meteorological droughts (Maccioni et al., 2015). For calculating SPEI, **P**otential **E**vapo**T**ranspiration (PET) is evaluated first. For the estimation of PET, Penman-Monteith, Thornthwaite and Hargreaves are the most widely used methods. In the present study, Hargreaves method is adopted to calculate PET because of its simplicity and lower data requirement. Then, difference between precipitation and PET is estimated as shown in Eq. 4.6.

$$D_i = P_i - PET \tag{4.6}$$

where, P_i= precipitation at i_{th} month, D_i= surplus or deficit in the i_{th} month.

The D_i values are then aggregated, probability distributions are fitted and the best fitted distribution is chosen using L-moments method because, it is more robust for outliers and is effective in characterizing various distribution functions compared to other methods. The CDF of the best fitted distribution is then normalized to evaluate SPEI for the selected region. Therefore, SPEI is estimated at three different monthly time scales (3, 6 and 12) using the IMD precipitation and temperature data available at the spatial resolution of 1°×1° from 2002 to 2016. Positive SPEI indicates wet condition and negative SPEI indicates a dry condition. Drought characteristics are well assessed with SPEI, as the index is consistent and flexible in terms of space and time in reproducing water deficiencies at different time scales.

4.2.4 Self-Calibrated Palmer Drought Severity Index (SC_PDSI)

Palmer (1965) developed an index called PDSI to assess moisture demand and supply on the basis of a two-layer soil water balance model. Wells et al. (2004), within the framework of PDSI, proposed SC_PDSI model that automatically adjusts the climatic characteristics (K) and the duration factors evaluated from historical climate data for a particular location. The SC_PDSI is calculated from the precipitation and temperature time series with fixed parameters of soil/surface characteristics at each location. This study considered the global gridded monthly SC_PDSI (0.5°×0.5°) values from 2002 to 2016.

4.2.5 GRACE Drought Severity Index (GRACE DSI)

This is a satellite-based drought index derived from the variations in TWSA from GRACE. GRACE DSI provides comparison of drought characteristic across regions and time intervals, without considering any impact of uncertainties related to soil water balance models or the influence of meteorological data. It also integrates the variations in water storage due to human interventions including withdrawal of groundwater. In this study, GRACE JPL RL06 land water storage data are used for the evaluation of GRACE DSI following the procedure developed by Zhao et al. (2017a). GRACE DSI is calculated as

$$GRACE - DSI_{u,v} = \frac{TWS_{u,v} - \overline{TWS_v}}{\sigma_v} \tag{4.7}$$

where u is the year from 2002–2016; v is the month ranging from January to December; and $\overline{TWS_v}$ and σ_v are mean and standard deviation of monthly anomalies, respectively. GRACE DSI is dimensionless quantity. Drought categories related to **W**et (W) and **D**ry (D) conditions for GRACE DSI are presented in Table 4.2.

Table 4.2: Drought categories related to Wet (W) and Dry (D) conditions for GRACE DSI and CCDI

Drought Category	GRACE DSI and CCDI
W4: Exceptionally Wet	2 or greater
W3: Extremely Wet	1.6 to 1.99
W2: Severely Wet	1.3 to 1.59
W1: Moderately Wet	0.8 to 1.29
W0: Abnormally Wet	0.5 to 0.79
N: Near Normal	0.49 to -0.49
D0: Abnormally Dry	-0.5 to -0.79
D1: Moderately Dry	-0.8 to -1.29
D2: Severely Dry	-1.3 to -1.59
D3: Extremely Dry	-1.6 to -1.99
D4: Exceptionally Dry	-2 or less

4.2.6 Combined Climatologic Deviation Index (CCDI)

CCDI integrates meteorological, hydrological and agricultural drought occurrences by incorporating precipitation and TWSA for drought assessment. Thus, the CCDI accounts for variations in surface and subsurface water storages. In this study, IMD gridded precipitation data and TWSA from JPL RL06 are used in calculating CCDI from 2002-2016 for the four river basins following the procedure proposed by Sinha et al. (2019). CCDI is calculated using the equations provided below i.e., from Eq. 4.8 to Eq. 4.14.

Precipitation anomalies are calculated as

$$PA_x = P_x - P_\mu \tag{4.8}$$

where, PA_x is precipitation anomaly, P_x represents monthly deviations of precipitation and P_μ represents the mean monthly deviations.

$$PA_y^{clim} = \frac{\sum_{y=1}^{12} PA_{x,y}}{N} \tag{4.9}$$

$$TWSA_y^{clim} = \frac{\sum_{y=1}^{12} TWSA_{x,y}}{N} \tag{4.10}$$

$$PA_x^{res} = PA_x - PA_{x,y}^{clim} \tag{4.11}$$

$$TWSA_x^{res} = TWSA_x - TWSA_{x,y}^{clim} \tag{4.12}$$

$$CD_x = PA_x^{res} + TWSA_x^{res} \tag{4.13}$$

$$CCDI_x = \frac{CD_x - CD_\mu}{CD_\sigma} \tag{4.14}$$

where subscript x varies from 1 to 177 months (the study period considered i.e., April 2002 to December 2016); y denotes each month of the calendar from 1 to 12; N is the total count of the considered month; $clim$ and res denote time series of climatology and residuals, respectively; and μ and σ are the mean and standard deviation respectively.

4.2.7 GRACE Groundwater Drought Index (GGDI)

The dimensionless GGDI is implemented to examine the drought characteristics related to groundwater. Firstly, monthly climatology, C_i (climatology for month i) is calculated as follows:

$$C_i = \frac{1}{n_i} \sum_{1}^{n_i} GWSA_i \tag{4.15}$$

where, i represents month $(i = 1, 2, \ldots 12)$ and n represents number of years. In the present study, TWSA from GRACE is considered from 2002-2016 with $n = 15$. The monthly climatology C_i is calculated for each month individually using GWSA. The effect of seasonality is removed by using the monthly climatology Thomas et al. (2017). Secondly, the monthly climatology is subtracted from GWSA to obtain **G**round**W**ater **S**torage **D**eviation (GWSD), that signifies the net deviation in the volume of GWSA based on seasonal variability. Finally, the GWSD is normalized by removing the mean and divided by standard deviation as follows:

$$GGDI = \frac{GWSD_t - \bar{x}_{GWSD}}{S_{GWSD}} \tag{4.16}$$

where, $\bar{x}_{GWSD}$ and S_{GWSD} are the mean and standard deviation of GWSD respectively. GGDI is the normalized net deviation in GWS volume and the GGDI classification is given in Table 4.3. For detailed information regarding GGDI, one can refer to Thomas et al. (2017).

Table 4.3: Classification of the GGDI

Grade	Classification	GGDI
I	No drought	$-0.5 <$ GGDI
II	Mild drought	$-1.0 <$ GGDI ≤ -0.5
III	Moderate drought	$-1.5 <$ GGDI ≤ -1.0
IV	Severe drought	$-2.0 <$ GGDI ≤ -1.5
V	Extreme drought	GGDI ≤ -2.0

The 'run theory' approach is used to determine the characteristics of drought, such as severity and duration from the considered drought indices. Drought duration is the period of time where the index remains below the fixed threshold (threshold value of -0.8). The minimum duration of drought is considered as one month, as the drought event is defined at aggregation of monthly time scale. Drought severity is the cumulative values of index within the drought duration.

4.3 RESULTS

4.3.1 Seasonal Analysis

Seasonal correlation analysis is performed for four seasons over four river basins using Pearson's correlation test. The t-test is evaluated to determine the significant difference between the means of two datasets for their corresponding 'p' values at the 95% confidence level for four seasons. The post-monsoon kharif and pre-monsoon seasons (see Fig. 4.2) have shown significant correlation for all the four basins considered in this study. In the monsoon season, parts of CRB and PCRB have shown insignificant correlation as they are not normally impacted by monsoon rains whereas the remaining parts have shown significant correlation. In the post-monsoon rabi season, parts of GRB, CRB and PCRB have shown insignificant correlation and the remaining part exhibited significant correlation. The correlation analysis as presented in this study offered insights into spatial and temporal variability between the basins.

4.3.1.1 Correlation between TWSA and SPI

To identify a suitable index for the assessment of storage and drought conditions, a Pearson correlation coefficient analysis is performed for TWSA and SPI for 3, 6 and 12 months represented by SPI3, SPI6 and SPI12. The results have shown significant correlation between TWSA and SPI in all seasons for KRB as shown in Fig. 4.2(a),

4.2(b) and 4.2(c) for SPI3, SPI6 and SPI12 respectively.

The post-monsoon kharif season has indicated high positive significant correlation followed by the post-monsoon rabi season for SPI. The pre-monsoon and monsoon seasons have shown positive correlation, with a few negative correlations in the upper Western Ghats and Southern Tungabhadra River for SPI 3, 6 and 12 months. CRB has shown significant correlation in post-monsoon kharif and pre-monsoon seasons and insignificant correlation is observed for both the monsoon and post-monsoon rabi seasons.

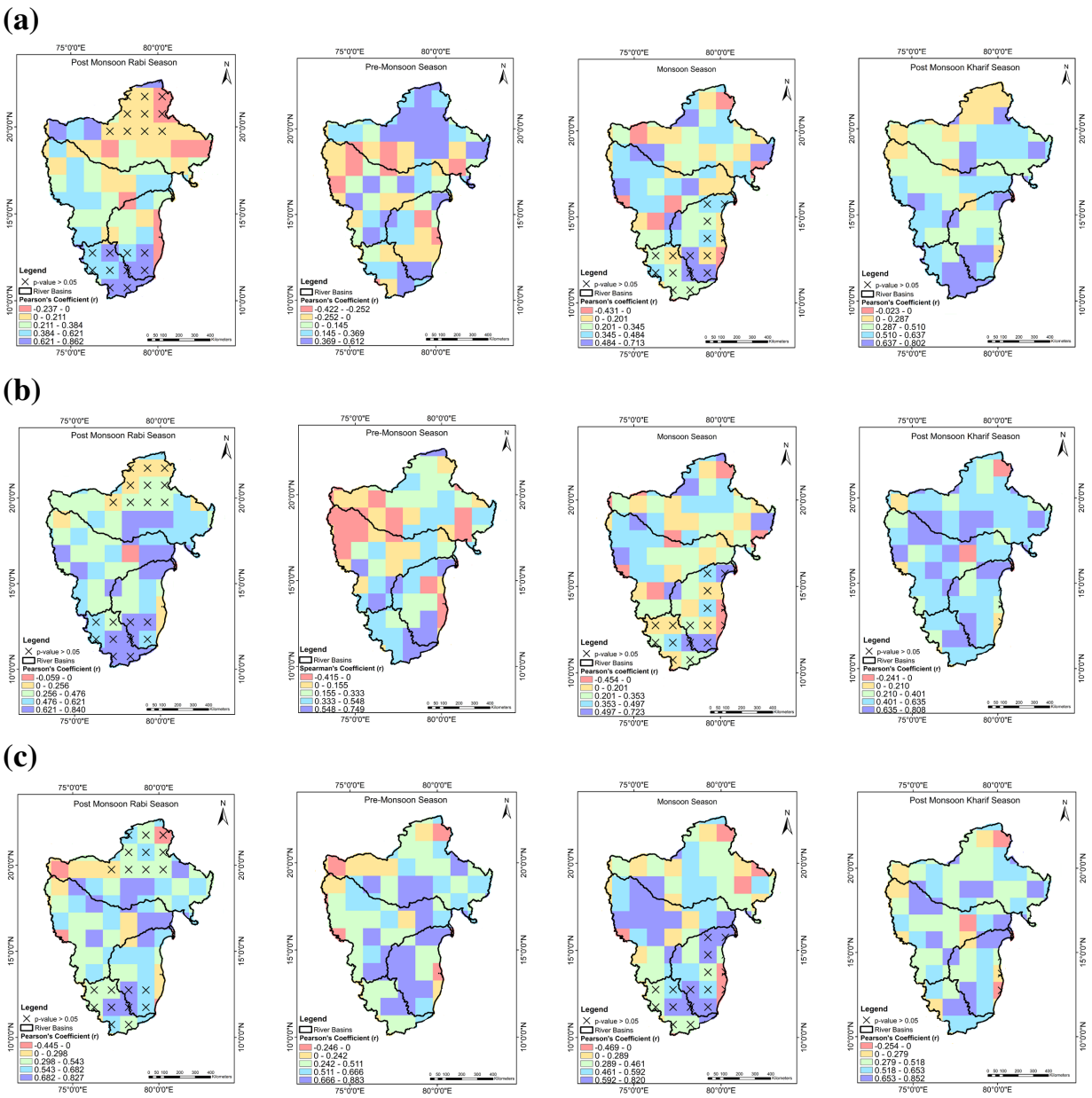

Figure 4.2: Pearson's correlation between (a) GRACE TWSA and SPI3, (b) GRACE TWSA and SPI6 and (c) GRACE TWSA and SPI12

From Fig. 4.2(c), GRB has shown almost positive significant correlation in the post-monsoon kharif season followed by the pre-monsoon and monsoon seasons with some negative significant correlations. In the post-monsoon rabi season, insignificant positive and negative correlations are observed in the mid to upper portions of GRB. In case of SPI3 and SPI6, GRB has shown significant positive correlation for post-monsoon kharif season whereas, for monsoon and pre-monsoon seasons significant positive and negative correlations are observed. PCRB has shown a significant positive correlation for SPI12 whereas, for SPI3 and SPI6 significant positive and negative correlation are observed in the pre-monsoon season. In the monsoon season, insignificant positive and negative correlations are observed in the middle and coastlines of PCRB. The post-monsoon kharif season has shown significant positive correlations. The post-monsoon rabi season has shown insignificant correlation in the South and significant correlation for remaining portion between TWSA and SPI.

4.3.1.2 Correlation between TWSA and SPEI

Similar analysis of correlation is performed between TWSA and SPEI for 3, 6 and 12 months represented by SPEI3, SPEI6 and SPEI12 respectively. The correlation of TWSA with SPEI3, SPEI6 and SPEI12 are presented in Fig. 4.3(a), Fig. 4.3(b) and Fig. 4.3(c) respectively. The post-monsoon rabi season has indicated highly significant positive correlation in SPEI6 and SPEI12, partly positive and negative significant correlation in SPEI3. The GRB has presented almost significant positive correlation in the post-monsoon kharif season (SPEI3 and SPEI6). The monsoon season of SPEI3 and SPEI6 and the pre-monsoon season of SPEI6 have exhibited more positive and a few negative significant correlations. The monsoon season of SPEI12, the pre-monsoon season of SPEI3 and SPEI12 have exhibited partially significant positive and negative correlations. The post-monsoon rabi season has indicated significant positive and negative correlations, and insignificant positive and negative correlations in the middle portion for SPEI6 and SPEI12. PCRB has shown positive correlation in the post-monsoon kharif and pre-monsoon seasons for SPEI. In the post-monsoon rabi season, insignificant correlations are observed in the South. Similarly, during the monsoon season, insignificant correlations (middle and coast) are observed. In CRB, highly significant positive correlations are observed in post-monsoon kharif and pre-monsoon seasons. Whereas, insignificant correlations are observed in the monsoon and post-monsoon rabi seasons at SPEI3, SPEI6 and SPEI12.

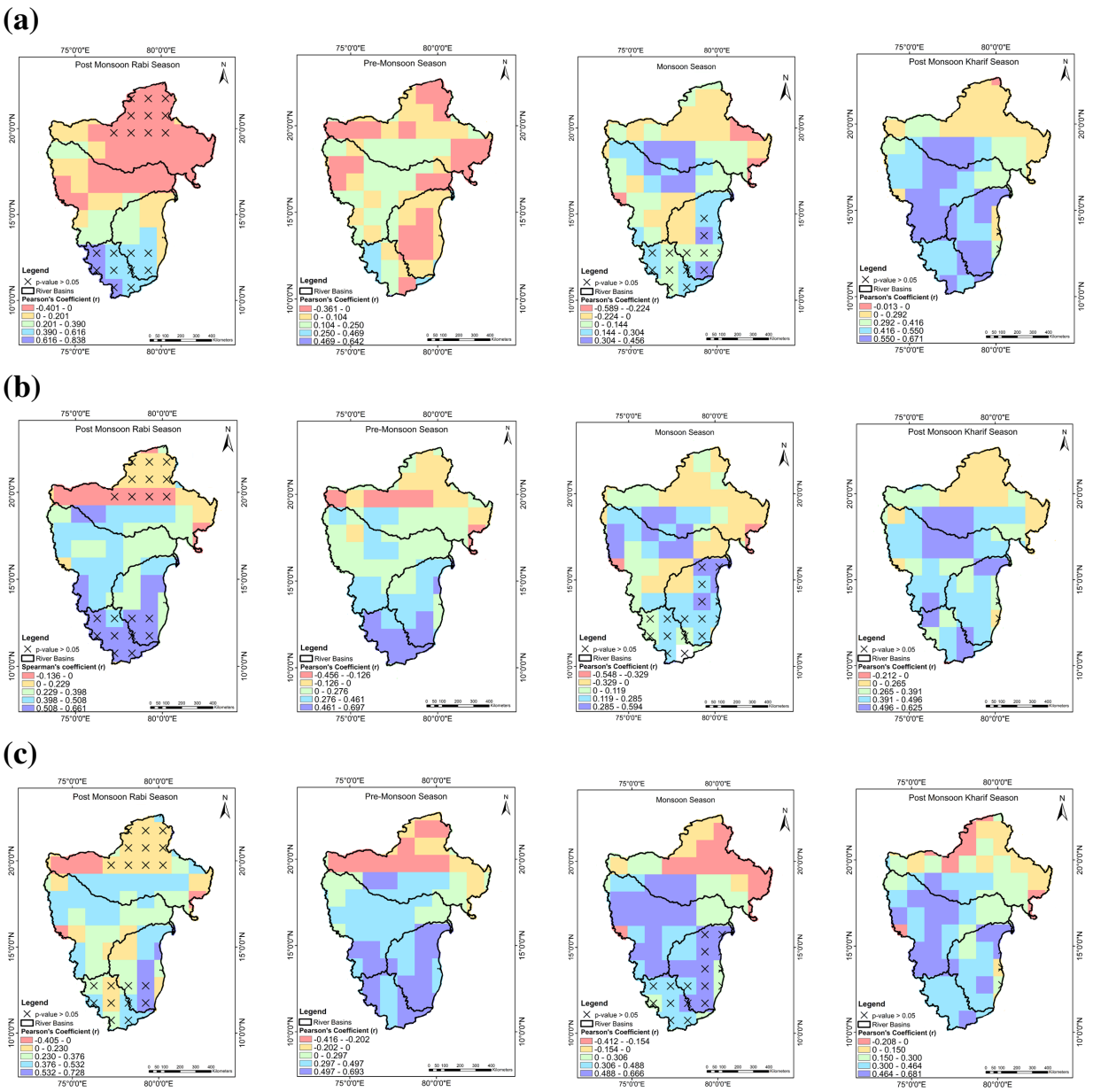

Figure 4.3: Pearson's correlation between (a) GRACE TWSA and SPEI3, (b) GRACE TWSA and SPEI6 and (c) GRACE TWSA and SPEI12

4.3.1.3 Correlation between TWSA and GRACE DSI

The analysis of TWSA and GRACE DSI Pearson correlation has shown highly positive correlation in almost all seasons as shown in Fig. 4.4. KRB has shown positive significant correlation in all seasons. GRB has indicated highly significant positive correlations in the pre-monsoon, post-monsoon kharif and monsoon seasons; however, insignificant correlations are observed in the middle and upper portions of the post-monsoon rabi season. CRB has shown significant highly positive correlations in the post-monsoon kharif and pre-monsoon seasons whereas insignificant correlations are observed in the monsoon and post-monsoon rabi seasons. PCRB has shown a

highly significant positive correlation in the pre-monsoon season. Insignificant positive correlations are observed in the post-monsoon rabi (down south) and monsoon seasons (along the coast and middle portion).

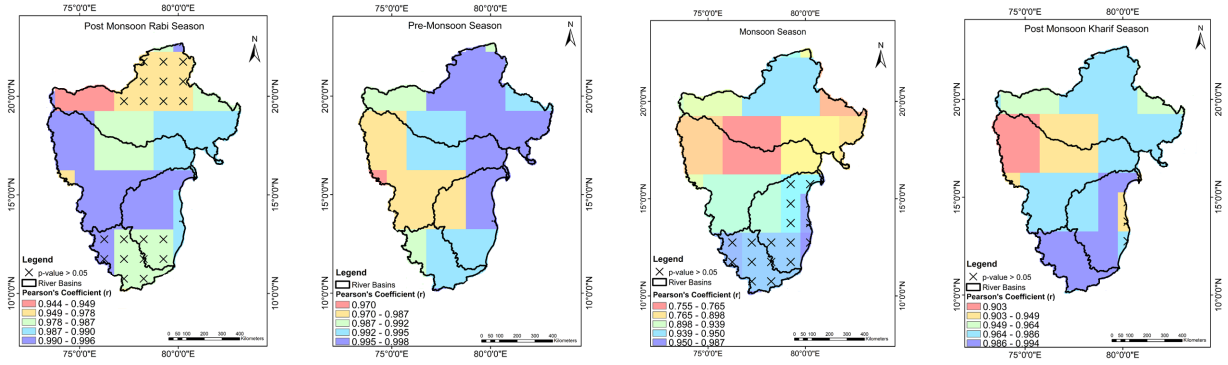

Figure 4.4: Pearson's correlation between GRACE TWSA and GRACE DSI

4.3.1.4 Correlation between TWSA and CCDI

The correlation of TWSA with CCDI has shown highly positive correlations for all seasons as shown in Fig. 4.5. KRB has shown highly significant positive correlation for all seasons due to anomalies of precipitation and TWS. GRB has shown highly significant positive correlation in the pre-monsoon and post-monsoon kharif seasons, followed by the monsoon season. In the post-monsoon rabi season, an insignificant positive correlation is noted over the upper portions of GRB. CRB has shown significant highly positive correlations in the post-monsoon kharif followed by the pre-monsoon season. The monsoon season has shown insignificant correlations followed by the post-monsoon rabi season. CCDI has shown the changes in surface, near surface and storage in the subsurface layers similar to TWSA.

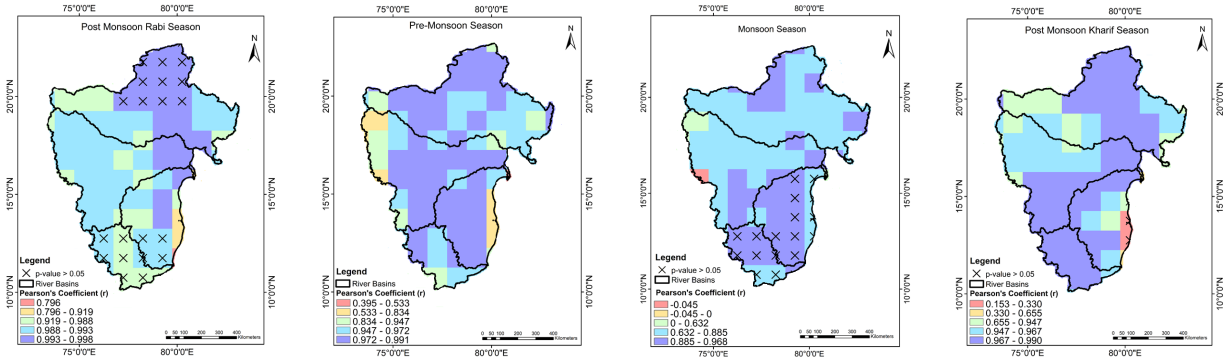

Figure 4.5: Pearson's correlation between GRACE TWSA and CCDI

4.3.1.5 Correlation between TWSA and SC_PDSI

Similar assessment of correlation for TWSA with SC_PDSI has shown positive correlation in almost all seasons as shown in Fig. 4.6. KRB has shown significant

positive correlation in the post-monsoon kharif and rabi seasons followed by the pre-monsoon and monsoon seasons. GRB has shown significant positive correlation in the post-monsoon kharif followed by pre-monsoon and monsoon seasons. CRB has shown highly significant positive correlations in the post-monsoon kharif and pre-monsoon seasons, whereas insignificant correlations are observed in the monsoon and post-monsoon rabi seasons. PCRB has shown both significant positive and negative correlation in the pre-monsoon season. The post-monsoon rabi season has shown insignificant correlation specifically in the South and significant positive correlation in the North and middle portion of PCRB. The post-monsoon kharif has shown significant positive correlation.

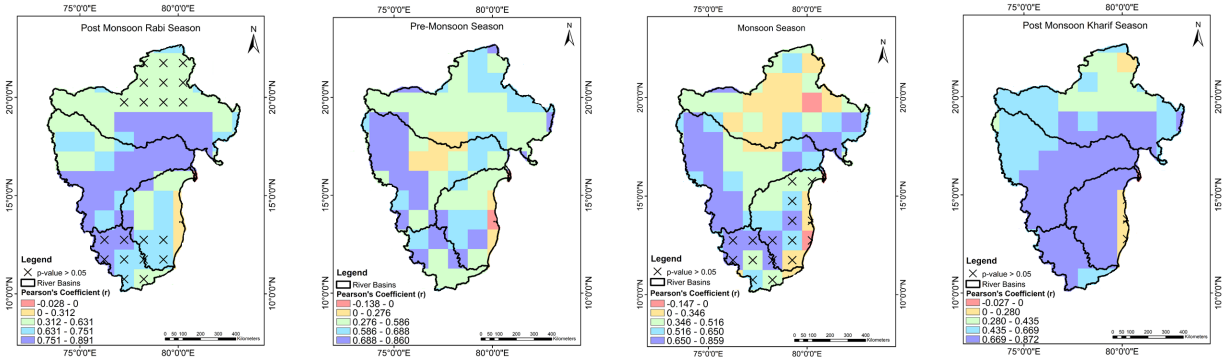

Figure 4.6: Pearson's correlation between GRACE TWSA and SC_PDSI

4.3.1.6 Correlation between TWSA and GGDI

The analysis of TWSA and GGDI Pearson correlation has shown highly positive correlation in almost all seasons as shown in Fig. 4.7. KRB has shown positive significant correlation in all seasons. GRB has shown highly significant positive correlations in the monsoon and post-monsoon rabi seasons. CRB and PCRB have shown significant highly positive correlations in the post-monsoon kharif and pre-monsoon seasons.

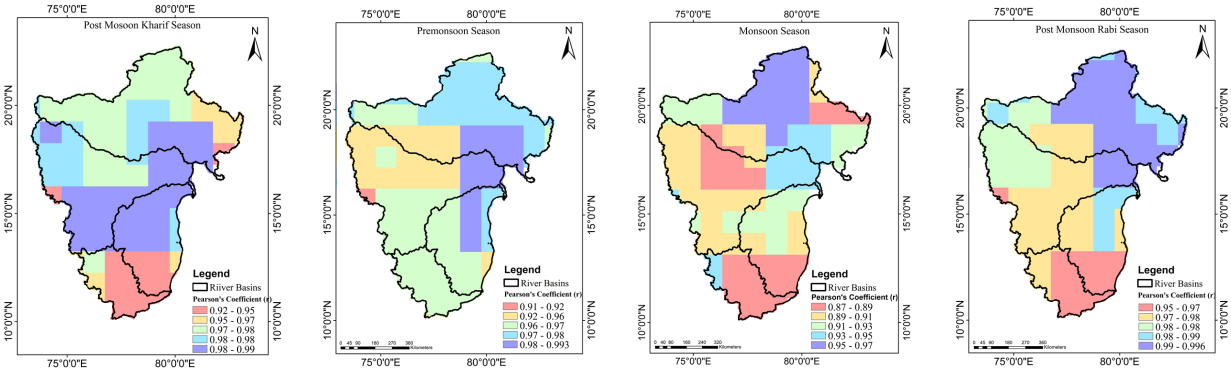

Figure 4.7: Pearson's correlation between GRACE TWSA and GGDI

4.3.2 Monthly Analysis

4.3.2.1 Correlation Analysis Among Commonly Used Drought Indices

The correlation matrix of CCDI, GRACE DSI, GGDI, SC_PDSI, SPEI12 and SPI12 drought indices over four basins is shown in Table 4.4. The correlation matrix of drought indices is evaluated from January 2003 to December 2016. The SPI and SPEI time series are compared over a 12-month time scale. There is a general agreement across multiple drought indices, despite some differences among the indices considered. The estimated correlation coefficients (r) between CCDI and GRACE DSI for GRB, KRB, CRB and PCRB are 0.79, 0.8, 0.92 and 0.81 respectively.

Table 4.4: Correlation matrix of drought indices for four river basins.

	CCDI	**GRACE DSI**	**SC_PDSI**	**SPEI12**	**SPI12**	**GGDI**
GRB						
CCDI	1					
GRACE DSI	0.79	1				
SC_PDSI	0.26	0.22	1			
SPEI12	0.18	0.17	0.15	1		
SPI12	0.73	0.59	0.30	0.78	1	
GGDI	0.93	0.77	0.28	0.15	0.7	1
KRB						
CCDI	1					
GRACE DSI	0.80	1				
SC_PDSI	0.82	0.67	1			
SPEI12	0.60	0.52	0.53	1		
SPI12	0.80	0.66	0.78	0.75	1	
GGDI	0.93	0.79	0.79	0.48	0.76	1
CRB						
CCDI	1					
GRACE DSI	0.92	1				
SC_PDSI	0.78	0.75	1			
SPEI12	0.59	0.59	0.68	1		
SPI12	0.74	0.67	0.68	0.71	1	
GGDI	0.94	0.93	0.78	0.56	0.71	1
PCRB						
CCDI	1					
GRACE DSI	0.81	1				
SC_PDSI	0.83	0.70	1			
SPEI12	0.50	0.51	0.65	1		
SPI12	0.75	0.61	0.77	0.74	1	
GGDI	0.93	0.84	0.82	0.51	0.71	1

A high correlation is observed between GGDI and CCDI, GRACE DSI. GGDI is also correlated well with SPEI12, SPI12 and SC_PDSI in all the river basins as shown in Table 4.4. As CCDI, GGDI and GRACE DSI are more responsive to TWSA variations from GRACE, there is a good correlation among CCDI, GGDI and GRACE DSI. The highest correlation between these three indices is observed in CRB. GRACE DSI is calculated using a single variable i.e., TWSA. Whereas, CCDI is evaluated using the combined effect of precipitation and TWSA. Therefore, the difference in correlation is observed between CCDI and GRACE DSI as the precipitation anomaly is included along with TWSA.

Similarly, scatter plots of CCDI with other indices (SC_PDSI, SPEI12 and SPI12) are also plotted for all basins and represented in Fig. 4.8.

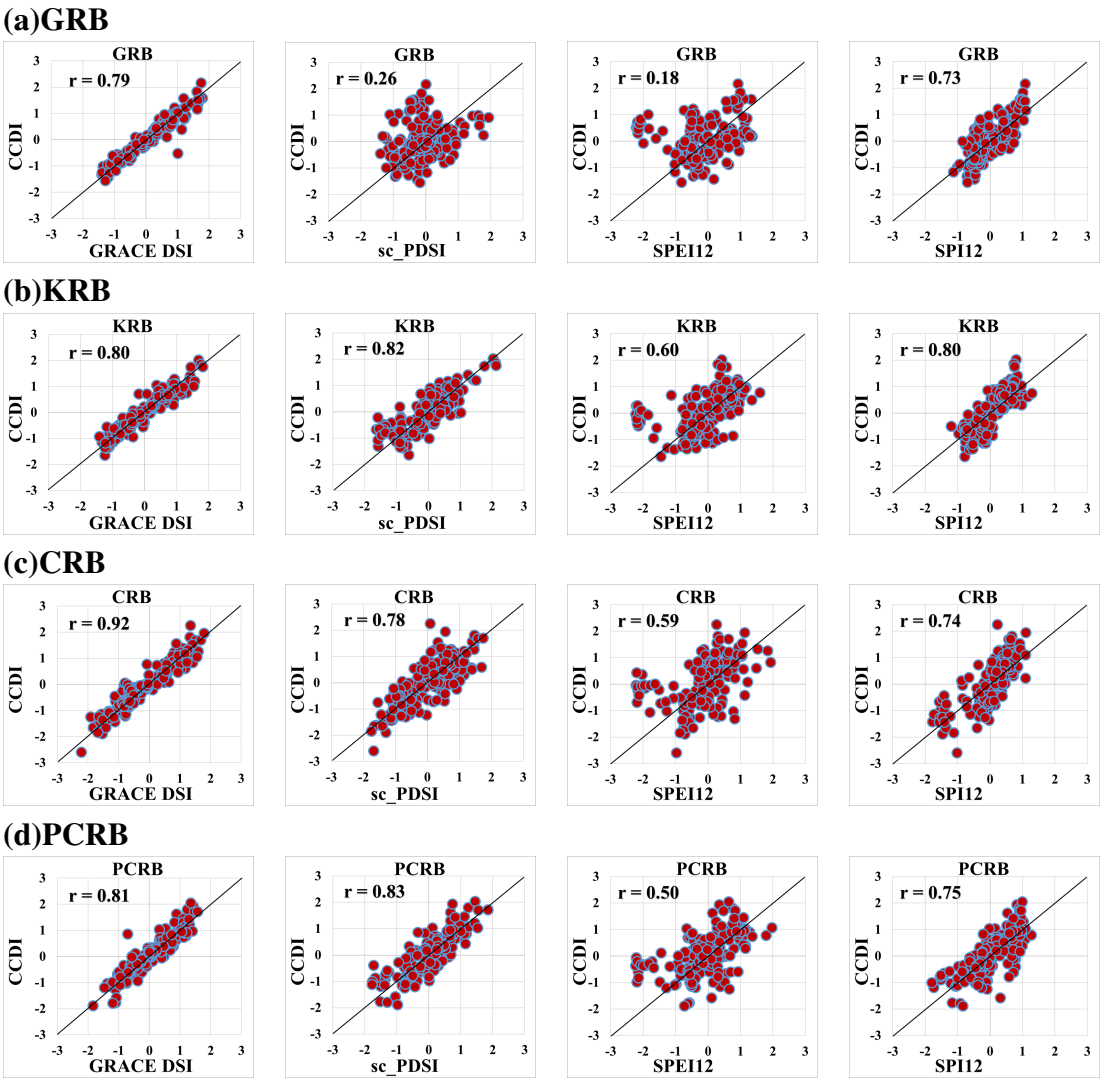

Figure 4.8: Basin wide scatter plots for (a) GRB, (b) KRB, (c) CRB and (d) PCRB between TWSA from GRACE and CCDI

As CCDI integrates precipitation and TWSA for drought assessment, SPI12 is evaluated using precipitation and a good correlation of 0.73, 0.80, 0.74 and 0.75 is observed between CCDI and SPI12 subsequent to GRACE DSI. Comparatively, CCDI has shown a good correlation with SPEI12 and SC_PDSI in the remaining three river basins (KRB, PCRB and CRB) as shown in Table 4.4. GRACE DSI is highly correlated with CCDI, moderately correlated with SPI12 and SPEI12, and poorly correlated with SC_PDSI.

GGDI is evaluated using TWSA from GRACE and LSM data (soil moisture and canopy water storage from GLDAS). Along with CCDI and GRACE DSI, GGDI has displayed high correlations with SPI12, SPEI12 and SC_PDSI in all the basins, except GRB. Among four basins, the highest correlation between GGDI and other indices is observed in CRB, followed by PCRB. GGDI has shown a correlation of $>$0.7 with SPI12 in all the basins.

The SC_PDSI has shown high correlation with CCDI and GRACE DSI compared to other drought indices for KRB, CRB and PCRB except GRB. Additionally, SC_PDSI has shown good correlation with SPI12 followed by SPEI12. Among the four river basins, the lowest correlation coefficient of r = 0.15 is observed between SC_PDSI and SPEI12 for GRB. SC_PDSI is capable at mid-term and long-term time spans whereas SPEI12 is convenient at a long-term span. SPI12 and SPEI12 are evaluated using precipitation and evapotranspiration and resulted in good correlation of 0.78, 0.75, 0.71 and 0.74 for GRB, KRB, CRB and PCRB respectively. SPI12 is well correlated with CCDI (0.80), GRACE DSI (0.66), SC_PDSI (0.78) and SPEI12 (0.75) for KRB and poorly correlated with other indices for GRB with the lowest being 0.3 between SPI12 and SC_PDSI. SPEI12 is well correlated with the remaining indices for CRB and poorly correlated for GRB. The major part of GRB consists of agricultural lands i.e., 60% and the forest area covers approximately 30%. Demand for surface water exceeds the availability. Therefore, the availability of water storage is less in GRB, which effects the correlation of TWSA with SPI12 and SC_PDSI.

4.3.2.2 Basin Wide Drought Event Analysis

The time series of CCDI, GGDI, GRACE DSI, SC_PDSI, SPEI12, SPI12 and TWSA for the four river basins considered in the study are represented in Fig. 4.9. The solid red, solid green, light green, black, orange, dashed blue and blue lines represent CCDI, GGDI, GRACE DSI, SPI12, SC_PDSI, SPEI12 and TWSA; the light red shaded area signifies the period of drought events described by the values of these four drought indices given by NRAA, India (NRAA, 2013). For the characterisation, dry spells of three or more months of drought are taken into account in this study (Thomas et al.,

2014). Drought events identified by the indices are denoted as 'DE' with the event order and river basin name. For instance, the drought event for GRB is denoted as $DE1^{GRB}$.

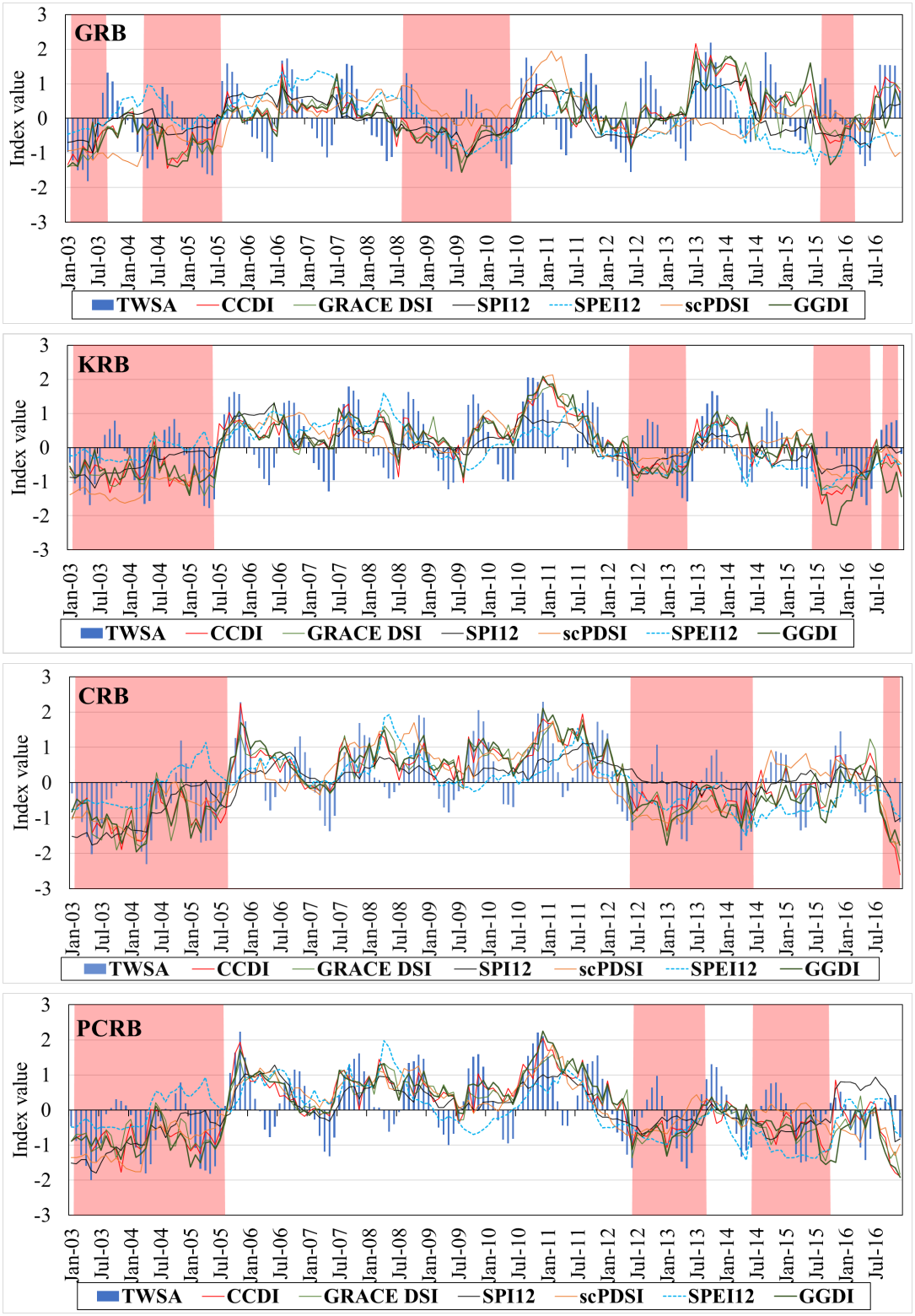

Figure 4.9: Monthly time series of TWSA from GRACE, CCDI, GRACE DSI, SPEI12, SC_PDSI and SPI12. (Red bands indicate major drought events).

In Fig. 4.9, with reference to CCDI, GGDI, GRACE DSI, SC_PDSI, SPEI12, SPI12 and TWSA; four drought events are observed in GRB i.e., during January 2003–August 2003 ($DE1^{GRB}$), April 2004–May 2005 ($DE2^{GRB}$), September 2008–May 2010 ($DE3^{GRB}$) and September 2015–February 2016 ($DE4^{GRB}$). Among the four drought events, $DE1^{GRB}$ and $DE3^{GRB}$ are characterised as D1 (moderate drought), $DE2^{GRB}$ is represented as D2 (severe drought) and $DE4^{GRB}$ as D0 (abnormal drought). $DE3^{GRB}$ is the longest drought period observed in GRB extending for 21 months between 2008 and 2010.

From Fig. 4.9, three drought events are observed for KRB, $DE3^{KRB}$ is characterised as D2 (severe drought) during July 2012–April 2013, $DE1^{KRB}$ and $DE2^{KRB}$ as D1 (moderate drought) during January 2003–May 2005 and June 2012–April 2013, respectively. $DE3^{KRB}$ is the most severe drought identified in the KRB. The longest drought period observed in KRB is $DE1^{KRB}$, which continued for 29 months from 2003 to 2005.

Three drought events are observed for CRB, $DE1^{CRB}$ is characterised as D3 (extreme drought) from January 2003 to August 2005, which is the longest drought period as shown in Fig. 4.9. $DE2^{CRB}$ and $DE3^{CRB}$ comes under D1 (moderate) and D3 (extreme) respectively. Three drought events are observed for PCRB during January 2003–July 2005 ($DE1^{PCRB}$: characterised as D1), 12 July–13 August ($DE2^{PCRB}$ characterised as D0) and 14 July–15 September ($DE3^{PCRB}$ characterised as D0) as shown in Fig. 4.9. Overall, CCDI and GGDI are observed as good predictors of drought for the four basins considered in the study.

4.3.3 Basin Wide Drought Characteristics Using CCDI

The severity and duration characteristics of CCDI for all the basins are presented in Table 4.5. In GRB, severity is observed as 11.72 for 22 months of duration (September 2008 to June 2010). A total of 62 months of drought duration is observed in GRB. In KRB, the highest severity (12.01) is observed for 17 months from January 2003 to May 2004. In PCRB, the highest severity (14.79) is observed for 16 months from January 2003 to April 2004. In CRB, the highest severity (18.89) is observed during the same period as in KRB. Drought duration of 62 months for GRB, 67 months for KRB, 71 months for PCRB and 78 months for CRB are observed.

Table 4.5: Summary of drought severity and duration from CCDI.

Time period	Severity	Duration (No. of months)
GRB		
Jan to Nov 2003	8.37	11
Mar 2004 to Jun 2005	10.84	16
Sep 2008 to Jun 2010	11.72	22
Feb to Jul 2012	2.29	6
Aug 2015 to Feb 2016	3.29	7
KRB		
Jan 2003 to May 2004	12.01	17
Jul 2004 to Jun 2005	9.90	12
May 2012 to May 2013	7.46	13
Jun to Dec 2014	2.00	7
Jul 2015 to Jun 2016	12.46	13
Aug to Dec 2016	2.51	5
PCRB		
Jan 2003 to Apr 2004	14.79	16
Aug 2004 to Aug 2005	10.36	13
May 2012 to Jul 2013	8.79	15
Jun 2014 to Oct 2015	9.07	17
Jan to May 2016	0.97	5
Aug to Dec 2016	6.68	5
CRB		
Jan 2003 to May 2004	18.89	17
Jul 2004 to Aug 2005	11.59	14
Dec 2006 to Jun 2007	0.91	7
May 2012 to May 2013	8.14	13
Jul 2013 to Jul 2014	6.34	13
Sep to Dec 2014	1.32	4
Feb to Jun 2015	0.70	5
Aug to Dec 2016	8.04	5

4.4 DISCUSSIONS

This study has investigated six different drought indices in four river basins of South India at three different time scales with TWSA. SPI, a precipitation-based drought index, is linked with various physical processes, topography, atmospheric and oceanic circulation, and local processes in India. Using a single precipitation indicator can be problematic in evaluating the Indian monsoon cycle as moisture, terrain and vegetation can affect variation in precipitation at the regional and basin scales (Wang et al., 2015b). The results suggest that SPI has shown almost good significant correlation in the pre-monsoon season and post-monsoon kharif followed by the monsoon and

post-monsoon rabi seasons. Significant correlation between TWSA and SPI is evident, indicating that TWSA can be used in combination with SPI for drought assessment. The agricultural land areas for GRB, KRB, PCRB and CRB are 59.57%, 75.86%, 58.64% and 66.21% respectively (www.india-wris.nrsc.gov.in). Due to different crop patterns in the agricultural land during monsoon and post-monsoon seasons, insignificant correlation is observed between TWSA and all other indices.

SPEI indicates the availability of water driven by climate demand similar to that of PDSI, whereas SPI does not include soil moisture. SPEI is the summation of precipitation and evapotranspiration and measures normalised changes in moisture availability. Evapotranspiration is mainly used to define soil moisture changes and water content in vegetation (Vicente-Serrano et al., 2010). Water levels and moisture conditions are affected by meteorological conditions (physical geography and human interventions) both spatially and temporally (Jing et al., 2015). A few studies have reported that SPEI is useful to examine variations temporally (Fei et al., 2016; Li et al., 2012). In arid regions, as precipitation and evapotranspiration can be constraints, SPEI produces poor fit results (Beguería et al., 2014). From this study, it is concluded that SPEI 3, 6 and 12 months have agreed well with TWSA and can be used as a suitable tool for drought assessment over large areas.

Correlation between SC_PDSI and TWSA has shown a better fit. In the calculation of SC_PDSI, soil moisture is considered to be evaluated with evapotranspiration (demand) and precipitation (supply) using the water balance equation. SC_PDSI is considered as a multifactorial water budget indicator that takes into account monthly precipitation, temperature and soil properties. Soil moisture storage is calibrated by separating the soil column into layers with available moisture at field capacity. The detailed procedure for the evaluation of PDSI and SC_PDSI can be found in Alley (1984); Karl (1986); Wells et al. (2004). SC_PDSI has shown good positive fit for all the seasons except in the monsoon season of PCRB and CRB, and the post-monsoon rabi of GRB, PCRB and CRB. This result is observed in other studies in which PDSI is constant, while the values of TWS decreased in the summer and spring (Dai et al., 2004; Long et al., 2013). This can be inferred from the fact that variation in the correlation is largely related to the spatial extent of precipitation and more commonly to the atmospheric circulation (Mika et al., 2005). Seasonal fluctuation is observed mainly in large river basins. A high correlation is noted between TWSA and SC_PDSI for China (Dai, 2011b). It is clear that the correlation between TWSA and SC_PDSI have shown highly positive correlation compared to all other indices followed by CCDI.

GGDI is evaluated using TWSA comprising surface and subsurface water components. GGDI is highly correlated with TWSA as it is based on direct measurements of the water balance components that account for water supply (from rainfall) and demand (from evapotranspiration and runoff) (Zhao et al., 2017b). GGDI and CCDI are also strongly correlated as source for the evaluation of these indices are the same i.e., TWSA from GRACE.

CCDI is a combined with anomalies of precipitation and TWSA. This explains changes in surface, near surface and groundwater conditions. It is important to understand that the combination of precipitation and storage differences may have triggered disagreements with other indices while it has been proved to be reasonable for good correlation with TWSA. It is also observed that CCDI and SC_PDSI correlations are almost identical in all the river basins for all seasons except for GRB.

The dataset of TWSA is a combination of hydroclimatic and anthropogenic factors. Various river basins of varying physical characteristics are considered in this study; therefore, different correlation values with drought indices have been observed. CCDI and GGDI has performed well compared to all other indices. Subsequently, SC_PDSI, GRACE-DSI, SPEI12 and SPI12 have exhibited good correlation. It is concluded from the results that CCDI and GGDI have performed better to characterise storage and drought.

In this study, the correlation matrix for drought indices: CCDI, GGDI, GRACE DSI, SC_PDSI, SPEI12 and SPI12 suggest that (see Table 4.4) all the basins had demonstrated high correlation between CCDI and GGDI, as both are calculated using TWSA dataset comprising all forms of water stored above and below the land surface. SPI12 and SPEI12 are more responsive to precipitation and evapotranspiration, resulting in a high correlation between them. The SC_PDSI has shown a better fit for CCDI and GGDI than other drought indices considered for analysis. This is because SC_PDSI considers the soil moisture content of the model algorithm, which is also the main component in TWSA. Notwithstanding the inconsistencies between the drought indices and the method used to compute the indices, it is clear that droughts can be better understood by a combination of indices.

4.5 CONCLUSIONS

During the period between 2002 and 2016, this study examined and evaluated the drought conditions in four major river basins in India. GRACE-satellite data provided important benefits to the field of hydrology, revealing information about large-scale groundwater depletion and droughts. CCDI, GGDI, GRACE DSI, SC_PDSI, SPEI12 and SPI12 are used to analyse and characterise the stressed regions with TWSA in four

river basins. In addition, multiple drought indices are compared and similarities and differences in drought conditions are investigated. Furthermore, basin scale drought events are evaluated using CCDI, GGDI, GRACE DSI, SPEI12, SPI12 and SC_PDSI. Drought characteristics are evaluated to observe the severity and duration among all the basins using CCDI. The following conclusions are made from the study of the first sub objective.

- CCDI and GGDI correlated well with TWSA in capturing both spatial and temporal drought conditions over four river basins.
- CRB experienced strongest association between CCDI and GGDI with other indices when compared to other basins.
- KRB manifested high storage anomalies leading to strong seasonal fluctuation in drought indices.
- From the drought event analysis of KRB, as it stands out among other basins during 2003 to 2005, the most severe drought lasted for 29 months. Assessment of these extreme hydrologic conditions are critical and possible when the analysis is aided with remote-sensing data for better management of regions the water resources.
- Drought severity and duration are evaluated using CCDI. From a total of 180 months, a period of 62 months for GRB, 67 for KRB, 71 for PCRB and 78 for CRB are observed. Knowledge about duration and spatial extent of drought from both hindcast and real-time analysis of drought indices within the context of TWSA serves as a powerful tool for planning and management of the land and water resources of these major river basins.
- Although differences are found between indices, the shifting trend and peak time are consistent.

CHAPTER 5

GGDI FOR DROUGHT CHARACTERIZATION AND ITS LINKAGE TO TELECONNECTION FACTORS

This chapter deals with the second sub objective that evaluates drought characteristics using GRACE groundwater drought index and its linkage to teleconnection factors.

5.1 INTRODUCTION

Due to large-scale climate variations in India, the spatio-temporal availability of surface and groundwater is very diverse and affects the agricultural and industrial productivity of the country (Bhuvaneswari et al., 2013). The 2016 drought in India affected 330 million people with more than $\$100$ billion loss in the economy. From this perspective, for the conservation of water resources, it is crucial to understand the variations of surface water and groundwater and its association with the teleconnection in India.

Many studies have investigated drought characteristics at regional and basin scales throughout the world using TWSA. These studies verified the capabilities of drought using GRACE data only but not the associations between droughts evaluated using GRACE data and teleconnection factors. It is clear from earlier studies that teleconnection factors have a major effect on drought (Dai, 2011a; Wang et al., 2015a). Many worldwide attempts have been made over past to establish the relationship between climate variability and TWSA, with most studies focused on ENSO. Climate variables directly or indirectly influence the drought that results in detailed investigation between them.

To the best of our knowledge, previous studies have focused on the relationship of several atmospheric variables like precipitation, temperature, vapor pressure and humidity with teleconnections in India (Gehlot et al., 2021; Gupta and Jain, 2020, 2021; Sharma et al., 2020). Nonetheless, a comprehensive and systematic analysis between GRACE and teleconnections is vague and in particular for India. Therefore, the second sub objective addresses the research gap by exploring the drought situation over South Indian River Basins with GGDI and identifying the linkages between drought and large-scale climate oscillations during 2003-2016. The effect of four major climate oscillations namely MEI, SOI, DMI and NINO3.4 on GGDI are assessed using TWSA dataset from GRACE during 2003–2016. The detailed analysis is

accomplished for GRB, KRB, PCRB and CRB to illustrate the linkages between GGDI and climate oscillations. Also, gridded monthly and seasonal drought trends are evaluated using the **M**odified **M**ann-**K**endall (MMK) trend test. Seasonal trends are evaluated for four seasons of India namely (i) post-monsoon rabi, (ii) pre-monsoon, (iii) monsoon and (iv) post-monsoon kharif. Flowchart of the second sub objective is presented in Fig. 5.1.

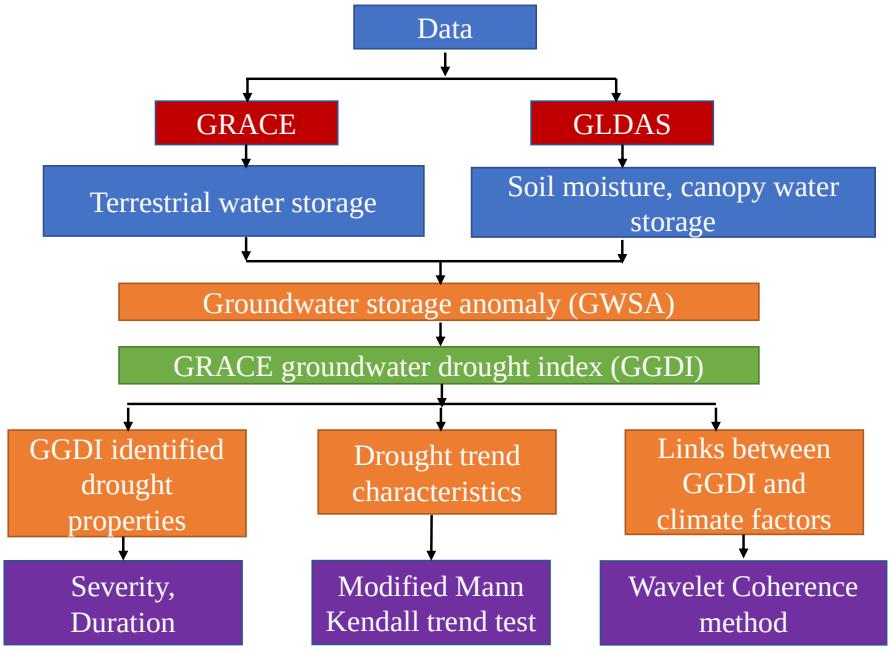

Figure 5.1: Flow chart of second sub objective

5.2 METHODOLOGY

5.2.1 Retrieval of Groundwater Storage Change from GRACE and GLDAS

TWSA is derived from GRACE satellite observations. The GWSA at any time t, has been calculated by subtracting **S**oil **M**oisture **S**torage **A**nomalies (SMSA), **C**anopy **W**ater **S**torage **A**nomalies (CWSA) from TWSA. The SMSA has been calculated for GLDAS Noah land surface model using the following equation

$$SMSA_t = SMS_t - \overline{SMS_{2004-2009}} \tag{5.1}$$

where, $SMSA_t$ = soil moisture storage anomaly w.r.t time t, SMS_t = soil moisture storage at time t, $\overline{SMS_{2004-2009}}$ = average soil moisture storage w.r.t the base line period from January 2004 to December 2009, same as that of GRACE. Similarly, CWSA has been calculated for GLDAS Noah land surface model using the following equation

$$CWSA_t = CWS_t - \overline{CWS_{2004-2009}} \tag{5.2}$$

where, $CWSA_t$ = canopy water storage anomaly w.r.t time t, CWS_t = canopy water storage at time t, $\overline{CWS_{2004-2009}}$ = average canopy water storage w.r.t the base line period from January 2004 to December 2009, same as that of GRACE. Therefore, GWSA is calculated as:

$$GWSA_t = TWSA_t - SMSA_t - CWSA_t \tag{5.3}$$

5.2.2 Modified Mann-Kendall (MMK) Trend Test

This study implemented MMK trend test to evaluate the spatial drought trend characteristics over four river basins of South India from 2003-2016. Consider a sequence X_T and divide it by the mean of this series to obtain a new series X_t. Null hypothesis (H_0) is: no trend in the series over time. Alternate hypothesis (H_1) is: existence of increasing or decreasing trend. The trend estimator β of the rank for the new series is calculated as:

$$\beta = median\left(\frac{x_i - x_j}{i - j}\right) \qquad 1 \leq i < j \leq n \tag{5.4}$$

where $\beta > 0$ represents upward trend and $\beta < 0$ represents downward trend. If the trend part T_t of the new series X_t is linear then trend part is removed to obtain the stationary series Y_t.

$$Y_t = X_t - T_t = X_t - \beta \times t \tag{5.5}$$

The rank corresponding to series Y_t is calculated and its corresponding autocorrelation coefficient r_i is obtained.

$$r_i = \frac{\sum_{k=1}^{n-i}(R_k - \bar{R})(R_{k+i} - \bar{R})}{\sum_{k=1}^{n}(R_k - \bar{R})^2} \tag{5.6}$$

where $\bar{R}$ is the average rank and R_i is the rank of y_i. The variance $V(S)$ of the trend statistic S of autocorrelation series is obtained as follows:

$$V(S) = \eta \times \frac{n(n-1)(2n+5)}{18} \tag{5.7}$$

$$\eta = 1 + \frac{2}{n(n-1)(n-2)} \times \sum_{i=1}^{n-1}(n-i)(n-i-1)(n-i-2)r_i \tag{5.8}$$

The test statistic Z is calculated as

$$Z = \begin{cases} \frac{S-1}{\sqrt{V(S)}} & S > 0 \\ 0 & S = 0 \\ \frac{S+1}{\sqrt{V(S)}} & S < 0 \end{cases} \tag{5.9}$$

At α significance level, the null hypothesis of no trend is rejected if the absolute value of standardized test statistic Z is greater than the theoretical value $Z_{1-\alpha/2}$. For example, at the 5% significance level, the null hypothesis is rejected if $Z > 1.96$. A higher magnitude of Z value indicates that the trend is more statistically significant.

5.2.3 Teleconnections

The atmospheric circulation transmits energy and water mass across very long distances to remote locations due to the interaction of ocean-atmosphere and land-atmosphere. As a result, climatologic fluctuations are transmitted via atmospheric circulation through heat, moisture and momentum fluxes. These transmitted atmospheric circulations are delivered in the form of precipitation and evaporation via the large-scale continental water cycle and ocean circulation (Wallace and Gutzler, 1981). As a result, atmospheric circulation can be thought of as a driving force that influences both land and sea, resulting in significant climate fluctuation (Alexander et al., 2002). This variability shows patterns that occur on a variety of time ranges, including diurnal, daily, weekly and monthly time scales, as well as intra-seasonal, seasonal and interannual time scales. As a result, teleconnections serve as a conceptual framework for summarising atmospheric interactions and describing transport processes, as well as a method for converting climate variability into a set of indices. The term teleconnection is introduced by Walker in 1924 (British meteorologist) to assess the correlations between atmospheric pressure, temperature and rainfall. A teleconnection map describes the connection between a region of interest and all other locations in the domain. Table 5.1 represents the commonly used climate indices, including their full names and acronyms. In the present study, the effect of four major climate oscillations, namely, MEI, SOI, DMI and NINO3.4 on TWSA are assessed for Indian River Basins. Fig. 5.2 represents the regions used to monitor ENSO, SOI and IOD events.

El Niño Southern Oscillation (ENSO): ENSO is a periodic fluctuation in sea surface temperature (El Niño) and the air pressure of the overlying atmosphere (Southern Oscillation) across the equatorial Pacific Ocean. ENSO is thought to be the most important source of global inter-annual climate fluctuation. In many places of the world, the presence of an El Niño, or its polar opposite, La Niño, sufficiently alters the

Table 5.1: The commonly used climate indices, including their full names and acronyms

Index full name	Acronym
El Niño Southern Oscillation	ENSO
Southern Oscillation Index	SOI
Multivariate ENSO Index	MEI
North Atlantic Oscillation	NAO
Oceanic Nino Index	ONI
Pacific Decadal Oscillation	PDO
Arctic Oscillation	AO
Pacific North America	PNA
Antarctic Oscillation	AAO
Indian Ocean Dipole	IOD
Sea Surface Temperature	SST
Indian Summer Monsoon Index	ISMI

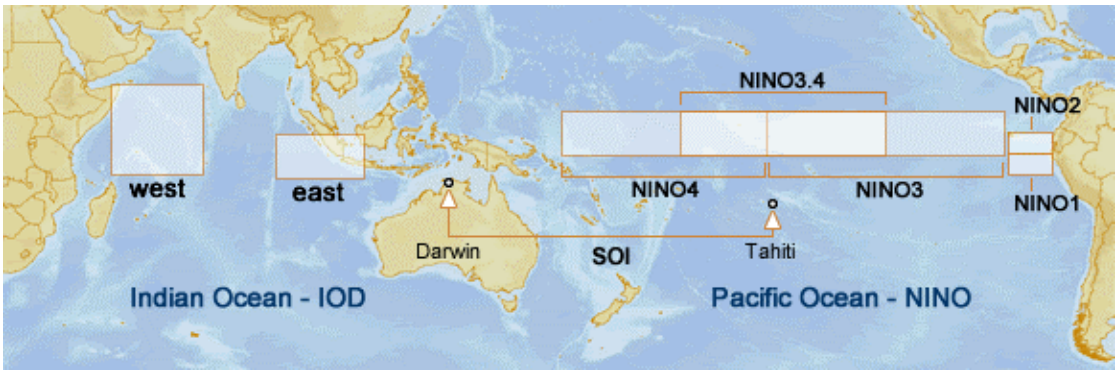

Figure 5.2: Regions used to monitor ENSO, SOI and IOD events.

general flow of the atmosphere to affect weather conditions. ENSO has been described by four indices namely Nino 1+2, Nino 3, Nino 4 and Nino 3.4 that are defined by SST anomalies in a specific region of the equatorial Pacific. The Niño 3.4 is the most widely used index covering the region between 5°S-5°N latitudes and 170°W-120°W longitudes. El Niño (warm sea surface temperature) conditions are indicated by positive values, whilst La Niño (cold sea surface temperature) conditions are indicated by negative values of the index.

Southern Oscillation Index (SOI): The SOI is a standardised index that is based on observed changes in sea level pressure between Tahiti and Darwin, Australia. During El Niño and La Niño phases, the SOI measures the large-scale air pressure fluctuations between the western and eastern tropical Pacific. Smoothed time series of the SOI often correlate well with variations in ocean temperatures in the eastern tropical Pacific. At Tahiti, the negative phase of the SOI reflects below-normal air pressure, while at Darwin, it represents above-normal air pressure. During El Niño (La Niño) occurrences,

prolonged periods of negative (positive) SOI values are associated with exceptionally warm (cold) ocean waters in the eastern tropical Pacific.

Multivariate ENSO Index (MEI): The MEI is a method that combines both oceanic and atmospheric variables to characterize the intensity of an ENSO event. The MEI is calculated from the first principal component of the six primary observed variables like sea level pressure, sea surface temperature, zonal and meridional components of surface wind, surface air temperature and total cloudiness fraction of the sky across the tropical Pacific. MEI is calculated using the **C**omprehensive **O**cean **A**tmosphere **D**ata **S**et (COADS). The MEI is calculated for each of the twelve sliding bi-monthly periods, such as December/January, January/February and so on. El Nino is represented by positive MEI values, while La Nina is represented by negative MEI values.

Dipole Mode Index (DMI): The IOD events are determined by the changes in the tropical Indian Ocean. IOD events are defined by long-term fluctuations in the SSTs over the tropical Western and Eastern Indian oceans. The IOD is generally assessed using an index defined as the difference between two tropical Indian ocean SST anomalies. The DMI is also known as IOD. IOD West covers the region between 50°E to 70°E and 10°S to 10°N. IOD East covers the region between 90°E to 110°E and 10°S to 0°S (see Fig. 5.2). When DMI is positive (or negative) then the water in the tropical Eastern Indian ocean is cooler (or warmer) and the water in tropical Western Indian ocean is warmer (or cooler) than the average.

Correlation analysis has been widely used to extract teleconnection patterns. As a method of building teleconnection maps, correlation analysis is simple and straight forward. The teleconnection map is a representation of the correlation between two points. For example, Wallace and Gutzler, 1981 performed the correlation analysis to examine the **N**orth **A**tlantic **O**scillation (NAO), the **N**orth **P**acific **O**scillation (NPO) and the **P**acific-**N**orth **A**merica (PNA). **P**rincipal **C**omponent **A**nalysis (PCA) is also a very commonly used approach to determine teleconnections patterns that are spatially and temporally orthogonal (Diaz et al., 2001). Furthermore, an enhanced PCA method known as rotated PCA has gained popularity for producing teleconnection patterns (McCabe et al., 2004). On the other hand, **E**mpirical **O**rthogonal **T**eleconnection (EOT), has been established to detect teleconnections by utilising linear regressions (Van den Dool et al., 2000). Other statistical methods, such as **M**ulti-channel **S**ingular **S**pectrum **A**nalysis (MSSA) and **I**ndependent **C**omponent **A**nalysis (ICA) (Eicker et al., 2016) have been used to successfully identify teleconnection patterns for climate studies. In recent studies, Wavelet transforms approach is considered as a powerful tool in analysing the relationship between meteorological connections with the large-scale climatic oscillations (Han et al., 2019).

5.2.4 Wavelet Transforms

The Fourier transform is a useful tool for examining the components of a stationary signal in which the signal parameters do not change. However, observation signals are frequently non-stationary. As a result, it necessitates more precise information on frequency variation across time. The Fourier transform provides information which is only related to the frequency domain. Whereas, the Wavelet transform produces a spectrum that is localised not only in frequency but also in time domains (Farge, 1992).

The Wavelet transform is based on a principle that is similar to that of the Fourier transformations. It does, however, provide you a lot more versatility when it comes to analysing all of the frequencies in a time series, from stationary to non-stationary and short to long term (Percival and Walden, 2000). This method is frequently utilised in the field of hydro-climatology and is widely employed in signal processing (Jiang et al., 2003; Xu et al., 2019). **W**avelet **T**ransformations (WT) are divided into two types: **C**ontinuous **WT** (CWT) and **D**iscrete **WT** (DWT). These two methods of WT have significant distinctions, which are summarised below. The time-frequency spectrum generated by the CWT is used in this study to examine the relationship between climate indices and TWS.

A wavelet is a wave-like oscillation whose amplitude starts at zero, grows and then drops back to zero. According to Farge (1992), a mother wavelet transformation basis function $\psi(t)$, satisfies the condition

$$C_\psi = 2\pi \int_\infty^\infty \frac{|\Psi(\omega)|^2}{|\omega|} d\omega \quad < \infty \tag{5.10}$$

where, C_ψ = admissibility constant. Integral is considered over all frequencies ω. $\Psi(\omega)$ = Fourier transform of the wavelet $\psi(t)$. In general, with sufficient decay, the mother wavelet satisfies the following conditions.

$$\Psi(0) = \int_\infty^\infty \psi(t) dt = 0 \tag{5.11}$$

$$\|\psi(t)\| = \int_\infty^\infty |\psi(t)|^2 \, dt = 1 \tag{5.12}$$

where, $\|.\|$ represents the magnitude. As a result of these two conditions, the wavelet function oscillates along time axis and decays rapidly in both directions of time. Therefore, CWT with respect to wavelet $\psi(t)$, for a time series $x(t)$ is defined as given below (Farge, 1992).

$$W_s(\tau, s) = \int_\infty^\infty x(t) \frac{1}{\sqrt{s}} \psi^* \frac{t-\tau}{s} dt = 0 \tag{5.13}$$

where, $W_s(\tau, s)$ = wavelet transform, with τ = time shift and s = scale factor. ψ = wavelet function and ψ^* = complex conjugate. $(s, \tau) = (1, 0)$ represents basic or mother wavelet.

The basic or mother wavelet is denoted by $\tau = 0$ and $s = 1$. The wavelet transform's flexibility comes from the scale variations in a time series, which allow it to capture both long and short frequencies. Also, the time series can be divided into high and low frequencies with $s > 1$ corresponds to high frequency of ψ. In general, by varying s and τ values, we obtain the wavelet spectrum at various time and frequency scales. The Morlet wavelet is one of the most widely used wavelet functions in hydro-climatology (Araghi et al., 2018) and is represented by below equation.

$$\varphi_0(\theta) = \pi^{-1/4} e^{i\omega_0\theta} e^{-\theta^2/2} \tag{5.14}$$

where, φ_0 represents mother wavelet; ω_0, θ denotes frequency and time respectively; with increase in ω_0, time resolution decreases and scale resolution increases, and vice versa.

5.2.4.1 Wavelet Coherence

Within the time-frequency space, wavelet coherence can be used to determine the relationship between two time series by estimating the correlation between them that varies between 0 and 1. In accordance with Torrence and Webster (1999) and Grinsted et al. (2004), coefficient of wavelet coherence between the two sets of time series data can be denoted as follows:

$$R^2(s, \tau) = \frac{\left|S(s^{-1} W_{xy}(s, \tau))\right|^2}{S(s^{-1} \left|W_x(s, \tau)\right|^2 . S(s^{-1} \left|W_y(s, \tau)\right|^2)} \tag{5.15}$$

where, $R^2(s, \tau)$ = coherence coefficient for a given time shift τ and scale s. $W_{xy}(s, \tau)$ = cross wavelet transforms between two series x and y. The wavelet coherence varies between 0 and 1 (Liu, 1994). The smoothing operator S is represented as given below (Chang et al., 2019):

$$S(W) = S_{scale}(S_{time}(W_{xy}(s, \tau))) \tag{5.16}$$

The smoothing along wavelet axis (scale and time) are represented as S_{scale} and S_{time} respectively. Designing the smoothing operator so that it has a similar footprint as the wavelet used is a common process and Torrence and Webster (1999) proposed a suitable smoothing operator for the Morlet wavelet, details can be found in Grinsted et al. (2004). Using Monte Carlo method, the statistical significance level is estimated

using 1000 ensemble surrogate pairs with **A**uto **R**egressive **1** (AR1) coefficients as the input datasets. Then we evaluate wavelet coherence for each pair and for each scale calculate the significance level using only values outside the cone of influence. Grinsted et al. (2004) specified that resolution chosen when computing the scale smoothing has a major impact on the significance level. Therefore, the number of scales per octave should be high enough to capture the rectangle shape of the scale smoothing operator while minimizing computing time. In the present study, the wavelet coherence is examined at 5% significance level or at the confidence interval $> 95\%$.

5.3 RESULTS

5.3.1 Changing Characteristics of TWSA

Seasonal and annual scale analysis of TWSA is performed for four basins. The results have shown distinct seasonal and annual TWSA characteristics over these river basins as shown in Fig. 5.3.

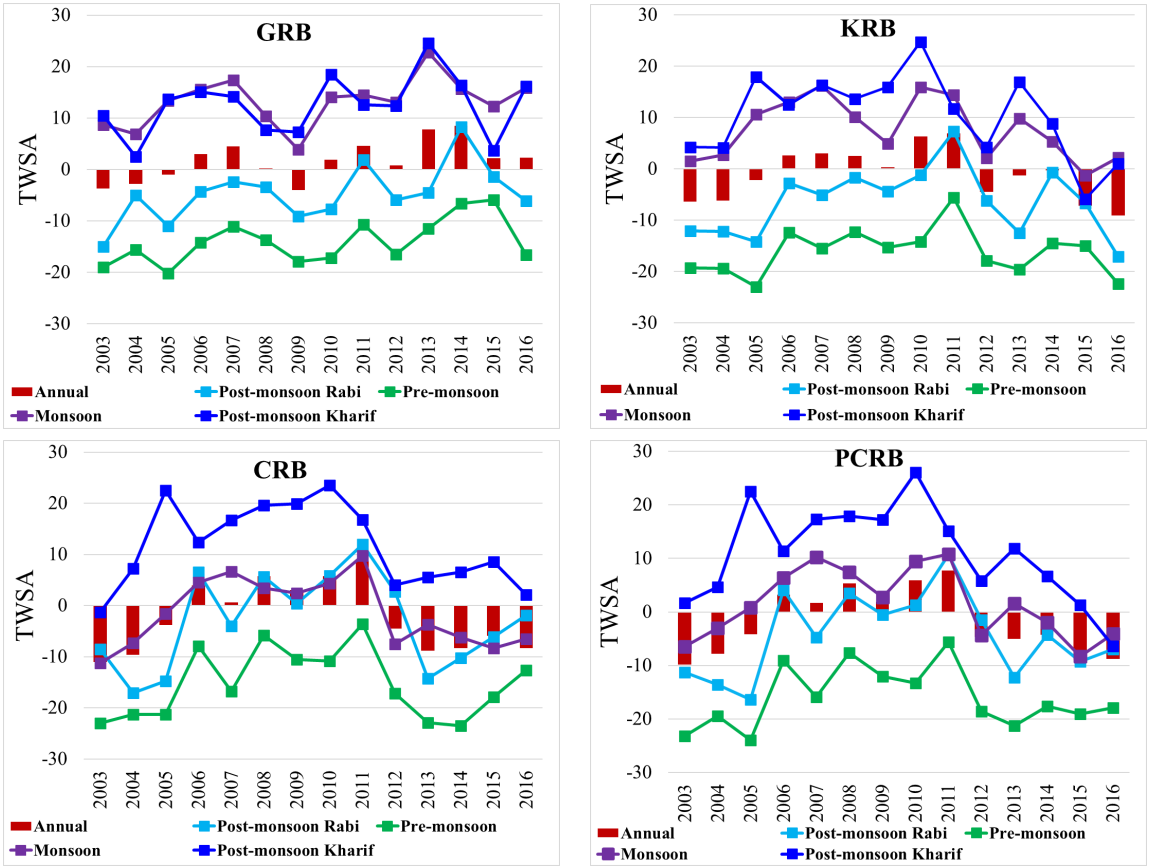

Figure 5.3: Multiscale (seasonal and annual) TWSA variations from 2003 to 2016.

In the monsoon and post-monsoon kharif seasons, the GRB has shown positive TWSA values, while negative TWSA values are detected in the pre-monsoon season. The positive and negative TWSA values are shown by the post-monsoon rabi season. On annual basis, TWSA displayed a significant upward trend with the highest values observed in 2013 and 2014. The TWSA in the GRB tends to decrease from 2003 to 2005, leading to a significant drought between 2003-2005 (see Fig. 5.3). Except for 2015, the KRB has shown positive TWSA values in the monsoon and post-monsoon kharif seasons. Except for the post-monsoon rabi season in 2011, the pre-monsoon and post-monsoon kharif seasons displayed negative TWSA values. Annual TWSA has shown a significant upward, downward trend and most of the negative trends are observed between 2003-2005 and 2012-2016, leading to severe droughts. The CRB and PCRB have shown positive and negative TWSA for post-monsoon kharif and pre-monsoon seasons respectively as shown in Fig. 5.3. Positive and negative TWSA values are observed in the monsoon and post-monsoon rabi seasons, with most of the negative values between 2003-2005 and 2012-2016. Annual TWSA has shown a downward trend between 2012 and 2016, leading to severe drought, followed by the 2003-2005 event. Overall, from the beginning of the 21st century, TWSA has shown a downward trend over the four river basins on seasonal and annual scales.

5.3.2 Basin Wise Drought Event Analysis

The temporal characteristics of drought and major drought events based on GGDI from 2003 to 2016 are shown in Fig. 5.4. The solid red line represents the GGDI and green shaded region indicates the period of drought events. The GGDI has shown upward and downward trends over each river basin with different change characteristics, demonstrating that the droughts reported using GGDI are increasing in these river basins during 2003–2016. For all the four basins, major decreasing trends are observed between 2003-2005, 2011-2013 and 2014-2016. From GGDI it is observed that droughts have become more frequent across these river basins in recent years. For the drought characterization, dry spells of more than three months are considered for drought event analysis (Thomas et al., 2014). The identified drought events are denoted as ‘DE’, followed by event order for that particular basin.

Four major drought events are detected with reference to GGDI in GRB i.e., during (i) DE1 - January to December 2003, (ii) DE2 - March 2004 to July 2005, (iii) DE3 - June 2008 to July 2010 and (iv) DE4 - August 2015 to February 2016 as shown in Fig. 5.4. The longest drought event over GRB extended for 26 months between 2008 and 2010 (DE3). Among four drought events DE1, DE2 and DE4 are characterized as moderate drought and DE3 as severe drought.

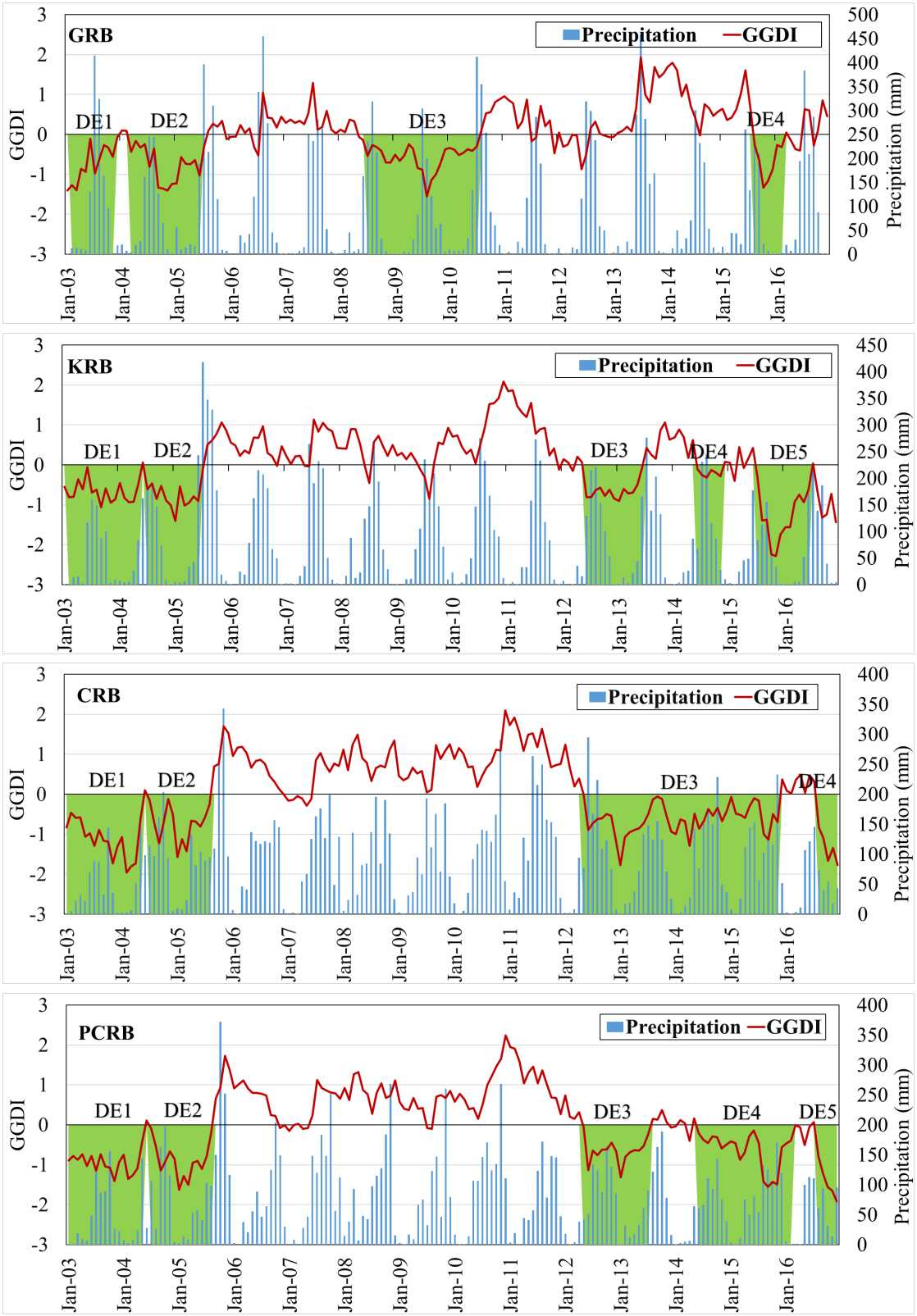

Figure 5.4: Monthly GGDI and precipitation time series with major drought events (green bands and 'DE' represents drought event).

Five major drought events are observed in KRB (i) DE1 - January 2003 to May 2004, (ii) DE2 - July 2004 to July 2005, (iii) DE3 - June 2012 to May 2013, (iv) DE4 - June to November 2014 and (v) DE5 - July 2015 to June 2016 as shown in Fig. 5.4. Among these drought events DE1, DE3 and DE4 are characterized as mild drought, DE2 as moderate drought and DE5 as extreme drought. For KRB, the longest drought is observed for 17 months between 2003 and 2004 (DE1).

Four major drought events are identified over CRB (i) DE1 - January 2003 to May 2004, (ii) DE2 - July 2004 to August 2005, (iii) DE3 - June 2012 to November 2015 and (iv) DE4 - August to December 2016 as shown in Fig. 5.4. DE1, DE3 and DE4 are characterized as severe drought and DE2 as moderate drought, with the longest drought extended for 42 months between 2012 to 2015 (DE3).

Five major drought events are observed in PCRB (i) DE1 - January 2003 to May 2004, (ii) DE2 - July 2004 to August 2005, (iii) DE3 - June 2012 to July 2013, (iv) DE4 - June 2014 to February 2016 and (v) DE5 - August to December 2016 as shown in Fig. 5.4. DE1 and DE3 are characterized as moderate drought; DE2, DE4 and DE5 are characterized as severe drought, with the longest drought extended for 21 months between 2014 to 2016 (DE4). Overall, for the four river basins of South India, GGDI can be considered as a strong indicator of drought.

5.3.3 SPEI12 based Drought Event Analysis

The SPEI12 time series with major drought events represented in red bands for four river basins are shown in Fig. 5.5. The SPEI12 has shown upward and downward trends over each river basin during 2003–2016. For all the four basins, major decreasing trends are observed between 2003-2004, 2012-2013 and 2014-2016. From the SPEI12 it is evident that droughts have become more recurrent and prolonged across four river basins in recent years.

Four major drought events are evident in GRB (i) DE1 - January 2003 to August 2003, (ii) DE2 - February 2009 to September 2010, (iii) DE3 - November 2011 to April 2013 and (iv) DE4 - April 2014 to December 2016 as shown in Fig. 5.5. DE1 and DE3 are characterized as moderate drought; DE2 and DE4 are characterized as severe drought, with the longest drought extended for 33 months between 2014 to 2016 (DE4).

Four major drought events are observed in KRB (i) DE1 - January 2003 to April 2004, (ii) DE2 - February 2009 to January 2010, (iii) DE3 - November 2011 to June 2013 and (iv) DE4 - February 2014 to December 2016 as shown in Fig. 5.5. DE1, DE2 and DE3 are characterized as moderate drought; DE4 is characterized as severe drought, with the longest drought extended for 35 months between 2014 to 2016 (DE4).

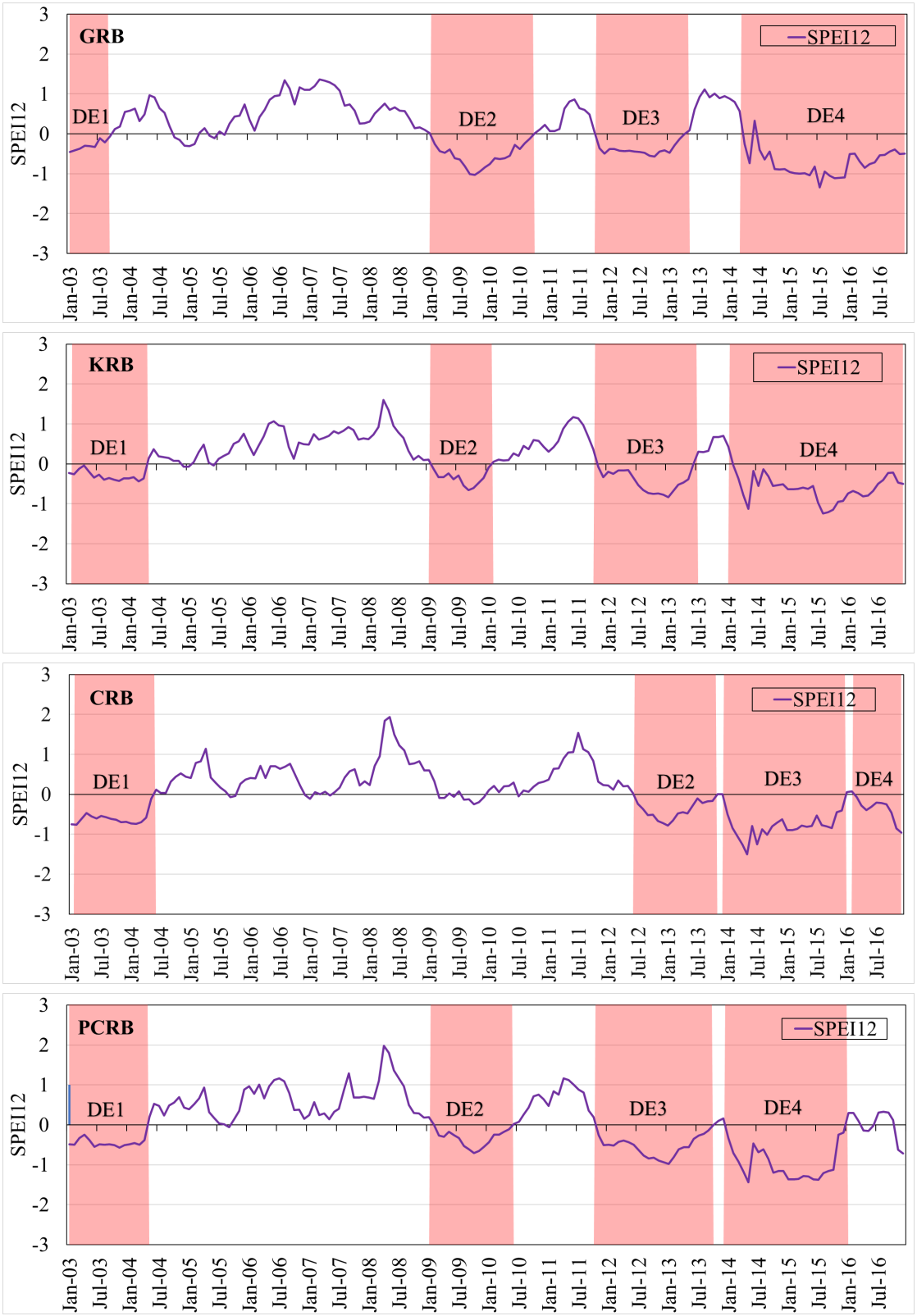

Figure 5.5: Monthly SPEI12 time series with major drought events (red bands and 'DE' represents drought event).

Four major drought events are observed in CRB (i) DE1 - January 2003 to May 2004, (ii) DE2 - June 2012 to October 2013, (iii) DE3 - January 2014 to December 2015 and (iv) DE4 - May 2016 to December 2016 as shown in Fig. 5.5. DE1, DE2 and DE4 are characterized as moderate drought; DE3 is characterized as severe drought, with the longest drought extended for 24 months between 2014 to 2015 (DE3).

Four major drought events are observed in PCRB (i) DE1 - January 2003 to April 2004, (ii) DE2 - February 2009 to May 2010, (iii) DE3 - November 2011 to September 2013 and (iv) DE4 - January 2014 to December 2015 as shown in Fig. 5.5. DE1, DE2 and DE3 are characterized as moderate drought; DE4 is characterized as severe drought, with the longest drought extended for 24 months between 2014 to 2015 (DE4).

The comparative analysis of GGDI with SPEI12 is done using Fig. 5.4 and 5.5. In GRB, drought events are commonly observed during 2008-2010 and 2015-2016 for GGDI and SPEI12. In KRB, three major drought events are observed between 2003-2004, 2012-2013 and 2015-2016 for both SPEI12 and GGDI. In CRB, for both SPEI12 and GGDI two major drought events are observed during 2003-2005 and 2012-2015. In PCRB, 2003-2004 and 2012-2016 are the two major drought events noticed for both SPEI12 and GGDI. Variations in the drought duration are observed between GGDI and SPEI12 based droughts. More drought events are observed using GGDI when compared with the SPEI12. As each drought index is different by construct and variables involved and differences in characterizing drought events are expected among the indices. So, variations in the drought events are observed between GGDI and SPEI12. Therefore, GGDI based drought analysis is important and may offer additional insights in identifying the extreme droughts for the river basins in which 50% of the population depends on agriculture.

5.3.4 Basin Wise Drought Characteristics Using GGDI

The drought characteristics (severity and duration) calculated from GGDI for four river basins is presented in Table 5.2. For GRB, the highest severity of 14.64 is observed for a duration of 26 months between June 2008 to July 2010. In KRB, the highest severity of 15.72 is observed for a duration of 12 months (July 2015 to June 2016), followed by 11.56 severity with a duration of 17 months (January 2003 to May 2004). The CRB experienced the height drought period among all the four basins, with severity of 27.02 observed for 42 months from June 2012 to November 2015. PCRB observed the highest severity 16.33 for a duration of 17 months (January 2003 to May 2004), followed by severity of 13.38 with the highest duration of 21 months (June 2014 to February 2016) in this basin. All the four basins experienced droughts during 2003 to 2005 and 2015 to 2016.

Table 5.2: Drought severity and duration from GGDI for GRB, KRB, CRB and PCRB

Time period	Severity	Duration (No. of months)
GRB		
Jan 2003 to Dec 2003	8.72	12
Mar 2004 to Jul 2005	12.91	17
Jun 2008 to Jul 2010	14.64	26
Aug 2015 to Feb 2016	4.87	7
KRB		
Jan 2003 to May 2004	11.56	17
Jul 2004 to Jul 2005	10.08	13
Jun 2012 to May 2013	8.47	12
Jun to Nov 2014	1.56	6
Jul 2015 to Jun 2016	15.72	12
Aug to Dec 2016	5.41	5
CRB		
Jan 2003 to May 2004	19.27	17
Jul 2004 to Aug 2005	10.56	14
Jun 2012 to Nov 2015	27.02	42
Aug to Dec 2016	6.71	5
PCRB		
Jan 2003 to May 2004	16.33	17
Jul 2004 to Aug 2005	12.52	14
Jun 2012 to Jul 2013	9.71	14
Jun 2014 to Feb 2016	13.38	21
Aug to Dec 2016	7.14	5

5.3.5 Analysis of Gridded Monthly and Seasonal Drought Trends based on GGDI

Gridded monthly and seasonal drought trends are performed using MMK trend test during 2003-2016 and presented in Fig. 5.6. GRB has shown monthly significant positive and negative trends from January to December (see Fig. 5.6). From January to July, GRB has shown positive trends at different significant levels (0.01, 0.05 and 0.1 significance level). The highest significant positive trends are observed in the month of May at the upper part of the basin, whereas the bottom part has shown downward trend from January to July. From August to December, significant negative trends are observed at 0.1, 0.05 and 0.01 significance level in the downward region of the basin. The highest significant negative trends are seen during August and September. Highly fluctuating positive and negative trends are observed in GRB compared to the other three basins.

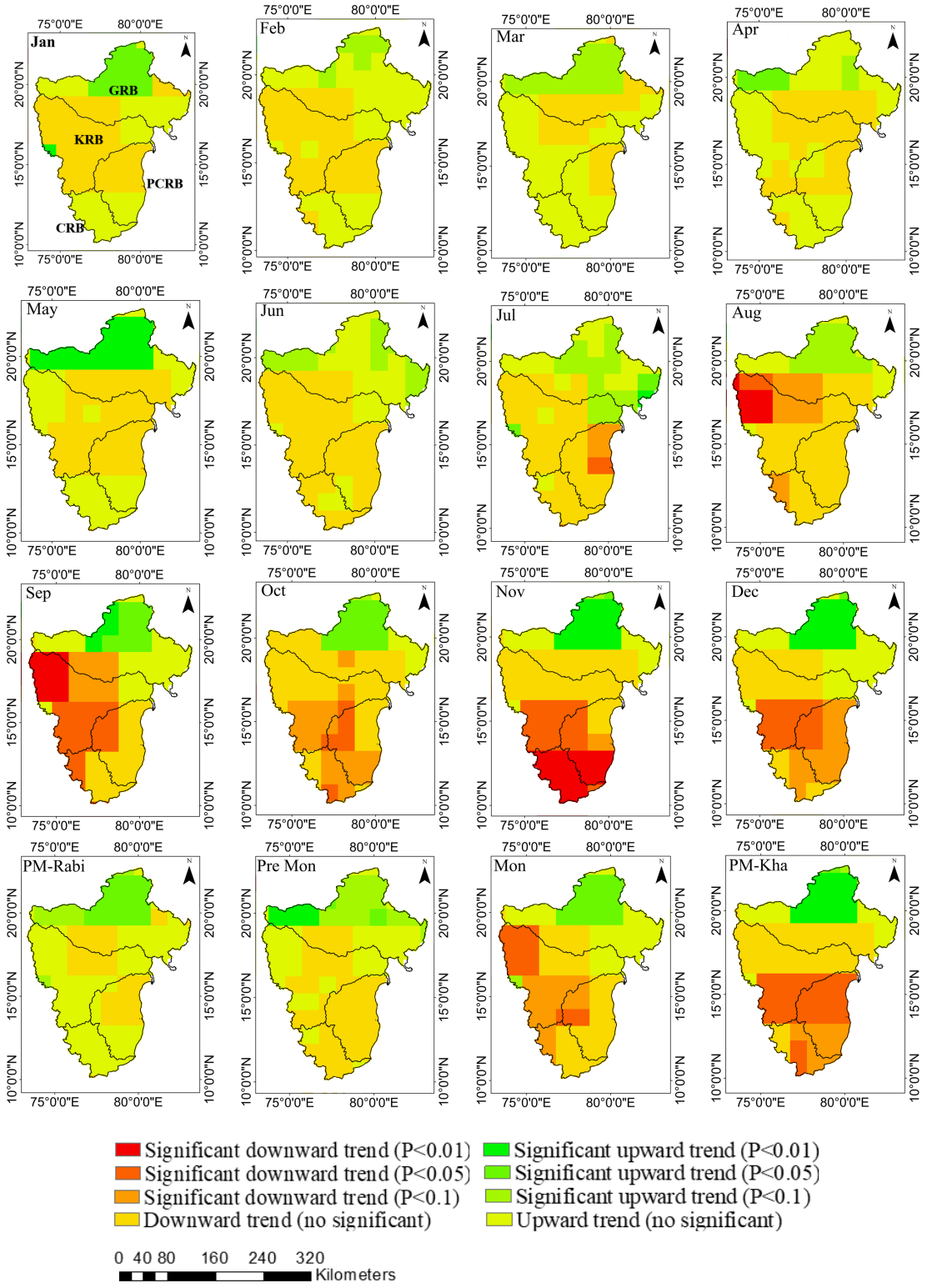

Figure 5.6: Monthly and seasonal trends of GGDI using the MMK test.

KRB displayed no significant monthly positive and negative trends from January to July. From August to December significant negative trends are observed at 0.01, 0.05 and 0.1 significance level. Most of the negative trends are observed in the month of September followed by August. No significant positive trends are observed in KRB.

PCRB and CRB have shown no significant monthly positive and negative trends from January to July (see Fig. 5.6). From August to December significant negative trends are observed at 0.01, 0.05 and 0.1 significance level. A complete downward trend is observed over CRB in the month of November and PCRB in the month of December.

The four seasons have shown significant positive trends over GRB. In KRB, CRB and PCRB, post-monsoon rabi and pre-monsoon seasons have shown upward and downward (no significant) trends. In comparison, KRB, CRB and PCRB have shown significant negative trends in the monsoon and post-monsoon kharif seasons. As shown in Fig. 5.6, most of the significant negative trends are observed in the post-monsoon kharif followed by the monsoon season. Overall, from season to season, significant positive trends are converted to significant negative trends, with highest significant negative trends have shown in post-monsoon kharif season. Decrease in precipitation is observed during 2002 to 2016 which led to nearly four major drought events.

5.3.6 Gridded Monthly and Seasonal Trends based on Precipitation

The monthly and seasonal precipitation trends using the MMK trend test for four river basins during 2003-2016 are shown in Fig. 5.7. GRB has shown monthly significant downward trends in lower and middle parts of the basin during January to December expect in March and June. Whereas upper part of the basin has shown significant upward trend expect in May and August. From January, August to December, GRB has shown significant downward trend (0.05 and 0.1 significance level). Highest significant positive trends are observed in the month of June and July at 0.01 and 0.05 levels, whereas downward trends are observed during November, December and January at 0.01, 0.05 and 0.1 significance level respectively. Highest significant negative trends are showed during August and September. Highly fluctuating positive and negative trends are observed in GRB compared to other three basins.

During February to April and December, KRB displayed monthly significant positive trends at 0.01, 0.05 and 0.1 significance level in upper part of the basin whereas other portion of the basin has shown significant negative trends (see Fig. 5.7). The basin is covered with significant negative trends in the months of May, September, October and November at 0.1 significance level. No significant positive trends are observed in KRB. Also, monthly significant positive trends are observed in June, August and December for PCRB and in the month of June and December for CRB at 0.01 and 0.05 significance level. Highly significant negative trends are observed during October in PCRB and CRB. Significant positive and negative trends are observed during January to May and September to November in PCRB and CRB at 0.01, 0.05 and 0.1 significance level.

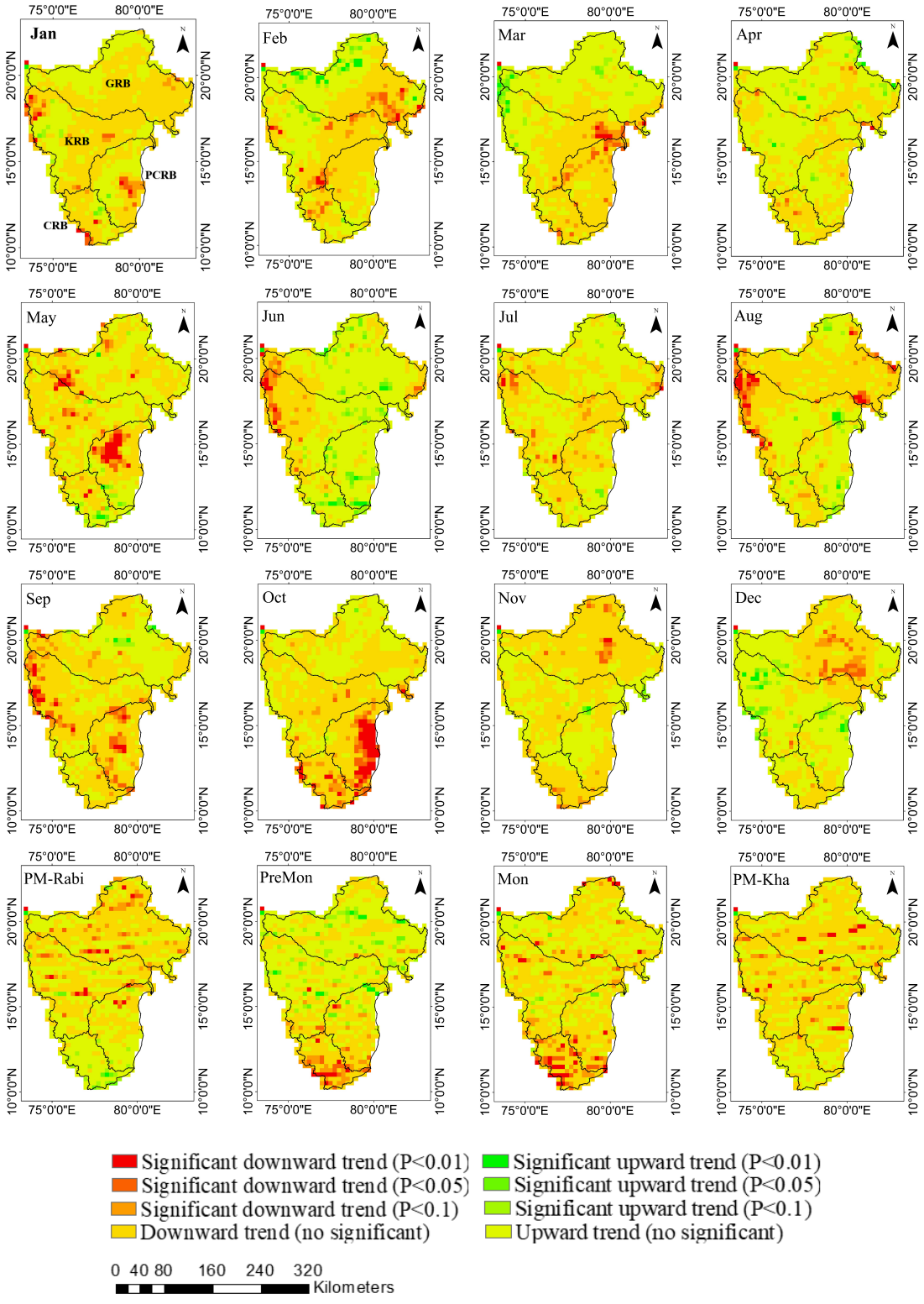

Figure 5.7: Monthly and seasonal precipitation trends using the MMK trend test over the four river basins during 2003–2016.

Seasonally (see Fig. 5.7), significant positive trends are observed during the pre-monsoon and monsoon seasons at 0.01, 0.05 significance level in GRB and KRB respectively. Significant negative and positive trends are observed during

post-monsoon rabi and kharif seasons over GRB, KRB, CRB and PCRB at 0.01, 0.05 and 0.1 significance level. Whereas, in case of pre-monsoon and monsoon seasons PCRB and CRB have shown most significant negative trends at 0.05 and 0.01 levels. Highly significant positive trends are observed in CRB compared to all other basins. Overall, from the analysis, GGDI is strongly influenced by variability of precipitation in the study region. Results stated that study region experienced significant decreasing trend in precipitation and GGDI. Assessment of GGDI and precipitation variability has shown a significant linear trend at both monthly and seasonal time scales.

5.3.7 The Correlation between GGDI and Teleconnection Factors

In this study, MEI, NINO3.4, SOI and DMI are chosen to describe the influences of teleconnections over droughts. Moreover, Wavelet coherence is employed to evaluate the link between GGDI and climate factors at South Indian River Basins during 2003-2016. The 95% confidence level is presented as thick contour and the relative phase relationship is represented by arrows with anti-phase pointing left and in-phase pointing right as shown in Fig. 5.8, 5.9, 5.10 and 5.11.

The Wavelet coherence between monthly GGDI and climate factors for GRB are presented in Fig. 5.8. The coherence at interannual variability is observed continuously

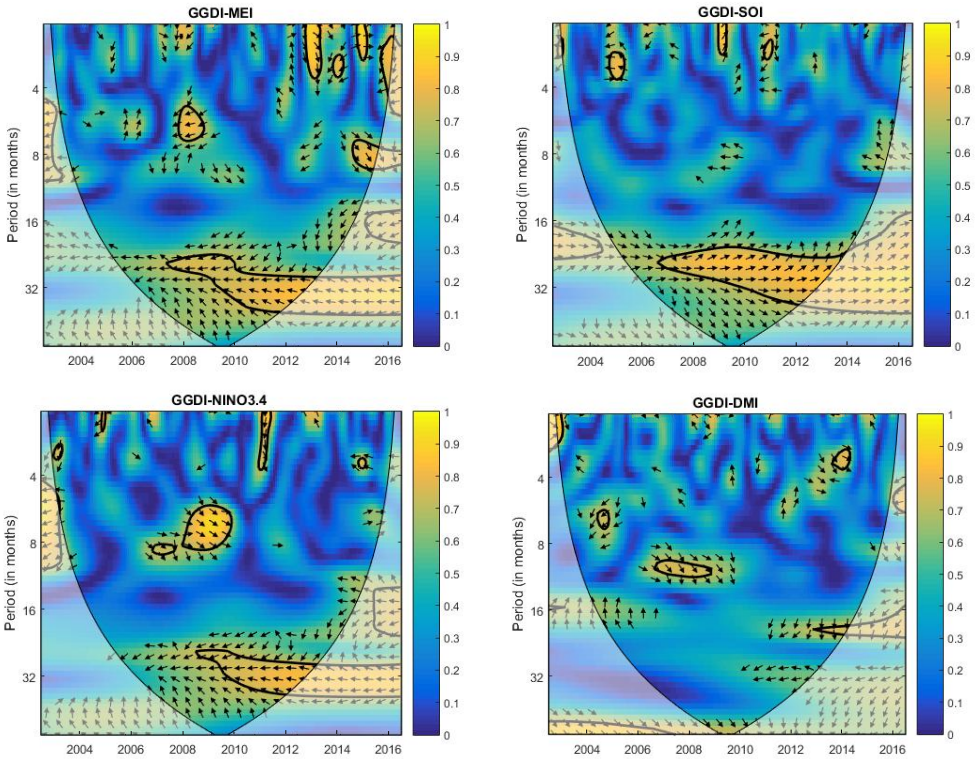

Figure 5.8: Wavelet coherence between monthly GGDI and MEI, SOI, NINO 3.4 and DMI for GRB.

between 2007-2016 on time scales of 20-36 months and intermittency is observed between 4-12 months at different years for MEI. In the case of SOI, coherence at interannual variability is observed between 2002-2005 and 2007-2016 periods on time scales varying from 16-40 months. For NINO3.4, intermittency is reduced between 2002-2007 period for time scales of 10-34 months and intermittency is observed at different years between 4-10 months. Compared to other teleconnections at different scales during different years, the effect of DMI is weak.

For KRB, the Wavelet coherence between GGDI and climate factors are provided in Fig. 5.9. High Wavelet coherence is noticed at an annual scale characterizing the dominant effect of groundwater for MEI, SOI, NINO 3.4 and DMI. Interannual variability is detected at time scales of 2 to 14 months for MEI, 4-10 months for SOI and 2-10 months for NINO3.4. Whereas, for DMI interannual variability is high varying for all months.

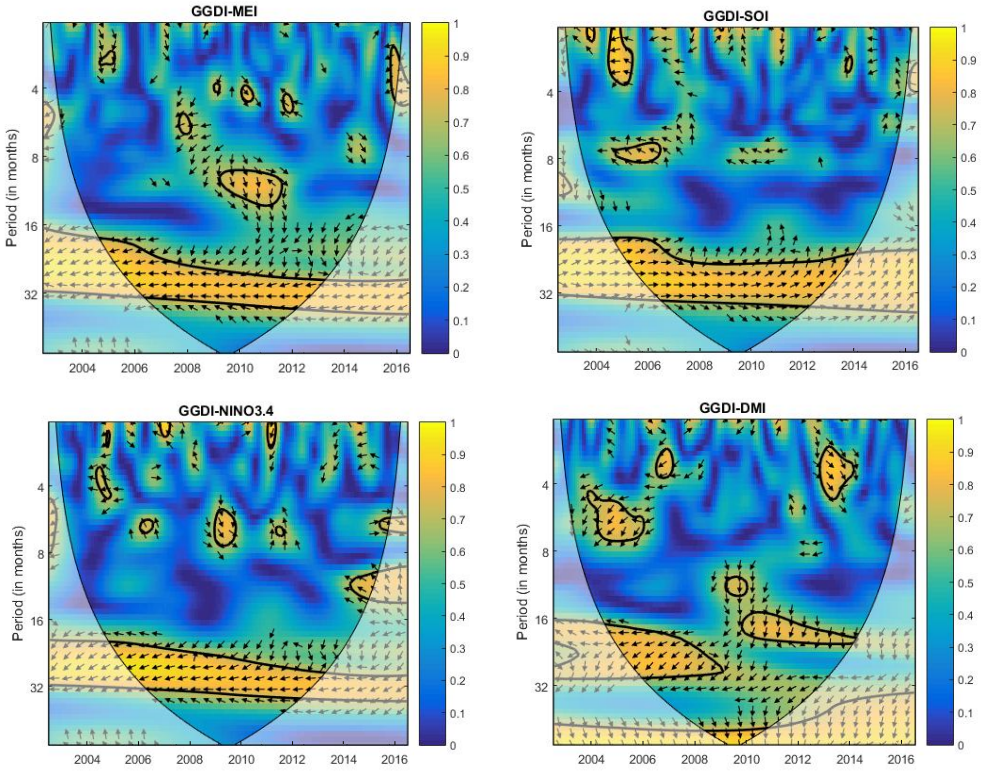

Figure 5.9: Wavelet coherence between monthly GGDI and MEI, SOI, NINO 3.4 and DMI for KRB.

For CRB, the Wavelet coherence between monthly GGDI and climate factors are presented in Fig. 5.10. The influence of MEI is observed over the time scales of 10-30 months for the period 2002-2011. Interannual variability of SOI is observed between 10–12-month time scale, whereas annual variability is observed for the time scale of 16-32 months over the period of 2002-2012. Annual variability of NINO3.4 is observed between 2002-2011 for an 18–32-month time scale and interannual

variability is observed for the time scale of 6-16 months. Influence of DMI is highly significant for the time scale of 14-40 months for the period 2002-2009, the annual variability is significantly high compared to NINO3.4, SOI and MEI.

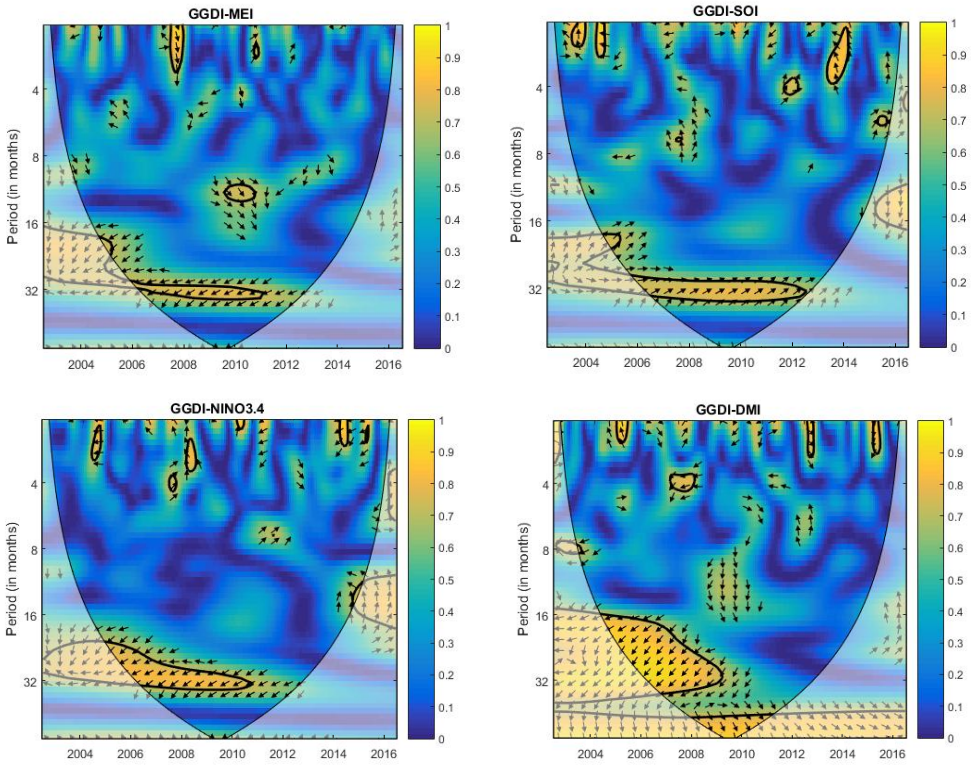

Figure 5.10: Wavelet coherence between monthly GGDI and MEI, SOI, NINO 3.4 and DMI for CRB.

For PCRB, the Wavelet coherence between monthly GGDI and climate factors are presented in Fig. 5.11. The annual variability of MEI is significantly dominant for all the years between the time scale of 16-32 months. Interannual variability is also observed between the time scale of 4-10 months at different years. The influence of interannual variability is observed at different years between the time scale of 2-14 months. Whereas, annual variability is seen for all the years between 16-32 months. Annual variability is comparatively less in NINO3.4 when compared with MEI, SOI and DMI. Interannual variability is observed between the time scales of 4-14 months over different years of 2009-2016. Annual variability of DMI is highly significant for 16–32 month time scales between the years 2002-2010 and continued for 33 to 40 month time scales for all the years. Also, interannual variability is observed between 4 to 14 month time scales for different years.

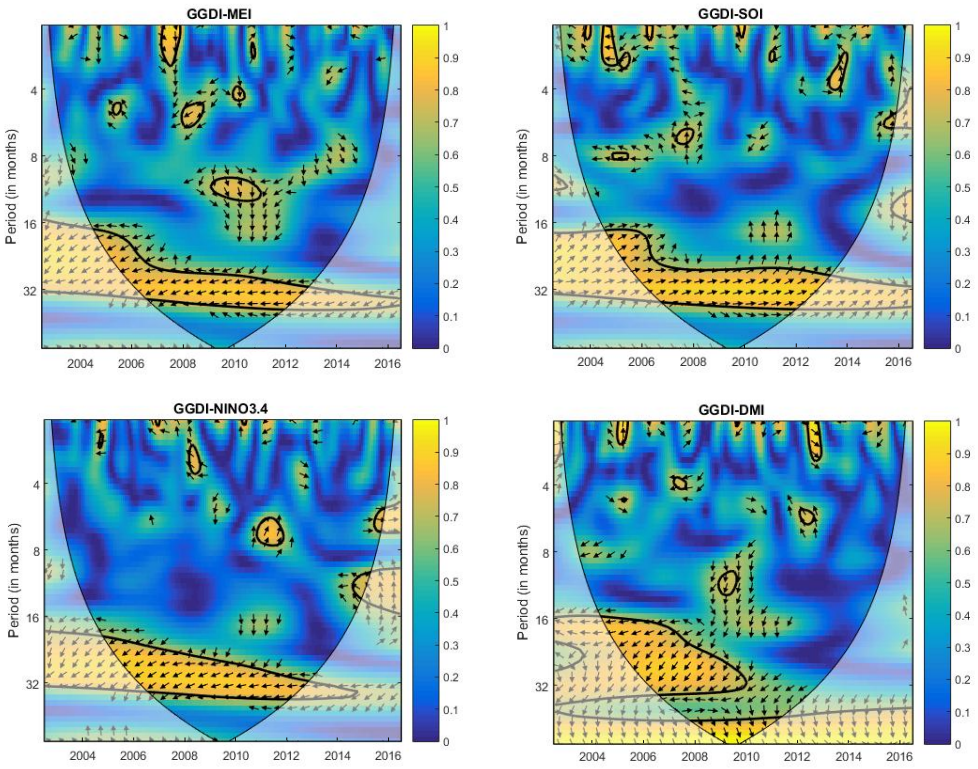

Figure 5.11: Wavelet coherence between monthly GGDI and MEI, SOI, NINO 3.4 and DMI for PCRB.

5.3.8 Spatial Distribution of Drought

Generally, most of the drought events are seen during 2003-2005, 2008-2010, 2012-2013 and 2014-2016. Spatial distribution of the yearly average GGDI time series is plotted to depict the spatial variation of drought throughout the basins as shown in Fig. 5.12. 2003, 2015 and 2016 are the most drought affected years in all the river basins. KRB has shown the severe drought throughout the basin in 2016 followed by PCRB and CRB. For GRB, the GGDI varied between -0.5 to -2 during 2003-2005, 2009, 2012, 2015 and 2016. For KRB, it varied between -0.5 to -2 for the years 2003-2005, 2009, 2012-2016. For CRB and PCRB, a range from -0.5 to -2 for the years 2003-2005 and 2012-2016 are noticed. KRB is the severely affected basin during the past decade compared to other basins. Drought had been considerably relieved during 2006, 2007 and 2011. Therefore, appropriate drought-resistant measures should be implemented in these river basins to reduce the impact of drought disaster and improve the capability of drought resistance.

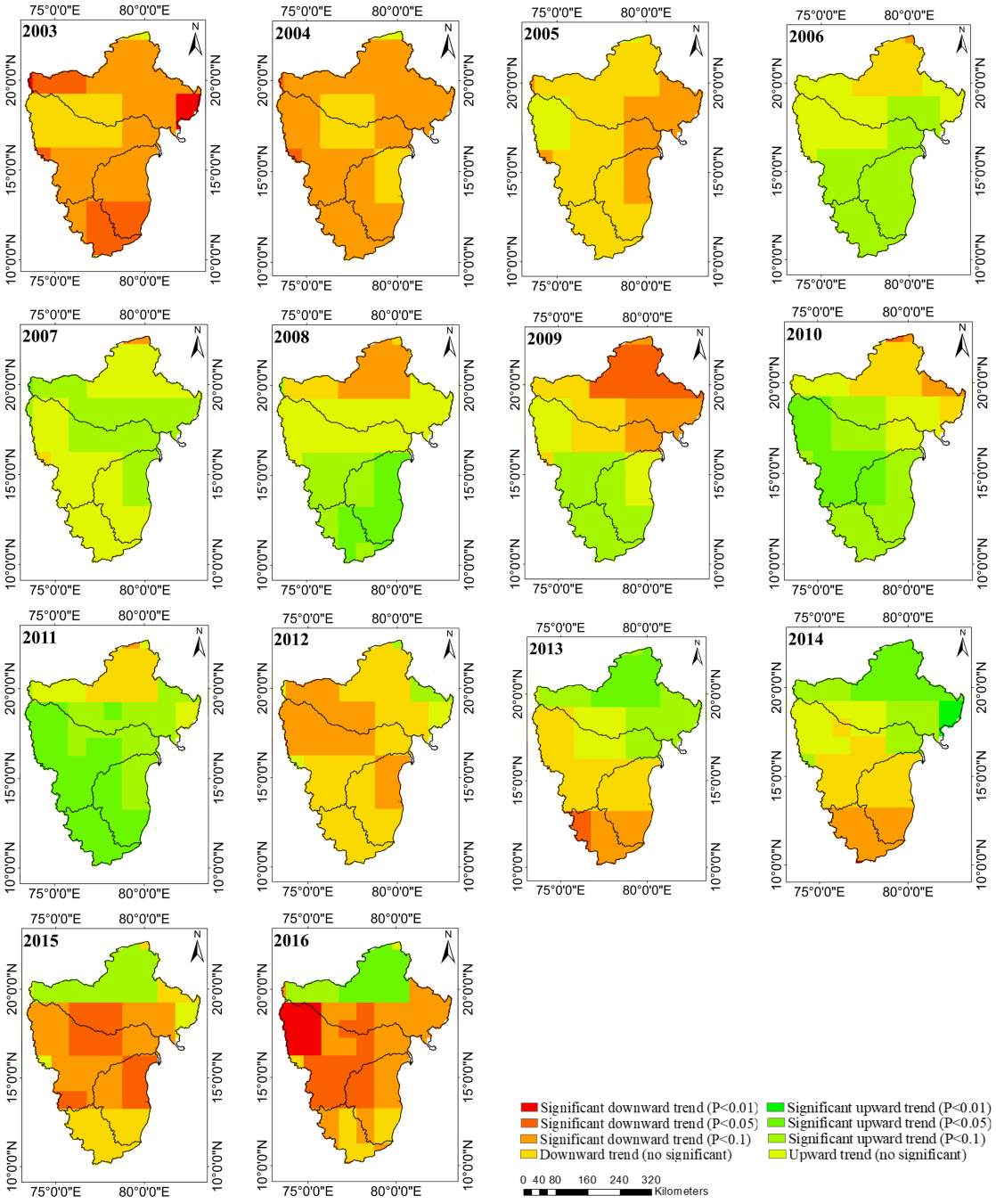

Figure 5.12: Spatial distribution of yearly averaged GGDI time series for GRB, KRB, CRB and PRB.

5.4 DISCUSSION

5.4.1 Influencing Factors of Drought

Droughts in India pose extraordinary challenges to the food production, socio-economic aspects, livelihood and gross domestic product. India has a long history of droughts with lasting effects on crops, surface and subsurface water resources and rural livelihoods (Mishra and Singh, 2010; Mooley and Parthasarathy,

1983). Water availability and crop production are affected by the recent drought of 2015-2016 over large parts of Southern India with reduced reservoir storage. Additionally, the 2015-16 drought affected around 330 million people and caused groundwater depletion in the South Indian states (Mishra, 2020). Failure of monsoon rainfall or its receipt in smaller quantities may often result in drought over major parts of India. There are many factors influencing the drought. These factors include anthropogenic factors along with natural factors, which cannot be overlooked. Due to the uneven distribution of rainfall spatially and temporally, surface and subsurface water resources are scarce over India. Mishra (2020) stated that the 2015-2018 drought affected groundwater and surface water availability in Southern India and is linked to climate indices. Farmers disproportionately use electricity and fossil fuels to pump groundwater to compensate for the lack of rainfall. In particular, cultivation costs for rice and other rainy season (kharif) crops are also rising due to increased use of energy and diesel for pumping of groundwater (Gautam, 2012). Excessive withdrawal of groundwater to save crops in drought conditions has drained groundwater in most parts of the world and then ultimately trigger a drought crisis.

Researchers have established that climate factors play a major role in the process of drought formation (Dai, 2011a; Sehgal and Sridhar, 2018). Additionally, the Wavelet coherence results have shown that climate factors (MEI, SOI, DMI and NINO3.4) have an extreme influence on drought evolution. In particular, for Indian regions, MEI, SOI and NINO3.4 have the greatest influence on drought (see Figs. 5.8, 5.9, 5.10 and 5.11). There are several teleconnections that influence the variability of TWSA along with its components over India. Though earlier studies primarily focused on the effect of ENSO over TWSA (Ni et al., 2018; Vissa et al., 2019), it is unlikely to consider a single indicator to represent all climatic variability features over large regions (Zhu et al., 2017). In the current study, four widely used climate factors are considered and their links with GGDI are evaluated; the results show that for each river basin the teleconnections differ considerably with GGDI. Therefore, TWSA attributions and predictions or indices calculated using TWSA (eg., GGDI) centered on a single teleconnection should be treated with caution and multiple teleconnections are suggested for the assessment of TWSA and their components.

The coherence of GGDI with teleconnections (MEI, SOI, DMI and NINO3.4) at $\sim$32 months period may be due to the correlation between climate indices (correlation of MEI with SOI/DMI/NINO3.4) as shown in Figs. 5.8, 5.9, 5.10 and 5.11. Therefore, analyzing the standalone effect of teleconnection factors on the GGDI series may provide better correlation between GGDI and teleconnection after removing the effect of other influential time series (Aryal and Zhu, 2020; Tan et al., 2016).

5.4.2 Uncertainty Analysis

Numerous areas of uncertainty are encountered in the present study. First, to avoid the uncertainty induced by observational and data processing, modern mascon solution data is considered instead of the spherical harmonic coefficients data (Swenson and Wahr, 2006). The mascon solutions developed by various organizations still have ambiguities due to diverse background models as well as data processing approaches. In addition, the JPL mascon solutions considered different hydrological models to adjust the scale factors, which eventually contributes to the presence of uncertainty. Second, to minimize the GLDAS uncertainty, the ensemble mean of several hydrological models (Noah, VIC, CLM, Mosaic) is suggested (Cao et al., 2015). However, similar to GRACE data, the Noah model has the same spatial resolution. Thus, this study adopted the GLDAS Noah model outputs to reduce the uncertainty related to spatial resolution in evaluating water storage calculations. Finally, using linear interpolation techniques, the missing GRACE data is filled out, which may trigger some uncertainties. However, since the approach is prevalent, easy and extensively used in the handling of missing data, the similar techniques is used in filling the GRACE dataset gaps (Sun et al., 2018) and the results suggest that the linear interpolation approach is appropriate.

5.4.3 Advantages and Limitations

GRACE satellite gravimetry plays an important role in the identification of drought in regions where data related to water storage variations is inadequate (Yirdaw et al., 2008). To reduce the influence of various errors in the GRACE spherical harmonic coefficients, various filtering processes are applied, yet results suggest the possibility of weak signals in the derived product. Therefore, scale factors are applied to recover the signal leakage caused by the filtering processes (Landerer and Swenson, 2012). In order to resolve these data processing errors, GRACE mascon solutions, which are equal to or superior to traditional GRACE spherical harmonic coefficients, are adopted in the current research (Hamed and Rao, 1998). Therefore, using GRACE mascon solutions, changing characteristics of TWSA, in identifying the teleconnections with GGDI and hence the drought situation over river basins in Southern India are explored. In regions where hydrometeorological data is minimal, GRACE data is an important means of estimating and managing the drought. The GGDI is a normalized index that can be used to objectively compare spatio-temporal drought, providing strong evidence for evaluating surplus and deficit groundwater availability. This study positively established the drought events between 2003-2005, 2008-2010 and 2013-2015, which are consistent with the results of Sinha et al. (2019). Severe drought events between 2008-2010 for GRB, 2015-2016 for KRB and 2003-2004 for PCRB are also reported

by Kumar et al. (2021), which are consistent with the drought events obtained using GGDI in this study (see Fig. 5.4 and Table 5.2). Moreover, the interaction of GGDI with climate indices has shown that teleconnections have a substantial effect on drought across Southern India's River Basins.

Though GGDI can be used to effectively and expediently categorize drought characteristics, there are still some limitations. GRACE datasets have only been available since 2002, covering only a few years of data; with longer temporal datasets, the results will therefore be more accurate (Thomas et al., 2014). Though GRACE data resolution is relatively low, but it considers the changes in water storage (including soil water and surface snow) that comes from rainfall, evapotranspiration, river transportation and deep underground infiltration. GRACE is the key technology in gravity satellite sensors to improve accuracy and monitoring gravity field in terrestrial hydrology. GRACE provides realistic spatiotemporal variations of vertically integrated measurement of water storage. The new GRACE FO satellite dataset will provide a valuable solution for the long-term evaluation of TWS variations and their associated studies, resulting in significant improvements in our knowledge of GRACE related studies. Moreover, the effect of anthropogenic activities (groundwater extraction, regional water division, mining) over mass changes of the earth surface cannot be overlooked (Tang et al., 2013). These effects are the influence of human activities and generally be ignored due to the lack of observed datasets, difficulties in the collection and measurement of relevant information. Therefore, analyzing the influence of anthropogenic activities on variations in water storage may provide a fresh insight into the future of science.

5.5 CONCLUSIONS

In the present study, during 2003-2016, the drought characteristics are examined and evaluated using GGDI over GRB, KRB, CRB and PCRB. The spatial distribution, temporal evolution of drought and trend characteristics are analyzed using GGDI. Then, using the Wavelet coherence method, the relationship between GGDI and climate factors is evaluated. GRACE datasets provide significant benefits in detecting droughts and revealing information about large-scale groundwater depletion, where hydrometeorological data is limited and data related to water storage variations is insufficient. This study provided reliable and robust quantitative results of GRACE water storage variations that provide a new approach to link surface and subsurface condition while investigating the drought and this methodology can be applied to any other regions. The key findings from this part of the study are given as follows:

- The distinct seasonal and annual variations of TWSA are observed in four river

basins. The pre-monsoon and post-monsoon rabi seasons have shown negative TWSA values; while monsoon and post-monsoon kharif seasons have shown positive variations of TWSA in all the river basins. Annually, TWSA values have shown significant upward and downward trends with most of the negative trends are observed between 2003-2005 and 2012-2016, indicating severe droughts.

- The GGDI-identified drought events have shown different temporal change characteristics in all the river basins. The most severe drought event is observed in CRB between 2012-2016 and followed by GRB between 2008-2010. All the four basins have shown drought events between 2003-2005 and KRB, CRB and PCRB experienced droughts between 2012-2016.

- Drought severity and duration are evaluated using GGDI for four river basins. The CRB experienced the longest drought period among all the four basins, with a severity of 27.02 observed for 42 months during June 2012 to November 2015.

- The monthly and seasonal trends are evaluated using MMK test. Significant monthly negative trends are observed during August to December in KRB, CRB and PCRB. Seasonal negative trends are also significant in monsoon and post-monsoon kharif seasons in CRB, KRB and PCRB except GRB.

- The Wavelet coherence analysis effectively demonstrated the teleconnection links between climate indices and drought events. The influence of SOI on drought is significantly high followed by NINO3.4 and MEI in all the basins. SOI has the strongest impact in detecting the progression of drought compared to other climate indices in these river basins.

CHAPTER 6

RECONSTRUCTION OF TWSA AND ITS VALIDATION WITH IN SITU GROUNDWATER WELL MEASUREMENTS

This chapter deals with the third sub objective that the reconstruction of GRACE terrestrial water storage from 1990 to 2020 and its validation with the in-situ groundwater well measurements.

6.1 INTRODUCTION

GRACE was originally intended to last for five years, but it got extended for another ten years till October 2017. The GRACE FO mission was initiated in May 2018, however between July and October 2018, the main instrument processing unit failed. As a result, there has been a one-year data gap. Many studies have attempted to bridge the gap between GRACE and GRACE FO satellite missions by utilizing various satellite observations. There is, however, no single satellite mission capable of filling this void with equal quality. As GRACE observations are the only ones that provide direct estimates of TWS, bridging the gap between these two missions is very important. Also, in order to investigate climate related applications, it is desirable to reconstruct TWSA prior to the period of record from the GRACE mission.

Machine learning techniques have recently advanced, opening new opportunities in hydrology and related domains (Hamshaw et al., 2018). Machine learning techniques proved to be effective in solving most complex problems, such as data prediction and reconstruction. In this study, a learning based model, namely MultiLayer Perceptron (MLP) is used to reconstruct (1960-2002) and predict (2017-2018) TWSA to obtain a continuous time series from 1960 to 2020. The ANN model is evaluated at both grid and basin scales, and its performance is compared to that of the existing GRACE and GRACE FO solutions. The learning based model developed will precisely reconstruct TWSA prior to the GRACE mission (1960-2002) and between the two missions (2017-2018).

In evaluating groundwater variations and trends, GRACE estimates have proven valuable at regional and global scales (Rodell et al., 2007). Using a satellite-based approach, previous studies have reported rapid groundwater storage depletion at basin or continental scales in various parts of the world. (Richey et al., 2015; Rodell et al.,

2009; Voss et al., 2013). In order to improve algorithms related to data retrieval techniques, satellite data products must be validated using ground estimates. As GRACE gravity processing algorithms are constantly evolving over time, GRACE outputs need additional validation studies all over the world (Watkins et al., 2015). Only a few studies have compared GRACE observations to groundwater level measurements around the world. Very few studies, particularly in India, have compared GRACE groundwater storage estimates with observation well networks (Bhanja et al., 2014; Chinnasamy et al., 2013; Long et al., 2016).

This is one of the first studies to reconstruct TWSA and validate it using a vast network of in-situ observation well data ($\sim$2000 observation wells) collected across Indian River Basins. The reconstructed TWSA datasets from four river basins are converted to Groundwater Storage Anomalies $(GWSA_{GRACE})$ and then validated using the GWSAs obtained from groundwater observation well data $(GWSA_{OBS})$. Because the observation well data is available from 1996 to 2020, the $GWSA_{GRACE}$ is also considered from 1996 to 2020, despite the reconstruction being from 1960 to 2020. The findings will aid hydrologists in selecting appropriate GRACE solutions for hydrologic applications in regional basin studies. The findings of this study could be used to fill gaps in GRACE data and promote the use of GRACE products to investigate long-term hydroclimatic aspects in global and basin-scale hydrologic research.

6.2 METHODOLOGY

Predictive models seek to identify a relationship between a group of predictors (GLDAS TWSA, precipitation, maximum temperature and minimum temperature) and the target variable (GRACE TWSA) (Bishop, 2006). In this study, MLP model is employed to predict (2017-2018) and reconstruct (1960-2002) TWSA to obtain a continuous time series from 1960-2020. Then, the model developed TWSA (1960-2020) is converted to GWSA. The obtained monthly GWSA is converted to seasonal GWSA for four seasons and validated using GWSA obtained from seasonal groundwater level monitoring sites from 1996 to 2020 across south Indian river basins. The methodology for reconstructing TWSA and validating it with $(GWSA_{OBS})$ is presented in Fig. 6.1.

6.2.1 Artificial Neural Networks (ANN)

The biological neural network in the brain, which consists of a billion linked neurons, is the basis for ANN. With advancements in information processing, ANNs have been used to simulate the brain's distributed storage properties and massive parallel processing. An ANN is a data processing system composed of a densely connected network of simple processing components known as neurons. These neurons are arranged in layers

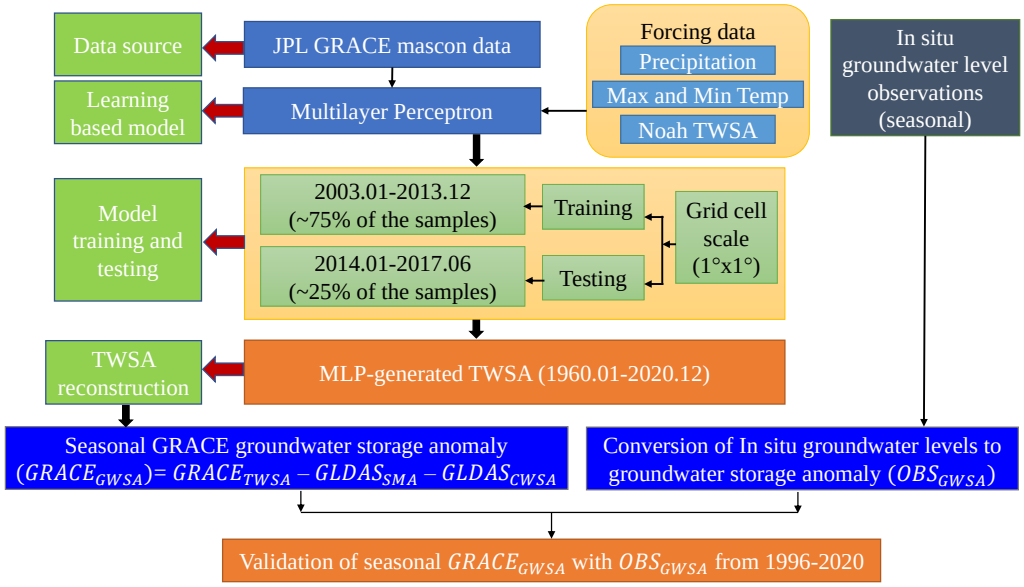

Figure 6.1: Flow chart of third sub objective

within the network by connecting to neurons in the next layer. The ”weight,” which is analogous to the signal intensity in a biological neural network, represents the strength of these connections between two neighbouring layers. During the training/learning phase, the weights of the interconnections are adjusted until the inputs produce desired output. To produce the desired output, different training rules for weight adjustment are required depending on the training data provided to the network (Long et al., 2014). MLP is a popular and widely used ANN model (Bishop and Nasrabadi, 2006; Long et al., 2014). MLP is used in this study to reconstruct TWSA dataset from 1960 to 2020. A brief overview of MLP is provided below.

6.2.2 Multi Layer Perceptron (MLP)

The MLP is made up of a network of interconnected nodes or neurons. The neurons are linked by weights and the output signals can be modified using a simple nonlinear transfer, or activation function (Sun, 2013). The commonly used activation functions are Unit step (Heaviside), Linear and Logistic (sigmoid). The connecting weights, scale the output of a node and feeds it forward as an input to the nodes in the next layer of the network. As a result of this information processing direction, the MLP is known as a feed-forward neural network, as shown in Fig. 6.2 (Bishop , 1995).

MLP may include one or more hidden layers, which are followed by an output layer. The output of one layer becomes the input of the following layer and so on. The input and output layers are the first and last of the neural network, whereas the other layers function as hidden layers within the network. Each neural link has its own weight. Perceptron activation functions (sigmoid) are the same for each layer.

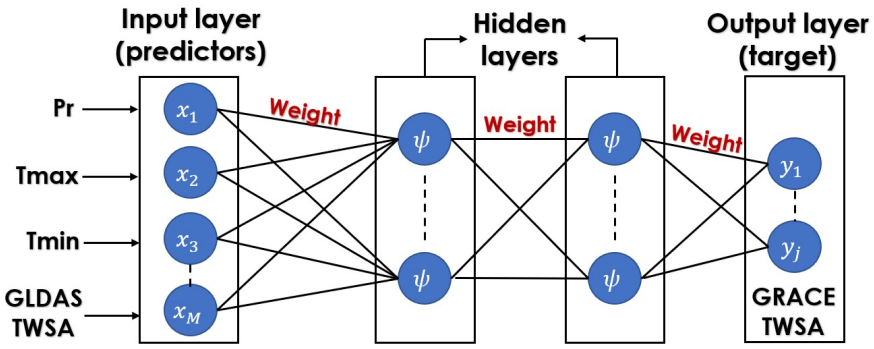

Figure 6.2: Structure of MLP.

Depending on the application, output layer could be a sigmoid or linear function (Long et al., 2014). The widely known MLP learning method uses back propagation technique, which is a generalisation of the Least Mean Squared rule (Du and Swamy, 2013). Back propagation is a weight correction technique that propagates errors from one layer to the next, beginning with the output layer and working backwards. The performance of MLP model is determined by the variables specified, the training dataset and the number of hidden layers. The use of a small number of hidden layers may result in a lower precision detection of the nonlinear function. Choosing a larger number of hidden layers, on the other hand, may overfit the training data. As a result, the optimal number of hidden layers for the analysis is determined.

MLP is a mathematical model that represents a functional mapping between predictors x and the target variable y (Bishop and Nasrabadi, 2006).

$$y = f(x) + \varepsilon \tag{6.1}$$

where, f is the mapping function and ε is process noise. An MLP is created by a series of transformations that combine layers one by one. First stage is to develop associations between the input and hidden layers. Let $\{x_i\}_{i=1}^{M}$ represents M predictors and a hidden layer containing K hidden neurons.

$$a_k = \sum_{i=1}^{m} W_{ki}^{(1)} x_i + W_{k0}^{(1)}, \qquad k = 1, ..., K \tag{6.2}$$

where, a_k = hidden neuron; $\left\{W_{ki}^{(1)}\right\}_{i=1}^{M}$ = unknown weights with respect to input neuron; $W_{k0}^{(1)}$ = bias term; superscript represents the layer number. Next, the above equation is passed through a transfer function in order to produce outputs from hidden neurons.

$$z_k = \psi(a_k), \qquad k = 1, ..., K \tag{6.3}$$

where, z_k represents the output; ψ denotes the transfer function i.e., sigmoid function, which ranges in [0, 1]. Finally, linear transfer functions are used to establish the connection between hidden and output layers.

$$y_j = \sum_{k=1}^{K} W_{jk}^{(2)} z_k + W_{j0}^{(2)} \tag{6.4}$$

where, y_j represents the output neuron i.e., model predictants $(j = 1, \ldots, J)$; $\left\{W_{jk}^{(2)}\right\}_{k=1}^{K}$ = unknown weights of the output layer; $W_{j0}^{(2)}$ = bias term. Back propagation techniques is used to solve unknowns in Eq. 6.2 and 6.4 during the training period in order to acquire the appropriate weights in each layer.

6.2.2.1 Performance Metrics

The performances of the developed MLPs are measured using Pearson's correlation coefficient (r) and **N**ash-**S**utcliff **E**fficiency (NSE).

Pearson's correlation coefficient It is a measure of linear correlation between two datasets which is represented as given below.

$$r = \frac{\sum_{i=1}^{n}(x_i - \bar{x})(y_i - \bar{y})}{\sqrt{\sum_{i=1}^{n}(x_i - \bar{x})^2 \sum_{i=1}^{n}(y_i - \bar{y})^2}} \tag{6.5}$$

where r = Pearson's correlation coefficient; x represents the TWSA dataset; and y represents the drought index. i is $1, 2 \ldots n$; $\bar{x}$,$\bar{y}$ are the means of x and y scores; n = the total number of observations; r ranges between -1 and +1, the highest r (positive or negative) represents the higher correlation between x and y.

Nash-Sutcliff Efficiency (NSE) The NSE measures the predictive skill of a model corresponding to the mean of observations. The NSE ranges between $-\infty$ to 1.

$$NSE = 1 - \frac{\sum_{i=1}^{n}(x_i - y_i)^2}{\sum_{i=1}^{n}(y_i - \overline{y})^2} \tag{6.6}$$

where, number of observations are represented by n; x and y are the observed and simulated datasets; $\overline{x}$, $\overline{y}$ are the means of x and y scores. The highest NSE (positive) value, better the correlation between x and y.

6.2.3 Retrieval of Groundwater Storage Change from Observation Wells

From 1996 to 2020, seasonal observation well data from GRB, KRB, CRB and PCRB are considered. Using the procedure outlined below, observation well data are converted into seasonal GWSAs.

- Calculate groundwater level anomalies (Δh) for individual wells by subtracting mean water level depths from seasonal observation values at all sites and reversing the sign for the depth conversion.

$$\Delta h = -(GWL_{individual\,well} - Mean\,GWL\,depth) \tag{6.7}$$

The obtained Δh for each river basin are provided in Table 6.1.

- Calculate observed groundwater storage (GWS_{OBS}) by multiplying S_y with Δh at each observation well. The basin averaged S_y values are considered form Bhanja et al. (2016) and provided in Table 6.1.

$$GWS_{OBS} = S_y \times \Delta h \tag{6.8}$$

Table 6.1: Basin wise number of observation wells, mean specific yield (S_y) and groundwater level (GWL) depth range

Basin	**No of wells**	**Specific yield** $(\mathbf{S_y})$	**GWL depth range** $(\mathbf{\Delta h})(\mathbf{m})^*$
GRB	822	0.023	∼35
KRB	550	0.022	∼48
PCRB	275	0.023	∼49
CRB	326	0.024	∼59

*According to the total number of observation wells used for each basin.

- Convert GWS_{OBS} to groundwater storage anomalies $GWSA_{OBS}$ by substracting it from the average GWS observed during January 2004 to December 2009.

$$GWSA_{OBS} = GWS_{OBS} - \overline{GWS_{2004-2009}} \tag{6.9}$$

6.2.4 Retrieval of Groundwater Storage Change from GRACE and GLDAS

In this study, the MLP method is used to reconstruct monthly TWSA from 1960-2020. These monthly TWSA datasets are converted to seasonal GWSA from 1996-2020 over four river basins using the procedure outlined below. The GWSA at any time t, is calculated by subtracting SMSA and CWSA (obtained from the GLDAS Noah model) from TWSA. The GLDAS Noah modelled datasets are considered from 1996-2020, allowing them to be related with the reconstructed TWSA (1996-2020). The following equation is used to determine SMSA using the Noah land surface model.

$$SMSA_t = SMS_t - \overline{SMS_{2004-2009}} \tag{6.10}$$

Similarly, CWSA for the Noah model is estimated using the following equation.

$$CWSA_t = CWS_t - \overline{CWS_{2004-2009}} \tag{6.11}$$

where, $SMSA_t$, $CWSA_t$ are the soil moisture and canopy water storage anomalies w.r.t time t respectively; SMS_t, CWS_t are the soil moisture and canopy water storage at time t respectively; $\overline{SMS_{2004-2009}}$, $\overline{CWS_{2004-2009}}$ are the average soil moisture and canopy water storage derived respectively from the base period of Jan 2004 to Dec 2009 and with the same base time period as TWSA. Then GWSA is calculated as:

$$GWSA_t = TWSA_t - SMSA_t - CWSA_t \tag{6.12}$$

Now the obtained seasonal GWSA from GRACE and GLDAS $(GWSA_{GRACE})$ from 1996-2020 are validated using the observation well-based seasonal GWSA $(GWSA_{OBS})$ from 1996-2020 over the study region.

6.2.5 Processing and Analysis of Data

For the development of an MLP model, four predictors (precipitation, maximum temperature, minimum temperature and GLDAS TWSA) and a predictand (TWSA from GRACE) are used. The GRACE TWSA is the combination of soil moisture, groundwater and canopy water storages as given in Eq. 6.13. The GLDAS Noah model products (soil moisture and canopy water storage) are considered to evaluate TWSAs. Like GRACE, GLDAS dataset play a major role in evaluating TWSA. As a result, TWSA is calculated from GLDAS by adding ΔSMS and ΔCWS. Because the GLDAS Noah model cannot evaluate changes in groundwater storages (ΔGWS), the TWSA is calculated using only two components, as given in Eq. 6.14.

$$\Delta TWS_{GRACE} = \Delta SMS + \Delta GWS + \Delta CWS \tag{6.13}$$

$$\Delta TWS_{GLDAS} = \Delta SMS + \Delta CWS \tag{6.14}$$

All the input datasets for the MLP model development are shown in Fig 6.3. Previous research has shown that GLDAS datasets have a strong resemblance to GRACE. Temperature is most likely a proxy for evapotranspiration and precipitation is the major factor that affects variations in TWSA. These two variables are frequently utilised in GRACE data reconstruction (Humphrey et al., 2017; Long et al., 2014). In all the four basins, TWSA exhibited average correlations with precipitation, with the best association in GRB (see Table 6.2). Maximum and minimum temperatures exhibited strong association with TWSA in four river basins. The inverse relationship between temperature and TWSA is shown by the negative correlation, as expected (Table 6.2).

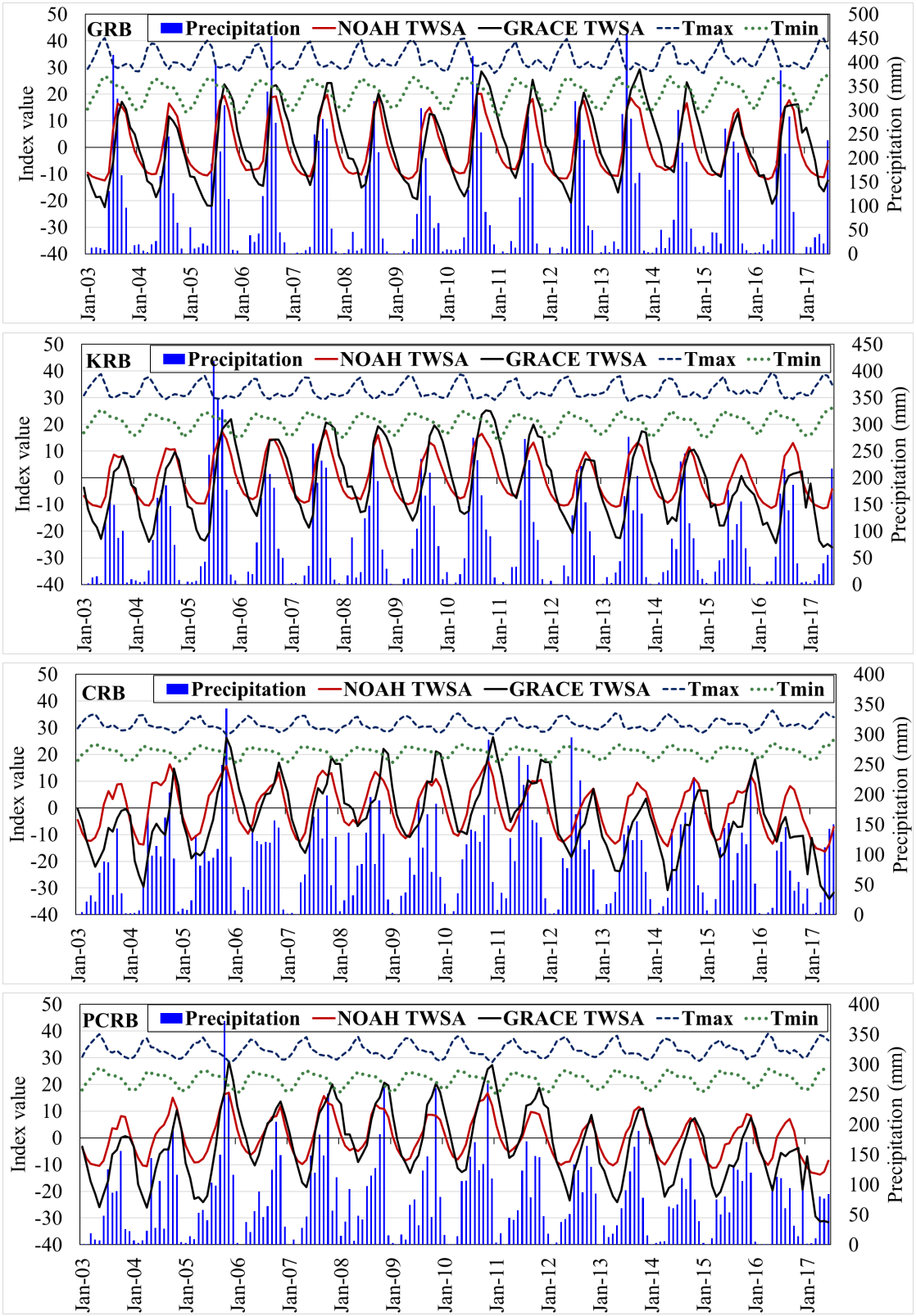

Figure 6.3: Input TWSA from GRACE and GLDAS Noah models, precipitation, maximum and minimum temperature for the development of MLP model.

Table 6.2: Correlation between predictand (TWSA) and perdictors (NOAH TWSA, precipitation (P), maximum temperature (TMax) and minimum temperature (TMin).

River Basins	GRACE TWSA			
	NOAH TWSA	P	Tmax	Tmin
GRB	0.82	0.55	-0.70	-0.48
KRB	0.75	0.44	-0.74	-0.59
CRB	0.85	0.41	-0.72	-0.54
PCRB	0.84	0.51	-0.77	-0.54

The lowest TWSA anomalies are observed during 2003-2005 and 2015-2017 in all the basins because of occurance of severe drought during these periods (Kumar et al., 2021). A strong correlation is observed between GRACE TWSA and NOAH TWSA with a correlation of 0.82, 0.85 and 0.84 for GRB, CRB and PCRB respectively. On the other hand, KRB has a lower correaltion of 0.75 when compared to the other basins (see Table 6.2). During the dry and wet periods, both the GRACE and GLDAS derived TWSA agreed well, with GRACE TWSA experiencing greater crest and trough in few years. NOAH TWSA has less variability than GRACE TWSA because it only considers soil moisture and canopy water storage for the evaluation of TWSA. The correlation strength between GLDAS and GRACE is largely determined by the climatology and the model's structure/parameterization. As a result, along with precipitation and temperature, GLDAS derived TWSA (see Eq. 6.14) is used as one of the predictors for the development of an MLP model.

The predictor and predictand datasets from January 2003 to December 2013 ($\sim$75% of the samples) are used to train the ANN model, while the datasets from January 2014 to June 2017 ($\sim$25% of the samples) are used to test the trained model performance at both grid and basin scales, as shown in Fig. 6.3. The trained ANN model is used to reconstruct and predict the TWSA from 1960-2020. The reconstructed TWSA for the period 2018-2020 is validated against the existing GRACE FO datasets. TWSA reconstruction is carried out from 1960 to 2020, resulting in a 60-year TWSA time series that could be utilised to investigate any long-term climate related applications.

The neural networks are trained at the grid scale in this study. First the training method (the Levenberg-Marquardt algorithm), learning rate (0.05), epochs (1000) and cost function (Mean Squared Error, MSE) are set using the trail and error method. The training is terminated when the MSE is less than 0.001, or when the number of iterations reached 1000. Once the termination requirements are met, the final model parameters and model prediction performance are recorded. These values are constant across all grid cells in the study. Second, grid search approach is used to modify the model hyper parameters to find the best one (i.e., the number of hidden layers, neurons

and activation function) at each grid cell. The range of hidden layers is set from 1 to 2; the neurons number of each hidden layer varies between 3 to 15. The activation functions are "tansig", "logsig" and "purelin", the most used functions in the field of hydrology.

The groundwater observation well data are available for four seasons namely, (i) post-monsoon rabi, (ii) pre-monsoon, (iii) monsoon and (iv) post-monsoon kharif, respectively. The seasonal observation well data is converted into groundwater storage anomalies. Then the monthly TWSA is converted into seasonal GWSAs ($GWSA_{GRACE}$) and validated with reference to GWSA obtained from groundwater observation well measurements ($GWSA_{OBS}$) at both grid and basin scale. For each grid, Pearson's correlation analysis is performed between $GWSA_{GRACE}$ and $GWSA_{OBS}$ to obtain the correlation coefficients.

6.3 RESULTS AND DISCUSSIONS

6.3.1 Model Evaluation at Grid and Basin Scale

The basin-scale study allows for a thorough evaluation of various models for reconstruction and prediction of TWSA. The actual training is performed at the grid level, whereas basin-scale analysis is done using grid averaged TWSA. During the training and testing period, the developed MLP model achieved high accuracy. The magnitudes and spatial patterns of two common metrics (NSE and r) produced by the observed and modelled TWSA during the testing period are compared. The NSE and r are both greater than 0.8 for the majority of grids in each basin as shown in Fig. 6.4. The GRB and KRB have relatively high NSE and r values. When compared to GRB and KRB, CRB and PCRB experienced lower NSE and r values. In general, high NSE and r levels are found in humid locations, while low values are found in dry places. GRB experienced a sub-humid climate, but CRB and PCRB experienced a semi-arid climate, resulting in the variation of NSE and r values (see Fig. 6.5 and Table 6.3). Another factor for the variations in NSE and r values is the area equipped for irrigation. In India, $>60\%$ of area is under irrigation with groundwater because of erratic nature of precipitation, increase in population and demand of water for irrigation, domestic and industrial usage. CRB and PCRB experienced more groundwater usage for irrigation compared to GRB and KRB, because of which low NSE and r values are observed between observed and modelled TWSA during the testing period (see Fig. 6.6). Also **G**round**W**ater **A**bstraction **R**atio (GWAR) defined as the ratio of groundwater withdrawals to groundwater availability is also high for CRB (52%) and PCRB (64%) and low for GRB (36%) and KRB (42%) resulting in high and low NSE and r values between observed and modelled TWSA (see Table 6.3).

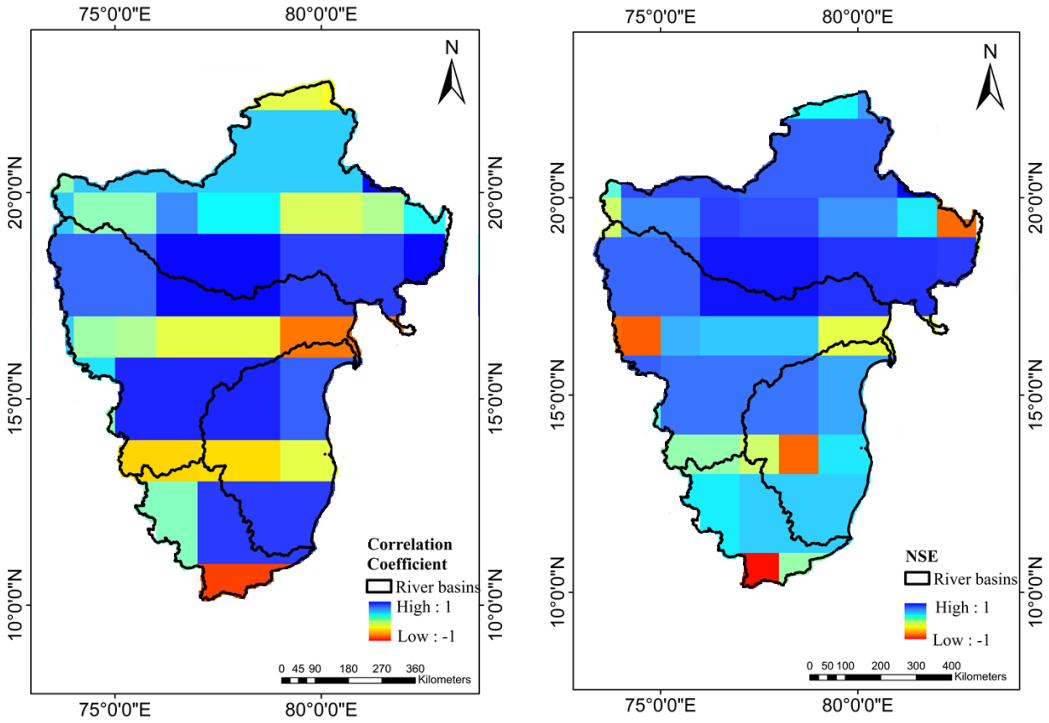

Figure 6.4: Spatial distributions of NSE and r values obtained from observed and MLP modelled TWSA during the testing period.

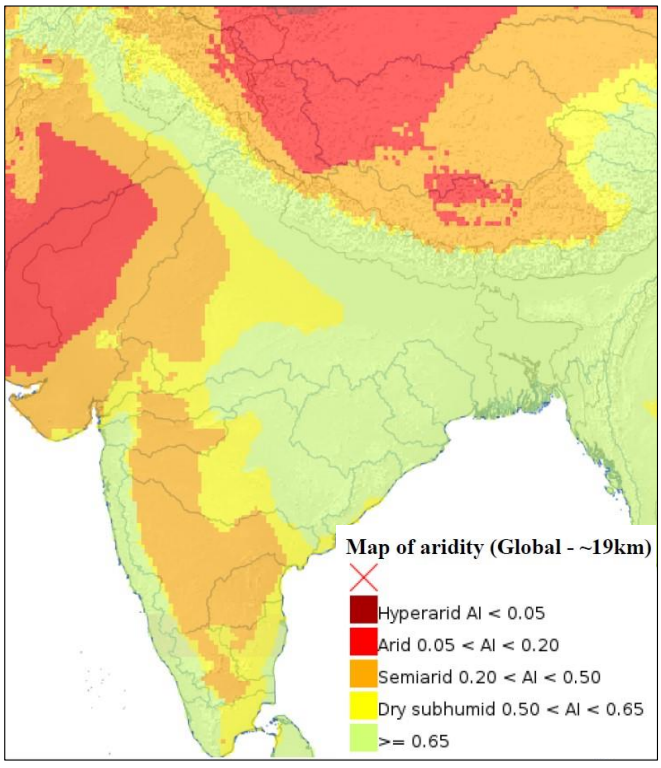

Figure 6.5: The **A**ridity **I**ndex (AI) map of India with major river basins. Higher AI values denote humid conditions and lower AI values representing higher aridity. Source: (https://data.apps.fao.org/catalog//iso/221072ae-2090-48a1-be6f-5a88f061431a)

Table 6.3: Basin-wide characteristics, aridity index and percentage of **G**round**W**ater **A**bstraction **R**atio (GWAR) values.

Basin	Area (Sq.km)	P (mm)	Aridity Index (AI)	Climate	Groundwater abstraction ratio (GWAR) (%)
GRB	3,12,812	1093.21	0.5 to 0.65	Sub humid	36
KRB	2,54,750	859.11	0.2 to 0.5	Semi-arid	42
CRB	1,17,889	770.18	0.5 to 0.65	Sub humid	52
PCRB	85,626	1075.23	0.5 to 0.65	Sub humid	64

Source: (https://data.apps.fao.org/catalog//iso/221072ae-2090-48a1-be6f-5a88f061431a) and Amarasinghe et al., 2005.

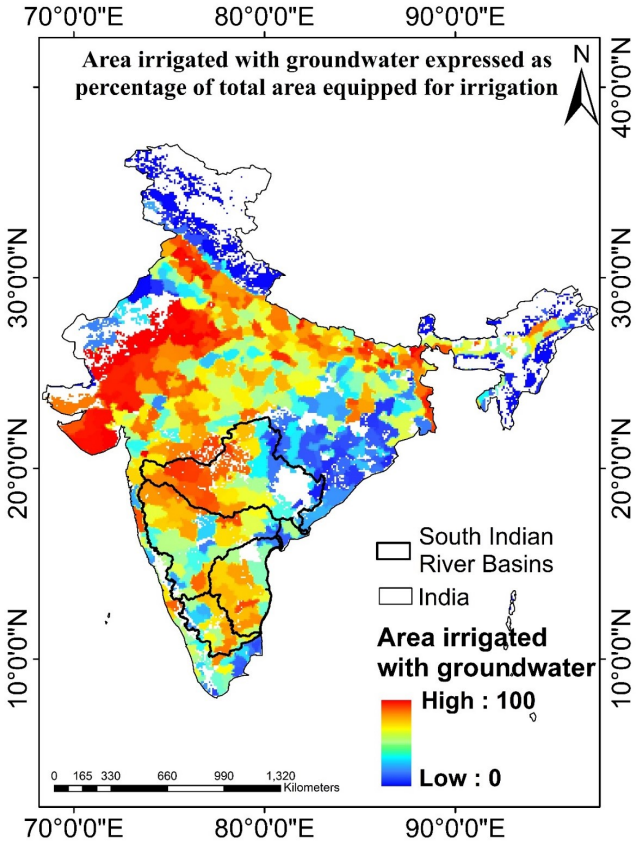

Figure 6.6: Area irrigated with groundwater based on **F**ood and **A**gricultural **O**rganization (FAO) Global Map of Irrigated Areas (http://www.fao.org/).

To examine the reconstructed TWSA more intuitively, the modeled and observed TWSA are compared during the test period, January 2014 to June 2017 (Fig. 6.7). The observed TWSA is highly correlated with the MLP modelled TWSA in four basins, with correlation coefficient ranging from 0.89 to 0.95. Out of four river basins, GRB exhibited the highest correlation (0.95), followed by KRB with 0.92, CRB with 0.9 and PCRB with 0.89. Groundwater abstractions are more in CRB and PCRB resulting in low correlation between the modeled and observed TWSA when compared with GRB

and KRB during the testing period (Amarasinghe et al., 2005; Meghwal et al., 2019). The trained leader MLP model for each basin is used for the reconstruction of GRACE TWSA from 1990 to 2020.

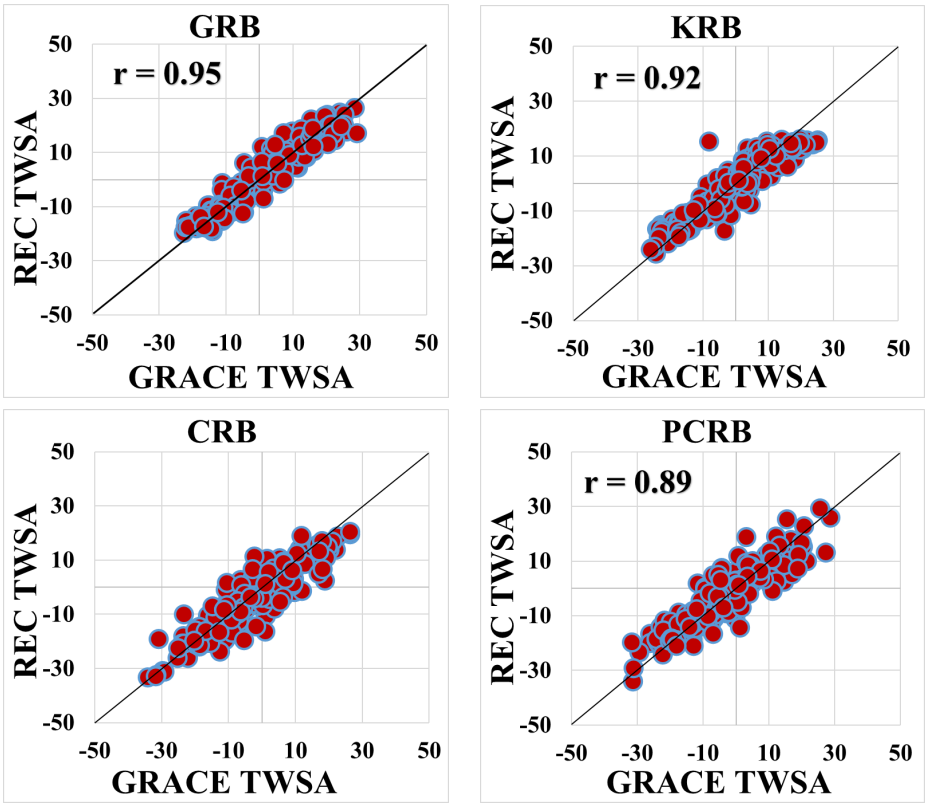

Figure 6.7: Scatterplots comparing observed and modelled TWSA during the test period derived by the MLP model.

6.3.2 Basin Scale Evaluation of the Reconstructed TWSA

The neural network model is developed at the grid scale using the training dataset and validated using the testing dataset. As shown in Fig. 6.8, the MLP model with the best correlation between the observed and modelled TWSA during the testing period is used to reconstruct the GRACE TWSA from 2003 to 2017. TWSA showed increasing interannual variability throughout the training period and decreasing interannual variability during the testing period. Increase in TWSA is due to the increase in precipitation anomalies during 2003-2013 in South India (Mishra et al., 2021; Satish Kumar et al., 2021).

Decreasing trends are observed in TWSA during the testing period because of precipitation variability. During 2015-2018, South India experienced worst drought, with precipitation deficits of more than 40%, resulting in a drop in TWSA (see Fig. 6.8) (Mishra et al., 2021). According to the findings, the developed MLP model performed well in each river basin. When compared to the observed TWSA, the

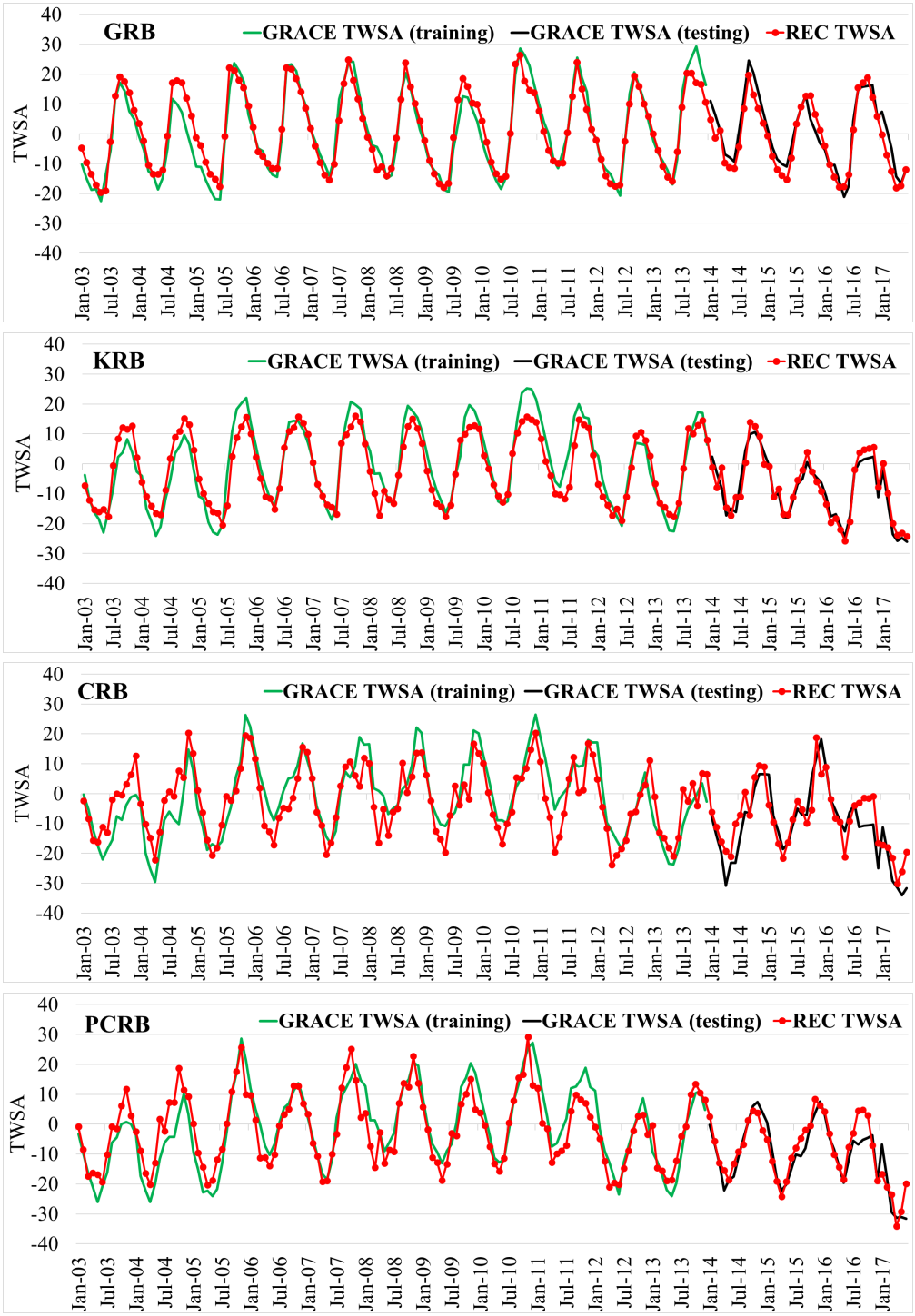

Figure 6.8: The training TWSA (green line), testing TWSA (black line) and the MLP model based TWSA (dotted red line) at the basin scale.

reconstructed TWSA is slightly underestimated in KRB and CRB during the training period (2003-2013). In general, the correlation is dependent on the aridity values. Higher correlations are primarily found in humid basins and low NSE values are found in relatively dry areas. CRB and PCRB experienced sem-arid to sub-humid climate resulting in low correlations between observed and reconstructed TWSA (see Fig. 6.5

and Table 6.3). During the training and testing period, the remaining river basins (GRB and PCRB) have shown a good correlation between observed and modelled GRACE TWSA because of subhumid climate in both the basins (see Fig. 6.5 and Table 6.3) (Liu et al., 2021; Sun et al., 2020).

Along with the observed TWSA from 2003 to 2017, the observed GRACE FO TWSA from 2018 to 2020 is also considered. As a result, the trained MLP models for each basin are used to predict the TWSA from 2017-2020 and validate the results against observed GRACE FO TWSA from 2018-2020. From the results (see Fig. 6.9) it is clear that there exists a good correlation between the predicted (2017-2018) and observed GRACE FO TWSA for four river basins. A decreasing trend is observed in all the four basins during 2017-2019. During 2016–18, South India experienced worst drought because of the failure of monsoon rainfall, with a precipitation deficit of ∼45% (Mishra et al., 2021). Because of the rainfall deficit drought has occurred during 2016–18 that led to the decreasing trends of TWSA during 2017-2019.

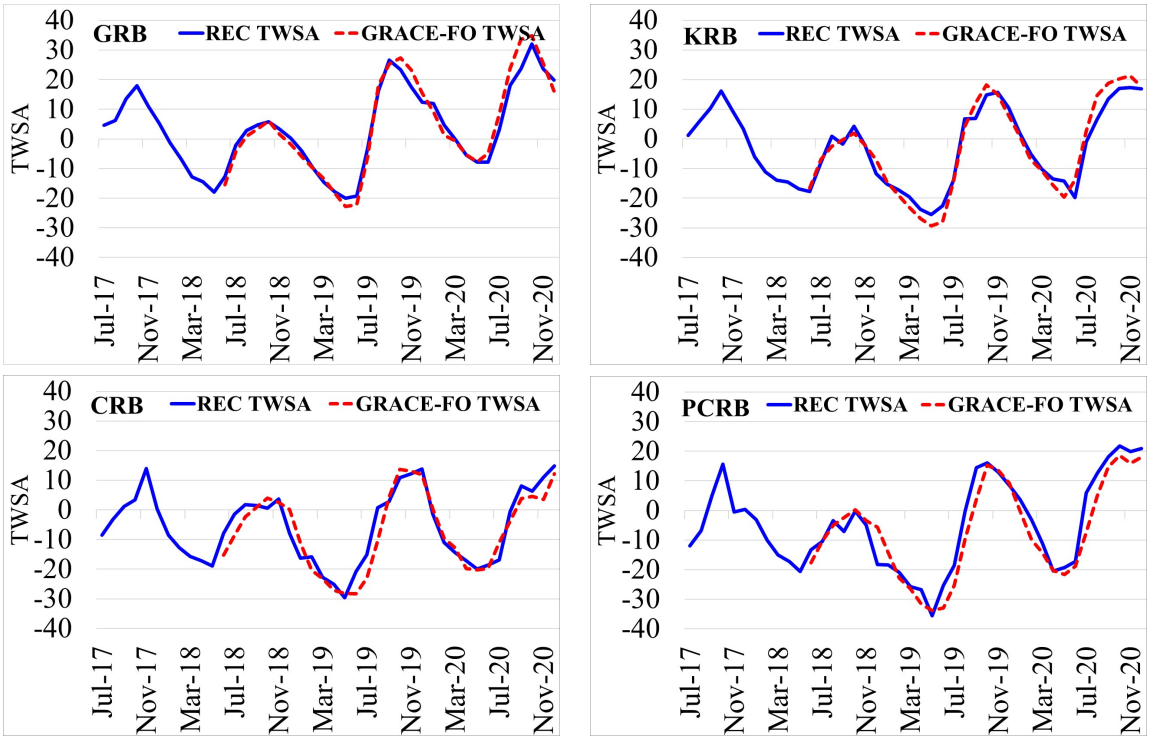

Figure 6.9: Comparison of reconstructed TWSA (blue line) and GRACE FO TWSA (red dotted line).

The best MLP model developed for each basin is used to reconstruct the past TWSA using the predictor datasets to obtain the reconstructed TWSA prior to the GRACE period (1960-2002). The MLP model based reconstructed TWSA time series from 1960 to 2002, as well as the observed (2003-2017), predicted (2017-2018) and GRACE FO (2018-2020) time series in the four basins is shown in Fig. 6.10.

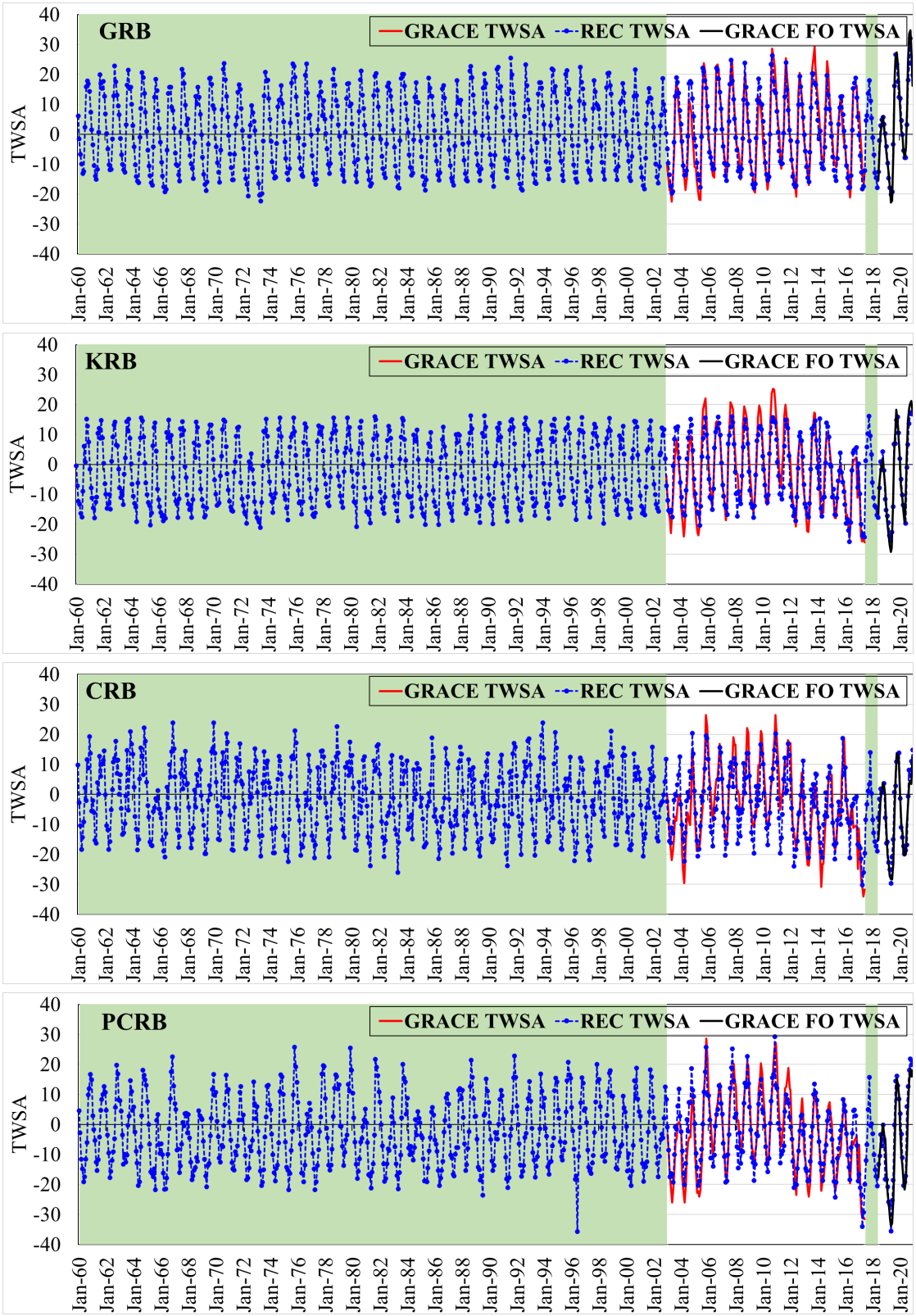

Figure 6.10: The MLP model based TWSA from 1960-2020 (dotted blue line). (The shaded region represents the reconstructed TWSA).

The long term TWSA series experienced decreasing and increasing trends during 1960-2020. GRB and KRB displayed decreasing trends during 1965-67, 1972-74,

1984-1988, 2002-2003, 2009-2010, 2014-2016 and 2017-2018. CRB and PCRB exhibited decreasing TWSA during 1965-67, 1968-1970, 1972-975, 1986-1988, 1996-1998, 2000-2003 and 2015-2018. Among the four basins CRB and PCRB experienced more decreasing and increasing trends compared to GRB and KRB because of anthropogenic abstractions of groundwater for irrigation purposes and climate factors (Asoka et al., 2017; Mishra et al., 2021). The decreasing TWSA trends during 1960-2020 matches with the previously occurred hydrological and meteorological droughts over Indian regions (Satish Kumar et al., 2021). The major hydrological and meteorological droughts are occurred in India during 1695-67, 1968-70, 1972-73, 1980-81, 1986-88, 2000-2003, 2009-2010 and 2015-2018 (Mishra, 2020). These previously observed droughts matches well with the reconstructed GRACE TWSA series from 1960-2020.

6.3.3 Grid Wise Seasonal Comparison of $GWSA_{GRACE}$ with $GWSA_{OBS}$

The reconstructed TWSA is converted to seasonal GWSA $(GWSA_{GRACE})$ and validated against the seasonal GWSA obtained from the in-situ observation well network $(GWSA_{OBS})$ during 1996-2020. This period is considered from 1996 to 2020, as the groundwater levels provided by **C**entral **G**round **W**ater **B**oard (CGWB, India) are available from 1996 onwards. In this study, comparison of seasonal $GWSA_{GRACE}$ with $GWSA_{OBS}$ is carried out using the Pearson's correlation analysis from 1996-2020 at grid scale over GRB, KRB, CRB and PCRB (see Fig. 6.11). Each grid had a minimum of 3 and a maximum of 60 observation wells over the study area. All the in situ observation well data is converted to $GWSA_{OBS}$ using the procedure described in the methodology section. The **I**nverse **D**istance **W**eightage (IDW) approach is used for each grid to convert the $GWSA_{OBS}$ at all observation well locations covering that grid into an average $GWSA_{OBS}$, which is then validated with $GWSA_{GRACE}$. In the post-monsoon rabi season, all the four basins exhibited moderate correlations between $GWSA_{GRACE}$ and $GWSA_{OBS}$. Only a few grids in the GRB and CRB displayed high positive correlations. Because of the limited availability of surface water during the post-monsoon rabi season, groundwater is used more for irrigation. As a result, there are moderate correlations between $GWSA_{GRACE}$ and $GWSA_{OBS}$ in the post-monsoon rabi season. During the pre-monsoon season, except for KRB, remaining three basins (GRB, PCRB and CRB) exhibited highly positive correlations between $GWSA_{GRACE}$ and $GWSA_{OBS}$. KRB, on the other hand, showed highly positive correlations on the Eastern side and negative correlation on the Western side of the basin. The majority of crops planted during the Rabi season in India are harvested during the pre-monsoon season. As a result, groundwater usage is lower than in Rabi season. Therefore, good correlations are observed between $GWSA_{GRACE}$ and $GWSA_{OBS}$ in the pre-monsoon season.

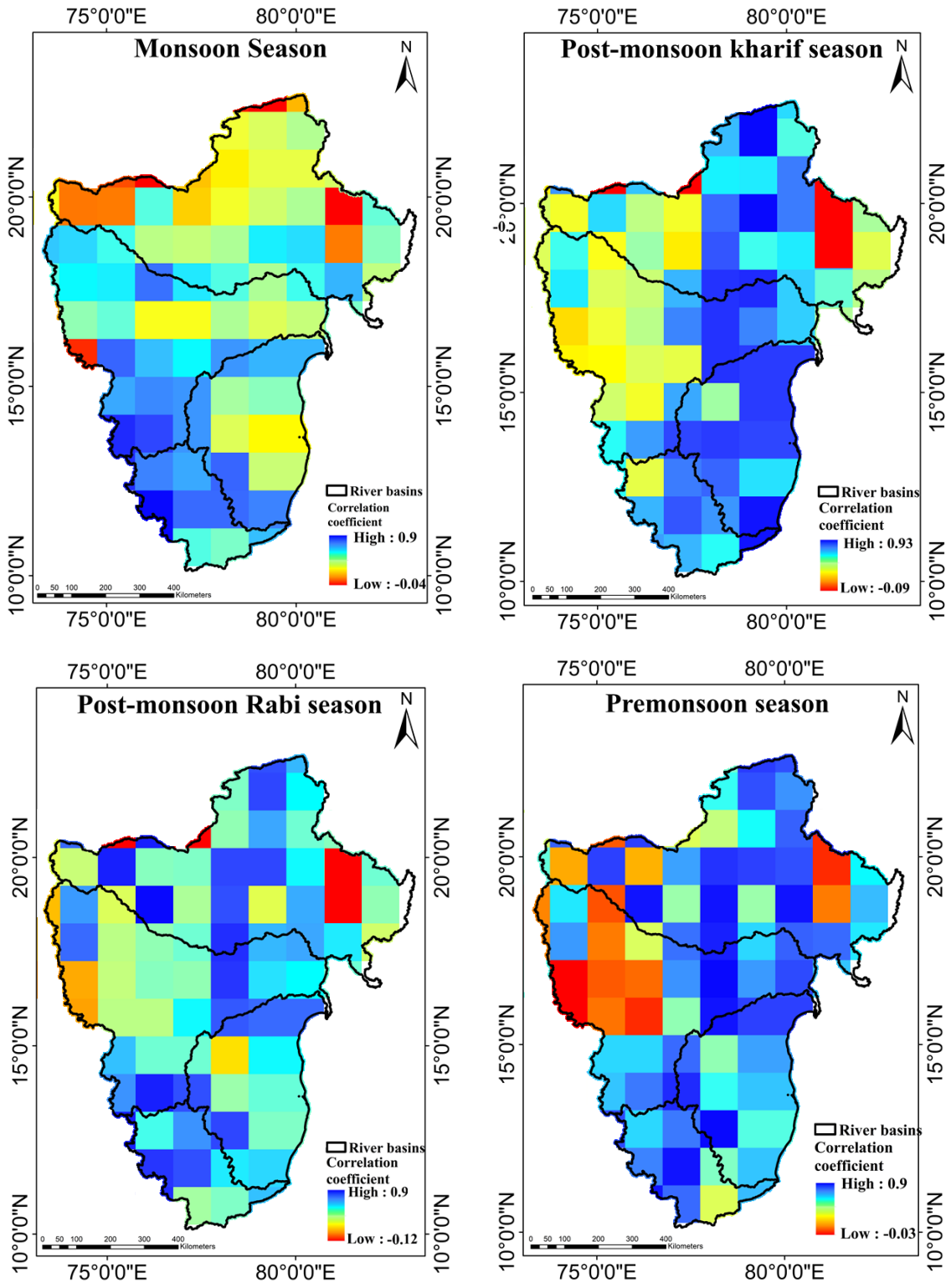

Figure 6.11: Grid wise seasonal correlation between $GWSA_{GRACE}$ and $GWSA_{OBS}$

During the monsoon season, GRB exhibited moderate correlation between $GWSA_{GRACE}$ and $GWSA_{OBS}$ over the entire basin, with the exception of a few grids with low correlations in the Western part of the basin. KRB also experienced moderate to high correlation, while PCRB experienced moderate to low correlation. In the

monsoon season, CRB experienced good correlation between $GWSA_{GRACE}$ and $GWSA_{OBS}$. Because of the monsoon rainfall fluctuations, more than 60% of the geographical area in South India is being irrigated using groundwater. Therefore, fluctuations in the correlation can be observed between $GWSA_{GRACE}$ and $GWSA_{OBS}$ because of the abstractions of groundwater for irrigation purposes. In the post-monsoon Kharif season, GRB exhibited moderate correlations, with the exception of a few grids with low correlations over the Western part of the basin. The KRB had high correlations in the Eastern part and moderate correlation in the Western part of the basin. Over the entire basins, PCRB and CRB showed strong correlations between $GWSA_{GRACE}$ and $GWSA_{OBS}$.

6.3.4 Basin Wise Seasonal Comparison of $GWSA_{GRACE}$ with $GWSA_{OBS}$

Pearson's correlation estimates (r) between seasonal $GWSA_{GRACE}$ and $GWSA_{OBS}$ are shown in Fig. 6.12. There is a strong significant correlation between $GWSA_{GRACE}$ and $GWSA_{OBS}$ in all the four basins. The 'r' values provided a vital information on closeness in the data magnitude. The highest correlation is observed in PCRB (r= 0.81) followed by CRB (r= 0.79) and GRB (r= 0.72). The least correlation is noticed in KRB with r= 0.68. The peaks of $GWSA_{GRACE}$ and $GWSA_{OBS}$ are well matched in CRB and PCRB. An increasing trend is observed in GWSAs from 2005 to 2011 in all the basins except GRB. Subsequently, a decreasing trend in GWSAs is observed from 2011 to 2014 in the KRB, CRB and PCRB.

The $GWSA_{GRACE}$ and $GWSA_{OBS}$ exhibited strong seasonality for all the four seasons across all the basins (see Fig. 6.12). The $GWSA_{GRACE}$ accurately matched the seasonality pattern from 1996 to 2013, but from 2014 to 2020, the pattern is slightly under or over estimated in all the four basins. During the monsoon season (June to September), the entire Indian region experiences the majority of the precipitation (**N**ational **C**limate **C**entre (NCC), 2013); however, in the Southern part of the country, the monsoon season extends into the months of October and November (NCC, 2013). As a result, the lowest GWS values are obtained during the pre-monsoon season, whereas the highest GWS values are obtained during the monsoon season in all the basins. Climate factors such as precipitation and evapotranspiration have an impact on seasonality in the groundwater storage, especially in areas with shallow groundwater tables (Eltahir and Yeh, 1999; Sridhar et al., 2018). Because the entire Southern part of India has a distinct monsoon season, the majority of the annual precipitation (>74%) has occurred during the months of June to September (Guhathakurta and Rajeevan, 2008). Other factors that effect groundwater inflow are modelled from canals and surface water bodies and agricultural return flow (Hoekema and Sridhar, 2011, 2013; Mukherjee et al., 2007). Pumping associated with irrigation,

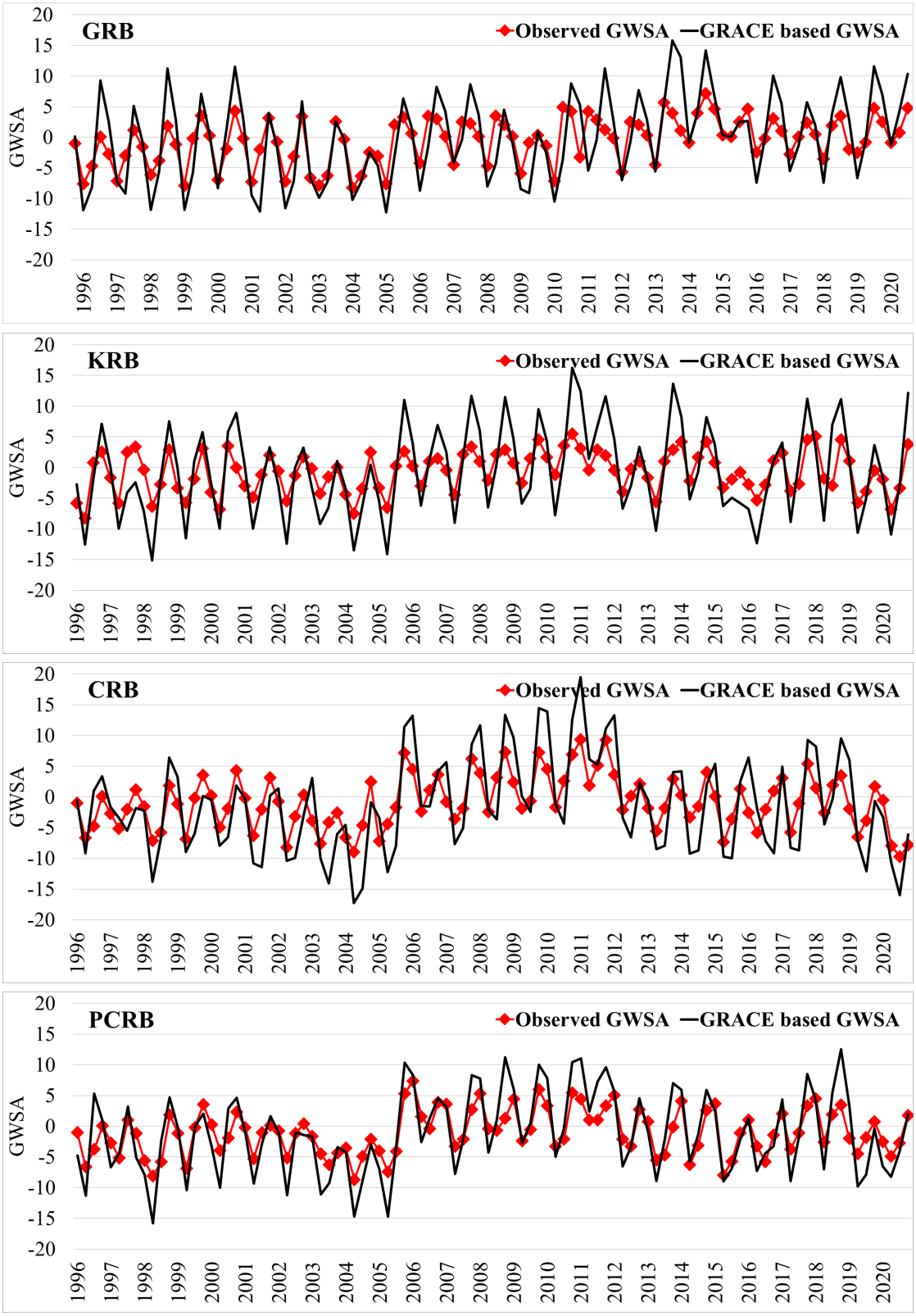

Figure 6.12: Comparison of $GWSA_{GRACE}$ with $GWSA_{OBS}$ in four river basins.

on the other hand, has significantly reduced groundwater storage (Saha and Agrawal, 2006). Other factors, such as baseflow and inter-aquifer flow, are also critical in maintaining groundwater storage.

6.3.5 Groundwater Storage Anomaly from Satellite-based Estimations

Between 1996 and 2020, $GWSA_{GRACE}$ estimates show the emergence of intense groundwater depletion zones in GRB, KRB, CRB and PCRB as shown in Fig. 6.13. Also, four river basins have decreasing GWSA in 2004-2005, 2012 and 2016-2019. Negative GWSAs are observed in GRB from 2003 to 2005, 2010 to 2012 and 2016 to 2019. 1997-1998, 2003-2005, 2012 and 2016-2019 for KRB. 2003-2005, 2012-2013, 2014-2015 and 2017-2020 for CRB and PCRB. Overall, CRB and PCRB have more negative GWSAs than GRB and KRB. The negative GWSA denotes a decrease in water storage and the occurrence of droughts.

The $GWSA_{GRACE}$ are consistent with previous studies on drought events conducted in Southern part of India (Bhanja et al., 2016; Mishra et al., 2021; Panda and Wahr, 2016; Soni and Syed, 2015). The 2015 drought had an impact on crop output and water availability in the central and Southern parts of the country (Mishra et al., 2016; Prakash, 2018). The 2015-2016 drought affected a large portion of South India, resulting in decreased reservoir storage and hydro-electric production. The 2015-2016 drought, which affected approximately 330 million people in ten states, particularly in India's Southern regions, resulted in significant groundwater depletion (UNICEF, 2016). From Mishra et al. (2021), there was a severe drought and worsened water scarcity in Southern India from 2016 to 2018. $GWSA_{GRACE}$ fluctuations in the current study are consistent with earlier records of occurrence of drought events in the Southern region of India, indicating that GRACE dataset can be used to evaluate drought-related studies.

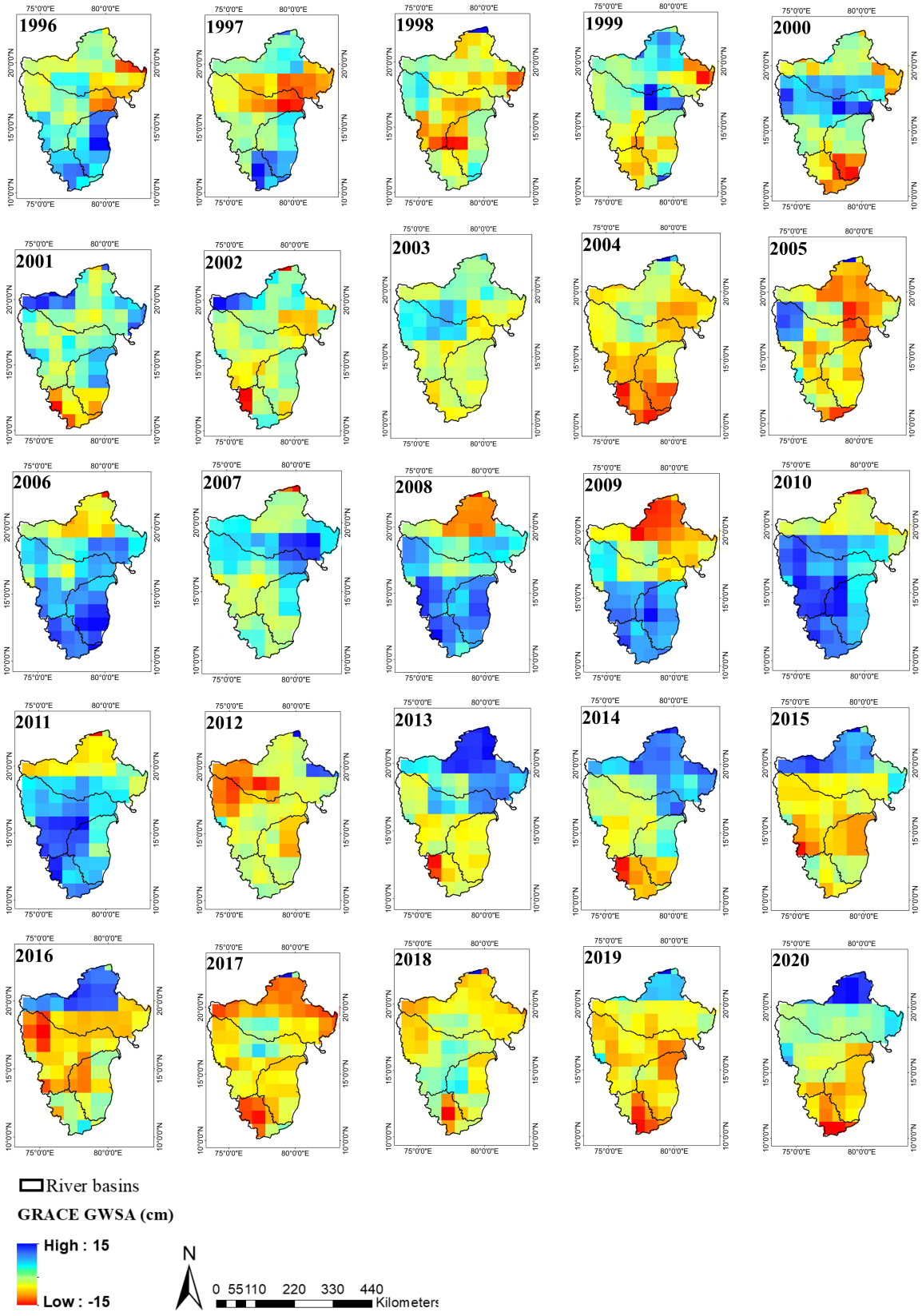

Figure 6.13: Maps of annual GWSA between 1996 and 2020.

6.4 CONCLUSIONS

In the present study, we reconstructed (1990-2002) and predicted (2017-2018) TWSA data by using the MLP model based on GRACE mascon's solution. The performance of the models is evaluated at the grid and basin level across GRB, KRB, CRB and PCRB. For the first time, we compared $GWSA_{GRACE}$ with $GWSA_{OBS}$ at seasonal scale between 1996 and 2020, using recently available GRACE datasets, i.e., RL06 mascon solutions. In South India, more than 1950 in-situ groundwater observation wells are utilised for water level data. Pearson's correlation analysis is used to compare seasonal $GWSA_{GRACE}$ with $GWSA_{OBS}$ at grid and basin scales from 1996 to 2020. In climatologically and hydro-geologically varied parts of South India, GRACE-based estimates matched well with ground estimates. The key findings from this part of the study are given as follows:

- All of the MLP models for each river basin performed reasonably well in reconstructing and predicting the TWSA at grid and basin scales.
- At the grid scale, the TWSA correlated well with the MLP modelled TWSA in four basins, with correlation coefficient ranging from 0.89 to 0.95. At the basin scale, GRB exhibited the highest correlation (r=0.95) between the modelled and observed TWSA, followed by KRB with r=0.92, CRB with r=0.9 and PCRB with r=0.89.
- The $GWSA_{GRACE}$ obtained from reconstructed TWSA is correlated well with $GWSA_{OBS}$ at grid and basin scales from 1996-2020 across four river basins.
- The $GWSA_{GRACE}$ estimates correlated well with $GWSA_{OBS}$ with highest correlation observed in PCRB (r= 0.81) followed by CRB (r= 0.79) and GRB (r= 0.72).
- Overall, the MLP technique is more effective at reconstructing TWSA and potentially bridging the gap between two satellite missions. It can also be used to rebuild pre-GRACE era changes in water storage.

Based on the findings of this study, we recommend using GRACE mascon solutions for groundwater assessments throughout the region, as well as in other parts of the world with similar meteorological, hydrogeological and groundwater withdrawal conditions.

CHAPTER 7

ANALYSIS OF SEVERITY-DURATION-FREQUENCY AND SEVERITY-AREA-FREQUENCY CURVES FOR GRB

This chapter deals with the fourth sub objective that the evaluation of drought frequency analysis and the development of **S**everity-**D**uration-**F**requency (SDF) and **S**everity-**A**rea-**F**requency (SAF) curves only for Godavari River Basin. This type of evaluation can be conducted on all the other basins under consideration in this study.

7.1 INTRODUCTION

Regional drought curves of SDF and SAF are developed under the conditions of drought in GRB, as it is one of the largest river basins with relatively high water potential in India. Currently, the concept of Copula has been widely used to measure the bivariate and multivariate joint probability distributions in Hydrology and water management engineering (Ganguli, 2014; Thilakarathne and Sridhar, 2017). In modeling the characteristics of two or more dependent variables such as drought severity, duration and area of drought, the Copula functions are highly effective and efficient. This is because of the function that maintains a strong correlation between the variables considered and is not bound to the identical distribution of marginal probability with regard to long-term predictions. The methodology for the development of SDF and SAF curves is provided in the form of flowchart in Fig. 7.1.

Reconstructed TWSA is used to calculate CCDI from 1960-2020. Then IMD precipitation dataset is used to evaluate 12-month SPI (SPI12). With the calculated CCDI and SPI12, the SDF and SAF curves are developed over GRB from 1960-2020. Here SPI12 based SAF and SDF curves are used as a standard metric to compare CCDI based SAF and SDF curves. The aim of this section is to check, whether the reconstructed TWSA can be utilized in developing SAF and SDF curves or not.

The analysis include: (i) identification of homogeneous drought regions by using Fuzzy C-Means Clustering approach; (ii) quantification of the changes in drought climatology with SPI12 (iii) development of SDF curves by employing copula-based methodology, by analysing the changes in joint return period of severity and duration and (iv) examination of SAF curves to identify the changes in drought return periods covering a specific percentage of areal extent and the corresponding severity values.

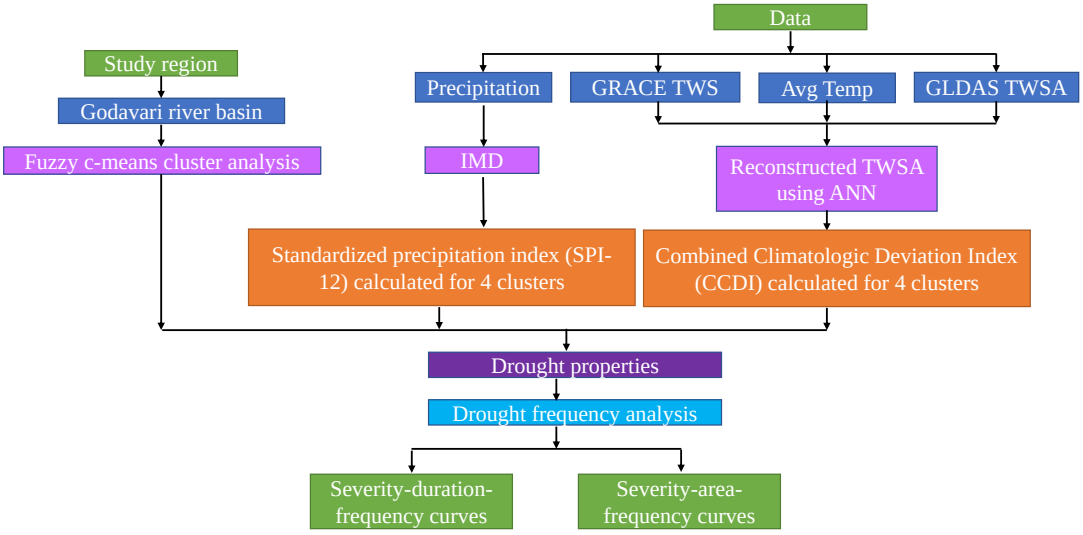

Figure 7.1: Flow chart of fourth sub objective.

7.2 METHODOLOGY

7.2.1 Fuzzy C-Means Clustering

Dunn (1973) proposed the concept of **F**uzzy **C**-**M**eans (FCM) clustering and Bezdek (1981) expanded it further. Consider a cluster c with M objects where Y_k is the data vector for k_{th} $(k = 1, 2, \ldots, M)$ object. The technique of FCM minimizes the objective function as given below

$$J(U, V) = \sum_{j=1}^{M} \sum_{i=1}^{c} u_{ik}^{\theta} \left\| Y_k - V_i \right\|^2 \tag{7.1}$$

where u_{ik} denotes the k_{th} point membership value in the i_{th} cluster, V_i is the centre of the i_{th} cluster $(i = 1, 2, \ldots, c)$, $\left\| Y_k - V_i \right\|^2$ is the squared Euclidean distance between k^{th} data point and V_i. θ is the fuzziness index or the fuzzifier that can have any value >1. The number of clusters and the data vector of the cluster center are randomly selected in the FCM algorithm and the membership matrix is then calculated as

$$u_{i<k}^{t} = \left[\sum_{j=1}^{c} \left(\frac{\left\| y_k - c_i \right\|}{\left\| y_k - c_j \right\|} \right)^{\frac{2}{\theta - 1}} \right]^{-1} \tag{7.2}$$

with the updated membership values, new cluster centers are calculated as follows

$$V_i = \frac{\sum_{k=1}^{M} u_{ik}^{\theta} y_k}{\sum_{k=1}^{M} u_{ik}^{\theta}} \tag{7.3}$$

using new cluster centers, the membership matrix is updated as

$$u_{i<k}^{t+1} = \left[\sum_{j=1}^{c} \left(\frac{\|y_k - c_i\|}{\|y_k - c_j\|} \right)^{\frac{2}{\theta-1}} \right]^{-1} \tag{7.4}$$

if $\left\| u_{i<k}^{t+1} - u_{i<k}^{t} \right\| < \varepsilon$ the algorithm will stop. If not, it goes back to step 1. In the present analysis, three validity indices are used to check the efficiency of clustering.

7.2.1.1 Separation Index (S_i)

The compactness and separation function (S_i) proposed by Xie and Beni (1991) is defined as the ratio of variance within clusters to the variance between clusters. The S_i value is lower, the clustering is better.

$$S_i(U, V : X) = \frac{\sum_{i=1}^{c} \sum_{k}^{M} (u_{ik}^{a}) \|c_i - y_k\|^2}{M \min\limits_{i \neq k} \|v_i - y_k\|^2} \tag{7.5}$$

7.2.1.2 Fuzziness Partition Index (F_{pi})

The membership (fuzziness) that various classes share (Bezdek, 1974) is calculated by the Fuzziness partition index.

$$F_{pi}(U) = \frac{1}{m} \sum_{i=1}^{c} \sum_{k=1}^{M} u_{ik}^2 \tag{7.6}$$

7.2.1.3 Partition Entropy (P_e)

Partition entropy is represented as

$$P_e(U) = \frac{1}{m} \sum_{i=1}^{c} \sum_{k=1}^{M} u_{ik} \log_a(u_{ik}) \tag{7.7}$$

Lower the P_e value, better the clustering and it varies between 0 and $\log(c)$. The Fuzzy C Means clustering analysis is performed using R software (package: ppclust; version 3.5.1; https://www.r-project.org/)

7.2.2 Copula Function

Copula is a function developed by Sklar (1959) that joins or couples two or more random variables. It transforms two or more marginal distributions into bivariate or multivariate distributions of random variables. Let X and Y be a pair of random variables with

marginal cumulative distribution functions $F_X(x)$ and $F_Y(y)$. From Sklar's theorem, using Copula function C, the joint distribution function $F_{XY}(x, y)$ of the two dependent random variables can be expressed as

$$P(X \leq x, Y \leq y) = F_{XY}(x, y) = C(F_X(x), F_Y(y)) = C(u, v) \tag{7.8}$$

where, $F_{XY}(x, y)$= joint CDF of the considered random variables X and Y. u and v are two uniformly distributed random variables expressed as $u = F_X(x)$ and $v = F_Y(y)$. The bivariate copula is a distribution function $C(\bullet)$ with mapping $C : [0, 1]^2 \rightarrow [0, 1]$. Each element (u, v) in the domain satisfies the following properties

- $C(u, 0) = 0 = C(0, v) \quad \forall\ u, v\ \in\ [0, 1]^2$
- $C(u, 1) = u; C(1, v) = v \quad \forall\ u, v\ \in\ [0, 1]^2$ and
- If $C(u, v)$ is a joint distribution function, then $C(u_2, v_2) - C(u_2, v_1) - C(u_1, v_2) + C(u_1, v_1) > 0$ for $0 \leq u_1 \leq u_2 \leq 1$ and $0 \leq v_1 \leq v_2 \leq 1$.

Copulas are established from different families and further information about different copula families and their properties are found in Nelsen (2007). The significant copula classes are Archimedean, Extreme, Elliptical and Plackett copulas. In this study, Gumbel, Clayton and Frank from Archimedean class, Galambos from Extreme class and Plackett copulas are used to model joint dependence of drought variables. The **C**umulative **D**istribution **F**unctions (CDF) expressions, the corresponding **P**robability **D**ensity **F**unctions (PDF) and the associated copula family set parameters are given in Table 7.1.

Table 7.1: Expression for CDF $(C(u, v))$ and parameter space of the copula families.

Copula family	$C(u, v)$	**Parameter Space**
Clayton	$(\ u^{-\theta}\ +\ v^{-\theta}\ -\ 1\ )^{-\frac{1}{\theta}}$	$\theta \geq 0$
Frank	$-\frac{1}{\theta} ln\left[1 + \frac{(e^{-\theta u}-1)(e^{-\theta v}-1)}{e^{-\theta}-1}\right]$	$\theta \neq 1$
Gumbel	$exp\left\{-\left[(-ln\, u)^{\theta} + (-ln\, v)^{\theta}\right]^{\frac{1}{\theta}}\right\}$	$\theta \geq 1$
Galambos	$uv\ exp\left\{\left[(-ln\, u)^{-\theta} + (-ln\, v)^{-\theta}\right]^{-\frac{1}{\theta}}\right\}$	$\theta \geq 0$
Plackett	$\frac{1}{2(\theta-1)}(s - q)$	$\theta \geq 0$

Note: u and v represents two dependent CDFs, θ is the copula parameter, $s = 1 + (\theta - 1)(u + v)$ and $q = \sqrt{s^2 - 4\, uv\, \theta(\theta - 1)}$.

7.2.2.1 Copula Parameter Estimation

The most frequently used methods for estimating copula parameters are: (i) **M**ethod **o**f **M**oments (MoM; Genest and Rivest (1993)), (ii) **I**nference **F**rom **M**argins (IFM; Joe (1997)), (iii) **E**xact **M**aximum **L**ikelihood (EML) and (iv) **M**aximum **P**seudo-**L**ikelihood (MPL; Genest et al. (1995)) methods. The MPL method is used in the present study for copula parameter estimation. In the MPL method, pseudo log-likelihood function is used the estimate copula parameters. Let $X \in X_{i,1}, X_{i,2}, ..., X_{i,d}$ are the observations of random variables from d-dimensional random vector X. The pseudo-observations are defined with the ranks of the observed data and estimating the empirical CDF using the following expression

$$U = U_{i,d} = \frac{Ranked\, data\, of\, X_{i,d}}{n+1} \quad \forall \; i = 1, 2, ..., n \tag{7.9}$$

$$U_{i,d} = \frac{1}{n+1} \sum_{j=1}^{n} 1 \left\{ X_{j,d} \; \leq X_{i,d} \right\} \quad \forall \; i = 1, 2, ..., n; \;\; j \neq i; \;\; d = 1, 2, ..., n \tag{7.10}$$

where, $U_{i,d}$= vector of pseudo-sample; For bivariate case, $U = \{U_{i,1}, U_{i,2}\}, \;\; \forall \; i = 1, 2, ..., n.$ Then on substituting the empirical CDFs into bivariate copula density produces log-likelihood function (Genest and Favre, 2007) of the form.

$$L_U(\theta) = \sum_{i=1}^{n} log \left[c_\theta (U_{i,1}, U_{i,2}) \right] = \sum_{i=1}^{n} log \left[c_\theta \left(\frac{R_i}{n+1}, \frac{S_i}{n+1} \right) \right] \;\; \forall \; i \in \{1, ..., n\} \tag{7.11}$$

where, c_θ= bivariate copula density; R_i, S_i are the ranks of observed data. Maximizing the rank-based pseudo log-likelihood function gives the parameter θ using the following expression

$$\hat{\theta} = arg \; max \left[ln \, L_U(\theta) \right] \tag{7.12}$$

7.2.2.2 Goodness of Fit

Identification of appropriate copula model is performed using distance-based statistics, such as **A**nderson–**D**arling (AD) and **A**kaike **I**nformation **C**riterion (AIC) methods are used to estimate the performance of fitted copulas. The empirical formulae of AD and AIC statistics are given as follows

$$AD = \max_{1 \leq i \leq n, \, 1 \leq j \leq n} \frac{\left| \hat{C}_n \left(\frac{i}{n}, \frac{j}{n} \right) - C_{p\theta} \left(\frac{i}{n}, \frac{j}{n} \right) \right|}{\sqrt{C_{p\theta} \left(\frac{i}{n}, \frac{j}{n} \right) \left[1 - C_{p\theta} \left(\frac{i}{n}, \frac{j}{n} \right) \right]}} \tag{7.13}$$

where, i and j denotes order statistics of the random variable u and v respectively.

$$AIC(m) = n\ log(MSE) + 2m \tag{7.14}$$

where, m= number of fitted parameters; n= number of observations; MSE= **M**ean **S**quare **E**rror of the fitted copula model and is expressed as follows

$$MSE = \frac{1}{n-m} \sum_{i=1}^{n} (O_i - P_i)^2 \tag{7.15}$$

where, O_i, P_i are the observed and simulated variables respectively. The best copula model represents the lowest AD and AIC test statistics (Amirataee et al., 2018; Janga Reddy and Ganguli, 2012).

7.2.3 Drought Frequency Analysis

In the present study, the definition of runs is adopted to measure the characteristics of drought (severity and duration) (Yevjevich, 1967). Suppose, X_t is a drought variable with a time series t, then a run is a portion of the time series where all the values are either above or below a fixed threshold X_0. Therefore, value above (or below) the threshold is denoted as positive run (or negative run). As the threshold level may vary or constant with time, the drought properties mainly depend on the chosen threshold (Mishra and Singh, 2010). A threshold of 20 percentile (about a threshold value of -0.8) of SPI12 vaule is selected so that a value below that threshold indicates an occurrence of drought (Reddy and Ganguli, 2013).

Several researchers have studied the drought properties using univariate frequency analysis (Cancelliere and Salas, 2004; Tallaksen et al., 1997). Therefore, researchers like Gupta et al. (2020); Janga Reddy and Ganguli (2012); Kim et al. (2006); Rajsekhar et al. (2015a); Shiau and Shen (2001) have generalized univariate cases to bivariate frequency analysis since the joint behavior of multiple characteristics is not revealed in univariate cases. It is therefore important to examine the joint actions of drought characteristics for regional drought assessment and planning. This has led to the development of SDF and SAF curves.

7.2.3.1 Severity-Duration-Frequency (SDF) Analysis

The SDF curves are useful multivariate tools for regional and global drought frequency analysis. The following are few studies from literature that performed SDF analysis for drought characteristics at different parts of the world. SDF analysis for wet periods and derived ISO-severity maps with return periods are performed for Greece by Dalezios et al. (2000). Similarly, for Iran, Saghafian et al. (2003) established SDF curves and

ISO-severity maps. Using either empirical or semi-empirical formulations, these studies developed SDF curves. An analytical approach using copula for the derivation of SDF curves is presented by Shiau and Modarres (2009). Adarsh et al. (2018); Gupta et al. (2020); Halwatura et al. (2015); Janga Reddy and Ganguli (2012); Rad et al. (2017); Samantaray et al. (2019) are other notable studies that have derived SDF curves based on copula. The following steps are involved in the derivation of the SDF curves using copula in this study.

- Standard goodness of fit statistics is selected to assess the best fitting marginal distribution for severity and duration.
- A joint and conditional marginal distribution is constructed for severity and duration using a best fit copula method.
- Relationship among severity, duration and frequency is established in terms of return period for drought events using the conditional recurrence interval provided by Shiau et al. (2007).

$$T_{S|D}(s|d) = \frac{1}{\gamma\left(1 - F_{S|D}(s|d)\right)} \tag{7.16}$$

where, d = drought duration, s = drought severity, γ = arrival rate, $F_{S|D}(s \mid d)$ and $T_{S|D}(s \mid d)$ are the conditional CDF and conditional recurrence interval of S given $D = d$ respectively. The expression for conditional CDF is given below

$$F_{S|D}(s|d) = \frac{\partial F_{S,D}(s,d)}{\partial F_D(d)} \tag{7.17}$$

where $F_{S,D}(s,d)$= joint CDF and $F_D(d)$ represents the CDF of drought duration.

- SDF curves for different return periods is derived from Eq. 7.16 and 7.17.

7.2.3.2 Severity-Area-Frequency (SAF) Analysis

The return period of a drought with severity covering a particular percentage of areal extent is defined by SAF curves and it indicates that drought has occurred (Burke and Brown, 2010). Few earlier studies that developed SAF curves are Amirataee et al. (2018); Bonaccorso et al. (2015); Gupta et al. (2020); Hisdal and Tallaksen (2003); Kim et al. (2002); Loukas and Vasiliades (2004); Mishra and Singh (2009); Santos (1983); Tase (1976). To evaluate SAF curves, the following procedure is adopted.

- Using run theory, annual severity is estimated at each grid point.
- Different thresholds of severity are computed for various areal extents and is expressed in terms of percentage of total area for each year.
- The parameters of different distributions are calculated using L-moments and the best fit distribution is identified for severity values for various areal extents.
- Finally, the frequency analysis is performed to calculate the return periods involved with different drought severity values for various percentage areal extents.

7.3 RESULTS

7.3.1 Formation of Homogeneous Regions

For GRB, the FCM concept is applied to the matrix containing mean annual precipitation, standard deviation, skewness and kurtosis. The selected variables are normalized before the application of cluster analysis because of the variation in the units. The efficiency of FCM depends on the fuzzifier index and optimum number of clusters. So, the clusters are varied from 2 to 6 (Urcid and Ritter, 2012) with a fuzzifier index of 2 (Pal and Bezdek, 1995). The optimum number of clusters are selected using validity indices S_i, F_{pi} and P_e as discussed in the methodology that are provided in Table 7.2. The S_i and P_e values are minimum at four and F_{pi} value is minimum at five number of clusters. Therefore, optimum number of clusters are assigned as four as shown in Fig. 7.2.

Table 7.2: Statistics of the validity indices

Clusters	$\mathbf{S_i}$	$\mathbf{F_{pi}}$	$\mathbf{P_e}$
2	0.67	0.83	0.87
3	0.57	0.77	0.78
4	0.35	0.74	0.73
5	0.39	0.72	0.74
6	0.41	0.76	0.77

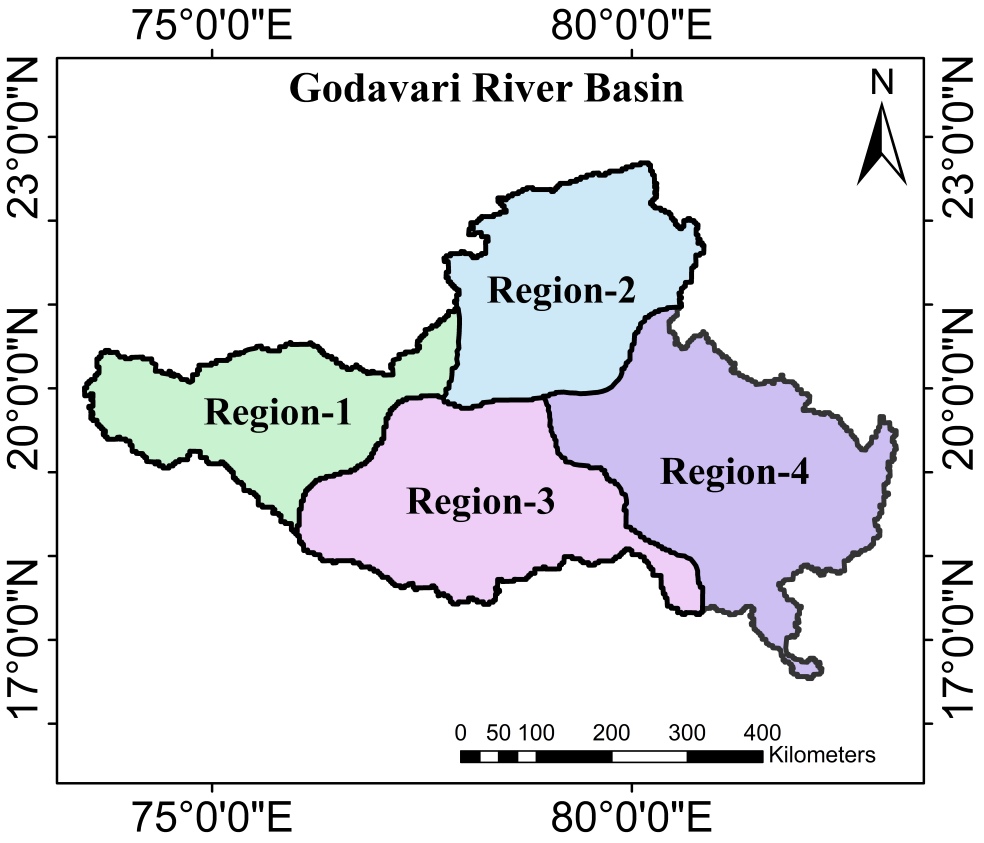

Figure 7.2: Clusters identified by FCM for GRB.

7.3.2 Characterization of Drought using SPI12

The SPI12 values are computed for each homogenous region for GRB using IMD (1960-2020) monthly precipitation dataset. The method of runs (Yevjevich, 1967) is applied to the SPI12 series with a threshold of -0.8 to evaluate drought characteristics (severity, duration and drought events) for four homogeneous regions. Top five drought events for each region of GRB are presented in Table 7.3. The most severe and longest drought is observed from August 2001 to June 2005 with a severity of 40.29 and a duration of 47 months for region 3. In region 1, with a severity of 39.23 and a duration of 43 months, the longest drought period is observed between October 1984 and April 1988. For region 2, the most severe drought is observed from July 1972 to May 1975, with a severity of 32.21 and a duration of 35 months. Whereas for region 4, the most recent drought occurred from June 2008 to August 2010 with 26.32 severity and 27 months of drought duration. All regions experienced droughts during 1971-1975, 2002-2003 and 2008-2010 periods. The scatterplot and histogram for observed dataset of drought intensity versus duration in these defined regions are shown in Fig. 7.3.

Table 7.3: The severe drought events (top five) based on SPI12 for each region.

Region	Starting month	Ending month	Severity	Duration (months)
Region 1	August 1971	August 1973	26.42	13
	October 1984	April 1988	39.23	43
	September 2000	May 2002	18.56	21
	July 201	September 2013	35.39	27
	July 2014	July 2016	28.61	26
Region 2	July 1972	May 1975	32.21	35
	July 1982	August 1983	17.78	14
	June 1987	August 1988	20.77	15
	January 1996	April 1998	29.45	28
	July 2004	August 2005	26.93	14
Region 3	August 1971	July 1973	32.34	24
	September 1991	September 1993	29.43	25
	August 2001	June 2005	40.29	47
	June 2008	August 2010	33.95	27
	July 2014	June 2016	37.96	24
Region 4	August 1965	July 1967	24.81	24
	July 1974	August 1975	25.29	14
	June 1981	June 1983	32.17	25
	August 1997	July 1999	38.63	24
	June 2008	August 2010	26.32	27

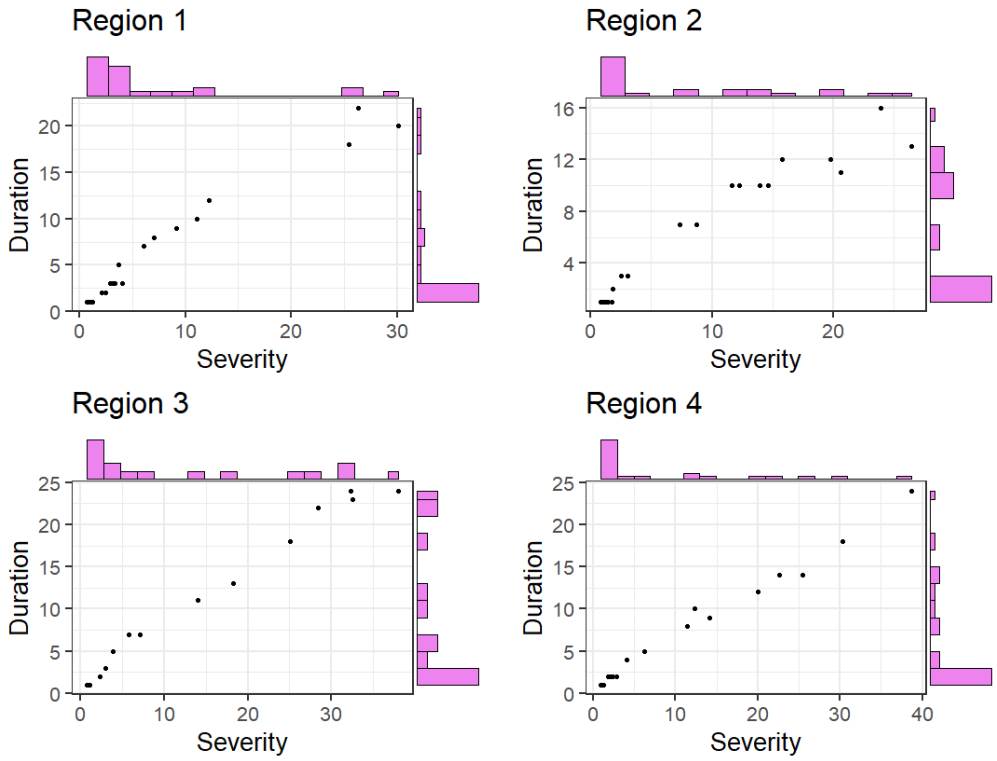

Figure 7.3: Scatterplot and histograms of severity and duration (months) for four regions of GRB.

The drought properties for each homogeneous region based on SPI12 from IMD dataset are shown in Table 7.4. Region 2 and 4 exhibited more number of drought when compared to region 1 and 3. The maximum severity of 40.29 is observed in region 3 followed by region 1 and 4. Region 1 and 3 has a longer drought inter-arrival time and hence it experiences fewer droughts. Maximum duration of 47 months is observed for region 3 followed by a severity of 43 months in region 1.

Table 7.4: Drought properties for each homogeneous region based on SPI12

Drought characteristics	**SPI12 from 1960-2020**			
	Region1	**Region2**	**Region3**	**Region4**
Number of droughts	17	26	21	26
Mean interarrival time (months)	27.3	23.6	29.3	21.6
Mean severity	6.7	8.1	12.5	8.4
Maximum severity	39.23	32.2	40.29	38.63
Mean duration (months)	6.1	5.6	9.6	6.8
Maximum duration (months)	43	35	47	27

The drought characteristics evaluated using SPI12 for each homogeneous drought region is presented in Fig. 7.4. The regions 2 and 4 experienced the highest number of drought events, followed by region 3. Whereas, the mean inter-arrival time is maximum for regions 3, followed by region 1. In case of maximum severity and duration, regions 1 and 3 experienced the highest values. With respect to the drought characteristics, decreasing trend is observed from region to region.

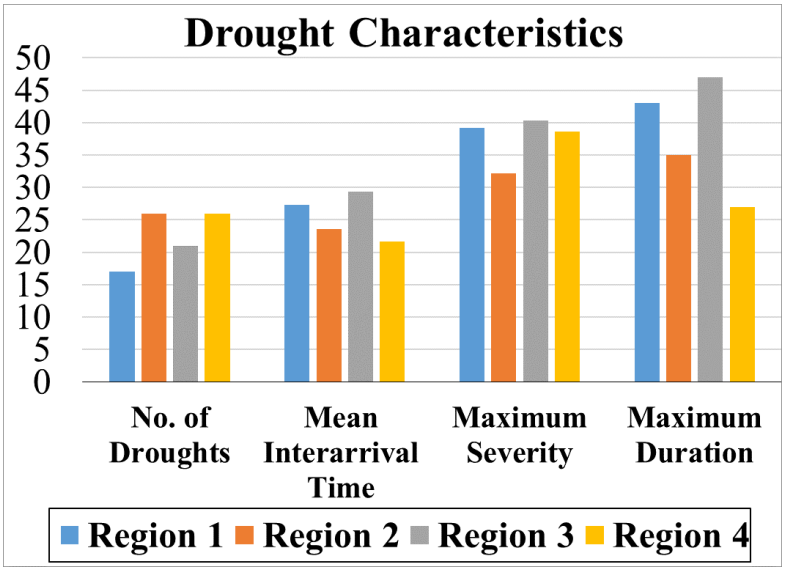

Figure 7.4: Drought characteristics for various homogeneous drought regions. (Units: Maximum duration and mean interarrival time are in months and no units for number of droughts and maximum severity).

Overall, regions 1 and 3 has fewer droughts with higher severity and high mean arrival time. Therefore, it is expected to experience a greater number of droughts with high mean arrival time, severity and duration for most part of the GRB. Gupta and Jain (2018) reported that, in most regions of the country, increase in the PET is observed at a higher rate compared to the rainfall. Increased dryness is therefore anticipated in the latter part of the 21st century, leading to a rise in the severity and duration of droughts.

The frequency of occurrence of different droughts classes (moderate, severe and extreme) over four homogeneous regions are presented in Fig. 7.5. The occurrence of moderate droughts is higher in all the regions for the study period. For region 4, the occurrence of moderate droughts are higher compared to other regions. Significant increase in the occurrence of moderate and severe droughts are observed in almost all regions. Extreme droughts are highly expected in region 2 and 3 of GRB. The availability of water in India depends primarily on the precipitation during monsoon season (June-September) where 70% of the annual rainfall occurs; therefore existence, movement and distribution of droughts are highly dependent on monsoon rainfall. Evaporation rate is expected to increase due to global warming which results in the drier conditions on the ground and increase of water vapor in the atmosphere over time.

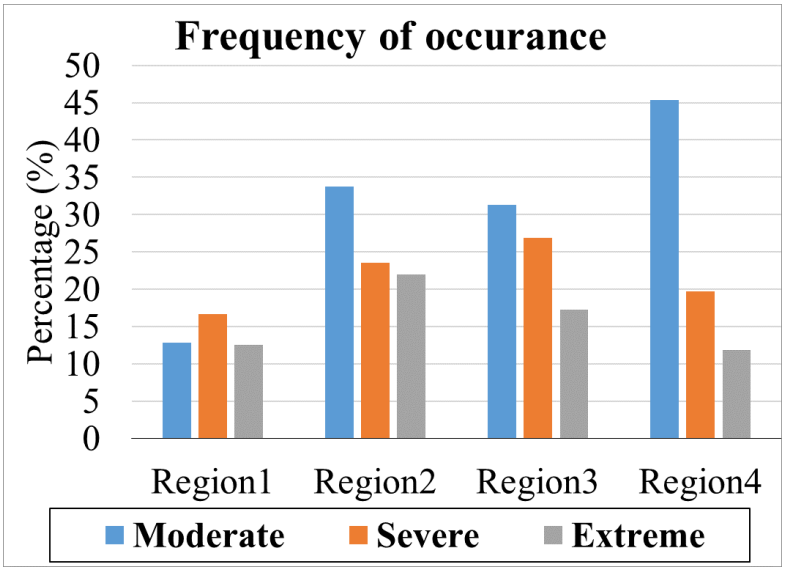

Figure 7.5: Frequency of occurrence of droughts for four homogeneous regions .

7.3.3 Drought Frequency Analysis using SPI12

7.3.3.1 Severity-Duration-Frequency (SDF) Analysis

The distribution with minimum **K**olmogorov-**S**mirnov (KS) and **A**nderson-**D**arling (AD) values are selected for the frequency analysis as shown in Table 7.5.

Clayton-copula is the best-fit copula for region 1; Gumbel-copula was the best-copula for region 2 and 3; and Frank-copula suits best for region 4 according to **L**og **L**ikelyhood (L-L) and AIC values as shown in Table 7.6. To analyse and visualize the results, scatter plots between observed and randomly simulated severity and durations from each best fitted copula class are plotted and presented in Fig 7.6. Then joint probability plots between severity and duration for four homogeneous regions are shown in Fig. 7.7.

Table 7.5: Best fit probability distributions for drought severity and duration.

Variable	**Distribution**	**KS**	**AD**	**KS**	**AD**	**KS**	**AD**	**KS**	**AD**
		Region 1		**Region 2**		**Region 3**		**Region 4**	
Drought severity	Exponential	0.22	1.19	0.25	1.93	0.23	1.57	0.28	2.32
	Normal	0.29	3.01	0.26	1.81	0.29	1.46	0.27	2.27
	Log normal	**0.12**	**0.48**	0.21	1.38	0.16	0.58	**0.17**	**1.15**
	Gamma	0.21	1.01	**0.19**	**1.33**	0.16	0.72	0.22	1.39
	Weibul	0.17	0.82	0.21	1.34	**0.16**	**0.66**	0.21	1.23
	Gumbel	0.25	2.06	0.25	1.96	0.24	1.43	0.28	2.31
Drought duration (months)	Exponential	0.21	0.87	**0.24**	**1.93**	0.18	0.9	0.27	1.52
	Normal	0.29	2.06	0.24	1.98	0.25	1.28	0.29	2.02
	Log normal	0.22	0.91	0.28	2.26	0.18	0.72	0.22	1.38
	Gamma	0.23	1.01	0.26	2.07	0.17	0.73	0.27	1.46
	Weibul	**0.17**	**0.86**	0.27	2.06	**0.17**	**0.72**	**0.21**	**1.32**
	Gumbel	0.28	1.62	0.25	2.27	0.21	1.14	0.3	2.06

Table 7.6: Best fitted copula model and copula parameter (θ), L-L and AIC values.

Copula	**parameter**	**L-L**	**AIC**	**Parameter**	**L-L**	**AIC**
	Region 1			**Region 2**		
Clayton	**6.38**	**17.51**	**-55.75**	5.67	17.24	-45.84
Frank	24.54	29.64	-65.27	18.9	20.59	-48.14
Gumbel	5.36	24.94	-59.88	**4.21**	**16.12**	**-42.21**
Galambos	4.85	22.38	-57.25	3.55	17.68	-43.65
Plackett	28.71	30.12	-64.01	18.45	20.15	-44.09
	Region 3			**Region 4**		
Clayton	5.63	15.07	-42.87	5.31	16.05	-37.77
Frank	17.15	17.58	-43.16	**13.79**	**15.83**	**-36.92**
Gumbel	**3.93**	**14.87**	**-37.25**	5.12	19.89	-39.52
Galambos	3.78	18.28	-39.32	4.77	20.22	-40.74
Plackett	20.35	22.18	-40.96	24.36	25.35	-42.15

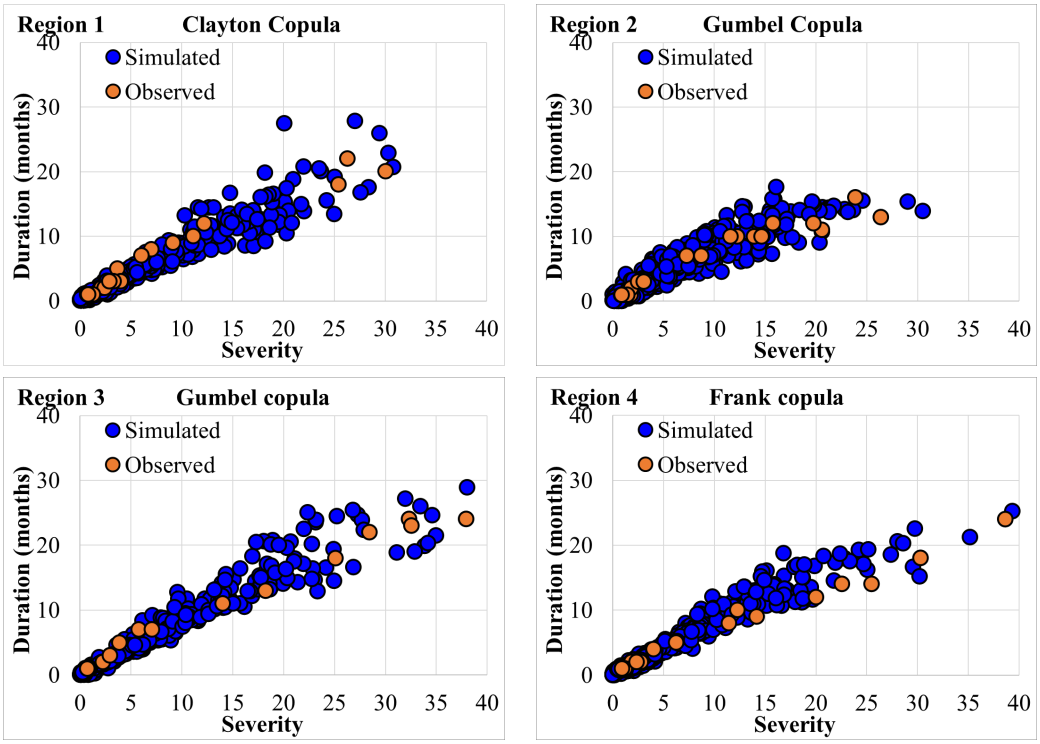

Figure 7.6: Scatterplots between observed and simulated severity duration values from best fit copula for each homogeneous region.

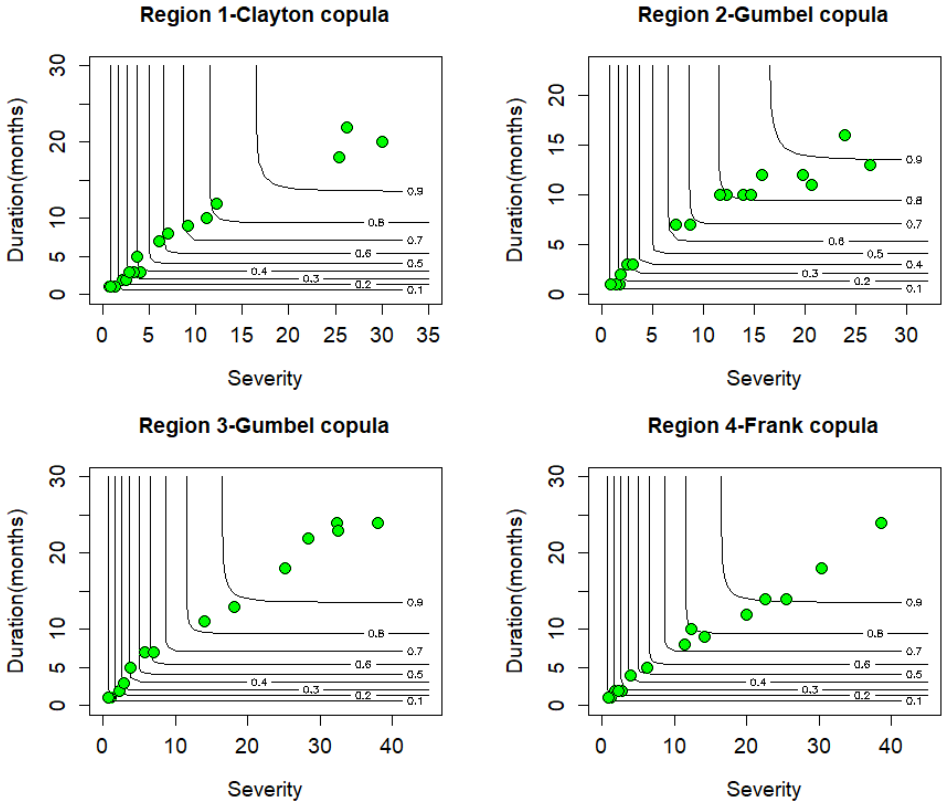

Figure 7.7: Joint probability plots between severity and duration for four homogeneous regions.

Further, best parameter values are analyzed and probabilities of duration are calibrated using inverse cumulative distribution of different univariate distributions fitted. Then joint probability dependence of various return periods is calculated by using inverse h-function of best-fit copula. For each homogenous region SDF curves are developed as shown in Fig. 7.8. Region 2,3 and 4 display higher severity for different return periods suggesting that a higher frequency of drought can be expected in the regions under consideration. Moreover, the SDF curves are concave upward for all the regions, specifying an increase in severity with an increase in duration.

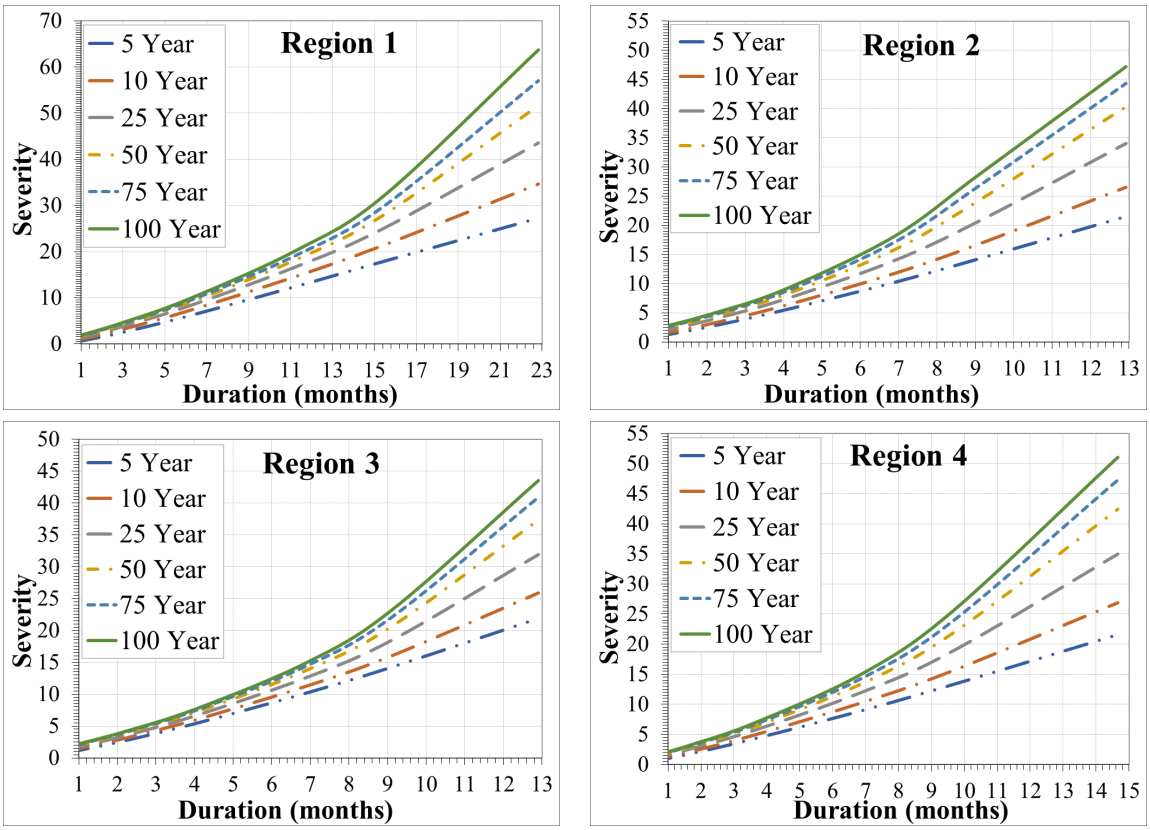

Figure 7.8: Joint probability plots between severity and duration for four homogeneous regions.

7.3.3.2 Severity-Area-Frequency (SAF) Analysis

For various spatial extents, gamma distribution is selected as the best fit. Distribution of the parameters are calculated using L-moments method. The SAF curves at various return periods (5, 10, 25, 50, 75, 100 years) are shown in Fig. 7.9. For regions 1-4; 1971-1976, 1984-1989, 1995-2000 and 2000-2005 respectively, are considered as most severe drought periods in comparison with projected SAF curves. It is observed from Fig. 7.9 that region 1 experienced more severity values and region 3 has a steeper slope compared to other regions that specifies drought risk is expected for small spatial extent. As the percentage of the area increases, the severity decreases and vice versa. It is observed from the SAF curves that severity values between 10 to 30 for 50% of the

area and decrease with increasing areal extent. Also, it is possible to estimate drought severity quantiles for specified percentage areal extent and return periods.

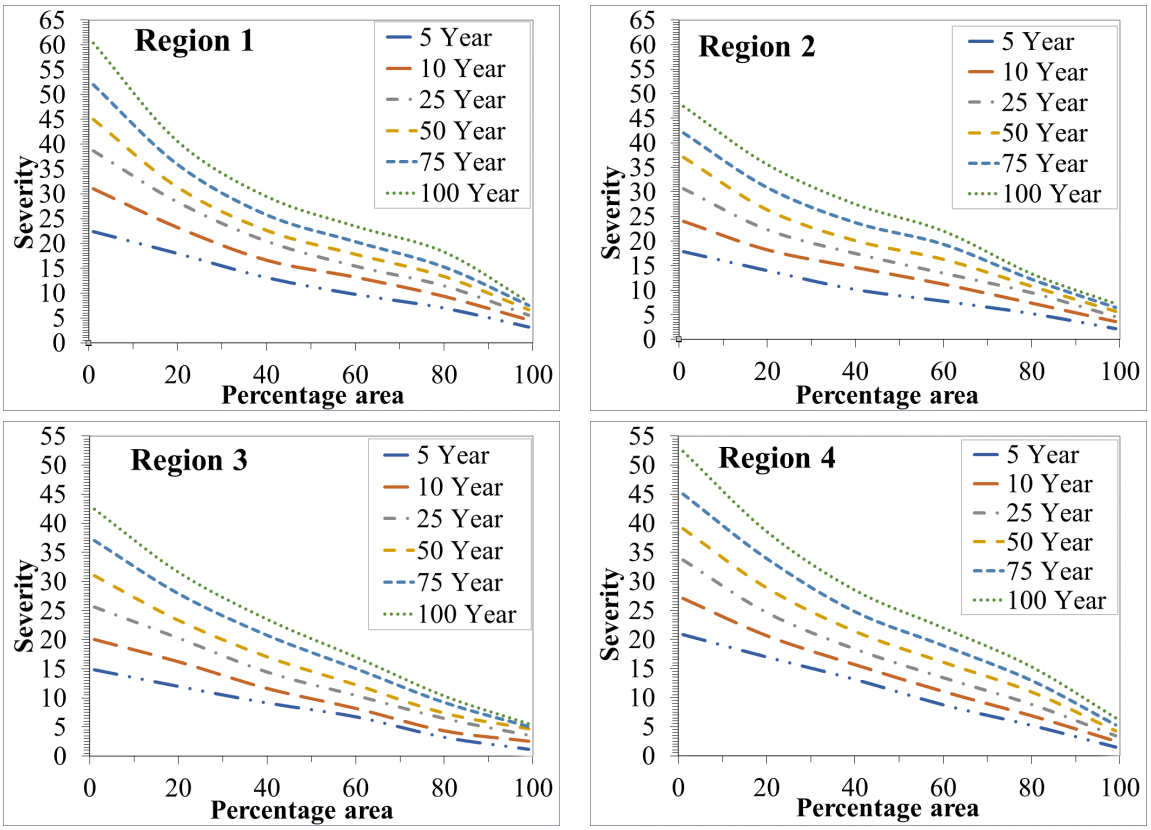

Figure 7.9: Drought SAF curves at various return periods for four homogeneous regions.

7.3.4 Drought Frequency Analysis using CCDI and SPI12

With the reconstructed TWSA from chapter 6 and precipitation datasets, CCDI and SPI12 time series have been generated for GRB from 1960-2020. A good correlation is observed between SPI12 and CCDI time series as shown in Fig. 7.10.

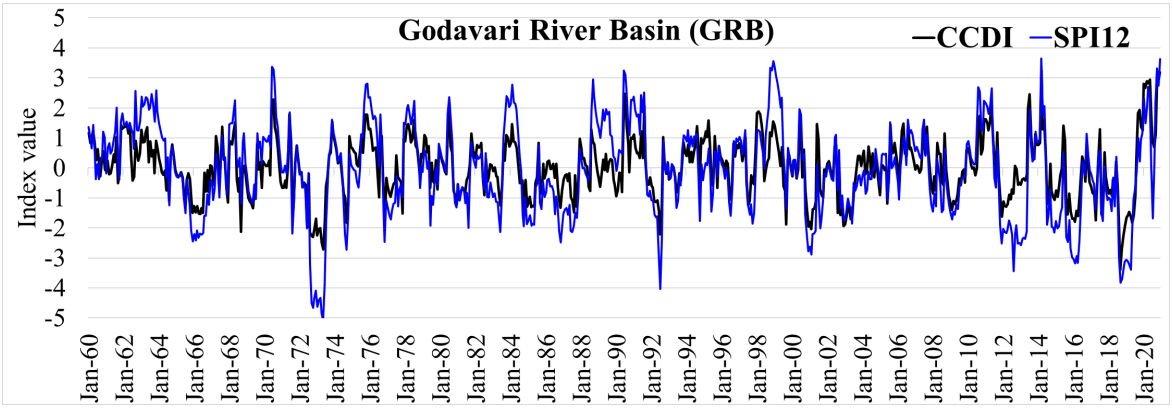

Figure 7.10: CCDI and SPI12 time series for GRB from 1960-2020.

The dry and wet spells between the two indices matched well (see Fig. 7.10). The obtained SPI12 and CCDI are used to develop basin averaged SAF and SDF curves for GRB. The SPI12 based drought frequency curves are used as a standard metric to compare with the frequency curves developed using CCDI.

The SDF curves developed using SPI12 and CCDI time series for GRB are shown in Fig. 7.11. Both SPI12 and CCDI based SDF curves displayed higher severity for different return periods suggesting that a higher frequency of drought can be expected in the regions under consideration. Both the SDF curves are concave upward, specifying an increase in severity with an increase in duration. Only variation is that, CCDI based SDF curve displayed droughts with shorter duration and severity when compared with the SPI12 based SDF curve.

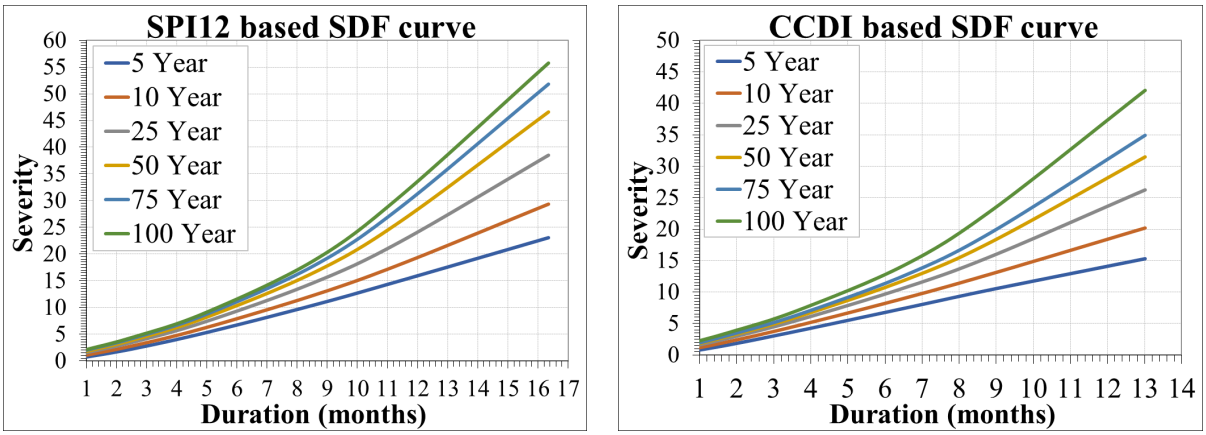

Figure 7.11: Basin averaged SDF curves developed using SPI12 and CCDI for GRB.

The developed SAF curves using SPI12 and CCDI time series for GRB are shown in Fig. 7.12. CCDI based SAF curve has a steeper slope compared to SPI12 based SAF curve that specifies drought risk is expected for small spatial extent. For SPI12 based SAF curve, at 50% of the area the corresponding severity varies between 10 for 5-year return period to 25 for 100-year return period. Whereas for CCDI based SAF curve, the severity varies between 5 for 5-year return period to 20 for 100-year return period. Most severe drought are observed using the SPI12 based SAF curve when compared with the other. Overall, there is a good match between both the SAF curves developed using SPI12 and CCDI. Therefore, reconstructed GRACE TWSA can be utilized as a metric to develop SAF and SDF curves over Indian river basins.

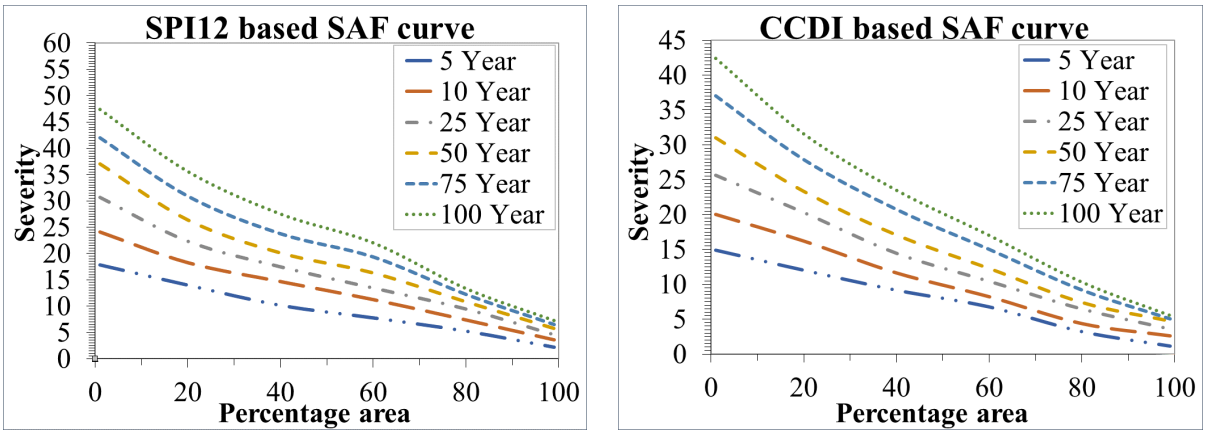

Figure 7.12: Basin averaged SAF curves developed using SPI12 and CCDI for GRB.

7.4 DISCUSSIONS

Closer analysis of the results shows that rising severity and duration of drought are noticed in almost all regions over all time-progressive regions. The study of the occurrence of various droughts (moderate, serious and extremely severe) reveals that the frequency of droughts is likely to increase in most regions, with the exception of region 1. The SDF curves show that for most of the regions considered, the severity rate increases with duration. However, critical drought events are likely to occur over multiple time scales in four homogeneous regions. In addition, the derived SAF curves suggest that droughts are likely to cover a greater areal scale for lesser severity values in all the regions.

Previously analyzed SAF study reports that greater areal extent of drought is expected in latter part of century (Gupta and Jain, 2018). Whereas steeper SAF curve slopes with high variability in topographical and hydrological characteristics have been observed for Indian regions. The SAF curves that have been developed can help to compare past droughts with future droughts. Therefore, it is noted from the results that India is experiencing severe droughts in GRB and has a major impact on population. Lack of soil moisture can also cause prolonged droughts, so turbulent heat flux and boundary layer distribution should be regulated because of surface energy loss (Alapaty et al., 1997; Sehgal et al., 2017). The local hydrological system depends primarily on soil moisture availability, absence of soil moisture disrupts agricultural production. In India, over 50 per cent of people depend primarily on agriculture. Historically, the share of agriculture in India in the total **G**ross **D**omestic **P**roduct (GDP) has gradually decreased from 39% in 1983 to 14% in 2014 (Ministry of Agriculture and Farmers' Welfare, 2016). Agriculture, therefore is economically and socially important for India's well-being. People's migration can be seen in almost all parts of the country due to lower agricultural profits and a lack of water availability. As

per the results of the study, severe droughts are expected in the twenty-first century, leading to the shortage of availability of water in basins. Therefore, it effects the long-term damage of plant species and leads to desertification.

Also, an increase in population results in the increase of energy demand. Presently after China and United States, India is the third largest user of energy. So, demand for electricity is increasing which directly affects the availability of water in the river basins over future periods. Therefore, better preparedness, monitoring and prediction of drought can be considered as the best adaptation technique for mitigating the hazard due to future droughts. Policies should be framed in case of local and regional vulnerabilities for successful mitigation of drought risk induced by climate change.

7.5 CONCLUSIONS

A regional study of the meteorological drought over India is carried out using SPI12 drought index, taking into account four distinct homogeneous drought regions. The run theory approach is used to determine the characteristics of drought, such as severity and duration. Copula-based methodology is adopted to derive SDF curves by analyzing the changes in the joint return period of severity and duration. SAF curves are developed which examine the changes in drought return periods covering a specific percentage of areal extent. A detailed spatiotemporal study of the occurrence, distribution and frequency of drought is performed over India in the twenty-first century to quantify drought risk. Then the CCDI based SAF and SDF curves are compared with the SPI12 based SAF and SDF curves. The key research outcomes are highlighted below:

- The occurrence of moderate and extreme drought conditions have increased gradually in almost all regions, while major increases in severe drought are expected in regions 2 and 3.
- For GRB, a high number of droughts with a high mean arrival time, high severity and duration are likely to be noticed in the future.
- It is observed from the SDF curves that region 2, 3 and 4 show higher severity for different return periods, indicating higher drought frequencies. Almost all SDF curves are concave upwards, indicating an increase in severity and duration.
- The rate of increase of drought severity is higher for longer durations whereas it decreases for shorter periods.
- Using the derived SAF relationships, it is possible to estimate drought severity quantiles for specified percentage areal extent and return periods.

- It is observed from the SAF curves that severity values vary between 10 to 30 for 50% of the area and decrease with increasing areal extent.
- A good match is observed between SPI12 and CCDI based SAF and SDF curves. From the results it is concluded that the reconstructed TWSA can be utilized as a metric to develop SAF and SDF curves for Indian river basins.

CHAPTER 8

CONCLUSIONS

This Chapter is organized as follows: Section 8.1 presents the summary of this thesis. Section 8.2 presents the conclusions of the study. Section 8.3 present future research directions for this research work.

8.1 SUMMARY OF THE THESIS

The potential of Gravity Recovery And Climate Experiment (GRACE) Terrestrial Water Storage Anomaly (TWSA) is analysed with different drought indices for Godavari River Basin (GRB), Krishna River Basin (KRB), Cauvery River Basin (CRB) and Pennar and East flowing Rivers between Pennar and Cauvery River Basins (PCRB). Seasonal and monthly correlation analysis of Combined Climatologic Deviation Index (CCDI) and GRACE Groundwater Drought Index (GGDI) are seen as the best drought indices applicable to the study regions. The GGDI is then, used to evaluate drought conditions and identify the linkages between GGDI and teleconnections over the study region. The TWSA dataset is limited to 15 years and hence, long term drought analysis is difficult to achieve. Therefore, reconstruction of TWSA is performed and validation is done with respect to in-situ groundwater well measurements. Severity-Duration-Frequency (SDF) and Severity-Area-Frequency (SAF) curves are developed for GRB using the reconstructed TWSA based CCDI as well as India Meteorological Department (IMD) precipitation based Standardized Precipitation Index at 12 month time scale (SPI12). The SPI12 based SAF and SDF curves are used as a standard metric to compare CCDI based SAF and SDF curves. The significant contributions of the study are presented in the next section.

8.2 CONCLUSIONS

- GGDI and CCDI are considered as the best drought indices for drought assessment at both seasonal and monthly scales for GRB, KRB, CRB and PCRB.
- The findings reveal an appreciable level of confidence in utilizing GGDI and CCDI ability to quantify droughts, which will further improve with better quantification and expanded availability of TWS information from GRACE FO mission.

- Extreme drought events are observed in KRB and CRB during 2003-2005 and 2012-2015 with a severity of 21.91 and 27.02 respectively.
- The association between TWSA and drought occurrences is closely related to SOI variability followed by NINO3.4.
- The MLP approach is effective in generating reconstructed TWSA and potentially bridge the gap between GRACE and GRACE FO missions over the study regions.
- The reconstructed TWSA can be used to analyse long-term climate related application in any river basin.
- A good match is observed between SDF / SAF curves developed using SPI12 and CCDI. Therefore, reconstructed TWSA can be utilized as a metric to develop SDF and SAF curves for Indian River Basins.
- The derived SAF curves can be useful to understand spatial characteristics of drought events (i.e., spatial coverage and severity values) and the associated risks.
- The derived drought SDF curves give risks associated with various values of drought severities at different return periods. This information can be very useful for environmental and agricultural planning in the drought prone regions.
- The results obtained based on the application of different statistical techniques used in this study, make it possible to recommend GRACE mascon solutions for drought and groundwater related studies over the region with similar climatic, hydrogeological and groundwater withdrawal conditions.

8.3 FUTURE SCOPE FOR THE RESEARCH WORK

- The entire hydrological mass change in a region is represented by TWS which is a sum of changes in soil moisture, surface water, groundwater, snow mass and canopy water. As a result, predicting change in one component is difficult and we require model-based estimations or in-situ measurements of other components. Since model uncertainties vary in space and time and in-situ information is scarce, using GRACE for hydrological studies concerning one component of TWS is a challenge. Therefore, separation of TWS signals into individual components e.g., soil moisture, groundwater in recent studies is still an active research field.
- In order to access changes in smaller geographical areas or basins (only a few tens of kilometers) improving the spatial resolution of GRACE products (now around 300-400 km on the Earth's surface) remains a technological and methodological challenge.

- As GRACE spatial resolution is around 300-400 km on the Earth's surface, spatial downscaling of GRACE by assimilating it with other hydrological observations can be performed to produce higher spatial resolution TWS products.
- With the launch of GRACE FO mission, reconstruction of TWSA is carried out in this study from 1960 to 2020, resulting in a 60-year TWSA time series that can be utilised to research any long-term climate-related applications.
- For better understanding of the behaviour of groundwater level change across the river basins, there is a need to understand the variation in the groundwater levels and availability with the changing aquifer system.

As a result of continuous developments, the GRACE products will become even more useful for studying hydrological and agricultural droughts worldwide. There is no doubt that GRACE based drought indices are an excellent tool to study hydrological and agricultural drought.

BIBLIOGRAPHY

Adarsh, S., Karthik, S., Shyma, M., Prem, G. D., Parveen, A. S., and Sruthi, N. Developing short term drought severity-duration-frequency curves for kerala meteorological subdivision, india using bivariate copulas. *KSCE Journal of Civil Engineering*, 22(3):962–973, 2018.

Ahmed, K., Shahid, S., Chung, E. S., Wang, X. J., and Harun, S. B. Climate change uncertainties in seasonal drought severity-area-frequency curves: Case of arid region of pakistan. *Journal of Hydrology*, 570:473–485, 2019a.

Ahmed, M., Sultan, M., Elbayoumi, T., and Tissot, P. Forecasting grace data over the african watersheds using artificial neural networks. *Remote Sensing*, 11(15):1769, 2019b.

Alamgir, M., Khan, N., Shahid, S., Yaseen, Z. M., Dewan, A., Hassan, Q., and Rasheed, B. Evaluating severity–area–frequency (saf) of seasonal droughts in bangladesh under climate change scenarios. *Stochastic Environmental Research and Risk Assessment*, 34(2):447–464, 2020.

Alapaty, K., Raman, S., and Niyogi, D. S. Uncertainty in the specification of surface characteristics: A study of prediction errors in the boundary layer. *Boundary-Layer Meteorology*, 82(3):475–502, 1997.

Alexander, M. A., Bladé, I., Newman, M., Lanzante, J. R., Lau, N. C., and Scott, J. D. The atmospheric bridge: The influence of enso teleconnections on air–sea interaction over the global oceans. *Journal of climate*, 15(16):2205–2231, 2002.

Allen, P., Harmel, R., Dunbar, J., and Arnold, J. Upland contribution of sediment and runoff during extreme drought: A study of the 1947–1956 drought in the blackland prairie, texas. *Journal of Hydrology*, 407(1-4):1–11, 2011.

Alley, W. M. The palmer drought severity index: limitations and assumptions. *Journal of Applied Meteorology and Climatology*, 23(7):1100–1109, 1984.

Alley, W. M., Reilly, T. E., and Franke, O. L. *Sustainability of ground-water resources*, volume 1186. US Department of the Interior, US Geological Survey, 1999.

Amarasinghe, U., Sharma, B. R., Aloysius, N., Scott, C., Smakhtin, V., and De Fraiture, C. *Spatial variation in water supply and demand across river basins of India*, volume 83. Iwmi, 2005.

Amirataee, B., Montaseri, M., and Rezaie, H. Regional analysis and derivation of copula-based drought severity-area-frequency curve in lake urmia basin, iran. *Journal of environmental management*, 206:134–144, 2018.

Anyah, R., Forootan, E., Awange, J. L., and Khaki, M. Understanding linkages between global climate indices and terrestrial water storage changes over africa using grace products. *Science of the Total Environment*, 635:1405–1416, 2018.

Araghi, A., Martinez, C. J., Adamowski, J., and Olesen, J. E. Spatiotemporal variations of aridity in iran using high-resolution gridded data. *International Journal of Climatology*, 38(6):2701–2717, 2018.

Aryal, Y and Zhu, J. Multimodel ensemble projection of meteorological drought scenarios and connection with climate based on spectral analysis. *International Journal of Climatology*, 40(7):3360–3379, 2020.

Asoka, A., Gleeson, T., Wada, Y., and Mishra, V. Relative contribution of monsoon precipitation and pumping to changes in groundwater storage in india. *Nature Geoscience*, 10(2):109–117, 2017.

Bauer, P., Thorpe, A., and Brunet, G. The quiet revolution of numerical weather prediction. *Nature*, 525(7567):47–55, 2015.

Beguería, S., Vicente-Serrano, S. M., Reig, F., and Latorre, B. Standardized precipitation evapotranspiration index (spei) revisited: parameter fitting, evapotranspiration models, tools, datasets and drought monitoring. *International journal of climatology*, 34(10):3001–3023, 2014.

Bettadpur, S. Utcsr level-2 processing standards document for level-2 product release 0005. *GRACE Rep*, 327:742, 2012.

Bezdek, J. C. Numerical taxonomy with fuzzy sets. *Journal of mathematical biology*, 1 (1):57–71, 1974.

Bezdek, J. C. Objective function clustering. In *Pattern recognition with fuzzy objective function algorithms*, pages 43–93. Springer, 1981.

Bhanja, S. N and Mukherjee, A. In situ and satellite-based estimates of usable groundwater storage across india: Implications for drinking water supply and food security. *Advances in Water Resources*, 126:15–23, 2019.

Bhanja, S. N., Mukherjee, A., Rodell, M., Velicogna, I., Pangaluru, K., and Famiglietti, J. S. Regional groundwater storage changes in the indian subcontinent: The role of anthropogenic activities. In *AGU Fall Meeting Abstracts*, volume 2014, pages GC21B–0533, 2014.

Bhanja, S. N., Mukherjee, A., Saha, D., Velicogna, I., and Famiglietti, J. S. Validation of grace based groundwater storage anomaly using in-situ groundwater level measurements in india. *Journal of Hydrology*, 543:729–738, 2016.

Bhanja, S. N., Mukherjee, A., and Rodell, M. Groundwater storage change detection from in situ and grace-based estimates in major river basins across india. *Hydrological Sciences Journal*, 65(4):650–659, 2020.

Bhuvaneswari, K., Geethalakshmi, V., Lakshmanan, A., Srinivasan, R., and Sekhar, N. U. The impact of el nino/southern oscillation on hydrology and rice productivity in the cauvery basin, india: application of the soil and water assessment tool. *Weather and Climate Extremes*, 2:39–47, 2013.

Bierkens, M. F. Global hydrology 2015: State, trends, and directions. *Water Resources Research*, 51(7):4923–4947, 2015.

Bishop, C. M and Nasrabadi, N. M. *Pattern recognition and machine learning*, volume 4. Springer, 2006.

Bishop, C. M. *Neural networks for pattern recognition*. Oxford university press, 1995.

Bisht, D. S., Chatterjee, C., Raghuwanshi, N. S., and Sridhar, V. Spatio-temporal trends of rainfall across indian river basins. *Theoretical and applied climatology*, 132 (1):419–436, 2018a.

Bisht, D. S., Chatterjee, C., Raghuwanshi, N. S., and Sridhar, V. An analysis of precipitation climatology over indian urban agglomeration. *Theoretical and Applied Climatology*, 133(1):421–436, 2018b.

Bisht, D. S., Sridhar, V., Mishra, V., Chatterjee, C., and Raghuwanshi, N. S. Drought characterization over india under projected climate scenario. *International Journal of Climatology*, 39(4):1889–1911, 2019.

Bonaccorso, B., Peres, D. J., Castano, A., and Cancelliere, A. Spi-based probabilistic analysis of drought areal extent in sicily. *Water Resources Management*, 29(2):459–470, 2015.

Bondarabadi, S. R., Saghafian, B., Razii, T., and Akhtari, R. Severity–area–frequency curves of drought and wet periods, 2008.

Burke, E. J and Brown, S. J. Regional drought over the uk and changes in the future. *Journal of hydrology*, 394(3-4):471–485, 2010.

Cammalleri, C., Vogt, J., and Salamon, P. Development of an operational low-flow index for hydrological drought monitoring over europe. *Hydrological Sciences Journal*, 62(3):346–358, 2017.

Cammalleri, C., Barbosa, P., and Vogt, J. V. Analysing the relationship between multiple-timescale spi and grace terrestrial water storage in the framework of drought monitoring. *Water*, 11(8):1672, 2019.

Cancelliere, A and Salas, J. D. Drought length properties for periodic-stochastic hydrologic data. *Water resources research*, 40(2), 2004.

Cao, Y., Nan, Z., and Cheng, G. Grace gravity satellite observations of terrestrial water storage changes for drought characterization in the arid land of northwestern china. *Remote Sensing*, 7(1):1021–1047, 2015.

Chang, X., Wang, B., Yan, Y., Hao, Y., and Zhang, M. Characterizing effects of monsoons and climate teleconnections on precipitation in china using wavelet coherence and global coherence. *Climate Dynamics*, 52(9):5213–5228, 2019.

Chaturvedi, R. K., Joshi, J., Jayaraman, M., Bala, G., and Ravindranath, N. Multi-model climate change projections for india under representative concentration pathways. *Current Science*, pages 791–802, 2012.

Chen, H., Zhang, W., Nie, N., and Guo, Y. Long-term groundwater storage variations estimated in the songhua river basin by using grace products, land surface models, and in-situ observations. *Science of the Total Environment*, 649:372–387, 2019.

Chen, J., Wilson, C., Tapley, B., Blankenship, D., and Ivins, E. Patagonia icefield melting observed by gravity recovery and climate experiment (grace). *Geophysical Research Letters*, 34(22), 2007.

Chen, J., Li, J., Zhang, Z., and Ni, S. Long-term groundwater variations in northwest india from satellite gravity measurements. *Global and Planetary Change*, 116:130–138, 2014.

Chen, J. L., Wilson, C. R., and Tapley, B. D. The 2009 exceptional amazon flood and interannual terrestrial water storage change observed by grace. *Water Resources Research*, 46(12), 2010.

Chinnasamy, P., Hubbart, J. A., and Agoramoorthy, G. Using remote sensing data to improve groundwater supply estimations in gujarat, india. *Earth Interactions*, 17(1): 1–17, 2013.

Dai, A. Drought under global warming: a review. *Wiley Interdisciplinary Reviews: Climate Change*, 2(1):45–65, 2011a.

Dai, A. Characteristics and trends in various forms of the palmer drought severity index during 1900–2008. *Journal of Geophysical Research: Atmospheres*, 116(D12), 2011b.

Dai, A. Increasing drought under global warming in observations and models. *Nature climate change*, 3(1):52–58, 2013.

Dai, A., Trenberth, K. E., and Qian, T. A global dataset of palmer drought severity index for 1870–2002: Relationship with soil moisture and effects of surface warming. *Journal of Hydrometeorology*, 5(6):1117–1130, 2004.

Dalezios, N. R., Loukas, A., Vasiliades, L., and Liakopoulos, E. Severity-duration-frequency analysis of droughts and wet periods in greece. *Hydrological sciences journal*, 45(5):751–769, 2000.

Das, P. K., Dutta, D., Sharma, J., and Dadhwal, V. Trends and behaviour of meteorological drought (1901–2008) over indian region using standardized precipitation–evapotranspiration index. *International Journal of Climatology*, 36(2): 909–916, 2016.

Diaz, H. F., Hoerling, M. P., and Eischeid, J. K. Enso variability, teleconnections and climate change. *International Journal of Climatology: A Journal of the Royal Meteorological Society*, 21(15):1845–1862, 2001.

Dirmeyer, P. A., Gao, X., Zhao, M., Guo, Z., Oki, T., Hanasaki, N. The second global soil wetness project (gswp-2): Multi-model analysis and implications for our perception of the land surface. *Bull. Amer. Meteor. Soc*, 2005.

Döll, P., Schmied, H. M., Schuh, C., Portmann, F. T., and Eicker, A. Global-scale assessment of groundwater depletion and related groundwater abstractions: Combining hydrological modeling with information from well observations and grace satellites. *Water Resources Research*, 50(7):5698–5720, 2014.

Dracup, J. A., Lee, K. S., and Paulson Jr, E. G. On the definition of droughts. *Water resources research*, 16(2):297–302, 1980.

Du, K. L and Swamy, M. N. *Neural networks and statistical learning*. Springer Science & Business Media, 2013.

Dunn, J. C. A fuzzy relative of the isodata process and its use in detecting compact well-separated clusters. 1973.

Eicker, A., Forootan, E., Springer, A., Longuevergne, L., and Kusche, J. Does grace see the terrestrial water cycle "intensifying"? *Journal of Geophysical Research: Atmospheres*, 121(2):733–745, 2016.

Eltahir, E. A and Yeh, P. J. On the asymmetric response of aquifer water level to floods and droughts in illinois. *Water Resources Research*, 35(4):1199–1217, 1999.

Famiglietti, J. S. Remote sensing of terrestrial water storage, soil moisture and surface waters. *Washington DC American Geophysical Union Geophysical Monograph Series*, 150:197–207, 2004.

Famiglietti, J. S., Lo, M., Ho, S. L., Bethune, J., Anderson, K., Syed, T. H., Swenson, S. C., de Linage, C. R., and Rodell, M. Satellites measure recent rates of groundwater depletion in california's central valley. *Geophysical Research Letters*, 38(3), 2011a.

Famiglietti, J. S., Lo, M., Ho, S. L., Bethune, J., Anderson, K., Syed, T. H., Swenson, S. C., de Linage, C. R., and Rodell, M. Satellites measure recent rates of groundwater depletion in california's central valley. *Geophysical Research Letters*, 38(3), 2011b.

Fan, K., Liu, Y., and Chen, H. Improving the prediction of the east asian summer monsoon: New approaches. *Weather and Forecasting*, 27(4):1017–1030, 2012.

Farge, M. Wavelet transforms and their applications to turbulence. *Annual review of fluid mechanics*, 24(1):395–458, 1992.

Fei, C., Shenbin, Y., Chunling, W., Runyuan, W., Heling, W., and Yue, Q. Spatial and temporal distribution of spring drought in northwest china based on standardized precipitation evapotranspiration index. *Journal of Arid Meteorology*, 34(1):34, 2016.

Ferreira, V. G., Andam-Akorful, S. A., Dannouf, R., and Adu-Afari, E. A multi-sourced data retrodiction of remotely sensed terrestrial water storage changes for west africa. *Water*, 11(2):401, 2019.

Flechtner, F., Morton, P., Watkins, M., and Webb, F. Status of the grace follow-on mission. In *Gravity, geoid and height systems*, pages 117–121. Springer, 2014.

Forootan, E., Khaki, M., Schumacher, M., Wulfmeyer, V., Mehrnegar, N., van Dijk, A. I., Brocca, L., Farzaneh, S., Akinluyi, F., Ramillien, G. Understanding the global hydrological droughts of 2003–2016 and their relationships with teleconnections. *Science of the Total Environment*, 650:2587–2604, 2019.

Ganguli, P. Probabilistic analysis of extreme droughts in southern maharashtra using bivariate copulas. *ISH Journal of Hydraulic Engineering*, 20(1):90–101, 2014.

Gautam, R. Impacts of drought on crops and ways to mitigate it. *Indian Farming*, 62 (6):13–19, 2012.

Gehlot, L. K., Jibhakate, S. M., Sharma, P. J., Patel, P., and Timbadiya, P. Spatio-temporal variability of rainfall indices and their teleconnections with el niño-southern oscillation for tapi basin, india. *Asia-Pacific Journal of Atmospheric Sciences*, 57(1): 99–118, 2021.

Genest, C and Favre, A. C. Everything you always wanted to know about copula modeling but were afraid to ask. *Journal of hydrologic engineering*, 12(4):347–368, 2007.

Genest, C and Rivest, L. P. Statistical inference procedures for bivariate archimedean copulas. *Journal of the American statistical Association*, 88(423):1034–1043, 1993.

Genest, C., Ghoudi, K., and Rivest, L. P. A semiparametric estimation procedure of dependence parameters in multivariate families of distributions. *Biometrika*, 82(3): 543–552, 1995.

Girotto, M., De Lannoy, G. J., Reichle, R. H., Rodell, M., Draper, C., Bhanja, S. N., and Mukherjee, A. Benefits and pitfalls of grace data assimilation: A case study of terrestrial water storage depletion in india. *Geophysical research letters*, 44(9): 4107–4115, 2017.

Grinsted, A., Moore, J. C., and Jevrejeva, S. Application of the cross wavelet transform and wavelet coherence to geophysical time series. *Nonlinear processes in geophysics*, 11(5/6):561–566, 2004.

Guhathakurta, P and Rajeevan, M. Trends in the rainfall pattern over india. *International Journal of Climatology: A Journal of the Royal Meteorological Society*, 28(11):1453–1469, 2008.

Gupta, V and Jain, M. K. Investigation of multi-model spatiotemporal mesoscale drought projections over india under climate change scenario. *Journal of Hydrology*, 567:489–509, 2018.

Gupta, V and Jain, M. K. Impact of enso, global warming, and land surface elevation on extreme precipitation in india. *Journal of Hydrologic Engineering*, 25(1):05019032, 2020.

Gupta, V and Jain, M. K. Unravelling the teleconnections between enso and dry/wet conditions over india using nonlinear granger causality. *Atmospheric Research*, 247: 105168, 2021.

Gupta, V., Jain, M. K., and Singh, V. P. Multivariate modeling of projected drought frequency and hazard over india. *Journal of Hydrologic Engineering*, 25(4): 04020003, 2020.

Halwatura, D., Lechner, A., and Arnold, S. Drought severity–duration–frequency curves: a foundation for risk assessment and planning tool for ecosystem establishment in post-mining landscapes. *Hydrology and Earth System Sciences*, 19 (2):1069–1091, 2015.

Hamed, K. H and Rao, A. R. A modified mann-kendall trend test for autocorrelated data. *Journal of hydrology*, 204(1-4):182–196, 1998.

Hamshaw, S. D., Dewoolkar, M. M., Schroth, A. W., Wemple, B. C., and Rizzo, D. M. A new machine-learning approach for classifying hysteresis in suspended-sediment discharge relationships using high-frequency monitoring data. *Water Resources Research*, 54(6):4040–4058, 2018.

Han, S.-C., Shum, C., Jekeli, C., and Alsdorf, D. Improved estimation of terrestrial water storage changes from grace. *Geophysical Research Letters*, 32(7), 2005.

Han, Z., Huang, S., Huang, Q., Leng, G., Wang, H., He, L., Fang, W., and Li, P. Assessing grace-based terrestrial water storage anomalies dynamics at multi-timescales and their correlations with teleconnection factors in yunnan province, china. *Journal of Hydrology*, 574:836–850, 2019.

Hayes, M., Svoboda, M., Wall, N., and Widhalm, M. The lincoln declaration on drought indices: universal meteorological drought index recommended. *Bulletin of the American Meteorological Society*, 92(4):485–488, 2011.

Hisdal, H and Tallaksen, L. M. Estimation of regional meteorological and hydrological drought characteristics: a case study for denmark. *Journal of Hydrology*, 281(3): 230–247, 2003.

Hoekema, D. J and Sridhar, V. Relating climatic attributes and water resources allocation: A study using surface water supply and soil moisture indices in the snake river basin, idaho. *Water Resources Research*, 47(7), 2011.

Hoekema, D. J and Sridhar, V. A system dynamics model for conjunctive management of water resources in the s nake r iver b asin. *JAWRA Journal of the American Water Resources Association*, 49(6):1327–1350, 2013.

Houborg, R., Rodell, M., Li, B., Reichle, R., and Zaitchik, B. F. Drought indicators based on model-assimilated gravity recovery and climate experiment (grace) terrestrial water storage observations. *Water Resources Research*, 48(7), 2012.

Huang, S., Huang, Q., Chang, J., and Leng, G. Linkages between hydrological drought, climate indices and human activities: a case study in the columbia river basin. *International Journal of climatology*, 36(1):280–290, 2016.

Humphrey, V and Gudmundsson, L. Grace-rec: a reconstruction of climate-driven water storage changes over the last century. *Earth System Science Data*, 11(3):1153–1170, 2019.

Humphrey, V., Gudmundsson, L., and Seneviratne, S. I. A global reconstruction of climate-driven subdecadal water storage variability. *Geophysical Research Letters*, 44(5):2300–2309, 2017.

Janga Reddy, M and Ganguli, P. Application of copulas for derivation of drought severity–duration–frequency curves. *Hydrological Processes*, 26(11):1672–1685, 2012.

Jiang, Z., Tai-Jen Chen, G., and Wu, M. C. Large-scale circulation patterns associated with heavy spring rain events over taiwan in strong enso and non-enso years. *Monthly Weather Review*, 131(8):1769–1782, 2003.

Jing, W., Zhao, X., Yao, L., Di, L., Yang, J., Li, Y., Guo, L., and Zhou, C. Can terrestrial water storage dynamics be estimated from climate anomalies? *Earth and Space Science*, 7(3):e2019EA000959, 2020.

Jing, Z., Deng-Hua, Y., Zhi-Yong, Y., Yong, H., Bai-Sha, W., and Bo-Ya, G. Improvement and adaptability evaluation of standardized precipitation evapotranspiration index. *Acta Physica Sinica*, 64(4), 2015.

Joe, H. *Multivariate models and multivariate dependence concepts*. CRC press, 1997.

Kang, H and Sridhar, V. Combined statistical and spatially distributed hydrological model for evaluating future drought indices in virginia. *Journal of Hydrology: Regional Studies*, 12:253–272, 2017.

Kang, H and Sridhar, V. Assessment of future drought conditions in the chesapeake bay watershed. *JAWRA Journal of the American Water Resources Association*, 54(1): 160–183, 2018.

Kang, H and Sridhar, V. Drought assessment with a surface-groundwater coupled model in the chesapeake bay watershed. *Environmental Modelling & Software*, 119: 379–389, 2019.

Kang, H and Sridhar, V. A novel approach combining simulated soil moisture and stochastic techniques to forecasting drought in the mekong river basin. *International Journal of Climatology*, 2020.

Kang, H., Sridhar, V., Mills, B. F., Hession, W. C., and Ogejo, J. A. Economy-wide climate change impacts on green water droughts based on the hydrologic simulations. *Agricultural Systems*, 171:76–88, 2019.

Karamouz, M., Nazif, S., and Falahi, M. *Hydrology and hydroclimatology: principles and applications*. CRC Press, 2012.

Karl, T. R. The sensitivity of the palmer drought severity index and Palmer's Z-index to their calibration coefficients including potential evapotranspiration. *Journal of Applied Meteorology and Climatology*, 25(1):77–86, 1986.

Kim, T. W., Valdés, J. B., and Aparicio, J. Frequency and spatial characteristics of droughts in the conchos river basin, mexico. *Water International*, 27(3):420–430, 2002.

Kim, T. W., Valdés, J. B., and Yoo, C. Nonparametric approach for bivariate drought characterization using palmer drought index. *Journal of Hydrologic Engineering*, 11 (2):134–143, 2006.

Kumar, K. S., Rathnam, E. V., and Sridhar, V. Tracking seasonal and monthly drought with grace-based terrestrial water storage assessments over major river basins in south india. *Science of The Total Environment*, 763:142994, 2021.

Kumar, P., Wiltshire, A., Mathison, C., Asharaf, S., Ahrens, B., Lucas-Picher, P., Christensen, J. H., Gobiet, A., Saeed, F., Hagemann, S. et al. Downscaled climate change projections with uncertainty assessment over india using a high resolution multi-model approach. *Science of the Total Environment*, 468:S18–S30, 2013.

Landerer, F. W. and Swenson, S. Accuracy of scaled grace terrestrial water storage estimates. *Water resources research*, 48(4), 2012.

Li, F., Kusche, J., Rietbroek, R., Wang, Z., Forootan, E., Schulze, K., and Lück, C. Comparison of data-driven techniques to reconstruct (1992–2002) and predict (2017–2018) grace-like gridded total water storage changes using climate inputs. *Water Resources Research*, 56(5):e2019WR026551, 2020.

Li, F., Kusche, J., Chao, N., Wang, Z., and Löcher, A. Long-term (1979-present) total water storage anomalies over the global land derived by reconstructing grace data. *Geophysical Research Letters*, 48(8):e2021GL093492, 2021.

Li, W. G., Yi, X., Hou, M. T., Chen, H. L., and Chen, Z. L. Standardized precipitation evapotranspiration index shows drought trends in china. *Chin. J. Eco-Agric*, 20(5): 643–649, 2012.

Liu, B., Zou, X., Yi, S., Sneeuw, N., Cai, J., and Li, J. Identifying and separating climate-and human-driven water storage anomalies using grace satellite data. *Remote Sensing of Environment*, 263:112559, 2021.

Liu, P. C. Wavelet spectrum analysis and ocean wind waves. In *Wavelet analysis and its applications*, volume 4, pages 151–166. Elsevier, 1994.

Liu, X., Feng, X., Ciais, P., and Fu, B. Widespread decline in terrestrial water storage and its link to teleconnections across asia and eastern europe. *Hydrology and Earth System Sciences*, 24(7):3663–3676, 2020.

Lobell, D. B., Burke, M. B., Tebaldi, C., Mastrandrea, M. D., Falcon, W. P., and Naylor, R. L. Prioritizing climate change adaptation needs for food security in 2030. *Science*, 319(5863):607–610, 2008.

Long, D., Scanlon, B. R., Longuevergne, L., Sun, A. Y., Fernando, D. N., and Save, H. Grace satellite monitoring of large depletion in water storage in response to the 2011 drought in texas. *Geophysical Research Letters*, 40(13):3395–3401, 2013.

Long, D., Shen, Y., Sun, A., Hong, Y., Longuevergne, L., Yang, Y., Li, B., and Chen, L. Drought and flood monitoring for a large karst plateau in southwest china using extended grace data. *Remote Sensing of Environment*, 155:145–160, 2014.

Long, D., Chen, X., Scanlon, B. R., Wada, Y., Hong, Y., Singh, V. P., Chen, ., Wang, C., Han, Z., and Yang, W. Have grace satellites overestimated groundwater depletion in the northwest india aquifer? *Scientific reports*, 6(1):1–11, 2016.

Longuevergne, L., Scanlon, B. R., and Wilson, C. R. Grace hydrological estimates for small basins: Evaluating processing approaches on the high plains aquifer, usa. *Water Resources Research*, 46(11), 2010.

Loukas, A and Vasiliades, L. Probabilistic analysis of drought spatiotemporal characteristics inthessaly region, greece. *Natural Hazards and Earth System Sciences*, 4(5/6):719–731, 2004.

Luthcke, S. B., Rowlands, D., Sabaka, T., Loomis, B., Horwath, M., and Arendt, A. Gravimetry measurements from space. *Remote Sensing of the Cryosphere*, pages 231–247, 2015.

Maccioni, P., Kossida, M., Brocca, L., and Moramarco, T. Assessment of the drought hazard in the tiber river basin in central italy and a comparison of new and commonly used meteorological indicators. *Journal of Hydrologic Engineering*, 20(8):05014029, 2015.

McCabe, G. J., Palecki, M. A., and Betancourt, J. L. Pacific and atlantic ocean influences on multidecadal drought frequency in the united states. *Proceedings of the National Academy of Sciences*, 101(12):4136–4141, 2004.

McKee, T. B., Doesken, N. J., Kleist, J. et al. The relationship of drought frequency and duration to time scales. In *Proceedings of the 8th Conference on Applied Climatology*, volume 17, pages 179–183. California, 1993.

Meghwal, R., Shah, D., and Mishra, V. On the changes in groundwater storage variability in western india using grace and well observations. *Remote Sensing in Earth Systems Sciences*, 2(4):260–272, 2019.

Mika, J., Horvath, S., Makra, L., and Dunkel, Z. The palmer drought severity index (pdsi) as an indicator of soil moisture. *Physics and Chemistry of the Earth, Parts A/B/C*, 30(1-3):223–230, 2005.

Mishra, A and Desai, V. Spatial and temporal drought analysis in the kansabati river basin, india. *International Journal of River Basin Management*, 3(1):31–41, 2005.

Mishra, A and Singh, V. P. Analysis of drought severity-area-frequency curves using a general circulation model and scenario uncertainty. *Journal of Geophysical Research: Atmospheres*, 114(D6), 2009.

Mishra, A., Singh, V., and Desai, V. Drought characterization: a probabilistic approach. *Stochastic Environmental Research and Risk Assessment*, 23(1):41–55, 2009.

Mishra, A. K and Singh, V. P. A review of drought concepts. *Journal of hydrology*, 391 (1-2):202–216, 2010.

Mishra, A. K and Singh, V. P. Drought modeling–a review. *Journal of Hydrology*, 403 (1-2):157–175, 2011.

Mishra, V. Long-term (1870–2018) drought reconstruction in context of surface water security in india. *Journal of Hydrology*, 580:124228, 2020.

Mishra, V., Aadhar, S., Asoka, A., Pai, S., and Kumar, R. On the frequency of the 2015 monsoon season drought in the indo-gangetic plain. *Geophysical Research Letters*, 43(23):12–102, 2016.

Mishra, V., Thirumalai, K., Jain, S., and Aadhar, S. Unprecedented drought in south india and recent water scarcity. *Environmental Research Letters*, 16(5):054007, 2021.

Mooley, D and Parthasarathy, B. Droughts and floods over india in summer monsoon seasons 1871–1980. In *Variations in the global water budget*, pages 239–252. Springer, 1983.

Mukherjee, A., Fryar, A. E., and Howell, P. D. Regional hydrostratigraphy and groundwater flow modeling in the arsenic-affected areas of the western bengal basin, west bengal, india. *Hydrogeology Journal*, 15(7):1397–1418, 2007.

Nagarajan, R. *Drought assessment*. Springer Science & Business Media, 2010.

Ndehedehe, C. E., Awange, J. L., Kuhn, M., Agutu, N. O., and Fukuda, Y. Climate teleconnections influence on west africa's terrestrial water storage. *Hydrological Processes*, 31(18):3206–3224, 2017.

Nelsen, R. B. *An introduction to copulas*. Springer Science & Business Media, 2007.

Ni, S., Chen, J., Wilson, C. R., Li, J., Hu, X., and Fu, R. Global terrestrial water storage changes and connections to enso events. *Surveys in Geophysics*, 39(1):1–22, 2018.

Nie, N., Zhang, W., Zhang, Z., Guo, H., and Ishwaran, N. Reconstructed terrestrial water storage change (δtws) from 1948 to 2012 over the amazon basin with the latest grace and gldas products. *Water Resources Management*, 30(1):279–294, 2016.

Pal, N. R and Bezdek, J. C. On cluster validity for the fuzzy c-means model. *IEEE Transactions on Fuzzy systems*, 3(3):370–379, 1995.

Palmer, W. Meteorological drought (vol. 30). us department of commerce, weather bureau, 1965.

Panda, D. K and Wahr, J. Spatiotemporal evolution of water storage changes in i ndia from the updated grace-derived gravity records. *Water Resources Research*, 52(1): 135–149, 2016.

Panofsky, H. A., Brier, G. W., and Best, W. H. Some application of statistics to meteorology. 1958.

Patle, G., Singh, D., Sarangi, A., Rai, A., Khanna, M., and Sahoo, R. Time series analysis of groundwater levels and projection of future trend. *Journal of the Geological Society of India*, 85(2):232–242, 2015.

Percival, D. B and Walden, A. T. *Wavelet methods for time series analysis*, volume 4. Cambridge university press, 2000.

Phillips, T., Nerem, R., Fox-Kemper, B., Famiglietti, J., and Rajagopalan, B. The influence of enso on global terrestrial water storage using grace. *Geophysical Research Letters*, 39(16), 2012.

Prakash, S. Capabilities of satellite-derived datasets to detect consecutive indian monsoon droughts of 2014 and 2015. *Current Science*, pages 2362–2368, 2018.

Qian, T., Dai, A., Trenberth, K. E., and Oleson, K. W. Simulation of global land surface conditions from 1948 to 2004. part i: Forcing data and evaluations. *Journal of Hydrometeorology*, 7(5):953–975, 2006.

Rad, A. M., Ghahraman, B., Khalili, D., Ghahremani, Z., and Ardakani, S. A. Integrated meteorological and hydrological drought model: a management tool for proactive water resources planning of semi-arid regions. *Advances in water resources*, 107:336–353, 2017.

Rajeevan, M., Bhate, J., and Jaswal, A. K. Analysis of variability and trends of extreme rainfall events over india using 104 years of gridded daily rainfall data. *Geophysical research letters*, 35(18), 2008.

Rajsekhar, D., Singh, V. P., and Mishra, A. K. Integrated drought causality, hazard, and vulnerability assessment for future socioeconomic scenarios: An information theory perspective. *Journal of Geophysical Research: Atmospheres*, 120(13):6346–6378, 2015a.

Rajsekhar, D., Singh, V. P., and Mishra, A. K. Hydrologic drought atlas for texas. *Journal of Hydrologic Engineering*, 20(7):05014023, 2015b.

Ramillien, G., Famiglietti, J. S., and Wahr, J. Detection of continental hydrology and glaciology signals from grace: a review. *Surveys in geophysics*, 29(4):361–374, 2008.

Rateb, A., Scanlon, B. R., Pool, D. R., Sun, A., Zhang, Z., Chen, J., Clark, B., Faunt, C. C., Haugh, C. J., Hill, M et al. Comparison of groundwater storage changes from grace satellites with monitoring and modeling of major us aquifers. *Water Resources Research*, 56(12):e2020WR027556, 2020.

Reddy, M. J and Ganguli, P. Spatio-temporal analysis and derivation of copula-based intensity–area–frequency curves for droughts in western rajasthan (india). *Stochastic environmental research and risk assessment*, 27(8):1975–1989, 2013.

Reddy, M. J and Singh, V. P. Multivariate modeling of droughts using copulas and meta-heuristic methods. *Stochastic environmental research and risk assessment*, 28 (3):475–489, 2014.

Richey, A. S., Thomas, B. F., Lo, M. H., Reager, J. T., Famiglietti, J. S., Voss, K., Swenson, S., and Rodell, M. Quantifying renewable groundwater stress with grace. *Water resources research*, 51(7):5217–5238, 2015.

Rodell, M and Famiglietti, J. S. The potential for satellite-based monitoring of groundwater storage changes using grace: the high plains aquifer, central us. *Journal of Hydrology*, 263(1-4):245–256, 2002.

Rodell, M., Houser, P., Jambor, U., Gottschalck, J., Mitchell, K., Meng, C. J., Arsenault, K., Cosgrove, B., Radakovich, J., Bosilovich, M, et al. The global

land data assimilation system. *Bulletin of the American Meteorological Society*, 85 (3):381–394, 2004.

Rodell, M., Chen, J., Kato, H., Famiglietti, J. S., Nigro, J., and Wilson, C. R. Estimating groundwater storage changes in the mississippi river basin (usa) using grace. *Hydrogeology Journal*, 15(1):159–166, 2007.

Rodell, M., Velicogna, I., and Famiglietti, J. S. Satellite-based estimates of groundwater depletion in india. *Nature*, 460(7258):999–1002, 2009.

Rogan, J., Franklin, J., Stow, D., Miller, J., Woodcock, C., and Roberts, D. Mapping land-cover modifications over large areas: A comparison of machine learning algorithms. *Remote Sensing of Environment*, 112(5):2272–2283, 2008.

Rowlands, D. D., Luthcke, S., Klosko, S., Lemoine, F. G., Chinn, D., McCarthy, J., Cox, C., and Anderson, O. Resolving mass flux at high spatial and temporal resolution using grace intersatellite measurements. *Geophysical Research Letters*, 32 (4), 2005.

Saghafian, B., Shokoohi, A., and Raziei, T. Drought spatial analysis and development of severity-duration-frequency curves for an arid region. *Proceedings of International Conference on Hydrology of the Mediterranean and Semiarid Regions*, 278, 01 2003.

Saha, D and Agrawal, A. Determination of specific yield using a water balance approach–case study of torla odha watershed in the deccan trap province, maharastra state, india. *Hydrogeology Journal*, 14(4):625–635, 2006.

Sahoo, A. K. Sheffield, J., Pan, M., and Wood, E. F. Evaluation of the tropical rainfall measuring mission multi-satellite precipitation analysis (tmpa) for assessment of large-scale meteorological drought. *Remote Sensing of Environment*, 159:181–193, 2015.

Samantaray, A. K., Singh, G., Ramadas, M., and Panda, R. K. Drought hotspot analysis and risk assessment using probabilistic drought monitoring and severity–duration–frequency analysis. *Hydrological Processes*, 33(3):432–449, 2019.

Santos, M. A. Regional droughts: a stochastic characterization. *Journal of Hydrology*, 66(1):183–211, 1983.

Sarkar, T., Kannaujiya, S., Taloor, A. K., Ray, P. K. C., and Chauhan, P. Integrated study of grace data derived interannual groundwater storage variability over water stressed indian regions. *Groundwater for Sustainable Development*, 10:100376, 2020.

Satish Kumar, K., AnandRaj, P., Sreelatha, K., Bisht, D. S., and Sridhar, V. Monthly and seasonal drought characterization using grace-based groundwater drought index and its link to teleconnections across south indian river basins. *Climate*, 9(4):56, 2021.

Save, H., Bettadpur, S., and Tapley, B. D. High-resolution csr grace rl05 mascons. *Journal of Geophysical Research: Solid Earth*, 121(10):7547–7569, 2016.

Scanlon, B. R., Longuevergne, L., and Long, D. Ground referencing grace satellite estimates of groundwater storage changes in the california central valley, usa. *Water Resources Research*, 48(4), 2012.

Scanlon, B. R., Zhang, Z., Save, H., Wiese, D. N., Landerer, F. W., Long, D., Longuevergne, L., and Chen, J. Global evaluation of new grace mascon products for hydrologic applications. *Water Resources Research*, 52(12):9412–9429, 2016.

Sehgal, V and Sridhar, V. Effect of hydroclimatological teleconnections on the watershed-scale drought predictability in the southeastern united states. *International Journal of Climatology*, 38:e1139–e1157, 2018.

Sehgal, V and Sridhar, V. Watershed-scale retrospective drought analysis and seasonal forecasting using multi-layer, high-resolution simulated soil moisture for southeastern us. *Weather and Climate Extremes*, 23:100191, 2019.

Sehgal, V., Sridhar, V., and Tyagi, A. Stratified drought analysis using a stochastic ensemble of simulated and in-situ soil moisture observations. *Journal of Hydrology*, 545:226–250, 2017.

Setti, S., Maheswaran, R., Radha, D., Sridhar, V., Barik, K., and Narasimham, M. Attribution of hydrologic changes in a tropical river basin to rainfall variability and land-use change: case study from india. *Journal of Hydrologic Engineering*, 25(8): 05020015, 2020.

Shamsudduha, M., Taylor, R., and Longuevergne, L. Monitoring groundwater storage changes in the highly seasonal humid tropics: Validation of grace measurements in the bengal basin. *Water Resources Research*, 48(2), 2012.

Sharma, P. J., Patel, P., and Jothiprakash, V. Hydroclimatic teleconnections of large-scale oceanic-atmospheric circulations on hydrometeorological extremes of tapi basin, india. *Atmospheric Research*, 235:104791, 2020.

Shewale, M and Kumar, S. Climatological features of drought incidences in india. *Meteorological Monograph (Climatology 21/2005). National Climate Centre, Indian Meteorological Department*, 2005.

Shiau, J. Return period of bivariate distributed extreme hydrological events. *Stochastic environmental research and risk assessment*, 17(1):42–57, 2003.

Shiau, J. Fitting drought duration and severity with two-dimensional copulas. *Water resources management*, 20(5):795–815, 2006.

Shiau, J and Modarres, R. Copula-based drought severity-duration-frequency analysis in iran. *Meteorological Applications: A journal of forecasting, practical applications, training techniques and modelling*, 16(4):481–489, 2009.

Shiau, J and Shen, H. W. Recurrence analysis of hydrologic droughts of differing severity. *Journal of water resources planning and management*, 127(1):30–40, 2001.

Shiau, J., Feng, S., and Nadarajah, S. Assessment of hydrological droughts for the yellow river, china, using copulas. *Hydrological Processes: An International Journal*, 21(16):2157–2163, 2007.

Sinha, D., Syed, T. H., Famiglietti, J. S., Reager, J. T., and Thomas, R. C. Characterizing drought in india using grace observations of terrestrial water storage deficit. *Journal of Hydrometeorology*, 18(2):381–396, 2017.

Sinha, D., Syed, T. H., and Reager, J. T. Utilizing combined deviations of precipitation and grace-based terrestrial water storage as a metric for drought characterization: A case study over major indian river basins. *Journal of Hydrology*, 572:294–307, 2019.

Sklar, M. Fonctions de repartition an dimensions et leurs marges. *Publ. inst. statist. univ. Paris*, 8:229–231, 1959.

Soni, A and Syed, T. H. Diagnosing land water storage variations in major indian river basins using grace observations. *Global and Planetary Change*, 133:263–271, 2015.

Sridhar, V., Billah, M. M., and Hildreth, J. W. Coupled surface and groundwater hydrological modeling in a changing climate. *Groundwater*, 56(4):618–635, 2018.

Sridhar, V., Ali, S. A., and Lakshmi, V. Assessment and validation of total water storage in the chesapeake bay watershed using grace. *Journal of Hydrology: Regional Studies*, 24:100607, 2019.

Srivastava, A., Rajeevan, M., and Kshirsagar, S. Development of a high resolution daily gridded temperature data set (1969–2005) for the indian region. *Atmospheric Science Letters*, 10(4):249–254, 2009.

Strassberg, G., Scanlon, B. R., and Rodell, M. Comparison of seasonal terrestrial water storage variations from grace with groundwater-level measurements from the high plains aquifer (usa). *Geophysical Research Letters*, 34(14), 2007.

Sun, A. Y. Predicting groundwater level changes using grace data. *Water Resources Research*, 49(9):5900–5912, 2013.

Sun, A. Y., Scanlon, B. R., Zhang, Z., Walling, D., Bhanja, S. N., Mukherjee, A., and Zhong, Z. Combining physically based modeling and deep learning for fusing grace satellite data: can we learn from mismatch? *Water Resources Research*, 55(2): 1179–1195, 2019.

Sun, Z., Zhu, X., Pan, Y., Zhang, J., and Liu, X. Drought evaluation using the grace terrestrial water storage deficit over the yangtze river basin, china. *Science of the Total Environment*, 634:727–738, 2018.

Sun, Z., Long, D., Yang, W., Li, X., and Pan, Y. Reconstruction of grace data on changes in total water storage over the global land surface and 60 basins. *Water Resources Research*, 56(4):e2019WR026250, 2020.

Svoboda, M., LeComte, D., Hayes, M., Heim, R., Gleason, K., Angel, J., Rippey, B., Tinker, R., Palecki, M., Stooksbury, D, et al. The drought monitor. *Bulletin of the American Meteorological Society*, 83(8):1181–1190, 2002.

Swenson, S and Wahr, J. Post-processing removal of correlated errors in grace data. *Geophysical research letters*, 33(8), 2006.

Syed, T. H., Famiglietti, J. S., Rodell, M., Chen, J., and Wilson, C. R. Analysis of terrestrial water storage changes from grace and gldas. *Water Resources Research*, 44(2), 2008.

Tallaksen, L. M and Van Lanen, H. A. Hydrological drought: processes and estimation methods for streamflow and groundwater. 2004.

Tallaksen, L. M., Madsen, H., and Clausen, B. On the definition and modelling of streamflow drought duration and deficit volume. *Hydrological Sciences Journal*, 42 (1):15–33, 1997.

Tan, X., Gan, T. Y., and Shao, D. Wavelet analysis of precipitation extremes over canadian ecoregions and teleconnections to large-scale climate anomalies. *Journal of Geophysical Research: Atmospheres*, 121(24):14–469, 2016.

Tang, Q., Zhang, X., and Tang, Y. Anthropogenic impacts on mass change in north china. *Geophysical Research Letters*, 40(15):3924–3928, 2013.

Tapley, B. D., Bettadpur, S., Ries, J. C., Thompson, P. F., and Watkins, M. M. Grace measurements of mass variability in the earth system. *Science*, 305(5683):503–505, 2004.

Tapley, B. D., Watkins, M. M., Flechtner, F., Reigber, C., Bettadpur, S., Rodell, M., Sasgen, I., Famiglietti, J. S., Landerer, F. W., Chambers, D. P, et al. Contributions of grace to understanding climate change. *Nature climate change*, 9(5):358–369, 2019.

Tase, N. *Area-deficit-intensity characteristics of droughts*. PhD thesis, Colorado State University. Libraries, 1976.

Thilakarathne, M and Sridhar, V. Characterization of future drought conditions in the lower mekong river basin. *Weather and Climate Extremes*, 17:47–58, 2017.

Thomas, A. C., Reager, J. T., Famiglietti, J. S., and Rodell, M. A grace-based water storage deficit approach for hydrological drought characterization. *Geophysical Research Letters*, 41(5):1537–1545, 2014.

Thomas, B. F., Famiglietti, J. S., Landerer, F. W., Wiese, D. N., Molotch, N. P., and Argus, D. F. Grace groundwater drought index: Evaluation of california central valley groundwater drought. *Remote Sensing of Environment*, 198:384–392, 2017.

Tiwari, V. M., Wahr, J., and Swenson, S. Dwindling groundwater resources in northern india, from satellite gravity observations. *Geophysical Research Letters*, 36(18), 2009.

Torrence, C and Webster, P. J. Interdecadal changes in the enso–monsoon system. *Journal of climate*, 12(8):2679–2690, 1999.

Urcid, G and Ritter, G. X. C-means clustering of lattice auto-associative memories for endmember approximation. In *Advances in Knowledge-Based and Intelligent Information and Engineering Systems*, pages 2140–2149. IOS Press, 2012.

Van den Dool, H., Saha, S., and Johansson, A. Empirical orthogonal teleconnections. *Journal of Climate*, 13(8):1421–1435, 2000.

Van Loon, A. F., and Van Lanen, H. A. Making the distinction between water scarcity and drought using an observation-modeling framework. *Water Resources Research*, 49(3):1483–1502, 2013.

Vicente-Serrano, S. M., Beguería, S., and López-Moreno, J. I. A multiscalar drought index sensitive to global warming: the standardized precipitation evapotranspiration index. *Journal of climate*, 23(7):1696–1718, 2010.

Vicente-Serrano, S. M., Beguería, S., and López-Moreno, J. I. Comment on "characteristics and trends in various forms of the palmer drought severity index (pdsi) during 1900–2008" by aiguo dai. *Journal of Geophysical Research: Atmospheres*, 116(D19), 2011.

Vishwakarma, B. D. Monitoring droughts from grace. *Frontiers in Environmental Science*, 2020.

Vissa, N. K., Anandh, P., Behera, M. M., and Mishra, S. Enso-induced groundwater changes in india derived from grace and gldas. *Journal of Earth System Science*, 128 (5):115, 2019.

Voss, K. A., Famiglietti, J. S., Lo, M., De Linage, C., Rodell, M., and Swenson, S. C. Groundwater depletion in the middle east from grace with implications for transboundary water management in the tigris-euphrates-western iran region. *Water resources research*, 49(2):904–914, 2013.

Wahr, J., Molenaar, M., and Bryan, F. Time variability of the earth's gravity field: Hydrological and oceanic effects and their possible detection using grace. *Journal of Geophysical Research: Solid Earth*, 103(B12):30205–30229, 1998.

Wahr, J., Swenson, S., Zlotnicki, V., and Velicogna, I. Time-variable gravity from grace: First results. *Geophysical Research Letters*, 31(11), 2004.

Wallace, J. M and Gutzler, D. S. Teleconnections in the geopotential height field during the northern hemisphere winter. *Monthly weather review*, 109(4):784–812, 1981.

Wang, F., Wang, Z., Yang, H., Di, D., Zhao, Y., and Liang, Q. Utilizing grace-based groundwater drought index for drought characterization and teleconnection factors analysis in the north china plain. *Journal of Hydrology*, 585:124849, 2020.

Wang, H., Chen, Y., Pan, Y., and Li, W. Spatial and temporal variability of drought in the arid region of china and its relationships to teleconnection indices. *Journal of hydrology*, 523:283–296, 2015a.

Wang, H., Rogers, J. C., and Munroe, D. K. Commonly used drought indices as indicators of soil moisture in china. *Journal of Hydrometeorology*, 16(3):1397–1408, 2015b.

Watkins, M. M., Wiese, D. N., Yuan, D. N., Boening, C., and Landerer, F. W. Improved methods for observing earth's time variable mass distribution with grace using spherical cap mascons. *Journal of Geophysical Research: Solid Earth*, 120(4): 2648–2671, 2015.

Wells, N., Goddard, S., and Hayes, M. J. A self-calibrating palmer drought severity index. *Journal of climate*, 17(12):2335–2351, 2004.

Wiese, D. N., Landerer, F. W., and Watkins, M. M. Quantifying and reducing leakage errors in the jpl rl05m grace mascon solution. *Water Resources Research*, 52(9): 7490–7502, 2016.

Wilhite, D. A., Sivakumar, M. V., and Pulwarty, R. Managing drought risk in a changing climate: The role of national drought policy. *Weather and Climate Extremes*, 3:4–13, 2014.

Xie, X. L., and Beni, G. A validity measure for fuzzy clustering. *IEEE Transactions on pattern analysis and machine intelligence*, 13(8):841–847, 1991.

Xu, L., Chen, N., Zhang, X., Chen, Z., Hu, C., and Wang, C. Improving the north american multi-model ensemble (nmme) precipitation forecasts at local areas using wavelet and machine learning. *Climate dynamics*, 53(1):601–615, 2019.

Yang, P., Zhang, Y., Xia, J., and Sun, S. Identification of drought events in the major basins of central asia based on a combined climatological deviation index from grace measurements. *Atmospheric Research*, 244:105105, 2020.

Yeh, P. J. F., Swenson, S. C., Famiglietti, J. S., and Rodell, M. Remote sensing of groundwater storage changes in illinois using the gravity recovery and climate experiment (grace). *Water Resources Research*, 42(12), 2006.

Yevjevich, V. M. *Objective approach to definitions and investigations of continental hydrologic droughts, An*. PhD thesis, Colorado State University. Libraries, 1967.

Yi, H and Wen, L. Satellite gravity measurement monitoring terrestrial water storage change and drought in the continental united states. *Scientific reports*, 6(1):1–9, 2016.

Yirdaw, S. Z., Snelgrove, K. R., and Agboma, C. O. Grace satellite observations of terrestrial moisture changes for drought characterization in the canadian prairie. *Journal of Hydrology*, 356(1-2):84–92, 2008.

Zhang, B., Zhao, X., Jin, J., and Wu, P. Development and evaluation of a physically based multiscalar drought index: The standardized moisture anomaly index. *Journal of Geophysical Research: Atmospheres*, 120(22):11–575, 2015a.

Zhang, D., Zhang, Q., Werner, A. D., and Liu, X. Grace-based hydrological drought evaluation of the yangtze river basin, china. *Journal of Hydrometeorology*, 17(3): 811–828, 2016.

Zhang, Y., Li, Y., Ge, J., Li, G., Yu, Z., and Niu, H. Correlation analysis between drought indices and terrestrial water storage from 2002 to 2015 in china. *Environmental Earth Sciences*, 77(12):1–12, 2018.

Zhang, Y., He, B., Guo, L., and Liu, D. Differences in response of terrestrial water storage components to precipitation over 168 global river basins. *Journal of Hydrometeorology*, 20(9):1981–1999, 2019.

Zhang, Z., Chao, B., Chen, J., and Wilson, C. Terrestrial water storage anomalies of yangtze river basin droughts observed by grace and connections with enso. *Global and Planetary Change*, 126:35–45, 2015b.

Zhao, M., Velicogna, I., and Kimball, J. S. Satellite observations of regional drought severity in the continental united states using grace-based terrestrial water storage changes. *Journal of Climate*, 30(16):6297–6308, 2017a.

Zhao, M., Velicogna, I., and Kimball, J. S. A global gridded dataset of grace drought severity index for 2002–14: Comparison with pdsi and spei and a case study of the australia millennium drought. *Journal of Hydrometeorology*, 18(8):2117–2129, 2017b.

Zhu, Z., Piao, S., Xu, Y., Bastos, A., Ciais, P., and Peng, S. The effects of teleconnections on carbon fluxes of global terrestrial ecosystems. *Geophysical Research Letters*, 44(7):3209–3218, 2017.

RESEARCH PUBLICATIONS

Referred Journals

1. Satish Kumar K, Rathnam E V, and Sridhar V. (2020) Tracking Seasonal and Monthly Drought with GRACE-based Terrestrial Water Storage Assessments over Major River Basins in South India. *Science of The Total Environment*, Elsevier, 763, 142994. doi: https://doi.org/10.1016/j.scitotenv.2020.142994.

2. Satish Kumar K, AnandRaj P, Sreelatha K, and Sridhar V. (2021) Regional analysis of drought severity-duration-frequency and severity-area-frequency curves in the Godavari River Basin, India. *International Journal of Climatology*, Wiley, 41(12), 5481-5501. doi: https://doi.org/10.1002/joc.7137.

3. Satish Kumar K, AnandRaj P, Sreelatha K, Bisht D S, and Sridhar V. (2021) Monthly and Seasonal Drought Characterization Using GRACE-Based Groundwater Drought Index and Its Link to Teleconnections across South Indian River Basins. *Climate*, MDPI, 9(4), 56. https://doi.org/10.3390/cli9040056.

4. Satish Kumar K and Rathnam E V. (2019) Analysis and Prediction of Groundwater Level Trends Using Four Variations of Mann Kendall Tests and ARIMA Modelling. *Journal of the Geological Society of India*, Springer, 94(3), 281-289. doi:https://doi.org/10.1007/s12594-019-1308-4.

5. Satish Kumar K and Rathnam E.V. (2020) Comparison of six trend detection methods and forecasting for monthly groundwater levels–a case study. *ISH Journal of Hydraulic Engineering*, Taylor and Francis, pp 1-10. https://doi.org/10.1080/09715010.2020.1715270.

Journals under review

1. Satish Kumar K, AnandRaj P, Sreelatha K, and Sridhar V. Reconstruction of GRACE total water storage changes (1960-2020) and its validation with in situ observation well network. (submitted to Science of The Total Environment).

BRIEF CURRICULUM VITAE

Mr. K Satish Kumar is a full-time research scholar in the Department of Civil Engineering, National Institute of Technology, Warangal-506004, India. He has received his undergraduate degree in Civil Engineering from Sri Venkateswara University, Tirupati and postgraduate degree in Water Resources Engineering from Maulana Azad National Institute of Technology (M.P.) Bhopal, India. His research interests are in the areas of drought and climate change impact assessment at river basin scales, groundwater storage assessments, remote sensing and GIS applications in hydrology. During his doctoral research, he has published 7 papers in International peer-reviewed and reputed journals and conferences.

DOCTORAL COMMITTEE

The Doctoral Committee of Mr. K Satish Kumar, full time Ph.D., Research Scholar (Enrolment Number: 717005) is as follows:

Doctoral Committee Chairman	**Dr. P Rathish Kumar** Professor, Department of Civil Engineering, National Institute of Technology, Warangal-506004.
Research Supervisor	**Dr. P Anand Raj** Professor, Department of Civil Engineering, National Institute of Technology, Warangal-506004.
Internal Member	**Dr. N V Umamahesh** Professor, Department of Civil Engineering, National Institute of Technology, Warangal-506004.
Internal Member	**Dr. K Venkata Reddy** Associate Professor, Department of Civil Engineering, National Institute of Technology, Warangal-506004.
External Member	**Dr. Debashis Dutta** Professor, Department of Mathematics, National Institute of Technology, Warangal-506004.